Hybrid Ionic Liquid Electrolytes for Lithium Battery Applications

Submitted in partial fulfilment of the requirements

of the degree of

Doctor of Philosophy

of the
Indian Institute of Technology, Bombay, India
and
Monash University, Australia

by

Sowmiya Theivaprakasam

Supervisors:

Prof. Sagar Mitra (IIT Bombay)

Prof. Douglas MacFarlane (Monash University)

The course of study for this award was developed jointly by
Monash University, Australia and the Indian Institute of Technology, Bombay
and was given academic recognition by each of them.
The programme was administrated by The IITB-Monash Research Academy

(2018)

Dedicated to my family & friends

Declaration

I declare that this written submission represents my ideas in my own words and where other's ideas or words have been included, I have adequately cited and referenced the original sources. I also declare that I have adhered to all principles of academic honesty and integrity and have not misrepresented or fabricated or falsified any idea/data/fact/source in my submission. I understand that any violation of the above will be cause for disciplinary action by the Institute and can also evoke penal action from the sources which have thus not been properly cited or from whom proper permission has not been taken when needed.

Notice 1

Notice 2

I certify that I have made all reasonable efforts to secure copyright permissions for third-party content included in this thesis and have not knowingly added copyright content to my work without the owner's permission.

Student Name	Sowmiya Theivaprakasam
IITB ID	[redacted]
Monash ID	[redacted]

Abstract

Electrolytes plays a significant role in terms of performance as well as safety of lithium batteries. Currently, $LiPF_6$ salts with alkyl carbonate solvents are used as electrolytes for lithium batteries. These have several drawbacks such as low thermal stability, narrow operating temperature range, and limited operation at high oxidation potentials. These issues challenge the high energy density, safety and operation of lithium-ion batteries at subzero temperatures. As a result, design of better electrolyte formulations will help in achieving better batteries. In the present work, we have studied a hybrid electrolyte (HE) formulation which involves the addition of 40 percent of room temperature ionic liquid (RTIL), N-Propyl-N-methylpyrrolidinium bis(trifluoromethanesulfonyl)imide to the conventional electrolyte. Ionic liquids are basically salts with an organic cation and inorganic anion which melts below room temperatures. They have negligible vapor pressures and better thermal stability. The physicochemical, electrochemical, and thermal properties of the HE were investigated in this work for lithium battery applications. It is inferred that the addition of ionic liquid to the conventional electrolyte will not cause any hindrance to the electrochemical performance of the electrolyte. Studies of HE with commercial $LiCoO_2$ cathodes indicate an ability to extract additional lithium ions from the system without compromising the structural stability. The operation of lithium-ion batteries using $LiFePO_4$ cathodes and $Li_4Ti_5O_{12}$ anodes was tested at subzero temperatures using a low temperature HE formulation. Further, the passivation mechanism of HE for aluminum current collector at higher oxidation potentials was investigated in this work. Thus, the potential application of HE in lithium-ion batteries is demonstrated in this work.

Table of Contents

Chapter 2 : Solution Structure and Electrochemical Characterization of N-methyl-N-propyl pyrrolidinium bis(trifluoromethanesulfonyl)imide in Alkyl-carbonate Hybrid Electrolyte

Chapter 3 : Studies of Hybrid Electrolyte with Lithium Cobalt Oxide Cathode

Chapter 4 : $LiFePO_4$ Based Batteries with Hybrid Electrolytes and Applications at Subzero Temperatures

Chapter 5 : Passivation Behavior of Aluminum Current Collector in Hybrid Electrolytes with [FSI] and [TFSI] anions

Chapter 6 : Inferences and Scope for Future Research

Abbreviations

1.	AES	Atomic Emission Spectroscopy
2.	AFM	Atomic Force Microscopy
3.	AGG	Aggregates
4.	Al_2O_3	Alumina
5.	AlF_3	Aluminum fluoride
6.	ATR	Attenuated Total Reflectance
7.	$[C_3mpyr][FSI]$	N-Methyl-N-propylpyrrolidinium bis(fluorosulfonyl)imide
8.	$[C_3mpyr][TFSI]$	N-methyl-N-propylpyrrolidinium bis(trifluoromethane sulfonyl)imide
9.	CA	Chronoamperometry
10.	CIP	Conjugated Ion Pair
11.	CMC	Carboxy methyl cellulose
12.	CO_2	Carbon dioxide
13.	CO_3^{2-}	Carbonate
14.	CPE	Constant Phase Element
15.	CPP	Cyclic Potentiodynamic Polarisation
16.	$CsNO_3$	Caesium nitrate
17.	CV	Cyclic Voltammetry
18.	DC	Direct Current
19.	DEC	Diethyl carbonate
20.	DFT	Density Functional Theory
21.	DMC	Dimethyl carbonate

22.	DSC	Differential Scanning Calorimetry
23.	DTA	Differential Thermal Analysis
24.	EA	Ethyl acetate
25.	EB	Ethyl butyrate
26.	EC	Ethylene carbonate
27.	E_{corr}	Corrosion Potential
28.	EDL	Electrochemical Double Layer
29.	EDXS	Energy Dispersive X-ray Spectroscopy
30.	EIS	Electrochemical Impedance Spectroscopy
31.	EMC	Ethyl methyl carbonate
32.	EP	Ethyl propionate
33.	ESI^+	Electrospray ionization
34.	EV	Electric Vehicle
35.	FEC	Fluroethylene carbonate
36.	FEGSEM	Field Emission Gun Scanning Electron Microscopy
37.	FSI	Fluorosulfonylimide
38.	FTIR	Fourier Transform Infrared Spectroscopy
39.	HE	Hybrid electrolyte
40.	HOMO	Highest Occupied Molecular Orbital
41.	HRTEM	High Resolution Transmission Electron Microscopy
42.	HT $LiCoO_2$	High Temperature $LiCoO_2$
43.	I_{corr}	corrosion current density
44.	KCl	Potassium chloride

45.	$Li_4Ti_5O_{12}$	Lithium titanium oxide
46.	$LiAsF_6$	Lithium hexafluoroarsenate
47.	LiB	Lithium-ion battery
48.	LiBs	Lithium-ion batteries
49.	$LiBF_4$	Lithium tetrafluroborate
50.	$LiClO_4$	Lithium perchlorate
51.	$LiCoO_2$	Lithium cobalt oxide
52.	$LiFePO_4$	Lithium iron phosphate
53.	LiFOB	Lithium difluoro oxalate borate
54.	$LiMn_2O_4$	Lithium manganese oxide
55.	$LiMnO_2$	Lithium manganese oxide
56.	$LiN(SO_2CF_3)_2$	Lithium Triflate
57.	$LiNiCoAlO_2$	Lithium nickel cobalt aluminum oxide
58.	$LiNiO_2$	Lithium nickel oxides
59.	$LiPF_6$	Lithium hexaflurophosphate
60.	LIPON	Lithium phosphorous oxynitride compounds
61.	LISCON	Lithium super ionic conductors
62.	LiTFS	Lithium trifluoromethanesulphonate
63.	LiTFSI	Lithium bis(trifluoromethanesulfonyl)imide
64.	$LiTi_2(PO4)_3$	Lithium Titanium Phosphate
65.	$Li_xV_2O_5$	Lithium vanadium oxides
66.	LSV	Linear Sweep Voltammetry
67.	LT $LiCoO_2$	Low Temperature $LiCoO_2$

68.	LUMO	Lowest Unoccupied Molecular Orbital
69.	LiV_3O_8	Lithium Vanadate
70.	MA	Methyl acetate
71.	MB	Methyl butyrate
72.	NCA	Lithium nickel cobalt aluminum oxide
73.	NMC	Lithium nickel manganese cobalt oxide
74.	NMR	Nuclear Magnetic Resonance
75.	OCV	Open Circuit Potential
76.	PA	Propyl acetate
77.	PAA	Poly (acrylic acid)
78.	PAN	Poly acrylonitrile
79.	PC	Propylene carbonate
80.	PEO	Poly ethylene oxide
81.	PPy	Polypyrrole
82.	PVC	Poly vinyl chloride
83.	PVDF	Polyvinylidene fluoride
84.	PVDF-HFP	Poly vinylidene fluoride copolymerized with hexafluoropropylene
85.	RSF	Relative Sensitivity Factors
86.	SEI	Solid Electrolyte Interface
87.	SEM	Scanning Electron Microscopy
88.	SSIP	Solvent-Separated Ion Pair
89.	TFSI	Trifluromethanesulphonylimide

90.	TGA	Thermogravimetric analysis
91.	TiO_2	Titanium dioxide
92.	TiP_2O_7	Titanium pyrophosphate
93.	TiS_2	Titanium disulphide
94.	VC	Vinylene carbonate
95.	VO_2	Vanadium (IV) oxide
96.	XPS	X ray Photoelectron Spectroscopy
97.	XRD	X ray Diffraction
98.	ZrO_2	Zirconium oxide

List of Figures

Chapter 2 : Solution Structure and Electrochemical Characterization of N-methyl-N-propyl pyrrolidinium bis(trifluoromethanesulfonyl) imide in Alkyl-carbonate Hybrid Electrolyte

Chapter 3 : Studies of Hybrid Electrolyte with Lithium Cobalt Oxide Cathode

Chapter 4 : $LiFePO_4$ Based Batteries with Hybrid Electrolytes and Applications at Subzero Temperatures

Chapter 5 : Passivation Behaviour of Aluminum Current Collector in Hybrid Electrolytes with [FSI] and [TFSI] anions

Chapter 6 : Inferences and Scope for Future Research

List of Tables

Chapter 4 : $LiFePO_4$ Based Batteries with Hybrid Electrolytes and Applications at Subzero Temperatures

Chapter 5 : Passivation Behaviour of Aluminum Current Collector in Hybrid Electrolytes with [FSI] and [TFSI] anions

Chapter 1

Introduction

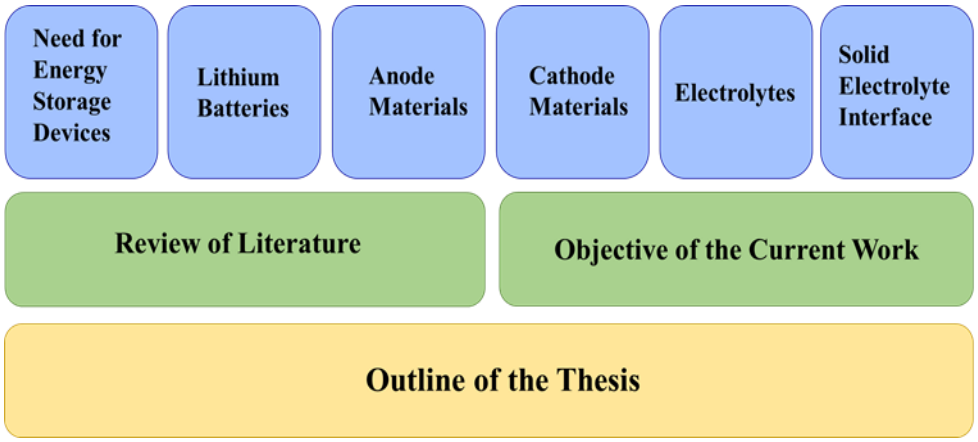

1.1 Energy storage

The quest for energy is one of the main pursuits of the current times. The world energy statistics[1] reveal that India stands third among the top-ten highest energy consuming countries, after China and the United States of America. The predominant source of energy production is fossil fuels[2], which are a non-renewable. There are serious concerns about the quantity of available fossil fuels to meet future energy demands and, currently, the post-processing and energy-conversion processes of these fuels have increased atmospheric carbon dioxide (CO_2) levels to more than 400 ppm[3]. There needs to be a reduction in these levels, if the earth is to become a better place to live[4]. Therefore, across the world, there has been an interest in the exploration of various alternative sources of renewable, clean, and green energy sources. The most promising renewable sources of energy are solar, wind, geothermal, and biofuel. However, there is no clear synchronization between the demand for energy and the production of energy. The disadvantage of these promising alternate energy sources[5] is their intermittent nature. This generates a need for better energy storage systems to meet the growing energy demands.

Energy can be stored in various forms, because the law of conservation of energy is always obeyed. The most preferred form of energy storage depends on factors such as convenience in handling, transport, and shelf life. In these cases, energy can be stored in different forms as chemical, electrochemical, mechanical, and electrical energy. Currently, electrical energy is the most desired form of energy, especially for portable devices. This necessitates portable energy-storage devices, of which the most commonly preferred are batteries that apply reversible chemistries to store energy.

1.2 Batteries

Batteries came into existence in early 200 BC (Parthian period), which can be seen in the reports of Baghdad batteries[6]. However, the scientific community started investigating the use of batteries in 1600 AD after the introduction of the concept of electric charge by William Gilbert [7]. The word, “battery,” was first coined by Benjamin Franklin in 1748, in order to represent a stack of dissimilar metal panels that were placed in a particular fashion to store energy. In 1800, voltaic piles enabled the scientific community to understand the concept of direct current (DC) electricity[8]. Thereafter, the development of batteries and their applications saw a rapid progress. The Voltaic cell was followed by the Daniel cell

with a slightly different design. A breakthrough technology that enabled the regeneration of electrode materials and the reusing of a battery through the concept of "recharging" the battery paved the way for secondary batteries. In 1859, Gaston Plante introduced the first secondary rechargeable batteries, which were called lead-acid batteries[9,10]. This significant technology is still powering automobiles.

Later, the concept of alkaline batteries that utilized alkaline aqueous electrolytes was reported in 1899 by Waldemar Jungne[11,12]. Further, in the 1970s, metal hydrogen and metal hydride batteries were introduced and were used in commercial communication satellites[13]. The lithium battery technology that was developed in the 1970s was a striking innovation at a time when high energy density materials were being investigated in order to power mobile electronic devices.

1.3 Evolution of Lithium Batteries

The potential of lithium metal in batteries was realized first in lithium iodine primary batteries, which were used in implantable devices[10]. After the lithium iodine batteries, lithium manganese dioxide batteries were regarded as successful primary batteries in the market[10]. The era of secondary lithium batteries began in 1978, based on the works of Whittingam et al. using titanium disulphide (TiS_2) materials[14]. Due to the formation of lithium dendrites and other safety-related issues, there was a constant search for better electrode materials. Later, Goodenough[15] et al., introduced a lithium battery which contained a layered metal oxide cathode, lithium cobalt oxide ($LiCoO_2$). This idea entered the commercial market as $Li/LiCoO_2$ rechargeable batteries. Due to lithium plating issues, these batteries were regarded as being safety threats, necessitating safer technologies. In 1991, Sony introduced graphite anodes to replace the lithium metal and proposed graphite/$LiCoO_2$ batteries. This invention paved the way for the concept of lithium-ion batteries (LiBs).

Today, these LiBs can be found in most portable electronic gadgets and in electric vehicles. However, there is a continued demand for high energy density batteries. Since energy density is defined as a product of capacity and voltage, we need to look for electrode materials that have higher capacity and/or voltage.

Although Sony introduced the first commercial LiBs in 1991, the constant research has made significant progress in the technology over the last 27 years. An article in ECS

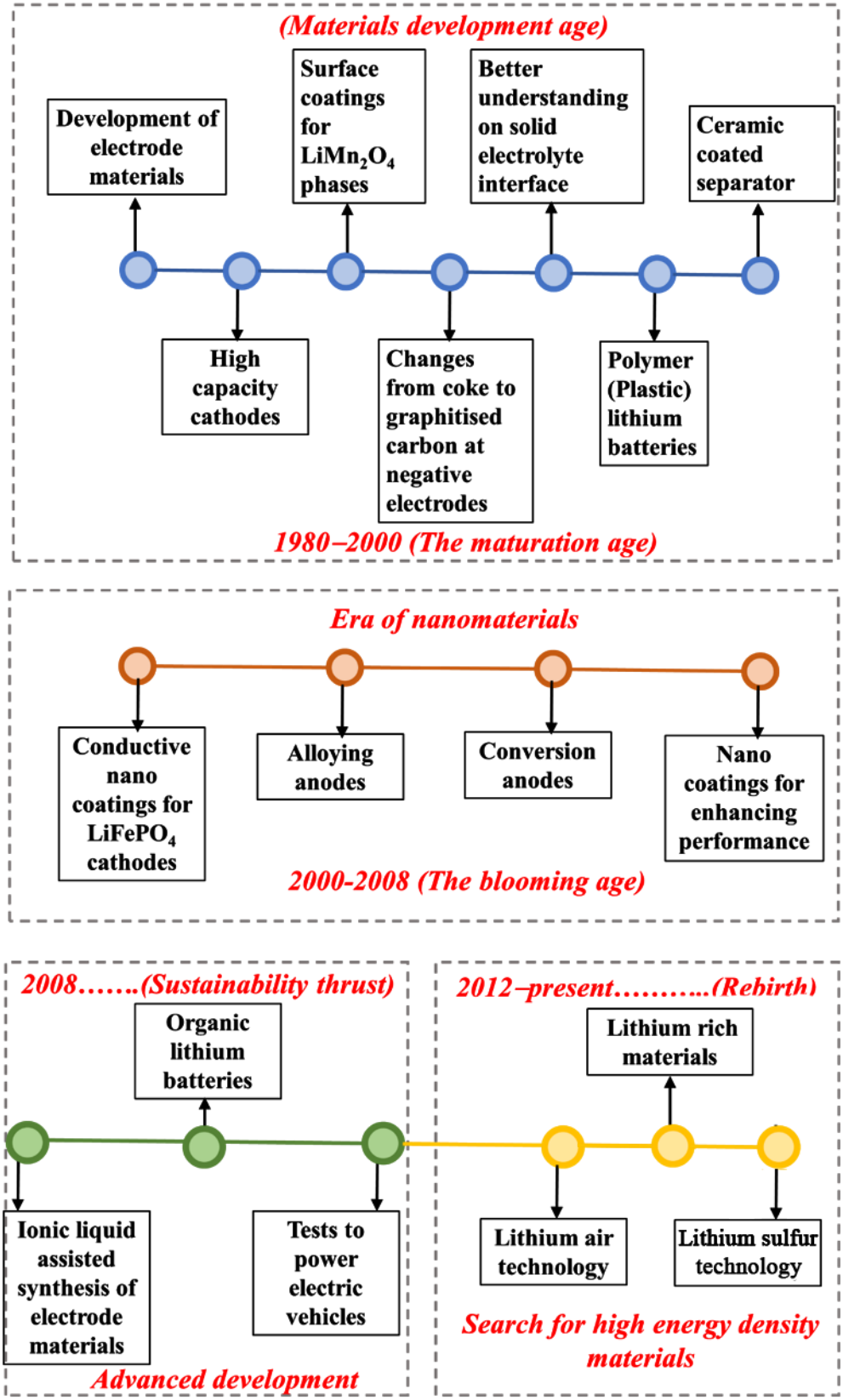

Figure 1.1 *Schematic representation of the evolution of lithium batteries over the years.*

Interface by Tarascon[16] marked the growth of LiBs over the years is represented pictorially in Figure 1.1. As can be observed from Figure 1.1, the first stage of research resulted in alternate and advanced electrode materials. The second stage of research is focused more on nanostructured materials and surface coatings to further enhance the performance and energy density of lithium batteries whereas the current research is on batteries to power electric vehicle, lithium rich materials, and lithium air technology.

1.4 Working Mechanism of Lithium Batteries

The reaction mechanism involves the reversible transfer of lithium ions between electrodes. At this juncture, it is essential to note the difference between lithium and LiB. The anode in the LiB is graphite, whereas in lithium batteries it is lithium metal. In short, the LiB does not employ any lithium metal as lithium batteries do. Thus, the difference in reaction mechanism is noted in the anodic site, as is shown in Equations 1.1 and 1.2.

In lithium battery $Li_{(metal)} \rightarrow Li^{+} + 1e^{-}$ (Equation 1.1)

In lithium-ion battery $6C + Li^{+} + 1e^{-} \rightarrow LiC_6$ (Equation 1.2)

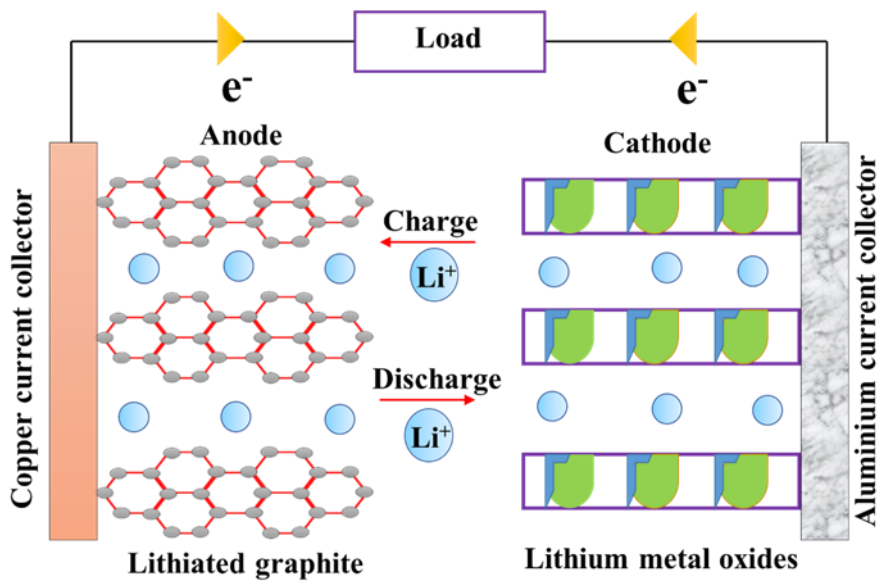

Figure 1.2 *Schematic representation of lithium-ion battery operation.*

The process of charging in the LiB involves the removal of lithium ions from the metal oxide (cathode) lattice, which on the other hand, can be viewed as the insertion of lithium-ion in the anode layers. The term discharge refers to the insertion of lithium ions into the cathode, which on the other hand, can be viewed as the removal of lithium ions from the

graphite lattice. Figure 1.2 represents the scheme of operation in the LiB. According to the rocking chair model, ion transfer occurs between the electrodes, whereas electron transfer happens through the external circuit. A selectively ion-conducting and electron-insulating membrane is used as separator and is placed between the electrodes in LiB. A detailed overview of the different constituents in the LiB and their development has been discussed in the following sections.

1.5 Anode Materials

In a lithium battery, lithium metal was traditionally used as the anode material due to its high energy density, yielding a theoretical capacity of 3860 mAh/g[11]. However, the use of lithium as the anode material had a major disadvantage of the undesirable formation of dendrite in lithium batteries.

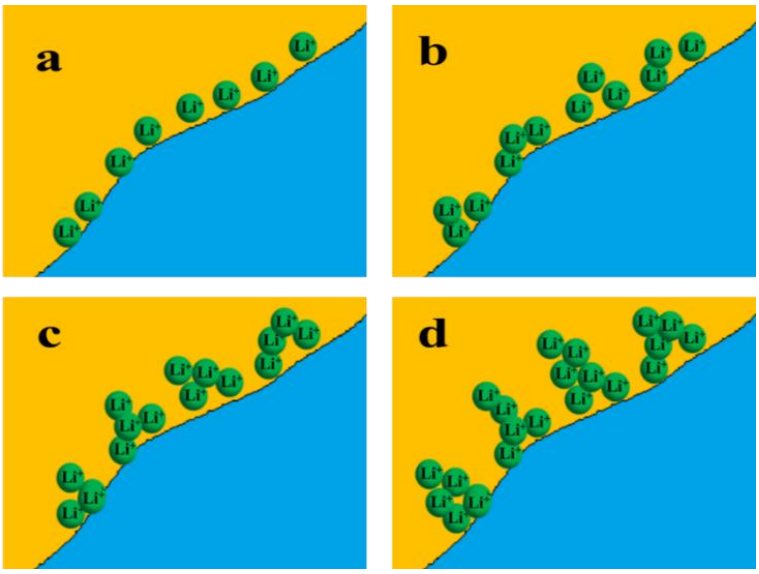

Figure 1.3 *Stepwise depiction of dendrite formation. From a–d, the deposition of lithium ions one over another in subsequent steps, which results in the spike-like deposition of lithium ions.*

Dendrite formation is the process of repeated deposition of lithium at a particular site, which creates spike-like structures over time, which in turn results in the puncturing of the separator in the batteries. Puncturing of separators creates severe threats to safety, such as the explosion of batteries. The stages involved in dendrite formation are shown in Figure 1.3. Dendrite-free deposition of lithium is being researched extensively[17–22]. Additionally,

battery technologies such as lithium air batteries and lithium sulfur batteries are promising if lithium metal is used as their anode material.

As mentioned earlier, LiB technology replaces lithium metal with carbon or other inorganic elements in order to avoid dendrite formation and to ensure safe batteries. In general, lithium storage happens in anode materials through three mechanisms, insertion, conversion, and alloying, as shown in Figure 1.4.

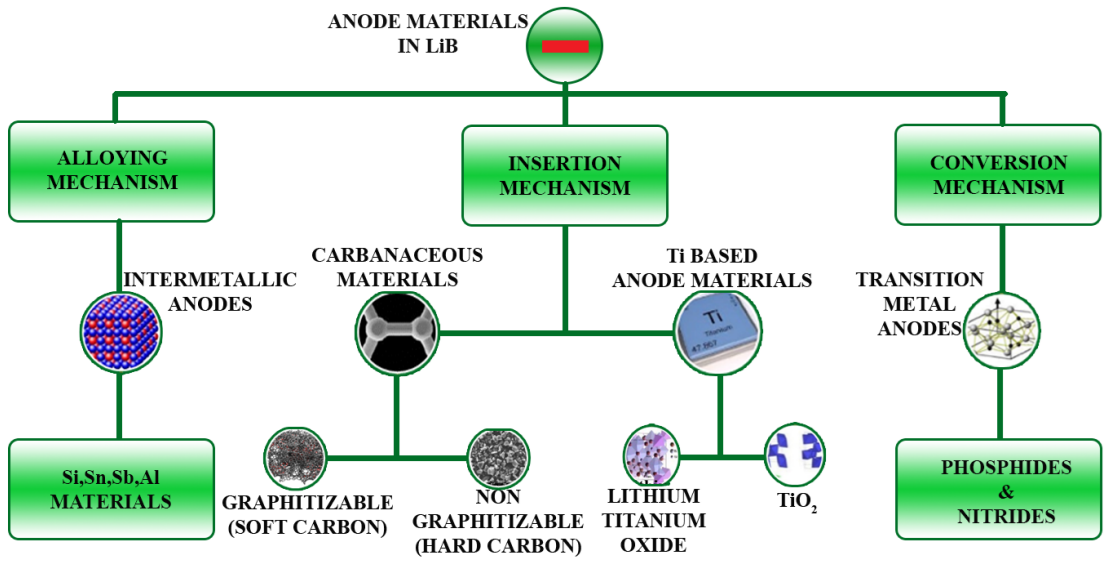

Figure 1.4 *Types of anodes used in lithium batteries*

1.5.1 Insertion Anodes

The insertion type of materials has layered structures in which lithium-ion is stored in between the layers. Insertion mechanisms are prevalent in LiB with carbonaceous and titanium-based anodes. Carbonaceous materials include hard (non-graphitized carbon) and soft (graphitized carbon) carbon, mesoporous carbon, carbon nanotubes, pitch-based carbon materials, carbon nanofibers, graphene, and artificial graphite materials[11]. Among all carbon materials that are used in LiB, graphitic carbon is the most commonly used commercial anode [23]. In the case of carbon materials, six carbon atoms provide the space to store one lithium ion as shown in Figure 1.5. The storage of one lithium-ion per six carbon atoms was seen as the reason for the low specific capacity of graphitic carbons in comparison with the conversion and alloying anodes[24]. The reversible mechanism of lithium storage found in these materials is as follows[11]:

$$C + xLi \rightarrow Li_xC \qquad \text{(Equation 1.3)}$$

The second-class of anodes, which follow the insertion mechanism, include titanium-based materials such as lithium titanium oxide and titanium dioxide. These materials have a potential of around 1.5 V versus Li/Li^+ and, hence, they do not have any of the lithium-plating issues that are seen in graphitic carbon materials[25] and are known as safe anode materials for LiB. Although layered materials have lower theoretical capacity than the conversion and alloying anodes, they possess good cycle life and capacity retention.

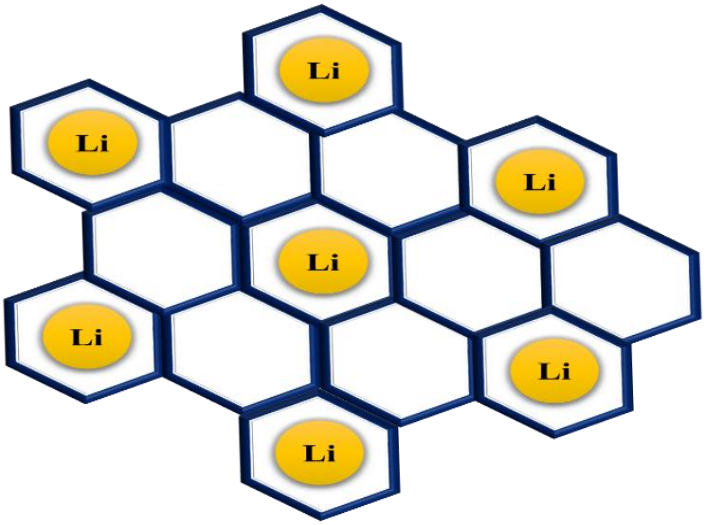

Figure 1.5 *Arrangement of lithium ions in graphitic layers*

1.5.2 Alloying Anodes

The second type of anodes is the intermetallic material, which follows the alloying mechanism for lithium storage. Materials such as silicon, tin, tin oxide, germanium and silicon dioxides, molybdenum oxide and the like follow the alloying mechanism for lithium storage[23]. These materials have good capacities in theory, but they have poor cycle life and capacity retention in comparison to the insertion type of anode materials. Alloying occurs through three different mechanisms, solid solution reactions, addition reactions, and displacement reactions[26].

In solid solution reaction as well as in addition mechanism, alloying of lithium ions with the metallic anodes occurs at the first place, as shown in Equation 1.4.

$$Li + xM \rightarrow Li_xM \qquad \text{(Equation 1.4)}$$

where M refers to an element or compound.

The further reaction steps are different in solid solution reactions and addition reactions. In a solid solution reaction, no phase change or structural change occurs when lithium enters the lattice[26]. It is a topotactic reaction, which can be seen during the reaction of lithium with magnesium and amorphous silicon materials[26]. In the case of an addition reaction, phase change occurs during alloying and, hence, the phase of M will be different from the parent compound, LiM_x. Crystalline materials such as silicon, aluminum, tin, and antimony follow this type of a reaction.

The type of third reaction is the displacement reaction, in which the active metal in the alloy participates in the reaction, as is shown in Equation 1.5.

$$Li + xMN_y \rightarrow LiM_x + xyN \qquad \text{(Equation 1.5)}$$

where MN_y is an alloy compound in which M actively participates in the reaction N is inactive.

In some cases, N can be active, and the reaction in N turns irreversible after the first cycle. In such cases, the reaction follows the addition or the solid solution reaction after the first cycle [26].

The third type of materials is the conversion-type of anode materials. These anode materials are reported to be promising for electric vehicles due to their high theoretical capacity. However, the conversion type of anode materials suffers from serious cyclability issues. The process of nanostructuring is believed to help conversion anodes in better cyclability [23]. The most commonly used types are metal oxides and phosphides. The general mechanism of lithium storage is as follows [23,27]:

$$M_xO_y + 2yLi^+ + 2ye^- \rightarrow xM^0 + yLi_2O \text{ (M is a transition metal)} \qquad \text{(Equation 1.6)}$$

Though insertion anodes are prevalent in the literature, conversion and alloying anodes for electric vehicle applications show greater potential due to their high capacity and rate capability.

1.6 Cathode materials

Cathode materials in LiB serve as the main source of lithium ions. The ideal cathode material in an LiB is expected to have the following characteristics[11]:

- High free energy of reaction with lithium;

- Reversible incorporation of a good number of lithium ions;
- Reversible structural changes for lithium incorporation but not structural damage.
- Good lithium-ion diffusivity;
- Good electronic conductivity;
- Capacity to be inert with electrolyte solution; and
- Possession of economically viable synthesis routes.

Goodenough et al., popularly known as the father of lithium-ion cathodes[28], made a significant contribution to the cathodes materials that are used in lithium batteries[15,29,30]. The common cathode materials that are used in LiB are lithium metal oxides in which lithium can reversibly move in the crystal lattices. Figure 1.6 and Figure 1.7 represent the different frameworks and structures of the cathode materials that are used in LiB.

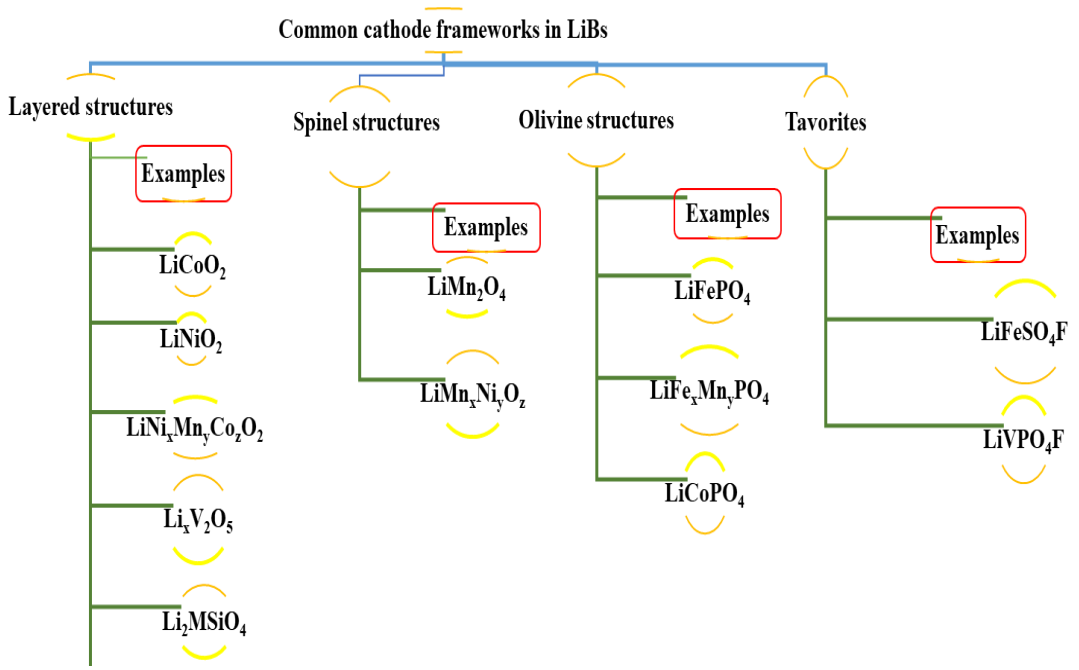

Figure 1.6 *Schematic illustration of the existing cathode materials in lithium batteries*

Table 1.1 presents an outline of the capacity, theoretical potentials, and the stages of development of the most commonly used cathode materials in LiB. The first class were the cathode materials that had layered structures, which were introduced in the early 1980s[15]. Materials such as lithium cobalt oxides ($LiCoO_2$), lithium nickel oxides ($LiNiO_2$), and lithium vanadium oxides ($Li_xV_2O_5$) are typical examples of layered cathode materials.

$LiCoO_2$ is the first known cathode material[15] for LiB, which also served as a significant commercial cathode. The good electrical conductivity of this cathode material in addition to its high open circuit voltage secured a notable place for it among the other newly developed cathode materials in LiB. Though the theoretical capacity of $LiCoO_2$ is 274mAh/g, the practical capacity is around 140 mAh/g, which means that only 50 percent of lithium can be reversibly extracted from this system without any undesired side reactions[31–35]. Excess lithium extraction ($Li_{1-x}CoO_2$, x>0.5) creates irreversible structural changes, and as a result, extraction of lithium to the extent of its theoretical capacity is not widely preferrred[36]. The extent of lithium extraction from $LiCoO_2$ can be controlled by its charging potential[36].

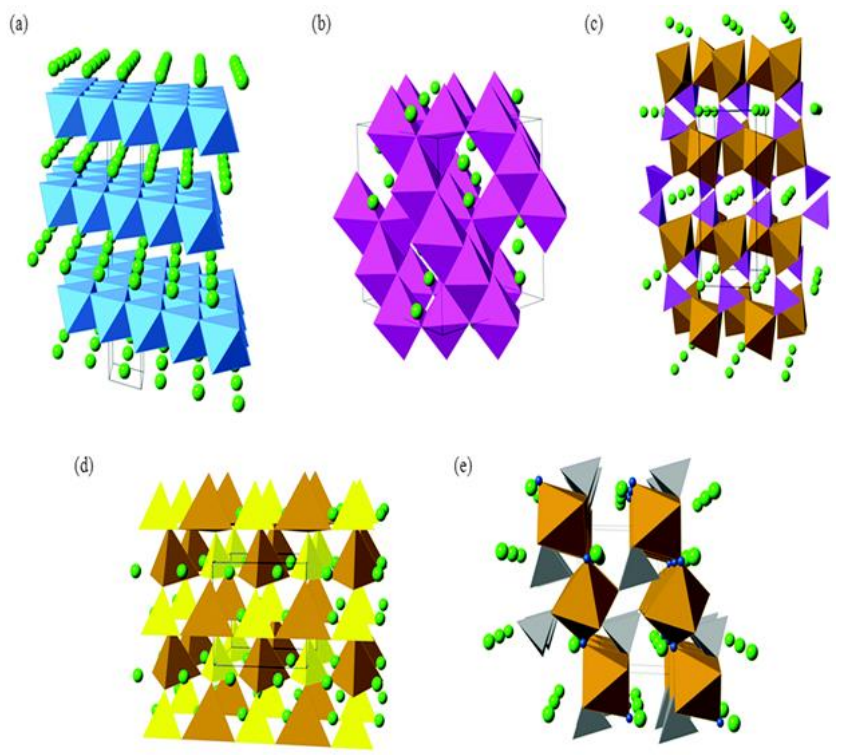

Figure 1.7 *Crystal structures of common cathode frameworks in LiB: (a) $LiCoO_2$ (layered), (b) $LiMn_2O_4$ (spinel), (c) $LiFePO_4$ (olivine), and (d) $LiFeSO_4F$ (tavorite). Reproduced with permission from Royal Society of Chemistry (2014)*[37].

On the other hand delithiated $LiCoO_2$ is thermally unstable when subjected to higher temperatures, which results in the evolution of oxygen from the crystal lattice, which then reacts with the electrolyte components and creates serious threats to safety in LiB[38,39]. The

cost of cobalt, toxicity, and safety issues limits this cathode material and paves way for further research in LiB[11].

$LiNiO_2$ is a layered cathode material that is studied mostly at the research level in LiB. Though the introduction of nickel in this system created a better cell voltage than that in $LiCoO_2$[40], the difficulties in synthesis and the Jahn Teller distortions that are associated with nickel added serious drawbacks and prevented the use of this cathode material at a commercial scale[41].

Table 1.1 *Electrochemical potentials and theoretical capacity of various cathode materials used in LiB* [40,42].

S.No.	Cathode material	Capacity (mAh/g)		Open circuit potential (OCV) (vs. Li/Li^+)	Level of development
		Theoretical	Practical		
1.	$LiCoO_2$	274	140	3.8	Commercialized
2.	$LiMn_2O_4$	148	120	4.1	Commercialized
3.	$LiNiO_2$	275	150	3.8	Research
4.	$LiFePO_4$	170	165	3.4	Commercialized
5.	$LiCoPO_4$	167	125	4.2	Research
6.	$LiNi_{0.33}Mn_{0.33}Co_{0.33}O_2$	280	160	3.7	Commercialized
7.	$LiNi_xMn_yAl_zO_2$	279	199	3.7	Commercialized
8.	$LiFeSO_4F$	151	120	3.7	Research
9.	$LiVPO_4F$	156	129	4.2	Research

$Li_xV_2O_5$ is also a layered cathode material that known for its high capacity as well as high rate applications. The advantages of $Li_xV_2O_5$ cathode materials over other cathodes is that they can store three lithium ions per unit formula; they can also be used in high rate applications[43]. Toxicity and poor cycle life prevents the widespread use of this material.

The second framework of cathodes that are studied in LiB includes spinel structures. Lithium manganese oxide ($LiMnO_2$) is the most common cathode material that is studied in this framework. This was the second most widely studied cathode material in 1984, after $LiCoO_2$[30]. The advantages of $LiMnO_2$ over layered $LiCoO_2$ cathodes are i) low cost; ii) better safety features; and iii) high power rate. On the other hand, structural instabilities, lesser specific capacity, manganese dissolution, and poor cycle life were considered to be serious drawbacks. The poor cycle life that is reported is mainly due to manganese dissolution, which occurs as a result of Jahn Teller distortion[41,44]. Olivine type cathode materials form the third framework of cathodes, in which $LiFePO_4$ is the most widely studied material. $LiFePO_4$ was reported in 1996 by Padhi et al.[29] and is considered to be the safe cathode with an excellent cycle life. These properties set apart olivine cathode materials from other layered and spinel cathode materials. Their better structural stability is associated with the strong PO_4^- bonds that hold this structure firmly. However, the low electronic conductivity of $LiFePO_4$ was seen as a hindrance to the rate performance of this system[45]. Possible solutions includes addition/coating with carbon additives and doping of elements in crystal lattice, which could enhance the electrical conductivity of the system[46–49]. Such enhanced $LiFePO_4$ were taken to the commercial scale and were preferred in electric vehicles due to their safe nature and better capacity [50]. Further modification in olivine structures was carried out by replacing iron with cobalt and manganese ions for better voltage[51–54]. However, these materials were not as successful as $LiFePO_4$ due to the stable electrochemical performance and safety of the cathodes[54].

In addition, the current research focuses on the doping of metals such as nickel, manganese, and aluminum ions into existing cathode frameworks in order to acquire cathodes with high capacity and rate performances for electric vehicle applications. Although the doping ratio and the elements may vary, a brief account of these high-capacity materials will be discussed in this section. Lithium-rich layered materials such as $Li[Li,Mn,Ni,Co]O_2$, exist as solid solutions between layered $Li[Li_{1/3}Mn_{2/3}]O_2$ (commonly designated as Li_2MnO_3) and $LiMO_2$ (M = Ni, Co, Mn). These materials were studied in the literature for their high capacity of around 250mAh/g and their high operating voltages[27,55–57]. Irrespective of their high capacity and voltage, these materials suffer from irreversible capacity loss and their capacities fade over the cycles. Although oxide coatings and metal doping were regarded to be alternative pathways, at a commercial and bulk scale, such methods were not regarded to be viable solutions[58].

The most notable, commercialized, high-capacity cathode materials include lithium nickel manganese cobalt oxide (NMC) and lithium nickel cobalt aluminum oxide (NCA) cathodes[59]. NCA was examined in early 1999[59], in order to develop safe and high-capacity cathode materials. Irrespective of their potential options, this material had certain issues in synthesis procedures, cost of nickel, cobalt, and structural stability issues[40,60,61].

The most popular cathode material that can potentially replace $LiCoO_2$ is NMC ($LiNi_{0.33}Mn_{0.33}Co_{0.33}O_2$) [58]. The process of replacing involves the doping of nickel, cobalt, and traces of other elements into lithium manganese oxide structures in order to extract better properties through synergy. The first patent on this material was published in early 2001[59]. Since 2001 this material has had great research importance because it was claimed that this material was a better cathode material for electrical vehicle applications (EV); it had higher capacity, higher voltage, and better safety features[40,59].

From among recent cases, polyanion cathode materials of the tavorite framework, such as $LiFeSO_4F$, $LiVPO_4F$, and $LiBO_3$, are being researched extensively[62,63]. These materials operate on the concept of the increasing of energy density by the increasing of voltage. The addition of electronegative fluorine anion to the phosphate group is expected to increase the electronegativity and the voltage of the cathode material[62]. Although these materials were known for their specific capacity, voltage, better ionic, and electronic conductivities, they are currently being researched more keenly in order to achieve scalable synthesis and stable performances[42].

1.7 Electrolytes

Electrolytes play a major role in the transport of lithium ions between the electrodes. The ideal characteristics of an electrolyte solution are pictorially depicted in Figure 1.8. In addition, the electrolyte should be able to withstand adequate mechanical, thermal, and electric wear and tear [64].

The electrochemical potential window of an electrolyte is a significant parameter that directs its electrochemical performance. It is defined as the difference between the oxidation and the reduction potential of the electrolyte. In terms of quantum chemistry, the potential window is the difference between the Highest Occupying Molecular Orbital (HOMO) and the Lowest Unoccupied Molecular Orbital[58] (LUMO), as shown in Figure 1.9.

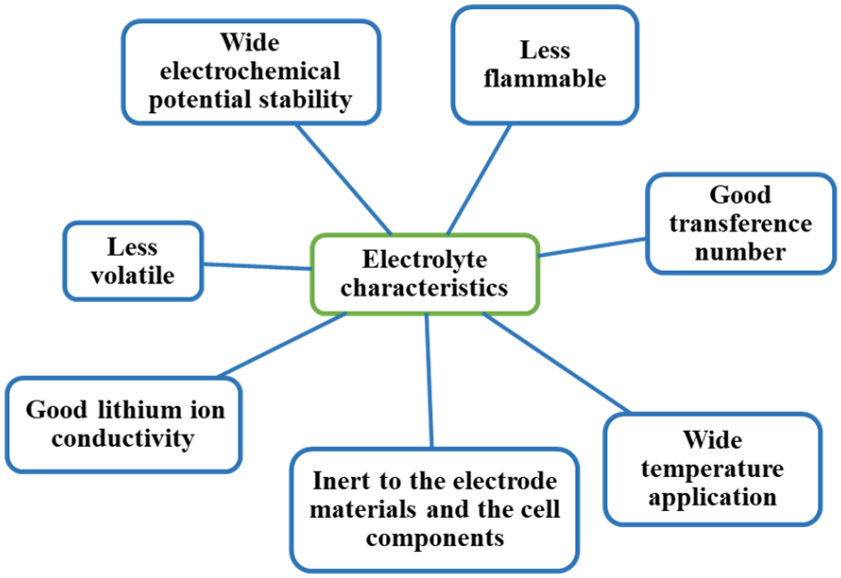

Figure 1.8 *Ideal characteristics of electrolytes in LiB*

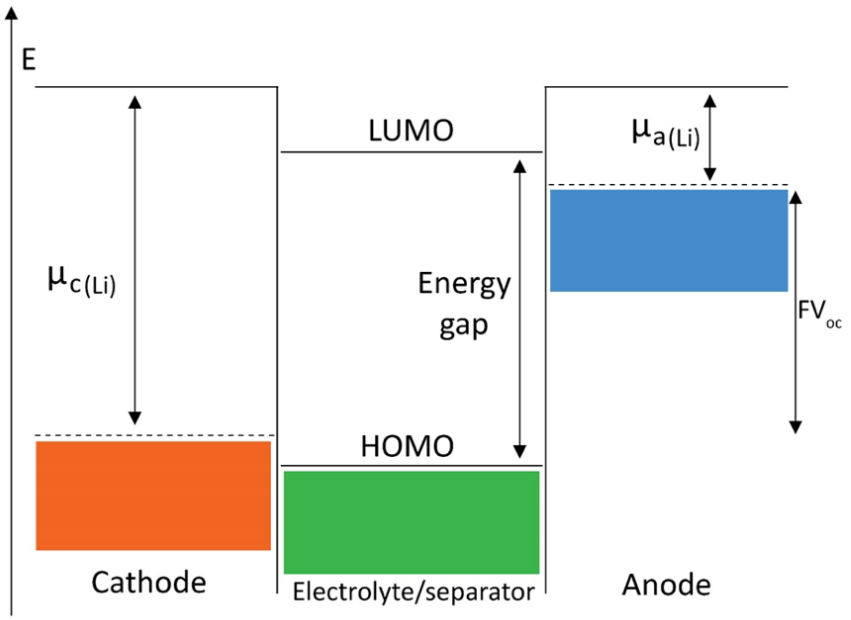

Figure 1.9 *Energy diagram of a lithium cell at an open circuit voltage condition, in which* $\mu_{a\,(Li)}$ *and* $\mu_{c(Li)}$ *point to the lithium chemical potential of the anode and the cathode, respectively*[58]**.**

The selection of the electrodes to be used depends on the potential window of the electrolyte. Ideally, the operating potential of the anode should be below the LUMO of the electrolyte, whereas the operating potential of the cathode should be above the HOMO of the electrolyte [58].It is always preferable to have wide potential window for the electrolyte especially in LiB. Generally, electrolytes in LiB exist in several forms, as is shown in Figure 1.10. Table 1.2 presents a short outline of the three types of electrolytes that are commonly used in LiBs.

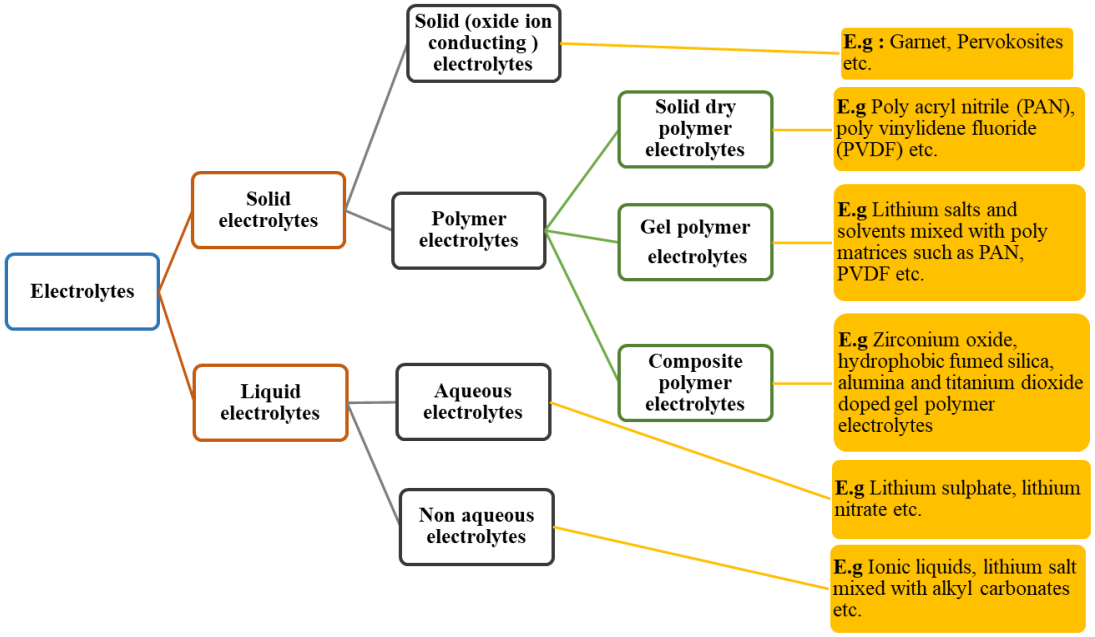

Figure 1.10 *Flow chart representing various types of electrolytes used in lithium batteries.*

1.7.1 Solid Electrolytes

Solid electrolytes are solid oxide ion conductors that help in the conducting of lithium ions[65]. In comparison to other metal ions, lithium ions are small enough to move between the interstitial lattice spaces; this helps in better ion transport in the system. Solid electrolytes are the safest electrolytes for lithium batteries even at high temperatures[65–67]. The solid electrolytes contribute to the safety of the batteries because they are leakproof and they can withstand dendrite formation[65,66].

The most commonly studied solid electrolytes are lithium halides, lithium super ionic conductors $Li_{2+x}(Al_{1+x}Ti_{1-x})(PO_4)_3$ (LISCON), garnets ($Li_7La_{2.75}Ca_{0.25}Zr_{1.75}Nb_{0.25}O_{12}$),

perovskites, lithium hydrides, argyrodites, and lithium phosphorous oxy-nitride

Table 1.2 *Outline of the different types of electrolytes in a lithium battery. Reproduced with permission from Chapman and Hall publications*[68].

Property	**Electrolyte Type and Characteristics**		
	Polymer	Liquid	Solid
Matrix	Flexible	Mobile	Fixed
Position of ion sites	Changes as chains flex	None	Fixed; accessibility affected by temperature
Solution	Yes	Yes	Not usually
Solvation	By matrix: roll-on mechanism	Forms mobile solvated ions	No
Concentration of solute	Usually high	Often low	Usually does not apply
Participation of charged ion clusters	Often yes	Usually no, except in molten salts	No
Contribution from migration of neutral species	Important	Usually unimportant	No
High cationic transference number	Usually no	Usually yes	Often unity for cation conductors

compounds (LIPON)[69]. Water-solvated amorphous glass electrolytes are the less expensive solid electrolytes that are commonly seen in supercapacitors and fuel cells but are not very common in LiBs[65]. In these electrolytes, the water ion is solvated by the existing amorphous glass solid ion.

In addition, the limiting factor that reduces the applicability of solid electrolytes in wide commercial use is their wettability with the electrodes and low ionic conductivity in comparison to existing commercial liquid electrolytes[65,70,71].

1.7.1.1 Polymer electrolytes

Polymer electrolytes are the subclass of solid electrolytes in which polymer membranes of appreciable ionic conductivity are regarded as being the medium of ion transport[72]. Further, the polymer can exists as solid dry polymer electrolytes, gel polymer electrolytes, and composite polymer electrolytes[70].

Dry polymer electrolytes are a mixture of lithium salts and polymers such as poly ethylene oxide (PEO), poly acrylonitrile (PAN), polyvinylidene fluoride (PVDF), poly vinylidene fluoride-hexafluoropropylene (PVDF-HFP), and poly vinyl chloride (PVC)[73]. Although these electrolytes have demonstrated notable performance, their cycle life is poor due to low ionic conductivity and wettability.

Gel polymer electrolytes are the second class of polymer electrolytes that covers the cohesive properties of solid electrolytes and the diffusive nature of liquids[70]. They provide better contact to the electrodes in comparison to other classes of solid electrolytes. These gel polymer electrolytes have a polymeric matrix that serves as a template. The polymer matrix is mixed with suitable salts, solvents, and gelation additives in which chemical or physical crosslinking is expected to form the gel polymer electrolyte. A gelled solution is identified at a point in which the mixture does not show any flow in the vessel in which it is contained [70].

The third class of polymer electrolytes includes composite polymer electrolytes in which electrochemically inert fillers such as zirconium oxide (ZrO_2), hydrophobic fumed silica, alumina (Al_2O_3), and titanium dioxide (TiO_2) are incorporated in the polymer matrix in order to enhance the ionic conductivity, mechanical strength and interfacial stability [48,49]. The gel polymer as well as the composite polymer electrolytes is regarded as being a better alternative to conventional liquid electrolytes for safe and flexible batteries.

1.7.2 Liquid Electrolytes

When compared to the solid electrolytes, liquid electrolytes usually have a simple preparation process, which involves the mixing of a lithium salt with a mixture of solvents. The general criteria for selecting salts and solvents for LiB are as follows,

- ***Salt***
  - ✓ *Good disassociation power*

- ✓ *High mobility for solvated ions*
- ✓ *Good electrochemical stability*
- ✓ *No side reaction in the operating environment (example : corrosion)*
- ✓ *Low vapor pressures*

➢ ***Solvent***

- ✓ *Low melting and high boiling point*
- ✓ *High dielectric constant*
- ✓ *Electrochemically stable in the operating potential window*
- ✓ *Economic*

Although non-aqueous electrolytes are not common in LiB, recent studies[75–77] demonstrate the appreciable role of aqueous electrolytes in LiB. In this context, both aqueous and non-aqueous the appreciable role of aqueous electrolytes in LiB. In this context, both aqueous and non-aqueous electrolytes are discussed briefly in the following sections.

1.7.2.1 Aqueous Electrolytes

The concept of aqueous electrolytes in lithium batteries was first proposed by Dahn et al. in 1994[75]. The first aqueous liquid battery had bronze phase vanadium dioxide and $LiMn_2O_4$ as the electrodes, and 5M $LiNO_3$ salt as the electrolyte.

Although the first prototype demonstrated significant performance, their cycle life was limited due to the side reactions between the electrode - electrolyte interface[77].

The major aspects of the poor cycle life were the dissolution of the electrode materials in the electrolyte as well as the intercalation of the H^+ ions from the electrolyte to the electrode materials[78,79].

Further research by Dahn et al.[75] has produced better electrodes and electrolyte composition for aqueous electrolytes, as shown in Table 1.3[77]. These aqueous batteries provide better energy density than the existing lead-acid and nickel-cadmium batteries[77]. In addition, they are a better choice in LiB when safety and cost are the major factors for consideration.

Table 1.3 *Review of the work carried out in aqueous electrolytes along with the respective electrodes. Reproduced with permission from Elsevier publication*[77].

Cathode	Anode	Electrolyte	Capacity retention (%) (per cycles)	Current density (mA g^{-1})	Capacity (mA h g^{-1})	Ref.
$LiFePO_4$	$LiTi_2(PO_4)_3$	Li_2SO_4 (1 M)	90% (1000)	6.0 C	55	80
$LiFePO_4$/C	VO_2	$LiNO_3$ (Saturated)	94% (50)	C/3	106	81
$LiFePO_4$/C	LiV_3O_8	$LiNO_3$ (9 M)	99% (100)	10 C	90	82
$LiFePO_4$	Activated carbon	Li_2SO_4 (0.5 M)	63% (10)	5 C	124	83
$LiFePO_4$	Activated carbon	Li_2SO_4 (0.5 M)	45%	20 C	58	84
$LiMn_2O_4$	VO_2	$LiNO_3$ (Saturated)	83% (42)	0.2 C	120	85
$LiMn_2O_4$	Activated carbon	Li_2SO_4 (0.5 M)	93% (10,000)	90 C	118	86
$LiMn_2O_4$	TiP_2O_7	$LiNO_3$ (5 M)	85% (10)	0.2 C	42	87
$LiMn_2O_4$	Activated carbon	Li_2SO_4 (0.5 M)	99% (200)	4.5 C	110	88
$LiMn_2O_4$	Activated carbon	Li_2SO_4 (0.5 M)	94% (1200)	4.5 C	110	89
$LiMn_2O_4$	$Li_xV_2O_5$–Ppy	$LiNO_3$ (5 M)	82% (60)	0.2 C	40	90
$LiCoO_2$	Ppy	Li_2SO_4 (Saturated)	63% (120)	0.1 C	104	91
$LiMn_{0.05}Ni_{0.05}Fe_{0.9}PO_4$	$LiTi_2(PO_4)_3$	Li_2SO_4 (Saturated)	53% (50)	0.2 C	87	92

1.7.2.2 Non-Aqueous Liquid Electrolytes

Non-aqueous liquid mixtures are generally a mixture of lithium salts and organic solvents. The most commonly used organic solvents are alkyl carbonate solvents such as ethylene carbonate (EC), diethyl carbonate (DEC), propylene carbonate (PC), dimethyl carbonate (DMC), and ethyl methyl carbonate (EMC)[64]. A variety of salts such as lithium hexaflurophosphate ($LiPF_6$), Lithium tetrafluroborate ($LiBF_4$), Lithium hexafluoroarsenate ($LiAsF_6$), Lithium perchlorate ($LiClO_4$), Lithium trifluoromethanesulphonate (LiTFS) and, Lithium bis(trifluoromethanesulfonyl)imide (LiTFSI) have been studied in the literature. The comparison of the ionic mobility of these salts aligns with the following order:

$LiBF_4$ > $LiClO_4$ > $LiPF_6$ > $LiAsF_6$ > LiTFS> LiTFSI,

whereas, the dissociation constant aligns with the following order:

LiTFS < $LiBF_4$ < $LiClO_4$ < $LiPF_6$ < $LiAsF_6$ < LiTFSI [64].

In spite of the various available salts, the most commonly preferred salt for the commercial LiB electrolyte was $LiPF_6$. The balanced properties of ionic mobility, dissociation constant, and the passive film formation on aluminum current collector rendered $LiPF_6$ the most favorable choice[64,93]. In the case of the solvents, ethylene carbonate was regarded as being a unreplaceable ingredient because of its ability to form better solid electrolyte interface with commonly used commercial graphite anodes[64]. On the other hand, the melting point of ethylene carbonate above room temperatures requires the addition of a suitable linear carbonate solvent in order to lower the freezing point in the electrolyte mixture.

Further, the lower boiling point of the linear carbonates introduces thermal instability to the electrolytes at above room temperatures[64]. As a result, steps were taken to increase the thermal stability of the electrolytes by adding various additives[94–96]. Although additives such as 1,3-benzoldioxole, vinylene carbonate (VC), tetra(ethylene glycol) and dimethyl ether were added in the electrolytes to increase the thermal stability in the early days, recently, ionic liquids are reported as additives and as electrolyte ingredients to impart better thermal stability in the electrolytes[97,98]. Detailed information about ionic liquids will be presented in the following subsection.

1.7.2.2.1 Ionic Liquids

Ionic liquids are generally salts that melt at temperatures that are less than the boiling point of water [99,100]. The application of ionic liquids to electrochemistry was much welcomed, considering the earlier contribution of molten salts[101]. Molten salts generally melt at high temperatures (> 200 ºC). They were used as electrolytes in molten salt batteries in the early 1940s[102]. As an electrolyte, ionic liquids have better properties such as high ionic conductivity and long shelf life[102]. Irrespective of the difference in properties and debates on whether ionic liquids can be the subset of molten salts, they have bigger advantages as standalone electrolytes. The first ionic liquid reported in the literature[103] by Gabriel et al. was ethanolammonium nitrate, with a melting point of 52–55 ºC. Similar to every other salt, ionic liquids have an organic cation (large asymmetric) and an inorganic anion (comparatively small). These ions are held together by weak van der Waals forces. As a result of this size difference, they have negligible vapor pressure, which results in better thermal stability[99].

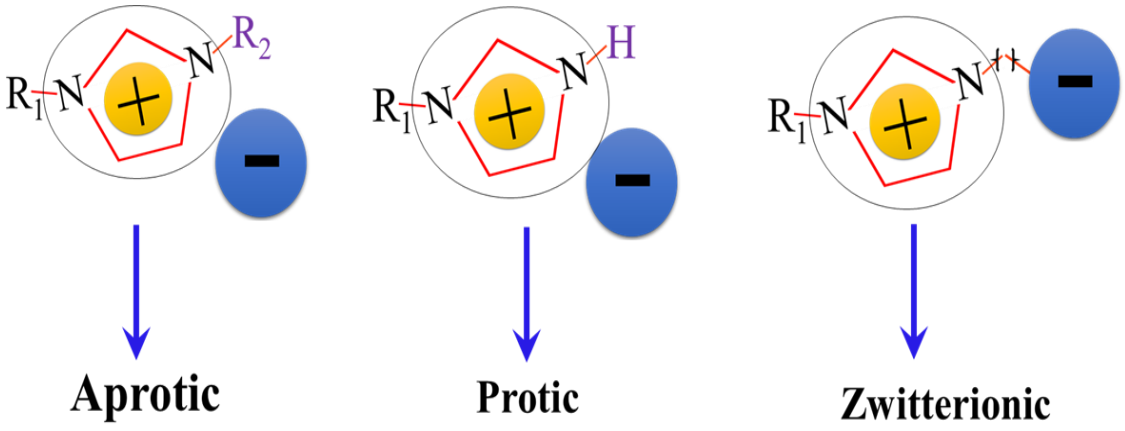

Figure 1.11 *Different classes of ionic liquids based on their compositions*

Ionic liquids can be completely tailored by choosing the cations and anions of interest. They mostly have an organic cation and an inorganic anion which are asymmetric and are held together by strong electrostatic interactions. Typical properties such as hydrophobicity, hydrophilicity, and viscosity can be tuned by a combination of suitable cations and anions[104]. Hence, on the basis of composition, there exist three classes of ionic liquids namely protic, aprotic, and zwitter-ionic liquids as shown in Figure 1.11.

As the name indicates, protic ionic liquids have a labile proton, which differentiates them from other subclasses of ionic liquids. Their formation involves the transfer of proton from a Bronsted acid to a Bronsted base, as shown in Equation 1.7. They have non-negligible vapor pressures, inexpensive synthesis process, and are distillable [105,106]. In the electrochemical domain, protic ionic liquids find applications in fuel cells[107].

Bronsted base (B) + Bronsted acid (A) → *Protic Ionic liquid* + A^- (Equation 1.7)

Aprotic ionic liquids differ from the protic ionic liquid due to the presence of an alkyl substituent instead of the proton in the cation structure. Aprotic ionic liquids have low melting points due to the inefficient packing of the cation and anion[108]. In the electrochemical domain, these ionic liquids find application in lithium batteries and super capacitors[107].

Zwitter-ionic liquids are formed by the tethering of the anion and the cation, which prevents the migration of ions under an electric field. In the electrochemical domain, these ionic liquids help to form membrane-based electrolytes for electrochemical systems[107].

RTILs contribute to a variety of applications. In chemical industries, they play a significant role in extraction[109–111], biosensors [112], photovoltaic cells [113], carbon dioxide reduction, and as lubricants[114]. In electrochemical devices, they act as safe electrolytes in rechargeable batteries (lithium, sodium, magnesium, and aluminum), catalysis, fuel cells, and photo electrochemical cells [107,115,116]. Ionic liquids as electrolytes in lithium batteries are discussed in detail in the literature review in section 1.10.

1.7.3 Additives

Additives are generally organic or inorganic substances that are added in *trace amounts* (not more than five per cent) to enhance battery performance[117]. Properties such as corrosion inhibition, solid electrolyte interface (SEI) formation, ionic conductivity and thermal stability can be enhanced by the additives. The brief outline on the common roles of the additives are discussed as follows,

1. *SEI enhancing Additives*

Several reducing agents such as sulfur dioxide, carbon disulfide and other sulfites were added to assist the SEI formation, through the adsorption of their reduced product on the catalytic active sites of graphite[117]. Polymerizable additives are also added in some cases to react with the solvent molecules in

the electrolyte to form a preliminary SEI layer on the surface of the graphite. The most common additives are VC and fluroethylene carbonate (FEC), which were generally preferred for better SEI and cycling properties even at lower temperatures.

2. Cathode protectors

These additives perform several functions to protect the cathode from the undesired side reactions either by forming a surface layer on the cathode or by acting as a scavenger to water and other acidic impurities in the system. It is reported that water is formed inevitably during charging on the surface of the cathode due to the oxidation of the solvents by the oxygen gas released from the cathodes[118].

3. Corrosion Inhibitors

Several salts such as Lithium bis(oxalato)borate and Lithium difluoro(oxalato)borate were reported for their ability to passivate the aluminium current collector when added around five mole percent. It was reported that the passivation layer is formed due to the reaction between the salt anion with the aluminum ions.

4. Overcharge protectors

Overcharging is a serious safety concern and additives helping to overcome overcharging are of two types namely, 1) shuttle additives and 2) shutdown additives. Shuttle additives prevent overcharging by forming redox products at slightly higher-potentials. Shutdown additives polymerize at high-potentials on the surface of the cathode to isolate the cathode from overcharging. Shutdown additives permanently stop the battery operation whereas the shuttle additives help the battery to resume operation after overcharging conditions.

In addition, additives can also act as fire retarders, wetting agents, and viscosity diluters[117].

1.8 Other Constituents in LiB

1.8.1 Current Collectors

The electrolyte, as well as the electrodes, form the major components in LiBs. In addition, the battery also has other miscellaneous components such as current collectors, binders, separators, and additives, which also contributes to the performance.

The current collectors are the conducting metallic films on which the electrodes are coated. They are solely electron collectors, which collect and transfer the electrons from the electrodes to and from the external circuit. The following properties are to be considered while choosing a current collector for LiBs.

- *Stability:* It is important that the current collector should remain stable at the operating electrochemical potential as well as the temperature.
- *Compatibility*: The active electrode material, conductive additives, and binders are coated on the current collectors. It is required that the current collector should be compatible to those materials to have better electrode coatings. Further, the current collector should also be compatible to the electrolyte used in the battery.
- *Weight*: The weight of the current collector will have a negative impact on the energy density of the battery as they add dead weight to the battery. As a result, thin metal foils are preferred for current collectors in LiBs.
- *Cost:* As the current collectors carry the electrode materials, long foils of current collectors are used in LiBs. In such cases, the cost of the current collector will have a significant impact on the total cost of the LiBs. They should be inexpensive.

Considering the above properties, the possible current collectors[119] that were studied for LiB applications are shown in Figure 1.12.

However, commercial LiBs use copper as current collector for anodes and aluminum as the current collector for cathodes. Aluminum is not stable at potentials below 3 V vs. Li/Li^+ whereas copper is not stable at potentials above 3.4 V vs. Li/Li^+[120,121]. Although the current collector is expected to play similar role irrespective of the cathode and anode, the electrochemical potential stability mandates the need to use different current collectors for the anode and cathode in LiB.

In addition, the most favorable property of aluminum current collectors is their better resistance to oxidation at higher potentials due to the passive film that is formed with the help of the PF_6^- anion in the electrolyte[122]. A detailed overview on the passive film formation on aluminum current collectors will be discussed in Chapter 5.

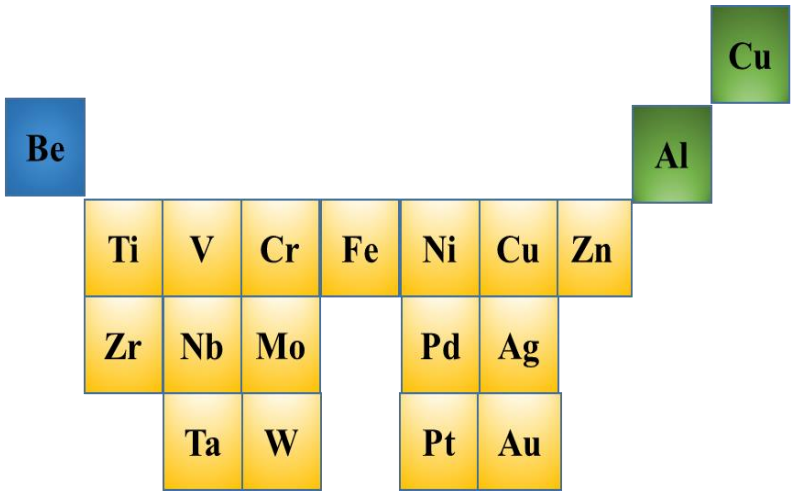

Figure 1.12 *Elements studied as current collectors in LiBs.*

1.8.2 Separators

A separator is a thin porous insulating membrane that that provides ideal separation between the electrodes. The ideal qualities that are expected from the separators are shown in Figure 1.13. Polymer materials such as polyethylene, polyethylene terephthalate, and polyvinyl fluorides are commonly used separators. In the case of polymer electrolytes, these polymers are mixed with lithium salts, and the cast membrane or gel can be used as a matrix to act both as an electrolyte and a separator. In general, LiB in mobile electronics applications use microporous separators that have a thickness of less than 25µm, whereas in HEV/EV applications, the thickness may be 40 µm in order to prevent cell punctures[123]. Typically, the separator should be moderately thick, because further increase in thickness will decrease the loading of the electrode material and vice versa[123].

In order to further analyze effectiveness of the separators, numbers such as the Macmullin number and the Gurley number are defined. The Macmullin number is the ratio of the resistivity of the separator with the electrolyte to the resistivity of the electrolyte. The Gurley number is defined in relation to air permeability and electrical resistivity for the given separator morphology[123]. These numbers should be low for better electrochemical performance[123].

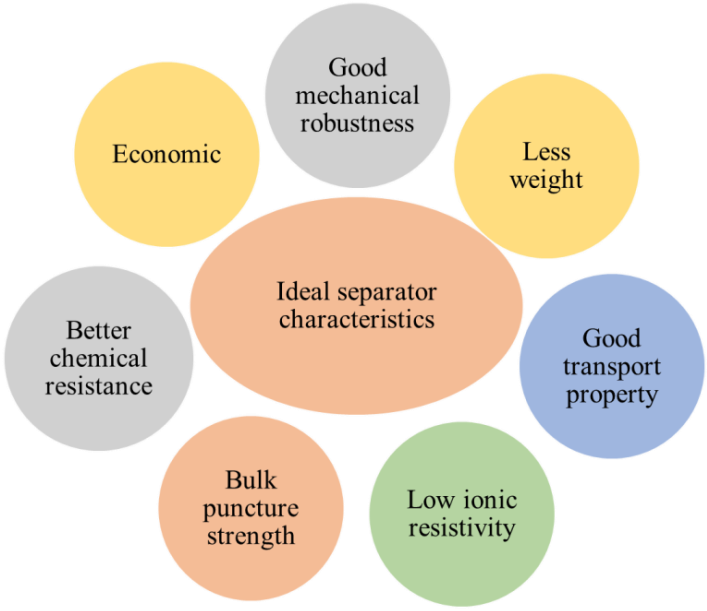

Figure 1.13 *Ideal characteristics of separators for LiB.*

1.8.3 Binders

Binders help in the better adhesion of the active electrode material to the current collector. Materials that can be used as binders include clay, SiO_2, MgO, kaolin, neoprene, latex, polytetrafluroethylene, potassium titanate, poly vinyldiene fluoride (PVDF), Polyvinyldiene fluoride copolymerised with hexaflurophosphate (PVDF-HFP), carboxy methyl cellulose (CMC), and poly (acrylic acid) (PAA)[11]. In the case of LiB, the commonly used binders are PVDF, PVDF-HFP, PAA, and CMC. The binders should be electrochemically inert and should be added in low quantities, because they contribute to dead weight in LiB. Efficient binders also help in stable electrochemical performance by maintaining proper adhesion with the current collectors[124].

1.9 SEI in LiBs

It is often expected that the SEI will be formed by the reaction between the anode surface and the electrolyte. In 1979, Peled et al.[125] proposed the formation of a surface film on alkali and alkaline earth metals that come into contact with non-aqueous electrolytes, which they termed as SEI. The film that is formed in this manner on the surface of the lithium metal exhibits the thickness of 20nm[126]. This film exhibits a distinct property of being electronically resistive while also being ionically conductive. It is expected that the electrolyte solvents will get reduced or decomposed and will form SEI on the surface. In

other words, the SEI can be regarded as the insoluble film that is formed as a result of the parasitic reactions between electrode surface and electrolyte solvents.

The film formation is instantaneous and happens in few milliseconds. The properties of the SEI absolutely depends on the electrolyte composition, nature of the electrode, the electrochemical potential, the temperature, and the applied current density in the system[126]. Although there are several unanswered questions, the models that are most commonly referred to and that explained the formation of SEI are 1) the Peled model, 2) the Mosaic model, and 3) the coulombic interaction model, as shown in Figure 1.14. The models are listed in the order in which they were reported.

In 1977, SEI was introduced by the Peled model[125,127], which explained that SEI is formed as a result of the preferential reduction of the components of the electrolyte. This reaction happens in steps and it is said to have Schottky defects for the lithium-ion to penetrate inside the surface.

In 1995, Kanamura et al. proposed the Mosaic model, which added further inputs to the Peled model and claimed that the SEI had a mosaic structure in which the surface layer was supposed to have several insoluble multiphase products in addition to the reduction products of electrolytes[128,129]. The movement of lithium-ion, according to this model, is through the boundary of the multiphase products[128,129].

In 1998, the Coulombic interaction model was proposed, which explained the ionic interaction between lithium and the electrode surface[130,131]. According to this model, lithium ions are considered to be the head and carbon, the foot, which forms a double layer-like structure on the interface. The formed layer, according to this model, is expected to have better adhesion than the earlier models. The major composition of the SEI is the lithium carbonate that is formed by the reaction of carbonate solvents with the lithium interface. Besides, the actual composition of the SEI is complicated and is often referred to as the Holy Grail of lithium batteries [16].

Irrespective of the SEI, the formation of dendrites still continues and prevents the practical applications of lithium batteries. The complexity of this film can be examined by various techniques such as atomic force microscopy (AFM), electrochemical impedance spectroscopy (EIS), x-ray photoelectron spectroscopy (XPS), electron microscopy, Fourier transform infra-red spectroscopy (FTIR), Raman spectroscopy, Atomic emission

spectroscopy (AES), and nuclear magnetic resonance (NMR) in ex situ as well as in situ modes [126]. The characteristic features of an ideal SEI film is as follows[126]:

- High lithium-ion conductivity;
- Good mechanical strength and flexibility; and
- Appropriate thickness and a compact structure.

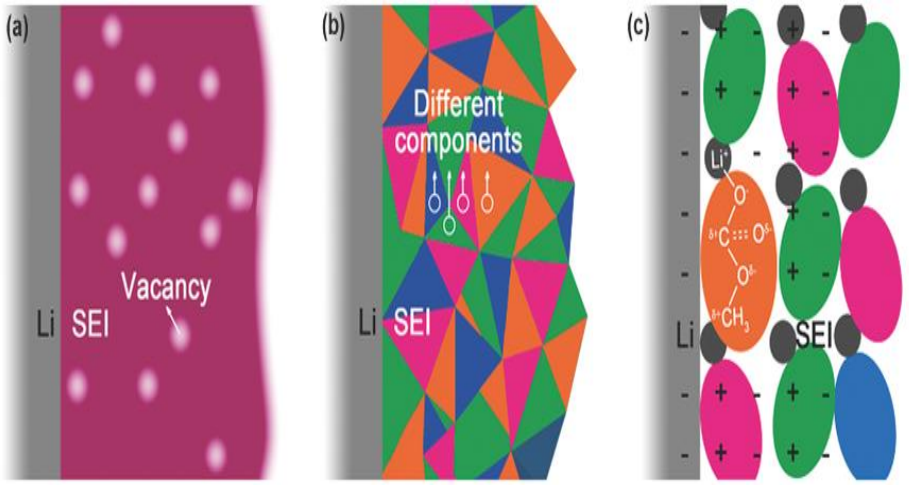

Figure 1.14 *Pictorial representation of SEI formation models a) Peled model, b) Mosaic model and c) Coulombic interaction model. Reproduced with permission from Wiley VCH publications*[126].

In the case of LiB, the phenomenon of SEI still exists in the anodes that operate below 1V versus. Li/Li^{+}[126]. The SEI that is formed in graphite is more stable than that formed in lithium metal, which favored the commercial LiB[16]. As mentioned earlier, the SEI that is formed on the lithium surface will not be same as that formed on the graphite anodes, because the nature of SEI will be directly dependent on the electrode under study. The extent of the selectivity of SEI can be understood from the variation in composition of SEI in different carbon allotropes.

In the case of graphite, the nature of SEI will differ from the basal to edge planes[25]. Lithium ions cannot enter through the basal planes because they are ionic insulators and will not contribute to the reversible capacity. On the contrary, reversible lithium-ion movement happens through the edge planes. This behavior complicates the understanding of the properties and the mechanism of SEI [25,132].

After graphite, the SEI on Si anodes were widely reported[133–135]. In addition to the carbonate species, the SEI in silicon is composed of silicon oxide and lithium silicates[133]. Thus, the electrode as well as the electrolyte composition plays a crucial role in determining the SEI and, thereby, the performance of lithium batteries.

1.10 Review of Literature

The research on ionic liquids as electrolyte components in lithium batteries increased due to their desirable properties such as thermal stability, flexibility in design, and wide electrochemical potential window. Since ionic liquids are composed completely of ions, their response to the electric filed will not similar to other organic solvents. Fedorov et al[136] states that the electrochemical performance of an electrode-RTIL interface is generally amplified by area when it is used for energy storage. The electrochemical double layer (EDL) of ionic liquids differs from that of the ordinary diluted electrolytes[136,137]. Endres et al[138] explains the solvation layers of ionic liquids have direct influence on the electrochemical reactions. Eftekhari et al.[101] described the various factors that are to be considered while using ionic liquids as electrolytes in lithium batteries. As a result, the following factors need to be considered[101].

1. *Choice of ionic liquid*

The use of RTILs as electrolytes in lithium batteries was reported in early 2000[97,139]. The RTILs were considered to be the safe electrolytes for lithium batteries due to their negligible vapor pressures[97,139]. Although, there exists a variety of ionic liquids, not all can be used as electrolytes for lithium batteries, because the following properties are expected in them prior to their being used:

1. *Wide electrochemical potential window (least 0.5–4.5V vs. Li/Li^+).*
2. *Good thermal stability.*
3. *Minimum viscosity and good ionic conductivity.*

As presented in Figure 1.15, a variety of ionic liquids was studied for energy applications. The most commonly studied cations for lithium battery applications are quaternary ammonium, pyrrolidinium, and phosphonium cations. The most commonly considered anion for lithium battery applications includes trifluoromethane sulphonylimide and fluorosulphonylimide[101,140]. In addition to these factors, the ease of pure synthesis is also a significant factor in choosing the ionic liquid for electrolyte applications. Although

imidazolium cations were less viscous and more conductive, the acidic C_2 protons and the double bonds in their structure limits their potential stability[141,142]. Quaternary ammonium salts have low ionic conductivity and high viscosity, which limits their application as lithium battery electrolytes[142]. The anodic stability of cations such as pyrrolidinium, piperidinium, and phosphonium are greater than 4 V versus Li/Li^+, and are widely preferred cations for lithium battery applications [140,142–144]. When compared to the piperidinium and phosphonium cations, pyrrolidinium cations are said to have lower viscosities and better thermal stabilities [142,143,145]. The cathodic potential stability of anions such as bis(trifluoromethanesulfonyl) imide and fluorosulfonylimide is less than 1V versus Li/Li^+ and, hence, are widely preferred anions in lithium batteries[142,146]. As a result, in this current study, the ionic liquids of interest are those with pyrrolidinium cations and bis(trifluoromethanesulfonyl)imide / fluoro sulfonyl imide anions.

2. <u>Operating temperature</u>

The operating temperature of LiBs is a significant factor which decides the temperature of operation of the battery powered devices. Due to various factors, the permissible charging temperature range of LiBs is from 0 ^oC to 45 ^oC whereas the discharging temperature is from -20 ^oC to 60 ^oC[147]. The most commonly reported reasons for the limited high temperature operation is the volatility of the organic solvents used in the battery electrolytes whereas, the limited low temperature performance is due to the slow lithium ion diffusion and the low ionic conductivity of the electrolyte. On the other hand, lithium plating is observed on the graphite electrodes cycled at low temperatures. As a result, intense research is dedicated to optimize the electrolyte formulation and choice of the electrodes which can ease the wide temperature operation of LiBs. In order to extend the operation at higher temperatures, additives such as ionic liquids and phosphamides were added to improve the thermal stability of the electrolytes[148,149]. On the contrary, electrolyte formulations for low temperature operations involves the addition of various organic solvents which can lower the freezing point of the electrolytes. The various available patents which describe the low temperature operation of LiBs are listed in Table 1.4. Further, Zhang et al.[150] reports the influence of charge transfer resistance in the low temperature operation of LiBs. It was believed that the slow kinetics of battery reactions is the major limitation to poor low temperature performance[150]. Ji et al. [151], reported that increasing the salt concentration in the electrolyte beyond 1.2 M may substantially the

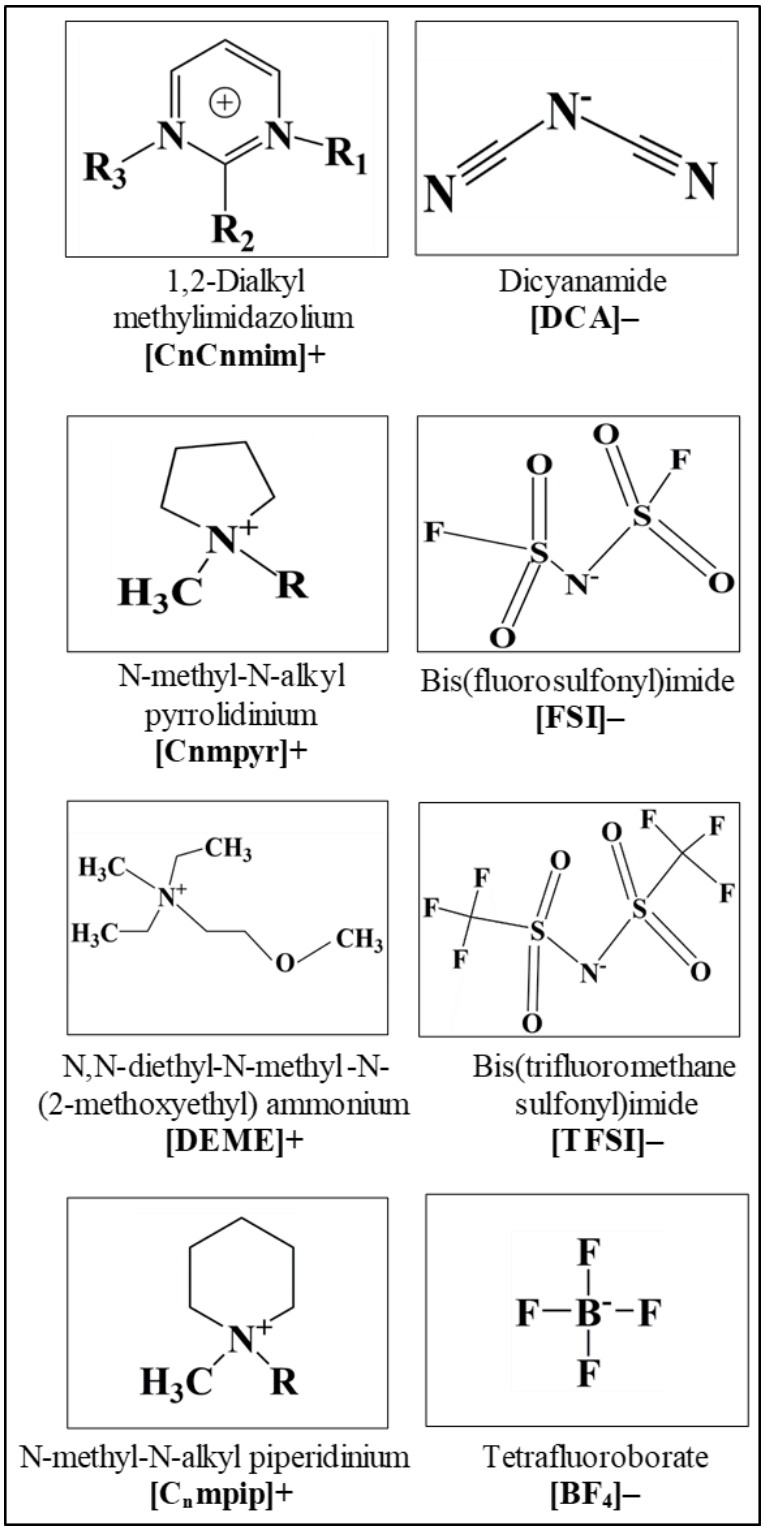

Figure 1.15 *Common anions and cations in ionic liquids used for energy applications and their corresponding acronyms. In this figure, "R" refers to ethyl, propyl, and butyl groups, and "n" refers to the number of carbons in the alkyl substituents.*

discharge capacity at room temperatures. Hence, lithium ion diffusion as well as electrolyte conductivity are equally important in optimizing the electrolytes for subzero temperature operations.

3. Wide potential window

The potential stability of ionic liquids is an important factor while considering electrolytes in lithium batteries[101,140]. Since lithium batteries operate in a wide potential window, the ionic liquids of choice are expected to have extreme oxidation and reduction potentials.

4. Thermal stability

Thermal stability is an attractive property in the choice between ionic liquids as electrolytesfor lithium batteries in which safety is a main concern. Researchers had been using ionic liquids as additives to enhance the thermal stability of electrolytes[96,152,153]. The thermal stability of ionic liquids also enabled the operation of batteries above room temperatures[143,154–156]. However, FSI (fluorosulfonylimide) anions were commonly reported for thermal instabilities, in comparison with other anions in ionic liquids[157,158]. The reason for the thermal instability can be ascribed to the weaker sulfur-fluorine bond in the FSI anion[145]. On the other hand, the better stability of the TFSI (trifluromethanesulphonylimide) anion can be ascribed to the carbon-sulfur bond in the TFSI anion[145]. Nonetheless, the better stability of N-methyl-N-propyl pyrrolidinium bis(trifluoromethanesulfonyl)imide over describes the role of the anion in the thermal stability of the ionic liquid[145].

5. Viscosity and ion diffusion

Ionic liquids are known for their relatively high viscosity in comparison to conventional electrolytes [136,159,160]. The viscosity was not seen as a concern when ILs were used as electrolytes in high-temperature batteries. However, viscosity of the electrolytes need to be taken into account when the performance is expected to be at room temperatures or below room temperatures. Although reports have shown that viscosity does not greatly slow down ion diffusion, which is contrary to expectation[101], the ionic liquids exhibit better diffusion-controlled properties and have diffusion coefficients in the order of 10^{-7} cm^2/s[101]. Apart from the diffusion properties, the wettability of the electrolytes was also seen as the indirect effect of the viscosity of the electrolyte. The wettability of the separator helps to

Table 1.4 *Patent literatures on the electrolyte formulations for subzero temperature operation of LiBs.*

S.No.	Patent Claim & Details	Battery Performance Details
1.	Electrolyte is a mixture of 0.8 ~ 1.5 M $LiPF_6$ and a mixed solvent composed of the following components in weight percent of the composition: 20 % – 40 % of EC, 5% – 30% of EMC, 30 % – 50 % of the methyl acetate MA, 0.5 % – 5 % of VC. *Patent Assignee:* Nanchang University *Patent number*[161]: CN103107364	The electrolyte can operate at –40 °C is initially allowed to stand for 16 ~ 24 h. Battery is cycled at C/20 rate. Relative capacity at –40 °C is 55 % whereas at –20 ^{o}C, the relative capacity is 90 %.
2.	Electrolyte is a mixture of $LiClO_4$, secondary lithium salt, organic solvents, and additives from group A or group B. *Secondary salts*: $LiPF_6$, $LiBF_4$, LiTFSI, LiTFS, lithium difluoro oxalate borate (LiFOB), and anhydrous lithium iodide. *Organic solvents*: Cyclic ester, linear esters, ethers, mixed solvents, and sulfones. *Additives Group A*: Benzoic acid, phenylacetic acid, benzoic anhydride, phthalic anhydride, isophthalic anhydride, and terephthalic acid anhydride. *Group B*: 2,6-di-tert-butyl-4-methyl phenol and butylhydroxyanisole. *Patent Assignee:* Zhangjiagang Guotai Huarong Chemical Industry New Materials Limited Company. *Patent number*[162]: CN103378360.	Lithium-MnO_2 cell measurements were carried out –20 ^{o}C in various electrolyte composition yielded an average relative capacity of 45%.

3.	One of the salt in the group is mixed with one of the solvents in group A and group B. *Salt:* $LiPF_6$, Lithium tetrafluoroborate ($LiBF_4$), Lithium hexafluoroarsenate ($LiAsF_6$), $LiCl_4$, lithium triflate ($LiN(SO_2CF_3)_2$, and a lithium perfluoro-sulfonate. *Solvent group A*: EC, PC, DEC, DMC, and EMC. *Solvent group B*: 3-methoxypropionitrile, 3-ethoxypropionitrile, methoxy acetonitrile, ethoxyacetonitrle, 2-acetoxyisobutyronitrile, 2-cyanoisopropyl methyl carbonate, 2-acetoxyacetonitrile, 2-cetoxyisopropionitrile, cyanomethyl methyl carbonate, and 1-cyanoethyl methyl carbonate. *PatentAssignee:* Policell Technologies. *Patent number*[163]: US2005123835.	Cells made from carbon anode and $LiCoO_2$ cathode in various compositions yielded an average relative capacity of 61 %. at –30 ºC.
4.	Electrolyte is a mixture of $LiPF_6$ salt, one of the organic solvent and one of the additive as mentioned below, *Organic solvents:* γ- butyrolactone, EMC and ethyl acetate. *Additives:* Ethylene glycol and dimethyl ether (molar ratio of ethylene glycol dimethyl ether is 1: 3 to 4.). *Patent Assignee:* Ningbo Weike Battery Co., Ltd. *Patent number*[164]: CN103779605.	$LiFePO_4$ cathode is tested at various temperatures such as 30ºC, –10 ºC, –25 ºC yielded 92 %, 89%, 84% capacity retention, respectively.

5.	Electrolyte is a mixture of LiFSI salt, PC and non-cyclic carbonate as mentioned below, *Non-cyclic carbonates:* EMC, DMC, Methyl butyrate (MB), and VC. *Patent Assignee:* Johnson Controls Technology Company, California Institute Of Technology. *Patent number*[165]: US 2016149263.	Graphite as well as LTO anodes and NMC cathodes were tested at temperatures –30 to 30 ^{o}C. The capacity retention at 20 ^{o}C, –20 ^{o}C, –25 ^{o}C, –30 ^{o}C are 100 %, 73 %, 69.4 %, and 64%, respectively.
6.	Electrolyte is a mixture of lithium salts $LiPF_6$ and $LiBF_4$ in a mass ratio of 3: 1 or 4: 1, one or more than one cyclic carbonate, linear carbonate and linear carboxylate as mentioned below, *Cyclic carbonates:* EC and PC *Linear carbonates:* DMC, DEC and EMC. *Linear carboxylates:* Methyl acetate (MA), ethyl acetate (EA), ethyl propionate (EP), ethyl butyrate (EB) and propyl acetate (PA) *Patent Assignee:* Huzhou Chuangya Power Battery Materials *Patent number*[166]: CN103078136.	The ionic conductivities of various additive added compositions used in this patent range from 0.87-1.37 mS/cm at –40 ^{0}C whereas, the 18650 battery performance was tested at –20°C yielded the maximum relative capacity of 84%.
7.	A quaternary mixed electrolyte is preferred wherein the solvent system contained only organic carbonates. In particular, the preferred solvent mixture was EC:DMC:EMC:DEC, in which EC is in the range of about 10 to 50 %, DMC is in the range of about 5 to 75 %, EMC is in the range of about 5 to 50 % and DEC is in the range of about 3 to 45%, by volume. *PatentAssignee:* Wilson Greatbatch Ltd. *Patent number*[167]: US6153338.	$LiCoO_2$/graphite cells tested with various claimed electrolyte compositions showed fairly better cyclic efficiency at –20 ^{o}C.

8.	The Electrolyte is a mixture of lithium salt, a non-aqueous solvent, 25 % ester based ionic liquid and additives. *Lithium salts :* $LiBF_4$, $LiPF_6$, LiTFSI, $LiClO_4$, and lithium bis (oxalate) borate salt. *Non-aqueous solvents:* EC, DMC, DEC, EMC, PC, VC butylene carbonate, ethylene sulfite, propylene sulfite, dimethyl sulfite, diethyl sulfite, ethyl acetate, methyl formate, methyl acetate, butyrate methyl, ethyl butyrate, methyl propionate, ethyl propionate, isopropyl acetate, isoamyl acetate, 1,3-propane sultone or 1,4-butane sultone. *Ionic liquid:* methyl acetate functionalized imidazolium ionic liquid *Additives:* Fluorine-containing carbonate, organic boride, sulfones organics, N, N-dimethyl-trifluoromethyl acetamide, vinylene carbonate, 1 3-propylene sulfite. *Patent Assignee:* Institute of Process Engineering - Chinese Academy of Sciences *Patent number*[168]: CN103151558.	Lithium manganese oxide, lithium cobalt oxide cathode and graphite anodes were tested in various formulations as described in the claim by charging at room temperature and discharging at low temperatures. The average relative capacity obtained is 60 % at – 40ºC.
9.	Electrolyte is a mixture of lithium salt; an organic solvent; 4-nitrophenyl 2-(trimethylsilyl) ethyl carbonate and an additive. *Additives:* LiBOB, caesium nitrate ($CsNO_3$), and 1,4-butane sultone. *Patent Assignee:* Original Assignee Johnson Controls Technology Co Wildcat Discovery Technologies Inc. *Patent number*[169]: US9466857B1.	Lithium metal oxide cathodes and graphite/silicon/oxide based anodes were studied for area specific impedances and battery performances in various claimed electrolyte compositions at –25 ºC.

10.	Electrolyte is a mixture of $LiPF_6$, $LiBF_4$ salts (1−2 M), organic solvents, and non-ionic organic additives as mentioned below, *Organic solvents :* EC, DMC, and EMC. *Non-ionic organic additives:* LiDFOB, LiBOB, lithium fluorododecaborate ($Li_2B_{12}H_xF_{12-x}$(x=0−3)), and LiTFSI, N,N-diethylamino trimethylsilane, 2,5-dihydrofuran, ethylmethyl sulfone, fluoroethylene carbonate, gamma-butyrolactone, monomer of polyethylene oxide, monomer of polyvinylidine fluoride. *PatentAssignee:* Envia Systems, Inc. *Patent number*[170]: US2013157147	Lithium metal oxide cathodes were tested with graphite and silicon anodes. The relative capacity at −30 ^oC and −40 ^oC are 40 % and 25 %, respectively.

keep the electrodes in good contact with the electrolytes, which, in turn help to increase the cycle life of batteries[171]. As a result, the wettability of the electrolyte is an essential parameter for the electrolyte[123]. In order to reduce the viscosity effects and to increase the wettability of an ionic liquid at room temperatures, the addition of organic solvents was considered to be useful because it reduced the viscosity of the electrolytes[172]. Recent studies about neat ionic liquids and mixtures with organic solvents have shown comparable capacities when compared with conventional electrolytes. In short, low viscosity ionic liquids will not greatly affect the specific capacities[101,142,149,160].

6. Lithium-ion solvation and SEI formation

In a lithium battery electrolyte, the solvation of lithium ions plays a critical role. In general, the lithium cation needs to be solvated by the solvent molecules. The solvated lithium ions will then move further toward the anode. At the anode, only the lithium ions need to intercalate inside the anodic layers. As a result, the solvated ion sheath breaks, allowing the lithium ions to move further inside the anode. On the other hand, the broken-down solvent molecules form the SEI layer on the anode surface. The schematic view of this process is shown in Figure 1.16. For the reasons mentioned above, this lithium solvation

is a factor in deciding the nature of the SEI film, which further defines the performance of the battery[130,173,174].

Thus far, in the literature, there has been no mention of lithium-containing ionic liquids of the kind that has been mentioned above. As a result, it is conventional to add lithium salt to the ionic liquid in lithium battery applications[101]. In such a case, lithium solvation is dominated more by the anion in the lithium salt or the ionic liquid anion[115,175–177] and the formation of SEI directly influences the anions in the system. As a result, the SEI in this section individually addresses the cases with different anodes (lithium /graphite/ silicon anodes), cations, and anions in the ionic liquid. In the case of lithium metal batteries, the SEI from ionic liquids is much appreciated because it creates the potential for the realization of high energy density lithium batteries. Basile et al.[176], studied the role of the [C_1mpyr][FSI] ionic liquid in a stable SEI formation with lithium for 1000 cycles in a Li/$LiFePO_4$ system. Howlett et al. and Sakaebe et al. reported effective SEI formation in lithium metal with ionic liquids of pyrrolidinium cations and TFSI anions[177,178]. As reported by Howlett et al. in [C_3mpyr][TFSI], the SEI is composed mostly of the reduction species of both the anion and the cation, in which the reduction products of the cation are seen trapped in the structure of the anion [177]. In addition, several other studies also suggest that the SEI that is formed along with the ionic liquids that are based on TFSI and FSI anions helps in effective passivation reaction[97,146].

In the case of graphite anodes, lithium solvation plays a major role because lithium ions have to intercalate between the graphite layers. It is expected that the solvation layers formed using ionic liquid anions break off and only lithium ions intercalate in the system[107]. In contrary, it was observed in the case of imidazolium and quaternary ammonium cations that the process of co-intercalation of the cation occurs with lithium-ion, which results in damage to the graphite structure, thereby degrading the performance of the cell[159,179]. As a result, imidazolium and quaternary cations were not widely preferred for LiB.

Despite the current research, there exists no commercial LiB with an ionic liquid as its electrolyte ingredient. Ionic liquids are expected to have moderate viscosity, ionic conductivity, and better SEI formation abilities in order to act as effective electrolyte ingredients in a lithium battery[159,172]. As a result, the phenomenon of hybrid electrolyte

(HE) combination was examined by researchers in order to improve the properties of electrolytes without compromising the inherent thermal stability[149,154,159,160].

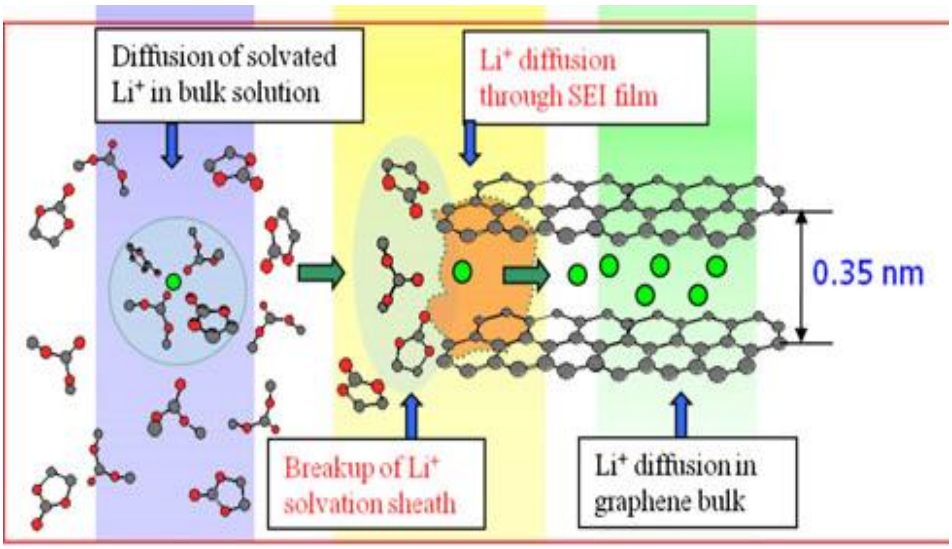

Figure 1.16 *Schematic view of solvated lithium ions and their role in SEI formation. Reproduced with permission from MRS*[180].

Allion et al.[172] reported the influence of the addition of organic solvents to ionic liquids, which decreases their viscosity and increases the ionic conductivity. Subsequently, Guerfi et al.[149,154] studied various proportions of ionic liquids and organic carbonate mixtures as electrolytes for lithium batteries. At that juncture, research was more focused on the optimizing of the proportion of the ionic liquid in the electrolyte mixture in order to achieve a better compromise between the electrolyte properties, which would result in performances that were comparable to conventional alkyl carbonate electrolytes.

The major expectation from this concept of HE is to formulate a safe electrolyte that performs better. In order to do so, the proportion of ionic liquid and conventional electrolyte in the HE mixture needs to be chosen carefully. In other words, balanced properties can be achieved in the HE by optimizing the proportion of ionic liquids. Although an increase in proportion of the ionic liquid increases the thermal stability, it will contribute to the increase in the viscosity of the electrolyte and vice versa. This phenomenon resembles the see-saw approach that is shown in Figure 1.17.

Kuhnel et al.[181] varied the proportion of the ionic liquid, N-butyl-N-methylpyrrolidinium bis(trifluoromethanesulfonyl)imide in propylene carbonate and examined the flammability

and physiochemical properties of the electrolyte. It was reported that the addition of propylene carbonate to the ionic liquids decreases the viscosity, extends the cathodic potential window, and lowers aluminum corrosion.

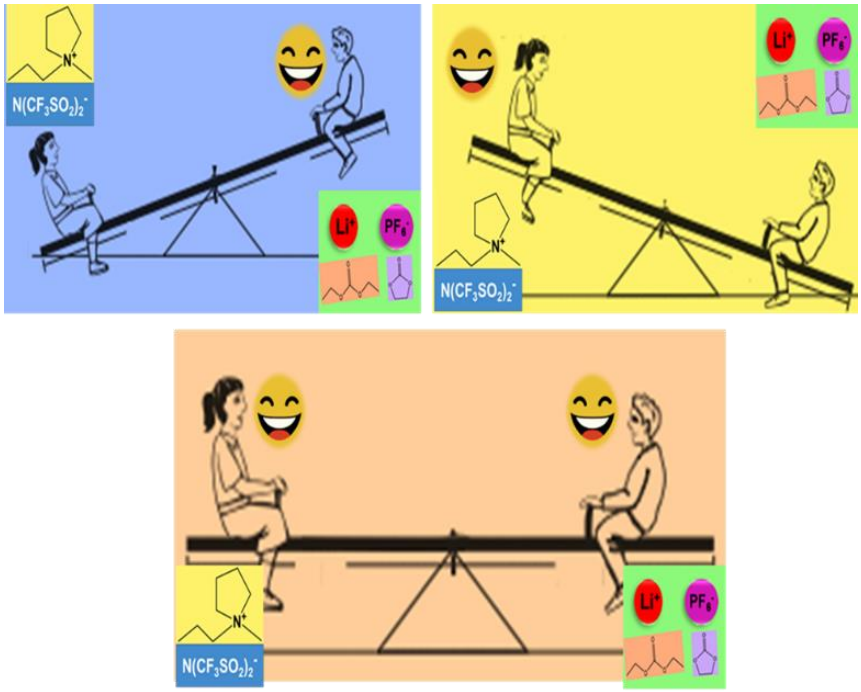

Figure 1.17 *The see-saw approach explains the need to have an optimized proportion of ionic liquid and alkyl carbonates.*

Quinzeni et al.[182] studied the various proportions of N-methoxy ethyl-N-methyl-N-propylpyrrolidinium bis(trifluoromethanesulfonyl)imide in LiTFSI : EC:DEC mixtures in order to achieve good hermal properties, potential window, anodic stabilities, and performance.

Further, several other works were carried out in [C_4mpyr][TFSI] and [C_3mpyr][TFSI] ionic liquids, which supports the fact that the hybrid combination containing 40 per cent of ionic liquids has better physicochemical and thermal properties[183,184]. Aguilera et al.[183] performed theoretical calculations as well as experimental studies on various proportions of ionic liquids in alkyl carbonate electrolyte mixtures. The findings reveal that the TFSI anions participate in lithium solvation when the proportion of ionic liquid in the solution is higher (>= 50%). As a result, the present study is carried out with an optimized proportion of 40 per cent of ionic liquid in the HE mixture.

1.11 Objective of the Current Work

The aim of the current work is to carry forward the initial studies about HE to realize its potential in the commercial market. As a result, studies were executed to validate the applicability of these HE in commercial LiB. In order to validate these electrolyte systems to commercial LiB, several factors need to be considered, as can be observed from Figure 1.18.

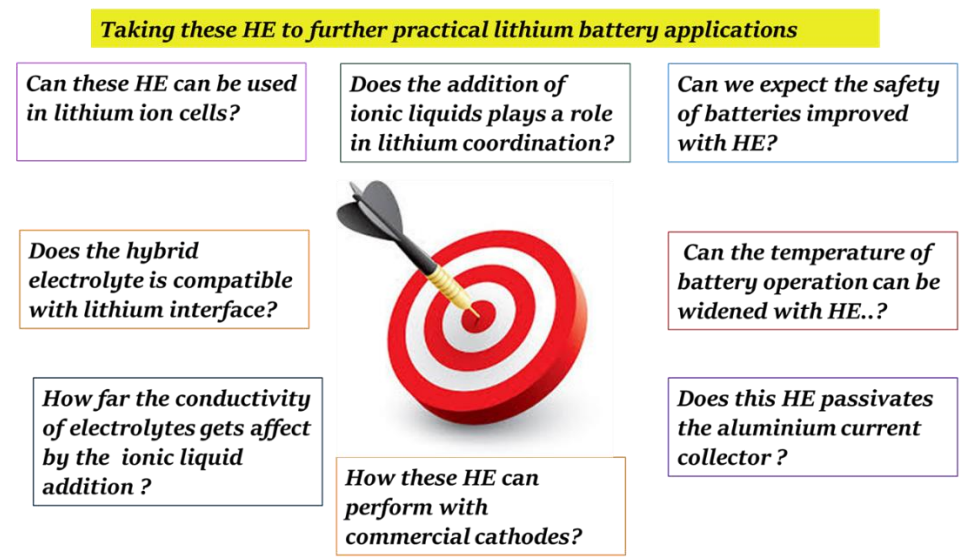

Figure 1.18 *Pictorial representation of the objectives of the current work.*

The framework here involves the development of a better understanding about the HE at an optimum composition. Initial studies about the physicochemical properties and electrochemical characterization of the HE are undertaken. Further, they are studied with commercial cathode materials in order to investigate the electrode-electrolyte compatibility. HE will also be studied in lithium-ion configuration. Further, it is important to identify the temperature window of the operation for the HE and this has been investigated here. In order to propose these electrolytes for high-potential applications, the stability of the cathodic current collector (aluminum) at high potentials is also studied in this work.

1.12 Outline of the Thesis

The focus of this thesis is the HE that is based on pyrrolidinium cation and bis(trifluoro methanesulfonyl)imide anion. It includes five chapters, and the chapters were ordered to

represent a stepwise understanding on the application of HE for lithium and lithium-ion batteries.

Chapter one presents an introduction to energy storage systems and the evolution of lithium batteries. It outlines the components in lithium batteries and lists the possible choices and criteria for the selection of the material of interest. The second part of this chapter reviews the literatures. Further, the motivation and scope of this current work is also discussed in the chapter.

Chapter two describes the physicochemical studies that were carried out in order to enable an initial understanding of this hybrid composition. Electrochemical studies and lithium solvation studies were performed in order to gain a clear understanding of the SEI. The thermal stability of the electrolytes was tested in this chapter.

Chapter three describes the next stage of studies about commercial cathodes. In this chapter, $LiCoO_2$ was tested with HE in the standard potential cutoff. Initial studies reveal a performance of the HE that is comparable to conventional electrolytes. The presence of ionic liquids in the present study motivated the extending of lithium extraction in $LiCoO_2$. As a result, research was carried out to study the performance at an extended potential cutoff (4.4V vs. Li/Li^+). In addition to the performance studies at extended potentials, the mechanism of the same has been explained in the chapter.

Chapter four describes the progress of the studies of a lithium-ion cell that contained $LiFePO_4$ and $Li_4Ti_5O_{12}$ anodes. Initial studies were carried out to check the compatibility of HE in the $LiFePO_4$ cathodes. The striking observation was the negligible iron dissolution from $LiFePO_4$ cathodes in HE when compared to the conventional electrolytes. In a lithium-ion cell, the cyclic performance was studied for 200 cycles with appreciable cyclic stability. Further, we optimized a special electrolyte composition by using ionic liquids in order to operate batteries at subzero temperatures. The subzero performances of those electrolytes were tested in lithium-ion cells with $LiFePO_4$ and $Li_4Ti_5O_{12}$ at −30 ^oC.

Chapter five discusses the possible applications of these HE in high-potential cathodes by investigating the compatibility of aluminum current collectors in high energy density applications. In this study, the corrosion of aluminum was tested against the conventional electrolyte and neat ionic liquids. Additionally, the ability to form a passivating film on

aluminum surfaces, the mechanism of film formation, and nature of the film were analyzed in detail in this chapter.

1.13 References

(1) Global Energy Statistical Yearbook 2017 https://yearbook.enerdata.net/ (accessed May 22, 2017).

(2) Crawley, G. M. *Fossil Fuels : Current Status and Future Directions*.

(3) Earth's CO_2 Home Page https://www.co2.earth/ (accessed May 22, 2017).

(4) Eshetu, G. G.; Grugeon, S.; Gachot, G.; Mathiron, D.; Armand, M.; Laruelle, S. LiFSI vs. $LiPF_6$ Electrolytes in Contact with Lithiated Graphite: Comparing Thermal Stabilities and Identification of Specific SEI-Reinforcing Additives. *Electrochim. Acta* **2013**, *102*, 133–141.

(5) Kowalski, K. M. *Alternative Energy Sources*; Marshall Cavendish Benchmark, 2010.

(6) Smith College Museum of Ancient Inventions: Baghdad Battery https://www.smith.edu/hsc/museum/ancient_inventions/battery2.html (accessed May 22, 2017).

(7) Early History of Electricity and Magnetism https://pwg.gsfc.nasa.gov/Electric/-E14-history.htm (accessed May 22, 2017).

(8) Alessandro Volta discovered methane, invented first electrochemical cell https://www.worldofchemicals.com/171/chemistry-articles/alessandro-volta-discoverer-of-methane.html (accessed May 22, 2017).

(9) Dell, R.; Rand, D. A. J. (David A. J. *Understanding Batteries*; Royal Society of Chemistry, 2001.

(10) Scrosati, B. History of Lithium Batteries. *J. Solid State Electrochem.* **2011**, *15*, 1623–1630.

(11) Linden, D.; Reddy, T. B. *HandBook of Batteries*; McGraw-Hill, Ed.; Third Edit.; 2002.

(12) Wikipedia. Alkaline batteries https://en.wikipedia.org/wiki/Alkaline_battery (acce

ssed Jul 18, 2017).

(13) Wikipedia. History of Batteries https://en.wikipedia.org/wiki/History_of_the_battery (accessed Jul 18, 2017).

(14) Whittingham, M. S. Electrical Energy Storage and Intercalation Chemistry. *Science (80-.).* **1976**, *192*.

(15) Mizushima, K.; Jones, P. C.; Wiseman, P. J.; Goodenough, J. B. LixCoO2 (0 < X <-1): A New Cathode Material for Batteries of High Energy Density. *Mater. Res. Bull.* **1980**, *15*, 783–789.

(16) Tarascon, J. M. The Li-Ion Battery: 25 Years of Exciting and Enriching Experiences. *Interface Mag.* **2016**, *25*, 79–83.

(17) Ding, F.; Xu, W.; Graff, G. L.; Zhang, J.; Sushko, M. L.; Chen, X.; Shao, Y.; Engelhard, M. H.; Nie, Z.; Xiao, J.; et al. Dendrite-Free Lithium Deposition via Self-Healing Electrostatic Shield Mechanism. *J. Am. Chem. Soc.* **2013**, *135*, 4450–4456.

(18) Yan, K.; Lee, H.-W.; Gao, T.; Zheng, G.; Yao, H.; Wang, H.; Lu, Z.; Zhou, Y.; Liang, Z.; Liu, Z.; et al. Ultrathin Two-Dimensional Atomic Crystals as Stable Interfacial Layer for Improvement of Lithium Metal Anode. *Nano Lett.* **2014**, *14*, 6016–6022.

(19) Pei, A.; Zheng, G.; Shi, F.; Li, Y.; Cui, Y. Nanoscale Nucleation and Growth of Electrodeposited Lithium Metal. *Nano Lett.* **2017**, *17*, 1132–1139.

(20) Wu, B.; Ren, Y.; Mu, D.; Liu, X.; Yang, G.; Wu, F. Effect of Lithium Carbonate Precipitates on the Electrochemical Cycling Stability of $LiCoO_2$ Cathodes at a High Voltage. *RSC Adv.* **2014**, *4*, 10196–10203.

(21) Zeng, X.-X.; Yin, Y.-X.; Li, N.-W.; Du, W.-C.; Guo, Y.-G.; Wan, L.-J. Reshaping Lithium Plating/Stripping Behavior via Bifunctional Polymer Electrolyte for Room-Temperature Solid Li Metal Batteries. *J. Am. Chem. Soc.* **2016**, *138*, 15825–15828.

(22) Zhang, Y.; Qian, J.; Xu, W.; Russell, S. M.; Chen, X.; Nasybulin, E.; Bhattacharya, P.; Engelhard, M. H.; Mei, D.; Cao, R.; et al. Dendrite-Free Lithium Deposition with Self-Aligned Nanorod Structure. *Nano Lett.* **2014**, *14*, 6889–6896.

(23) Goriparti, S.; Miele, E.; De Angelis, F.; Di Fabrizio, E.; Proietti Zaccaria, R.;

Capiglia, C. Review on Recent Progress of Nanostructured Anode Materials for Li-Ion Batteries. *J. Power Sources* **2014**, *257*, 421–443.

(24) Kaskhedikar, N. A.; Maier, J. Lithium Storage in Carbon Nanostructures. *Adv. Mater.* **2009**, *21*, 2664–2680.

(25) An, S. J.; Li, J.; Daniel, C.; Mohanty, D.; Nagpure, S.; Wood, D. L. The State of Understanding of the Lithium-Ion-Battery Graphite Solid Electrolyte Interphase (SEI) and Its Relationship to Formation Cycling. *Carbon N. Y.* **2016**, *105*, 52–76.

(26) Zhang, W.-J. Lithium Insertion/extraction Mechanism in Alloy Anodes for Lithium-Ion Batteries. *J. Power Sources* **2011**, *196*, 877–885.

(27) Yu, S.-H.; Lee, S. H.; Lee, D. J.; Sung, Y.-E.; Hyeon, T. Conversion Reaction-Based Oxide Nanomaterials for Lithium Ion Battery Anodes. *Small* **2016**, *12*, 2146–2172.

(28) Good enough http://ceramics.org/ceramic-tech-today/father-of-lithium-ion-cathode-innovates-new-material-to-charge-the-future-of-sodium-ion-batteries (accessed May 28, 2017).

(29) Padhi, A. K.; Nanjundaswamy, K. S.; Goodenough, J. B. Phospho-Olivines as Positive-Electrode Materials for Rechargeable Lithium Batteries. *J. Electrochem. Soc.* **1997**, *144*, 1188.

(30) Thackeray, M. M.; Johnson, P. J.; de Picciotto, L. A.; Bruce, P. G.; Goodenough, J. B. Electrochemical Extraction of Lithium from $LiMn_2O_4$. *Mater. Res. Bull.* **1984**, *19*, 179–187.

(31) Cho, J.; Kim, Y. J.; Park, B. Novel $LiCoO_2$ Cathode Material with Al2O3 Coating for a Li Ion Cell. *Chem. Mater.* **2000**, *12*, 3788–3791.

(32) Takahashi, M.; Tobishima, S.; Takei, K.; Sakurai, Y. Reaction Behavior of $LiFePO_4$ as a Cathode Material for Rechargeable Lithium Batteries. *Solid State Ionics* **2002**, *148*, 283–289.

(33) Wang, H.; Jang, Y.; Huang, B.; Sadoway, D. R.; Chiang, Y. TEM Study of Electrochemical Cycling-Induced Damage and Disorder in LiCoO2 Cathodes for Rechargeable Lithium Batteries. *J. Electrochem. Soc.* **1999**, *146*, 473–480.

(34) Xia, H.; Lu, L.; Meng, Y. S.; Ceder, G. Phase Transitions and High-Voltage

Electrochemical Behavior of $LiCoO_2$ Thin Films Grown by Pulsed Laser Deposition. *J. Electrochem. Soc.* **2007**, *154*, A337–A342.

(35) Chung, K. Y.; Yoon, W.-S.; McBreen, J.; Yang, X.-Q.; Oh, S. H.; Shin, H. C.; Cho, W. Il; Cho, B. W. Structural Studies on the Effects of ZrO2 Coating on LiCoO2 during Cycling Using In Situ X-Ray Diffraction Technique. *J. Electrochem. Soc.* **2006**, *153*, A2152–A2157.

(36) Amatucci, G. G.; Tarascon, J. M.; Klein, L. C. CoO2, The End Member of the Li_xCoO_2 Solid Solution. *J. Electrochem. Soc.* **1996**, *143*, 1114–1123.

(37) Islam, M. S.; Fisher, C. A. J. Lithium and Sodium Battery Cathode Materials: Computational Insights into Voltage, Diffusion and Nanostructural Properties. *Chem. Soc. Rev.* **2014**, *43*, 185–204.

(38) Dina G. Kellerman, V. V. K.; Blinovskov, V. S. G. A. Y. N. Investigation of Thermal Stability of $LiCoO_2$ and $Li_{1-x}CoO_2$. *Chem. Sustain. Dev.* **2002**, *10*, 721–726.

(39) Lee, K. T.; Jeong, S.; Cho, J. Roles of Surface Chemistry on Safety and Electrochemistry in Lithium Ion Batteries. *Acc. Chem. Res.* **2013**, *46*, 1161–1170.

(40) M. Julien, Christian and Mauger, Alain and Zaghib, Karim and Groult, H. Comparative Issues of Cathode Materials for Li-Ion Batteries. *Inorganics* **2014**, *2*, 132–154.

(41) y de Dompablo, M. E.; Marianetti, C.; der Ven, A.; Ceder, G. Jahn-Teller Mediated Ordering in Layered $LixMO_2$ Compounds. *Phys. Rev. B* **2001**, *63*, 144107.

(42) Nitta, N.; Wu, F.; Lee, J. T.; Yushin, G. Li-Ion Battery Materials: Present and Future. *Mater. Today* **2015**, *18*, 252–264.

(43) Sarkar, S.; Banda, H.; Mitra, S. High Capacity Lithium-Ion Battery Cathode Using LiV_3O_8 Nanorods. *Electrochim. Acta* **2013**, *99*, 242–252.

(44) Ouyang, C. Y.; Shi, S. Q.; Lei, M. S. Jahn–Teller Distortion and Electronic Structure of $LiMn_2O_4$. *J. Alloys Compd.* **2009**, *474*, 370–374.

(45) Wang, C.; Hong, J. Ionic/Electronic Conducting Characteristics of LiFePO 4 Cathode Materials The Determining Factors for High Rate Performance. **2007**.

(46) Bewlay, S. L.; Konstantinov, K.; Wang, G. X.; Dou, S. X.; Liu, H. K. *Conductivity Improvements to Spray-Produced $LiFePO_4$ by Addition of a Carbon Source*; 2004; Vol. 58.

(47) Delacourt, C.; Wurm, C.; Laffont, L.; Leriche, J.-B.; Masquelier, C. Electrochemical and Electrical Properties of Nb- And/or C-Containing $LiFePO_4$ Composites. *Solid State Ionics* **2006**, *177*, 333–341.

(48) Chung, S.-Y.; Bloking, J. T.; Chiang, Y.-M. Electronically Conductive Phospho-Olivines as Lithium Storage Electrodes. *Nat. Mater.* **2002**, *1*, 123–128.

(49) Hsu, K.-F.; Tsay, S.-Y.; Hwang, B.-J.; Lisi, M.; Scaccia, S.; Carewska, M.; Minarini, C.; Pasquali, M. Synthesis and Characterization of Nano-Sized $LiFePO_4$ Cathode Materials Prepared by a Citric Acid-Based Sol–gel Route. *J. Mater. Chem.* **2004**, *14*, 2690–2695.

(50) $LiFePO_4$ Batteries: A Breakthrough For Electric Vehicles - Meta Efficient https://metaefficient.com/rechargeable-batteries/innovative-lifepo4-batteries-electric-vehicles.html (accessed May 29, 2017).

(51) Wang, D.; Buqa, H.; Crouzet, M.; Deghenghi, G.; Drezen, T.; Exnar, I.; Kwon, N.-H.; Miners, J. H.; Poletto, L.; Grätzel, M. *High-Performance, Nano-Structured LiMnPO4 Synthesized via a Polyol Method*; 2009; Vol. 189.

(52) Martha, S. K.; Markovsky, B.; Grinblat, J.; Gofer, Y.; Haik, O.; Zinigrad, E.; Aurbach, D.; Drezen, T.; Wang, D.; Deghenghi, G.; et al. $LiMnPO_4$ as an Advanced Cathode Material for Rechargeable Lithium Batteries. *J. Electrochem. Soc.* **2009**, *156*, A541.

(53) Amine, K.; Yasuda, H.; Yamachi, M. Olivine $LiCoPO_4$ as 4.8 V Electrode Material for Lithium Batteries. *Electrochem. Solid-State Lett.* **1999**, *3*, 178.

(54) Zaghib, K.; Mauger, A.; Julien, C. M. Olivine-Based Cathode Materials. In *Rechargeable Batteries*; Zhang, Z.; Zhang, S. S., Eds.; Springer, 2015; pp. 25–65.

(55) Arunkumar, T. A.; Manthiram, A. Influence of Lattice Parameter Differences on the Electrochemical Performance of the 5 V Spinel $LiMn_{1.5-y}Ni_{0.5-z}M_{y+z}O_4$ (M=Li, Mg, Fe, Co, and Zn). *Electrochem. Solid-State Lett.* **2005**, *8*, A403.

(56) Lu, Z.; Dahn, J. R. Understanding the Anomalous Capacity of Li/Li[$Ni_xLi_{(1/3-2x/3)}Mn_{(2/3-x/3)}O_2$ Cells Using In Situ X-Ray Diffraction and Electrochemical Studies. *J. Electrochem. Soc.* **2002**, *149*, A815.

(57) Lu, Z.; Beaulieu, L. Y.; Donaberger, R. A.; Thomas, C. L.; Dahn, J. R. Synthesis, Structure, and Electrochemical Behavior of $LiNi_xLi_{(1/3-2x/3)}Mn_{(2/3-x/3)}O_2$. *J. Electrochem. Soc.* **2002**, *149*, A778.

(58) Manthiram, A. Materials Challenges and Opportunities of Lithium Ion Batteries. *J. Phys. Chem. Lett.* **2011**, *2*, 176–184.

(59) Lu, Z.; Dahn, J. R. Cathode Compositions for Lithium-Ion Batteries, 2005.

(60) Scrosati, B.; Garche, J. Lithium Batteries: Status, Prospects and Future. *J. Power Sources* **2010**, *195*, 2419–2430.

(61) Erickson, E. M.; Schipper, F.; Penki, T. R.; Shin, J.-Y.; Erk, C.; Chesneau, F.-F.; Markovsky, B.; Aurbach, D. Review—Recent Advances and Remaining Challenges for Lithium Ion Battery Cathodes. *J. Electrochem. Soc.* **2017**, *164*, A6341–A6348.

(62) Gong, Z.; Yang, Y.; Voss, A.; Thomas, A.; Oswald, S.; Gruner, W.; Trots, D. M.; Bramnik, N. N.; Ehrenberg, H.; Graff, G. L.; et al. Recent Advances in the Research of Polyanion-Type Cathode Materials for Li-Ion Batteries. *Energy Environ. Sci.* **2011**, *4*, 3223.

(63) Xu, B.; Qian, D.; Wang, Z.; Shirley Meng, Y. Recent Progress in Cathode Materials Research for Advanced Lithium Ion Batteries. *Mater. Sci. Eng. R* **2012**, *73*, 51–65.

(64) Xu, K. Nonaqueous Liquid Electrolytes for Lithium-Based Rechargeable Batteries. *Chem. Rev.* **2004**, *104*, 4303–4418.

(65) Goodenough, J. B.; Singh, P. Review—Solid Electrolytes in Rechargeable Electrochemical Cells. *J. Electrochem. Soc.* **2015**, *162*, A2387–A2392.

(66) Xia, L.; Yu, L.; Hu, D.; Chen, G. Z.; Jacobson, M. Z.; He, M.; Krzysztof, F.; Elżbieta, F.; Petr, N.; Erik, J. B.; et al. Electrolytes for Electrochemical Energy Storage. *Mater. Chem. Front.* **2017**, *2*, 148.

(67) Porcarelli, L.; Gerbaldi, C.; Bella, F.; Nair, J. R. Super Soft All-Ethylene Oxide Polymer Electrolyte for Safe All-Solid Lithium Batteries. *Sci. Rep.* **2016**, *6*, 19892.

(68) Linford, R. . *Applications of Electroactive Polymers*; Scrosati, B., Ed.; Chapman and Hall: London, 1993.

(69) What's the difference between a Li-ion and solid-state battery? | AndroidAuthority http://www.androidauthority.com/lithium-ion-vs-solid-state-battery-726142/ (accessed May 31, 2017).

(70) Song, J. Y.; Wang, Y. Y.; Wan, C. C. Review of Gel-Type Polymer Electrolytes for Lithium-Ion Batteries. *J. Power Sources* **1999**, *77*, 183–197.

(71) Kalhoff, J.; Eshetu, G. G.; Bresser, D.; Passerini, S. Safer Electrolytes for Lithium-Ion Batteries: State of the Art and Perspectives. *ChemSusChem* **2015**, *8*.

(72) Sequeira, C.; Santos, D. *Polymer Electrolytes ; Fundamentals and Applications*; Sequeira, C.; Santos, D., Eds.; Woodhead Pub, 2010.

(73) Manuel Stephan, A. Review on Gel Polymer Electrolytes for Lithium Batteries. *Eur. Polym. J.* **2006**, *42*, 21–42.

(74) Borghini, M. C.; Mastragostino, M.; Passerini, S.; Scrosati, B. Electrochemical Properties of Polyethylene Oxide-Li[(CF_3SO_2N]-Gamma-$LiAlO_2$ Composite Polymer Electrolytes. *J. Electrochem. Soc.* **1995**, *142*, 2118.

(75) Li, W.; Dahn, J. R.; Wainwright, D. S. Rechargeable Lithium Batteries with Aqueous Electrolytes. *Science (80-.).* **1994**, *264*, 1115–1118.

(76) Tang, W.; Zhu, Y.; Hou, Y.; Liu, L.; Wu, Y.; Loh, K. P.; Zhang, H.; Zhu, K.; Zhu, K.; Holze, R. Aqueous Rechargeable Lithium Batteries as an Energy Storage System of Superfast Charging. *Energy Environ. Sci.* **2013**, *6*, 2093.

(77) Alias, N.; Mohamad, A. A. Advances of Aqueous Rechargeable Lithium-Ion Battery: A Review. *J. Power Sources* **2015**, *274*, 237–251.

(78) Choi, J.; Alvarez, E.; Arunkumar, T. A.; Manthiram, A. Proton Insertion into Oxide Cathodes during Chemical Delithiation. *Electrochem. Solid-State Lett.* **2006**, *9*, A241.

(79) Manthiram, A.; Choi, J. Chemical and Structural Instabilities of Lithium Ion Battery Cathodes. *J. Power Sources* **2006**, *159*, 249–253.

(80) Luo, J.-Y.; Cui, W.-J.; He, P.; Xia, Y.-Y. Raising the Cycling Stability of Aqueous

Lithium-Ion Batteries by Eliminating Oxygen in the Electrolyte. *Nat. Chem.* **2010**, *2*, 760–765.

(81) Vujković, M.; Stojković, I.; Cvjetićanin, N.; Mentus, S. Gel-Combustion Synthesis of $LiFePO_4$/C Composite with Improved Capacity Retention in Aerated Aqueous Electrolyte Solution. *Electrochim. Acta* **2013**, *92*, 248–256.

(82) Zhao, M.; Zhang, B.; Huang, G.; Zhang, H.; Song, X. *Excellent Rate Capabilities of ($LiFePO_4$/C)//LiV_3O_8 in an Optimized Aqueous Solution Electrolyte*; 2013; Vol. 232.

(83) He, P.; Liu, J.-L.; Cui, W.-J.; Luo, J.-Y.; Xia, Y.-Y. Investigation on Capacity Fading of $LiFePO_4$ in Aqueous Electrolyte. *Electrochim. Acta* **2011**, *56*, 2351–2357.

(84) He, P.; Zhang, X.; Wang, Y.-G.; Cheng, L.; Xia, Y.-Y. Lithium-Ion Intercalation Behavior of $LiFePO_4$ in Aqueous and Nonaqueous Electrolyte Solutions. *J. Electrochem. Soc.* **2008**, *155*, A144.

(85) Zhao, M.; Zheng, Q.; Wang, F.; Dai, W.; Song, X. Electrochemical Performance of High Specific Capacity of Lithium-Ion Cell LiV_3O_8//$LiMn_2O_4$ with $LiNO_3$ Aqueous Solution Electrolyte. *Electrochim. Acta* **2011**, *56*, 3781–3784.

(86) Qu, Q.; Fu, L.; Zhan, X.; Samuelis, D.; Maier, J.; Li, L.; Tian, S.; Li, Z.; Wu, Y. Porous LiMn2O4 as Cathode Material with High Power and Excellent Cycling for Aqueous Rechargeable Lithium Batteries. *Energy Environ. Sci.* **2011**, *4*, 3985.

(87) Wang, H.; Huang, K.; Zeng, Y.; Yang, S.; Chen, L. Electrochemical Properties of TiP2O7 and LiTi2(PO4)3 as Anode Material for Lithium Ion Battery with Aqueous Solution Electrolyte. *Electrochim. Acta* **2007**, *52*, 3280–3285.

(88) Tang, W.; Tian, S.; Liu, L. L.; Li, L.; Zhang, H. P.; Yue, Y. B.; Bai, Y.; Wu, Y. P.; Zhu, K. Nanochain $LiMn_2O_4$ as Ultra-Fast Cathode Material for Aqueous Rechargeable Lithium Batteries. *Electrochem. commun.* **2011**, *13*, 205–208.

(89) Tang, W.; Liu, L. L.; Tian, S.; Li, L.; Li, L. L.; Yue, Y. B.; Bai, Y.; Wu, Y. P.; Zhu, K.; Holze, R. $LiMn_2O_4$ Nanorods as a Super-Fast Cathode Material for Aqueous Rechargeable Lithium Batteries. *Electrochem. commun.* **2011**, *13*, 1159–1162.

(90) Wang, H.; Zeng, Y.; Huang, K.; Liu, S.; Chen, L. Improvement of Cycle

Performance of Lithium Ion Cell $LiMn_2O_4/Li_xV_2O_5$ with Aqueous Solution Electrolyte by Polypyrrole Coating on Anode. *Electrochim. Acta* **2007**, *52*, 5102–5107.

(91) Wang, G. J.; Yang, L. C.; Qu, Q. T.; Wang, B.; Wu, Y. P.; Holze, R. An Aqueous Rechargeable Lithium Battery Based on Doping and Intercalation Mechanisms. *J. Solid State Electrochem.* **2010**, *14*, 865–869.

(92) Liu, X.-H.; Saito, T.; Doi, T.; Okada, S.; Yamaki, J. Electrochemical Properties of Rechargeable Aqueous Lithium Ion Batteries with an Olivine-Type Cathode and a Nasicon-Type Anode. *J. Power Sources* **2009**, *189*, 706–710.

(93) Xu, K. Electrolytes and Interphases in Li-Ion Batteries and Beyond. *Chem. Rev.* **2014**, *114*, 11503–11618.

(94) Hu, L.; Tornheim, A.; Zhang, S. S.; Zhang, Z. Additives for Functional Electrolytes of Li-Ion Batteries. In *Rechargeable Batteries*; Springer International Publishing, 2015; pp. 263–290.

(95) Xia, L.; Wang, D.; Yang, H.; Cao, Y.; Ai, X. An Electrolyte Additive for Thermal Shutdown Protection of Li-Ion Batteries. *Electrochem. commun.* **2012**, *25*, 98–100.

(96) Herstedt, M.; Rensmo, H.; Siegbahn, H.; Edström, K. Electrolyte Additives for Enhanced Thermal Stability of the Graphite Anode Interface in a Li-Ion Battery. *Electrochim. Acta* **2004**, *49*, 2351–2359.

(97) Howlett, P. C.; MacFarlane, D. R.; Hollenkamp, A. F. High Lithium Metal Cycling Efficiency in a Room-Temperature Ionic Liquid. *Electrochem. Solid-State Lett.* **2004**, *7*, A97--A101.

(98) Theivaprakasam, S.; MacFarlane, D. R.; Mitra, S. Electrochemical Studies of N-Methyl N-Propyl Pyrrolidinium Bis(trifluoromethanesulfonyl) Imide Ionic Liquid Mixtures with Conventional Electrolytes in LiFePO4/Li Cells. *Electrochim. Acta* **2015**, *180*, 737–745.

(99) Forsyth, S. A.; Pringle, J. M.; MacFarlane, D. R. Ionic Liquids—an Overview. *Aust. J. Chem.* **2004**, *57*, 113–119.

(100) MacFarlane, D. R.; Forsyth, M.; Izgorodina, E. I.; Abbott, A. P.; Annat, G.; Fraser,

K.; Endres, F.; Abedin, S. Z. El; Smiglak, M.; Metlen, A.; et al. On the Concept of Ionicity in Ionic Liquids. *Phys. Chem. Chem. Phys.* **2009**, *11*, 4962.

(101) Eftekhari, A.; Liu, Y.; Chen, P. Different Roles of Ionic Liquids in Lithium Batteries. *J. Power Sources* **2016**, *334*, 221–239.

(102) Wikipedia. No Title https://en.wikipedia.org/wiki/Molten-salt_battery (accessed Jun 12, 2017).

(103) Gabriel, S.; Weiner, J. Ueber Einige Abkömmlinge Des Propylamins. *Berichte der Dtsch. Chem. Gesellschaft* **1888**, *21*, 2669–2679.

(104) Castiglione, F.; Raos, G.; Battista Appetecchi, G.; Montanino, M.; Passerini, S.; Moreno, M.; Famulari, A.; Mele, A. Blending Ionic Liquids: How Physico-Chemical Properties Change. *Phys. Chem. Chem. Phys.* **2010**, *12*, 1784.

(105) Zhao, C.; Burrell, G.; Torriero, A. A. J.; Separovic, F.; Dunlop, N. F.; MacFarlane, D. R.; Bond, A. M. Electrochemistry of Room Temperature Protic Ionic Liquids. *J. Phys. Chem. b* **2008**, *112*, 6923–6936.

(106) Greaves, T. L.; Calum J. Drummond. Protic Ionic Liquids: Properties and Applications. *Chem. Rev.* **2007**, *108*, 206–237.

(107) Armand, M.; Endres, F.; MacFarlane, D. R.; Ohno, H.; Scrosati, B. Ionic-Liquid Materials for the Electrochemical Challenges of the Future. *Nat. Mater.* **2009**, *8*, 621–629.

(108) Pakiari, A. H.; Siahrostami, S.; Ziegler, T. An Insight into Microscopic Properties of Aprotic Ionic Liquids: A DFT Study. *J. Mol. Struct.* **2010**, *955*, 47–52.

(109) Tan, S. S. Y.; MacFarlane, D. R. Ionic Liquids in Biomass Processing. In; 2009; pp. 311–339.

(110) Vijayaraghavan, R.; MacFarlane, D. R. Living Cationic Polymerisation of Styrene in an Ionic Liquid. *Chem. Commun.* **2004**, 700–701.

(111) Kumar, S. S. D.; Surianarayanan, M.; Vijayaraghavan, R.; Mandal, A. B.; MacFarlane, D. R. Curcumin Loaded Poly (2-Hydroxyethyl Methacrylate) Nanoparticles from Gelled Ionic liquid–In Vitro Cytotoxicity and Anti-Cancer Activity in SKOV-3 Cells. *Eur. J. Pharm. Sci.* **2014**, *51*, 34–44.

(112) Zhang, J.; Bond, A. M.; MacFarlane, D. R.; Forsyth, S. A.; Pringle, J. M.; Mariotti, A. W. A.; Glowinski, A. F.; Wedd, A. G. Voltammetric Studies on the Reduction of Polyoxometalate Anions in Ionic Liquids. *Inorg. Chem.* **2005**, *44*, 5123–5132.

(113) Izgorodin, A.; Winther-Jensen, O.; Winther-Jensen, B.; MacFarlane, D. R. CdS Thin-Film Electrodeposition from a Phosphonium Ionic Liquid. *Phys. Chem. Chem. Phys.* **2009**, *11*, 8532–8537.

(114) Somers, A. E.; Khemchandani, B.; Howlett, P. C.; Sun, J.; MacFarlane, D. R.; Forsyth, M. Ionic Liquids as Antiwear Additives in Base Oils: Influence of Structure on Miscibility and Antiwear Performance for Steel on Aluminum. *ACS Appl. Mater. Interfaces* **2013**, *5*, 11544–11553.

(115) MacFarlane, D. R.; Pringle, J. M.; Howlett, P. C.; Forsyth, M. Ionic Liquids and Reactions at the Electrochemical Interface. *Phys. Chem. Chem. Phys.* **2010**, *12*, 1659–1669.

(116) MacFarlane, D. R.; Forsyth, M.; Howlett, P. C.; Kar, M.; Passerini, S.; Pringle, J. M.; Ohno, H.; Watanabe, M.; Yan, F.; Zheng, W.; et al. Ionic Liquids and Their Solid-State Analogues as Materials for Energy Generation and Storage. *Nat. Rev. Mater.* **2016**, 15005.

(117) Zhang, S. S. A Review on Electrolyte Additives for Lithium-Ion Batteries. *J. Power Sources* **2006**, *162*, 1379–1394.

(118) Wang, E.; Ofer, D.; Bowden, W.; Iltchev, N.; Moses, R.; Brandt, K. Stability of Lithium Ion Spinel Cells. III. Improved Life of Charged Cells. *J. Electrochem. Soc.* **2000**, *147*, 4023.

(119) Iwakura, C.; Fukumoto, Y.; Inoue, H.; Ohashi, S.; Kobayashi, S.; Tada, H.; Abe, M. Electrochemical Characterization of Various Metal Foils as a Current Collector of Positive Electrode for Rechargeable Lithium Batteries. *J. Power Sources* **1997**, *68*, 301–303.

(120) Whitehead, A. H.; Schreiber, M. Current Collectors for Positive Electrodes of Lithium-Based Batteries. *J. Electrochem. Soc.* **2005**, *152*, A2105.

(121) Myung, S.-T.; Hitoshi, Y.; Sun, Y.-K.; Schechter, A.; Lemondant, D.; Kodama, R.; Nakai, I.; Marcus, P. Electrochemical Behavior and Passivation of Current

Collectors in Lithium-Ion Batteries. *J. Mater. Chem.* **2011**, *21*, 9891.

(122) Zhang, S. S.; Jow, T. R. Aluminum Corrosion in Electrolyte of Li-Ion Battery. *J. Power Sources* **2002**, *109*, 458–464.

(123) Arora, P.; Zhang, Z. (John). Battery Separators. *Chem.Rev* **2004**, *104*, 4419–4462.

(124) Terborg, L.; Ling, M.; Nie, K.; Dahi, A.; Wu, C.; Guo, J.; Ross, P. N.; Liu, G.; Kostecki, R. The Effect of Polymer Binder on the Electrochemical Performance of Si/C Anodes. *Meet. Abstr.* **2016**, *MA2016-02*, 494–494.

(125) Peled, E. The Electrochemical Behavior of Alkali and Alkaline Earth Metals in Nonaqueous Battery Systems?The Solid Electrolyte Interphase Model. *J. Electrochem. Soc.* **1979**, *126*, 2047.

(126) Cheng, X.-B.; Zhang, R.; Zhao, C.-Z.; Wei, F.; Zhang, J.-G.; Zhang, Q. A Review of Solid Electrolyte Interphases on Lithium Metal Anode. *Adv. Sci.* **2016**, *3*, 1500213.

(127) Peled, E.; Straze, H. The Kinetics of the Magnesium Electrode in Thionyl Chloride Solutions. *J. Electrochem. Soc.* **1977**, *124*, 1030.

(128) Kanamura, K.; Tamura, H.; Shiraishi, S.; Takehara, Z. XPS Analysis of Lithium Surfaces Following Immersion in Various Solvents Containing LiBF[sub 4]. *J. Electrochem. Soc.* **1995**, *142*, 340.

(129) Kanamura, K.; Shiraishi, S.; Takehara, Z. Electrochemical Deposition of Very Smooth Lithium Using Nonaqueous Electrolytes Containing HF. *J. Electrochem. Soc.* **1996**, *143*, 2187.

(130) Ein-Eli, Y. A New Perspective on the Formation and Structure of the Solid Electrolyte Interface at the Graphite Anode of Li-Ion Cells. *Electrochem. Solid-State Lett.* **1999**, *2*, 212.

(131) Ein-Eli, Y.; McDevitt, S. F.; Laura, R. The Superiority of Asymmetric Alkyl Methyl Carbonates. *J. Electrochem. Soc.* **1998**, *145*, L1.

(132) Verma, P.; Maire, P.; Novák, P. A Review of the Features and Analyses of the Solid Electrolyte Interphase in Li-Ion Batteries. *Electrochim. Acta* **2010**, *55*, 6332–6341.

(133) Benitez, L.; Seminario, J. M. Electron Transport and Electrolyte Reduction in the

Solid-Electrolyte Interphase of Rechargeable Lithium Ion Batteries with Silicon Anodes. *J. Phys. Chem. C* **2016**, *120*, 17978–17988.

(134) Nadimpalli, S. P. V; Sethuraman, V. A.; Dalavi, S.; Lucht, B.; Chon, M. J.; Shenoy, V. B.; Guduru, P. R. Quantifying Capacity Loss due to Solid-Electrolyte-Interphase Layer Formation on Silicon Negative Electrodes in Lithium-Ion Batteries.

(135) Nie, M.; Abraham, D. P.; Chen, Y.; Bose, A.; Lucht, B. L. Silicon Solid Electrolyte Interphase (SEI) of Lithium Ion Battery Characterized by Microscopy and Spectroscopy. *J. Phys. Chem. C* **2013**, *117*, 13403–13412.

(136) Fedorov, M. V; Kornyshev, A. A. Ionic Liquids at Electrified Interfaces. *Chem. Rev.* **2014**, *114*, 2978–3036.

(137) Ivaništšev, V.; V.Fedorov, M. Interfaces between Charged Surfaces and Ionic Liquids: Insights from Molecular Simulations. *Electrochem. Soc. Interface* **2013**, 65–69.

(138) Endres, F.; Höfft, O.; Borisenko, N.; Gasparotto, L. H.; Prowald, A.; Al-Salman, R.; Carstens, T.; Atkin, R.; Bund, A.; Zein El Abedin, S.; et al. Do Solvation Layers of Ionic Liquids Influence Electrochemical Reactions? *Phys. Chem. Chem. Phys.* **2010**, *12*, 1724.

(139) Garcia, B.; Lavallée, S.; Perron, G.; Michot, C.; Armand, M. Room Temperature Molten Salts as Lithium Battery Electrolyte. *Electrochim. Acta* **2004**, *49*, 4583–4588.

(140) MacFarlane, D. R.; Tachikawa, N.; Forsyth, M.; Pringle, J. M.; Howlett, P. C.; Elliott, G. D.; Davis, J. H.; Watanabe, M.; Simon, P.; Angell, C. A.; et al. Energy Applications of Ionic Liquids. *Energy Environ. Sci.* **2014**, *7*, 232–250.

(141) M.Montannio; S.Passerini; G.B Appetecchi. Electrolytes for Rechargeable Lithium Batteries. In *Rechargeable lithium batteries : from fundamentals to applications*; Franco, A. A., Ed.; Woodhead Publishing, 2015; pp. 73–114.

(142) Li, Q.; Chen, J.; Fan, L.; Kong, X.; Lu, Y. Progress in Electrolytes for Rechargeable Li-Based Batteries and beyond. *Green Energy Environ.* **2016**, *1*, 18–42.

(143) Girard, G. M. A.; Hilder, M.; Zhu, H.; Nucciarone, D.; Whitbread, K.; Zavorine, S.;

Moser, M.; Forsyth, M.; MacFarlane, D. R.; Howlett, P. C. Electrochemical and Physicochemical Properties of Small Phosphonium Cation Ionic Liquid Electrolytes with High Lithium Salt Content. *Phys. Chem. Chem. Phys.* **2015**, *17*, 8706–8713.

(144) Hilder, M.; Girard, G. M. A.; Whitbread, K.; Zavorine, S.; Moser, M.; Nucciarone, D.; Forsyth, M.; MacFarlane, D. R.; Howlett, P. C. Physicochemical Characterization of a New Family of Small Alkyl Phosphonium Imide Ionic Liquids. *Electrochim. Acta* **2016**, *202*, 100–109.

(145) Eshetu, G. G.; Jeong, S.; Pandard, P.; Lecocq, A.; Marlair, G.; Passerini, S. Comprehensive Insights into the Thermal Stability, Biodegradability and Combustion Chemistry of Pyrrolidinium-Based Ionic Liquids. *ChemSusChem* **2017**.

(146) Howlett, P. C.; Izgorodina, E. I.; Forsyth, M.; Macfarlane, D. R. Electrochemistry at Negative Potentials in Bis(trifluoromethanesulfonyl)amide Ionic Liquids. *Z. Phys. Chem* **2006**, *220*, 1483–1498.

(147) Charging Batteries at High and Low Temperatures – Battery University http://batteryuniversity.com/learn/article/charging_at_high_and_low_temperatures (accessed Aug 29, 2017).

(148) Cao, X.; Li, Y.; Li, X.; Zheng, J.; Gao, J.; Gao, Y.; Wu, X.; Zhao, Y.; Yang, Y. Novel Phosphamide Additive to Improve Thermal Stability of Solid Electrolyte Interphase on Graphite Anode in Lithium-Ion Batteries. *ACS Appl. Mater. Interfaces* **2013**, *5*, 11494–11497.

(149) Guerfi, A.; Dontigny, M.; Charest, P.; Petitclerc, M.; Lagacé, M.; Vijh, A.; Zaghib, K. Improved Electrolytes for Li-Ion Batteries: Mixtures of Ionic Liquid and Organic Electrolyte with Enhanced Safety and Electrochemical Performance. *J. Power Sources* **2010**, *195*, 845–852.

(150) Zhang, S. S.; Xu, K.; Jow, T. R. The Low Temperature Performance of Li-Ion Batteries. *J. Power Sources* **2003**, *115*, 137–140.

(151) Ji, Y.; Zhang, Y.; Wang, C.-Y. Li-Ion Cell Operation at Low Temperatures. *J. Electrochem. Soc.* **2013**, *160*, A636–A649.

(152) Lin, X.; Kavian, R.; Lu, Y.; Hu, Q.; Shao-Horn, Y.; Grinstaff, M. W. Thermally-Responsive, Nonflammable Phosphonium Ionic Liquid Electrolytes for Lithium

Metal Batteries: Operating at 100 Degrees Celsius. *Chem. Sci.* **2015**, *6*, 6601–6606.

(153) Kerner, M.; Plylahan, N.; Scheers, J.; Johansson, P. Ionic Liquid Based Lithium Battery Electrolytes: Fundamental Benefits of Utilising Both TFSI and FSI Anions? *Phys. Chem. Chem. Phys.* **2015**, *17*, 19569–19581.

(154) Guerfi, A.; Duchesne, S.; Kobayashi, Y.; Vijh, A.; Zaghib, K. LiFePO4 and Graphite Electrodes with Ionic Liquids Based on Bis(fluorosulfonyl)imide (FSI)− for Li-Ion Batteries. *J. Power Sources* **2008**, *175*, 866–873.

(155) Murmann, P.; Niehoff, P.; Schmitz, R.; Nowak, S.; Gores, H.; Ignatiev, N.; Sartori, P.; Winter, M.; Schmitz, R. Investigations on the Electrochemical Performance and Thermal Stability of Two New Lithium Electrolyte Salts in Comparison to LiPF6. *Electrochim. Acta* **2013**, *114*, 658–666.

(156) Kannan, A. M.; Rabenberg, L.; Manthiram, A. High Capacity Surface-Modified LiCoO2 Cathodes for Lithium-Ion Batteries . *Electrochem. Solid-State Lett.* **2003**, *6*, A16–A18.

(157) Huang, J.; Hollenkamp, A. F. Thermal Behavior of Ionic Liquids Containing the FSI Anion and the Li^+ Cation. *J. Phys. Chem. C* **2010**, *114*, 21840–21847.

(158) Vijayaraghavan, R.; Surianarayanan, M.; Armel, V.; MacFarlane, D. R.; Sridhar, V. P. Exothermic and Thermal Runaway Behaviour of Some Ionic Liquids at Elevated Temperatures. *Chem. Commun.* **2009**, 6297–6299.

(159) Navarra, M. A. Ionic Liquids as Safe Electrolyte Components for Li-Metal and Li-Ion Batteries. *MRS Bull.* **2013**, *38*, 548–553.

(160) Lombardo, L.; Brutti, S.; Navarra, M. A.; Panero, S.; Reale, P. Mixtures of Ionic Liquid – Alkylcarbonates as Electrolytes for Safe Lithium-Ion Batteries. *J. Power Sources* **2013**, *227*, 8–14.

(161) Shijiang, L.; Hongjun, H.; Huachun, Y.; Xujin, X.; Shengjun, G.; Xi, L.; Jianjun, H.; Fengfeng, X.; Chengguo, L. A Cryogenic Lithium Ion Battery and a Lithium Ion Battery Electrolyte. CN103107364B, 2016.

(162) Kunlin, X.; Qun, H.; Xiangyun, Y.; Xiaorong, C.; Sheng, Y. A Method for Improving the Low Temperature Performance of Lithium Manganese Battery

Organic Electrolyte. CN103378360A, 2015.

(163) Sun, L. Non-Aqueous Electrolytes Having an Extended Temperature Range for Battery Applications. US 20050123835, 2005.

(164) Xuedong, Y.; Meizhi, P.; Changhe, C. Low-Temperature Lithium Iron Phosphate Ion Battery Electrolyte and Preparation Method Thereof. CN103779605, 2014.

(165) Hallac, B.; Smart, M. C.; Frederick C. Krause, Bernhard M. Metz, R. V. B. Lithium Ion Electrolytes with Lifsi for Improved Wide Operating Temperature Range. US 20160149263 A1, 2016.

(166) Liu Pengpeng; Jing, D.; Zhaoqiang, L.; Bo, H.; Xisheng, F. A Low Temperature Ratio Lithium Ion Battery Electrolyte. CN103078136 B, 2015.

(167) Hong Gan; Takeuchi, E. S. Nonaqueous Organic Electrolytes for Low Temperature Discharge of Rechargeable Electrochemical Cells. US6153338, 2000.

(168) Suojiang, Z.; Tao, D.; Yingjun, C.; Liang, Z. Ester-Based Ionic Liquid Electrolyte Solution for Low Temperature Lithium Ion Battery. CN 201310046352, 2013.

(169) Cheng, G.; Zhu, Y.; Strand, D.; Hallac, B.; Metz, B. M. Electrolyte Formulations for Lithium Ion Batteries. US9466857 B1; US20160380308; WO2016209839A1, 2016.

(170) Li, B.; Amiruddin, S. Low Temperature Electrolyte for High Capacity Lithium Based Batteries. US20130157147A1, US20130157147, WO2013090417A1, 2013.

(171) Sheng Shui Zhang. A Review on the Separators of Liquid Electrolyte Li-Ion Batteries. *J. Power Sources* **2007**, *164*, 351–364.

(172) Le, M. L. P.; Cointeaux, L.; Strobel, P.; Leprêtre, J.-C.; Judeinstein, P.; Alloin, F. Influence of Solvent Addition on the Properties of Ionic Liquids. *J. Phys. Chem. C* **2012**, *116*, 7712–7718.

(173) Yamada, Y.; Iriyama, Y.; Abe, T.; Ogumi, Z. Kinetics of Lithium Ion Transfer at the Interface between Graphite and Liquid Electrolytes: Effects of Solvent and Surface Film. *Langmuir* **2009**, *25*, 12766–12770.

(174) Abe, T.; Fukuda, H.; Iriyama, Y.; Ogumi, Z. Solvated Li-Ion Transfer at Interface Between Graphite and Electrolyte. *J. Electrochem. Soc.* **2004**, *151*, A1120.

(175) Shkrob, I. A.; Marin, T. W.; Zhu, Y.; Abraham, D. P. Why Bis(fluorosulfonyl)imide Is a ?Magic Anion? For Electrochemistry. *J. Phys. Chem. C* **2014**, *118*, 19661–19671.

(176) Basile, A.; Bhatt, A. I.; O'Mullane, A. P. Stabilizing Lithium Metal Using Ionic Liquids for Long-Lived Batteries. *Nat. Commun.* **2016**, *7*, 1–11.

(177) Howlett, P. C.; Brack, N.; Hollenkamp, A. F.; Forsyth, M.; MacFarlane, D. R. Characterization of the Lithium Surface in N-Methyl-N-Alkylpyrrolidinium Bis (Trifluoromethanesulfonyl) Amide Room-Temperature Ionic Liquid Electrolytes. *J. Electrochem. Soc.* **2006**, *153*, A595--A606.

(178) Matsumoto, H.; Sakaebe, H.; Tatsumi, K.; Kikuta, M.; Ishiko, E.; Kono, M. Fast Cycling of Li/LiCoO2 Cell with Low-Viscosity Ionic Liquids Based on Bis(fluorosulfonyl)imide [FSI]−. *J. Power Sources* **2006**, *160*, 1308–1313.

(179) Sakaebe, H.; Matsumoto, H.; Tatsumi, K. Application of Room Temperature Ionic Liquids to Li Batteries. *Electrochim. Acta* **2007**, *53*, 1048–1054.

(180) Xu, K.; von Wald Cresce, A. Li+-Solvation/desolvation Dictates Interphasial Processes on Graphitic Anode in Li Ion Cells. *J. Mater. Res.* **2012**, *27*, 2327–2341.

(181) Kühnel, R.-S.; Böckenfeld, N.; Passerini, S.; Winter, M.; Balducci, A. Mixtures of Ionic Liquid and Organic Carbonate as Electrolyte with Improved Safety and Performance for Rechargeable Lithium Batteries. *Electrochim. Acta* **2011**, *56*, 4092–4099.

(182) Quinzeni, I.; Ferrari, S.; Quartarone, E.; Tomasi, C.; Fagnoni, M.; Mustarelli, P. Li-Doped Mixtures of Alkoxy-N-Methylpyrrolidinium Bis(trifluoromethanesulfonyl)-Imide and Organic Carbonates as Safe Liquid Electrolytes for Lithium Batteries. *J. Power Sources* **2013**, *237*, 204–209.

(183) Aguilera, L.; Scheers, J.; Matic, A. Enhanced Low-Temperature Ionic Conductivity via Different Li^+ Solvated Clusters in Organic Solvent/ionic Liquid Mixed Electrolytes. *Phys. Chem. Chem. Phys.* **2016**, *18*, 25458–25464.

(184) Li, H.; Pang, J.; Yin, Y.; Zhuang, W.; Wang, H.; Zhai, C.; Lu, S. Application of a Nonflammable Electrolyte Containing Pp_{13}TFSI Ionic Liquid for Lithium-Ion Batteries Using the High Capacity Cathode Material $Li[Li_{0.2}Mn_{0.54}Ni_{0.13}]O_2$. *RSC*

Adv. **2013**, *3*, 13907–13914.

Chapter 2

Solution Structure and Electrochemical Characterization of N-methyl-N-propyl pyrrolidinium bis(trifluoromethane sulfonyl)imide in Alkyl-carbonate Hybrid Electrolyte

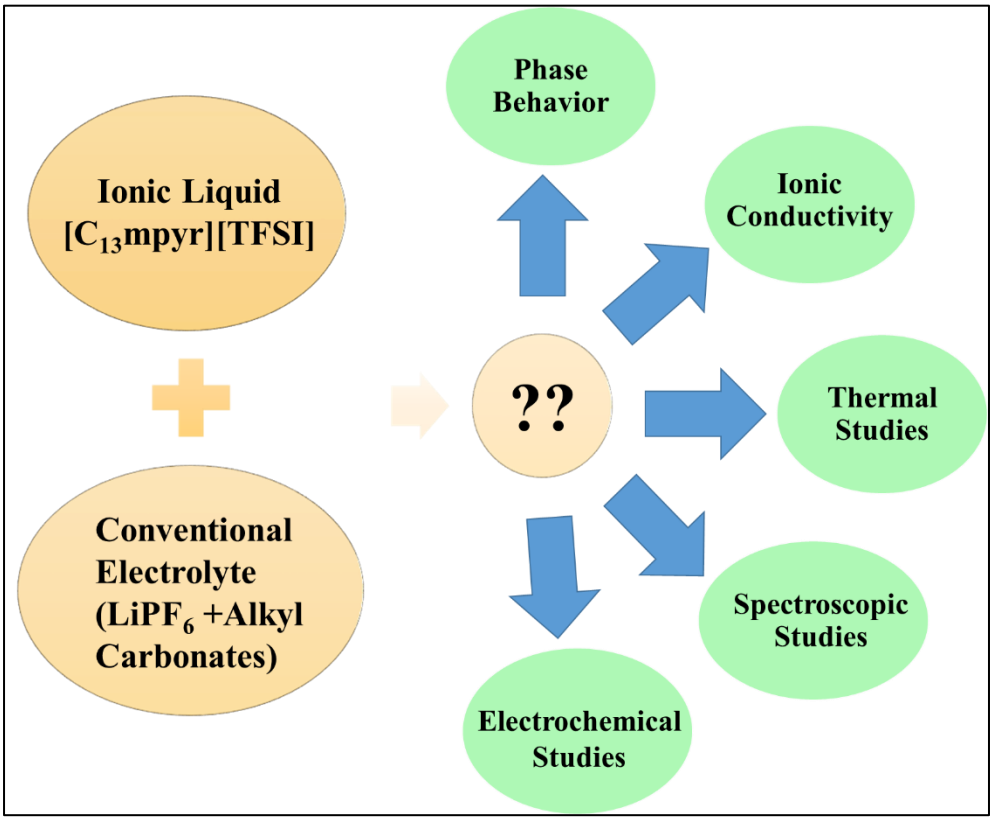

Part of this chapter is published as a journal publication:

Theivaprakasam, S.; MacFarlane, D. R.; Mitra, S. Electrochemical Studies of N-Methyl N-Propyl Pyrrolidinium Bis(trifluoromethanesulfonyl) Imide Ionic Liquid Mixtures with Conventional Electrolytes in $LiFePO_4$/Li Cells. *Electrochim. Acta* **2015**, *180*, 737–745.

2.1 Introduction

Currently, lithium batteries dominate the energy market by powering mobile electronic devices as well as electric vehicles[1–3]. In electric vehicles, the lithium battery technology requires further enhancement in terms of energy density and safety[2,4,5]. A better understanding of the interfacial chemistry will help in enhancing the performance of LiBs[6–8]. To do so, the most important aspect is the understanding of the SEI, which dictates the performance of the lithium battery[6,9–11]. As mentioned earlier, the solvents in the electrolyte solvate the lithium ions preferentially than the anion of the lithium salt[12]. Such solvent molecules travels towards the graphite electrode, get reduced further at the site of the electrode and forms the SEI. As a result, the composition of the SEI has a direct influence on the composition of the electrolyte[13]. In such circumstances, understanding the physicochemical properties such as viscosity, ionic conductivity, lithium ion solvation, and the electrochemical behavior of the electrolytes will help to understand their effective role in enhancing the performance of lithium batteries.

Ionic liquids are an emerging class of electrolytes in lithium batteries[14–17]. In the case of room temperature applications, molecular solvents are required to be added in order to reduce the viscosity of the mixtures[18–20]. In spite of the hybrid combination with the molecular solvents, it is expected that these ionic liquid mixtures will introduce notable thermal stability to the electrolytes[21,22].

Generally, the solution structure involves the solvation of the ions in the salt with the solvent molecules. In case of LiBs, it is potentially quite complex and has been studied with the help of density functional theory (DFT) calculations and spectroscopic analyses[17,23–28]. Recently, with the emergence of ionic liquid electrolytes, studies were carried out to understand lithium and sodium ion solvation in solvate ionic liquid electrolytes[17,18,29–31].

Since the role played by the individual electrolyte ingredients in the conventional electrolyte is very specific, this chapter aims to understand the solution structure of the hybrid mixture with 40 percent of the ionic liquid in the conventional electrolyte system[6,21,32]. Further, the electrochemical understanding of hybrid electrolytes in terms of their behavior at the cathodic and anodic regions, their compatibility, and the lithium interfaces was studied to acquire a preliminary understanding of the HE before proceeding

with further testing on commercial cathodes. Thus, the present chapter make efforts to understand the solution structure, physicochemical, and electrochemical characterization of the hybrid electrolyte in comparison with the conventional electrolyte.

2.2 Experimental

2.2.1 Electrolyte Compositions

N-methyl-N-propylpyrrolidinium bis(trifluoromethanesulfonyl)imide ([C_3mpyr][TFSI], Solvoionic, France) of about 40 percent (by weight) was mixed with 1M $LiPF_6$ in ethylene carbonate (EC) and diethyl carbonate (DEC) (1:1) in order to make the hybrid electrolyte. The composition of the conventional electrolyte (LP30, Merck) is 1M $LiPF_6$ in ethylene carbonate (EC) and dimethyl carbonate (DMC) whereas the composition of LP40 is 1M $LiPF_6$ in ethylene carbonate (EC) and diethyl carbonate (DEC) (1:1) (LP40, Sigma–Aldrich).

2.2.2 Differential Scanning Calorimetry (DSC) Measurements

DSC measurements were carried out by using TA thermal analysis in the temperature range of –120 ^{o}C to 30 ^{o}C. Electrolyte filling and sealing of the crucibles were carried out inside the glove box, and the sealed crucible was loaded for the study. For the analysis, the temperature sweep rate was kept at 5 degrees per minute.

2.2.3 Density and Viscosity Measurements

Density measurements were carried out using Anton Paar DMA5000. About 1 ml of the electrolyte was injected into the U tube of the density meter, and the measurements were carried out in steps of 5 ^{o}C from 20 to 90 ^{o}C. Viscosity measurements were carried out using the rolling ball method in Anton Paar Lovis 2000ME. The electrolytes were filled into a 10-mm-long capillary that had a diameter 1.5 mm inside the glove box. Steel balls were used for the measurements. The measurements were carried out from 20 ^{o}C to 90 ^{o}C with a tilting angle of 30°.

2.2.4 Ionic Conductivity Measurements

Ionic conductivity measurements were carried out by using a dip cell that contained two platinum wires that were connected to a glass tube, as shown in Figure 2.1. This cell was inserted inside a glass bottle that was filled with the electrolyte and was sealed using a

rubber O ring inside the glove box. The cell was further connected to the Eurotherm 2240E temperature controller and then to the Biologic MTZ-35 impedance analyzer for ionic conductivity measurements. The temperature for the measurements ranged from 298 K to 373 K in steps of 10 K. The ramp rate was 0.5 K/min. The cell constant was determined by using a solution of 0.01M of potassium chloride (KCl).

2.2.5 Thermal Analysis

Thermogravimetric analysis (TGA) and Differential thermal analysis (DTA) were carried out in Mettler–Toledo thermal analysis over a temperature range of 25 ^{o}C–800 ^{o}C in a nitrogen gas atmosphere at a heating rate of 5 K/minute.

2.2.6 FTIR Spectroscopy

FTIR spectroscopy was carried out by using the Perkin Elmer Spectrum 400 FTIR. The sample from the sealed cells was introduced on the Attenuated total reflectance (ATR) crystal and the measurements were carried out. Enough care was taken to lower the exposure of the sample to the environment. The spectra were convoluted by using Gaussian and Lorentzian Fit using Origin 9 software.

2.2.7 Mass Spectrometry

Mass spectrometry by Electrospray Ionization (Micromass Platform II API QMS Electrospray Mass Spectrometer) was carried out by using methanol as a solvent (cone voltage 25 V).

2.2.8 Electrochemical Characterization

Electrochemical potential window studies were carried out using Linear Sweep Voltammetry (LSV) on carbon: binder electrodes (90 percent carbon black and 10 percent PVDF-HFP) at a scan rate of 0.1 mV/s.

Symmetric cell studies were made by using lithium disks (diameter = 1.2 cm) on both sides, separated by polypropylene separators (thickness of 20 micron).

For lithium interfacial studies, symmetric cells were used. After fabrication, the symmetric cells were equilibrated for 24 h before cycling. They were cycled at a current density of 1 mA/cm^2 with 16 minutes of lithium plating and stripping cycles. All the electrochemical measurements in this chapter were carried out at 20 ^{o}C.

2.3 Results and Discussion

2.3.1 Physicochemical Characterization

Physicochemical characterization of the electrolyte can be considered as being the preliminary process in the characterization of the electrolyte. Properties such as density and viscosity are related to the ion conducting property of the electrolyte. The ionic conductivity of the electrolyte is one of the significant properties that determine the performance of any electrochemical device. As a result, a detailed analysis of the density, viscosity, and ionic conductivity of the electrolytes was performed in order to understand the behavior of HE. In addition, due to safety issues, the thermal stability of the HE is discussed in this chapter.

2.3.1.1 Phase Behavior of Electrolytes

The phase behaviour of the electrolytes accounts for its liquidus and solidus temperatures. Although the phase behaviours of the individual constituents are well known in the literature, the properties of the mixtures change significantly. For instance, the liquidus range of the linear carbonates is lowered by the addition of $LiPF_6$ in the system[33].

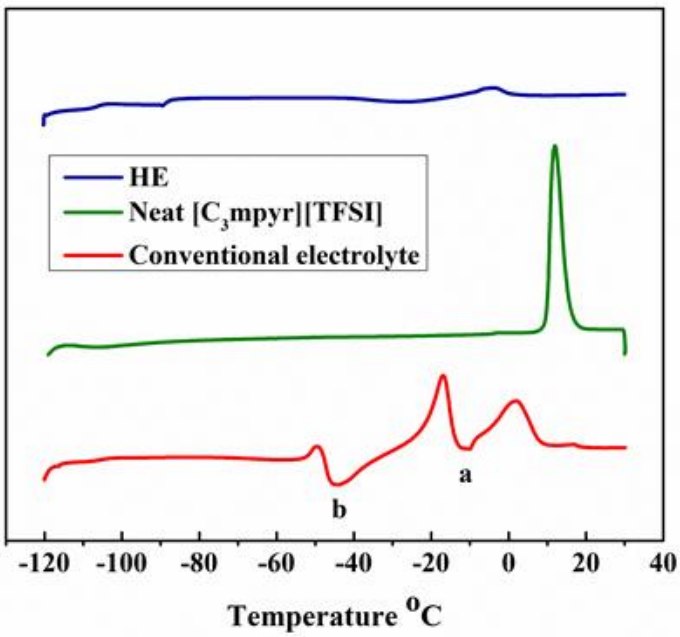

Figure 2.1 *DSC analysis of neat ionic liquid, conventional electrolytes as well as the HE.*

From Figure 2.1, it can be seen that the melting transition occurs at 12 ^{o}C in [C_3mpyr] [TFSI], which matches the data that is mentioned in the literature[34–36]. In the case of the conventional battery electrolyte, many crystallization peaks occur at low temperatures. This can be due to the crystallization of the organic solvents that have high freezing points, which are used in the mixture. It was noted that the melting point of pure ethylene carbonate in the electrolyte mixture is about 37 ^{o}C, whereas the melting point decreases on addition of lithium salt[37]. Further, in a mixture of lithium salts and linear carbonates, the melting point further drops to ~ 10 ^{o}C, which is marked "a" as shown in Figure 2.2. The second downward peak, which is marked "b" in the figure, arises due to the melting of a linear carbonate such as the diethyl carbonate. There is no glass transition in the neat ionic liquid, whereas the transition occurs in the hybrid and conventional electrolytes. It is to be noted that the addition of an ionic liquid did not introduce any significant change in the glass transition temperatures, whereas the crystallization peaks of the conventional battery electrolyte as well as those of neat ionic liquids are suppressed.

2.3.1.2 Ionic Conductivity Studies

The variable temperature ionic conductivity of HE was studied in comparison with the conventional lithium battery electrolyte, as shown in Figure 2.2.

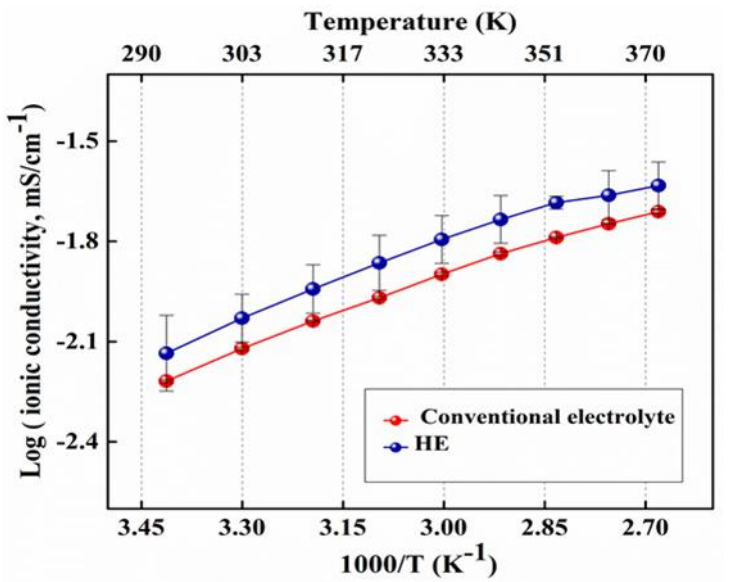

Figure 2.2 *Ionic conductivity of hybrid electrolytes in comparison with the conventional lithium battery electrolyte at various temperatures from 273 to 373 K.*

Ionic conductivity is an important factor in determining the ion transport of the electrolyte. In the case of LiB, the conductivity of the cation (Li^+) is more important than the anion, whereas ionic conductivity estimates the conductivity of both the cations and anions in the system. However, easy instrumentation and non-availability of data on disassociation degree and ion mobility make it an alternative metric to study the transport ability of the electrolyte on the basis of the assumption that the Li cationic conductivity relates at least partially to the conductivity of the system[32]. It was found that the ionic conductivity of the HE was on par (slightly greater) with the electrolytes of conventional batteries. Although there is a slight increase in viscosity when ionic liquids are added to conventional electrolytes, the ionic conductivity of the electrolytes are comparable near room temperature.

2.3.1.3 Walden Plot Analysis

The Walden plot is based on the Walden rule[38]:

$$\Lambda\eta = k \qquad \text{(Equation. 2.1)}$$

where Λ is the molar conductivity, η is the viscosity, and k denotes the temperature-dependent constants. In order to calculate the molar conductivities, we have measured the viscosity and density of the electrolytes, as shown in Figure 2.3. It was observed that the addition of ionic liquids did not significantly increase the density and viscosity of the electrolytes. The Walden plot was drawn by combining the density, viscosity, and ionic conductivity values, as shown in Figure 2.4.

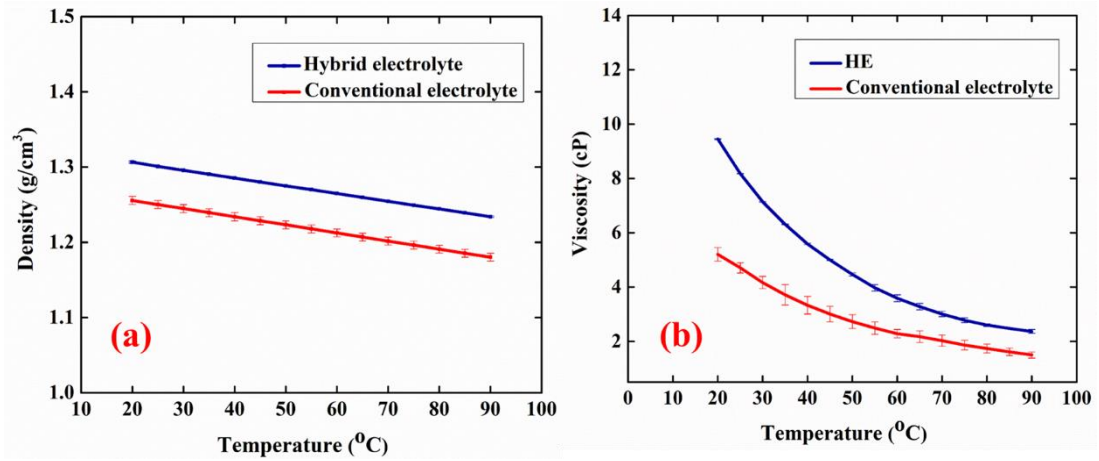

Figure 2.3 *(a) Density and (b) Viscosity of the conventional electrolyte and the HE at various temperatures, from 20 °C to 90 °C.*

KIA dilute aqueous solution of KCl is taken as a reference line for the Walden plot due to the similar-sized ions in KCl[39]. Thus the KCl line separates the graph into two regions such that the solutions that fall above the KCl line exhibit some type of super-ionic mechanism, whereas the solutions that fall below this line are not fully ionizable[39]. Though ionic liquids are composed completely of ions, not all of them are free to contribute to the conductivity of the system[39]. Hence, this Walden rule will help to understand the free as well as the neutral ions in the system. The plot is drawn by using the logarithmic values of both the viscosity and molar conductivity. From Figure 2.4, it can be seen that the HE and conventional have very similar behavior.

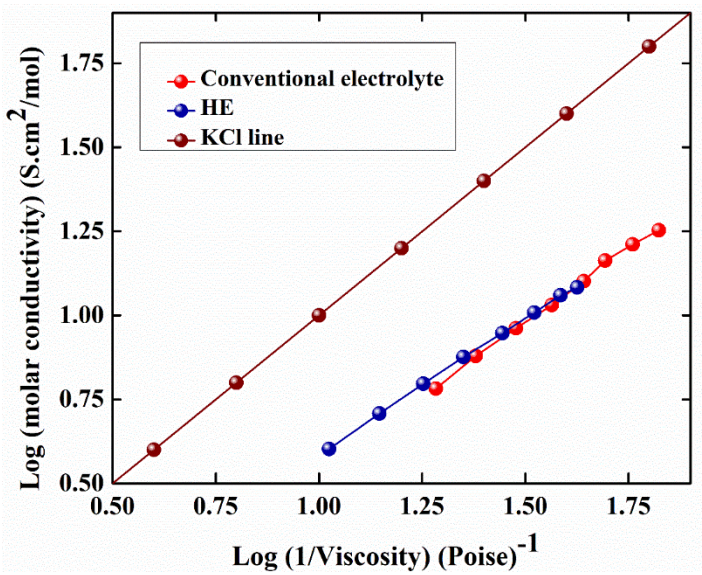

Figure 2.4 *Walden plot of HE in comparison with the conventional lithium battery electrolyte at various temperatures, from 293 to 363 K.*

2.3.1.4 Thermal Analysis

Thermal analysis is a significant study that helps to probe the safety of lithium batteries. The most significant safety threat in the battery is “thermal runaway,” which occurs when local heating reaches a threshold and any further heating in the system can no longer be dissipated. This triggers several adverse exothermic reactions inside the cell, which may lead to the explosion of the battery. Therefore, the thermal stability of the electrolyte is a significant factor in the assessing the safety of battery designs. In the present case, TGA, DTA, and isothermal TGA were measured to understand the effect of the ionic liquid in

the system. Figure 2.5 shows a comparison of TGA studies of the conventional electrolyte, the HE, and the [C_3mpyr] [TFSI] ionic liquid. Consistent with other reports[21,40], the thermal stability of [C_3mpyr] [TFSI] is retained until 377 ^oC.

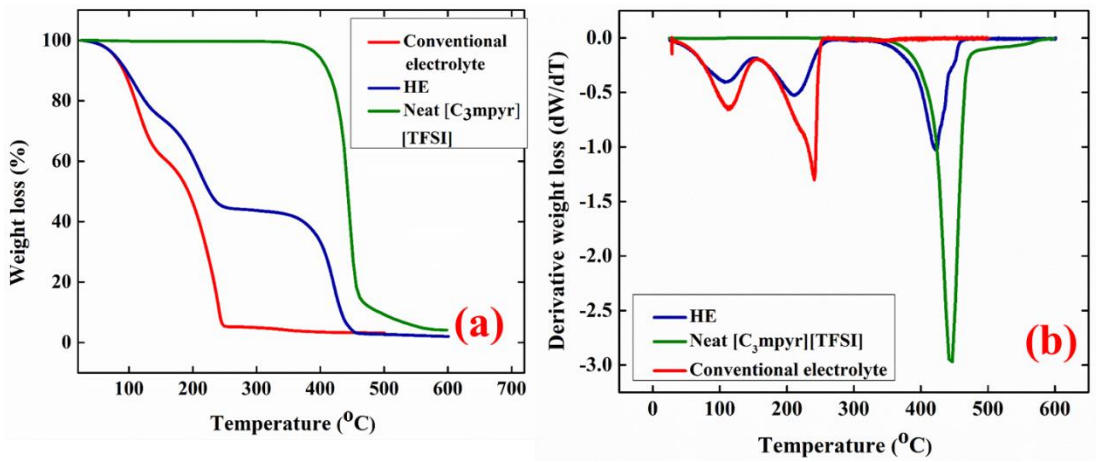

Figure 2.5 *Thermal Analysis of the conventional electrolyte, HE, and neat [C_3mpyr][TFSI] carried out from (a) Thermogravimetric Analysis and (b) Differential thermal Analysis.*

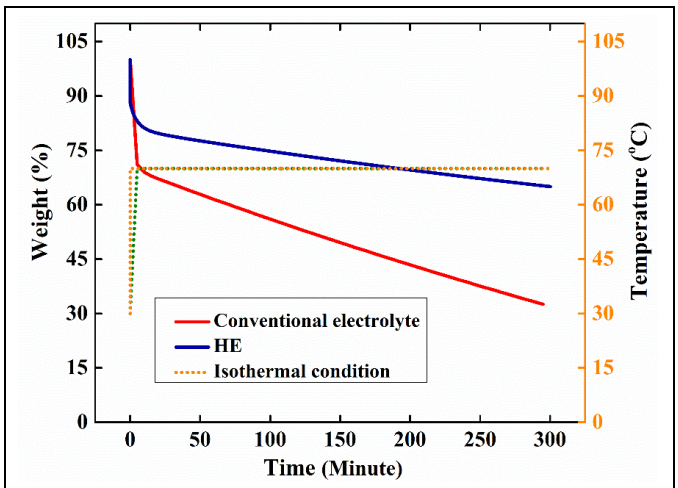

Figure 2.6 *Isothermal TGA of conventional electrolyte and HE at 70 ^oC.*

In the case of the conventional electrolyte and HE, the initial weight losses can be attributed to the evaporation of the volatile solvents that are present in the electrolyte mixture. As reported by Huifeng et al.[22], the addition of an ionic liquid to the conventional electrolyte mixture delays the evaporation of the solvent, which can be observed in the difference in

the mass loss with respect to the temperature. As can be seen in Figure 2.5 (a), almost 95 percent of the electrolyte is lost below 254 ^{o}C in the conventional electrolyte, 445 ^{o}C in HE, and 550 ^{o}C in neat [C_3mpyr] [TFSI]. The partial loss in the HE below 250 °C appears to be related to the loss of the volatile solvent components.

From the DTA that is shown in Figure 2.5, it can be observed that after 111 ^{o}C, an endothermic transition appears in the cases of the conventional electrolyte and the HE curve due to the evaporation/ decomposition of carbonate solvents in the mixture[41]. The thermal instability of $LiPF_6$ is well known for the fact that it decomposes to lithium fluoride salt with the evolution of PF_5 gas[42].

$$LiPF_6 \longrightarrow LiF\downarrow + PF_5\uparrow \qquad \text{(Equation 2.2)}$$

The endothermic peak at 240 ^{o}C can also be attributed to the decomposition of $LiPF_6$ in the mixture, as is evidenced by the peak in the conventional electrolyte as well as in the HE curves.

In isothermal TGA, it was found that after one hour, 60 percent of the conventional electrolyte mass and 77 percent of HE mass were present in the system, whereas, at the end of five hours, 30 percent of the conventional electrolyte mass and 65 percent HE mass are present in the system as shown in Figure 2.6. The mass losses in the HE are inevitable due to the presence of alkyl carbonates in the system, whereas the extent of mass loss is controlled by the presence of ionic liquids in the system. In short, it is apparent that the ionic liquid addition imparts better thermal stability to the electrolytes.

2.3.1.5 Lithium-ion Solvation

Lithium-ion solvation plays a major role in the understanding of the SEI that is formed on the anode-electrolyte interface in LiB[8,13,27]. In general, three of the most commonly seen forms of salt-solvent interaction are shown in Figure 2.7.

1. *Solvent-separated ion pair (SSIP)*

   The SSIP is formed when the cation and anion of the salt are capable of better disassociation, and the solvent molecules surround the ions individually[37]. These solvated entities are comparatively smaller than other types of solvation. This type of solvation is common in LiB due to their smaller size and charge[37].

2. *Conjugated ion pair (CIP)*

   In CIP, the ions are not well disassociated, and the solvent molecules surround the whole salt molecule.

3. *Aggregates (AGG)*

   In the case of AGG type of interaction, more than one salt pair is surrounded by the solvent species.

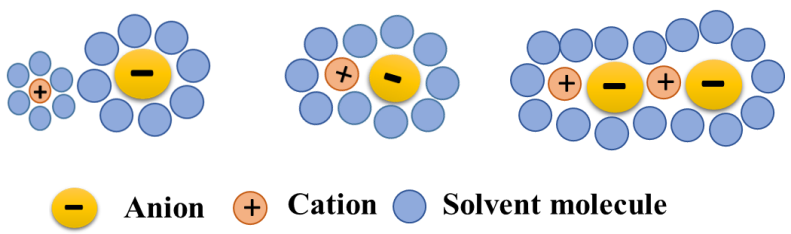

Figure 2.7 *Schematic representation of different forms of salt-solvent interactions.*

Seo et al.[43] reported that solvation in lithium battery electrolytes exists both in SSIP and CIP forms. SSIP was found in electrolytes that had lower lithium-ion solvation (< 1.2 M), whereas CIP was found in electrolytes that had higher lithium salt concentrations (> 2 M).

In this chapter, attempts were made to understand the solvation phenomenon that occurs in HE. The focus was on developing an understanding of whether the usual lithium solvation is altered by the addition of a significant amount of ionic liquid in the conventional electrolyte or not. In order to have proper understanding on solvation, FTIR and mass spectrometry studies were carried out in this subsection.

2.3.1.5.1 FTIR Analysis

The FTIR analysis of the HE in comparison with conventional electrolyte is shown in Figure 2.9. Closer analysis of this spectrum reveals the carbonyl absorptions, C=O, including the solvent coordinated as well as the uncoordinated regions. As reported in the literature[13,43], the coordinated peaks of EC and DEC are found at 1805 and 1715 cm^{-1}, whereas the uncoordinated peaks of EC and DEC are reported at 1755 and 1724 cm^{-1}.

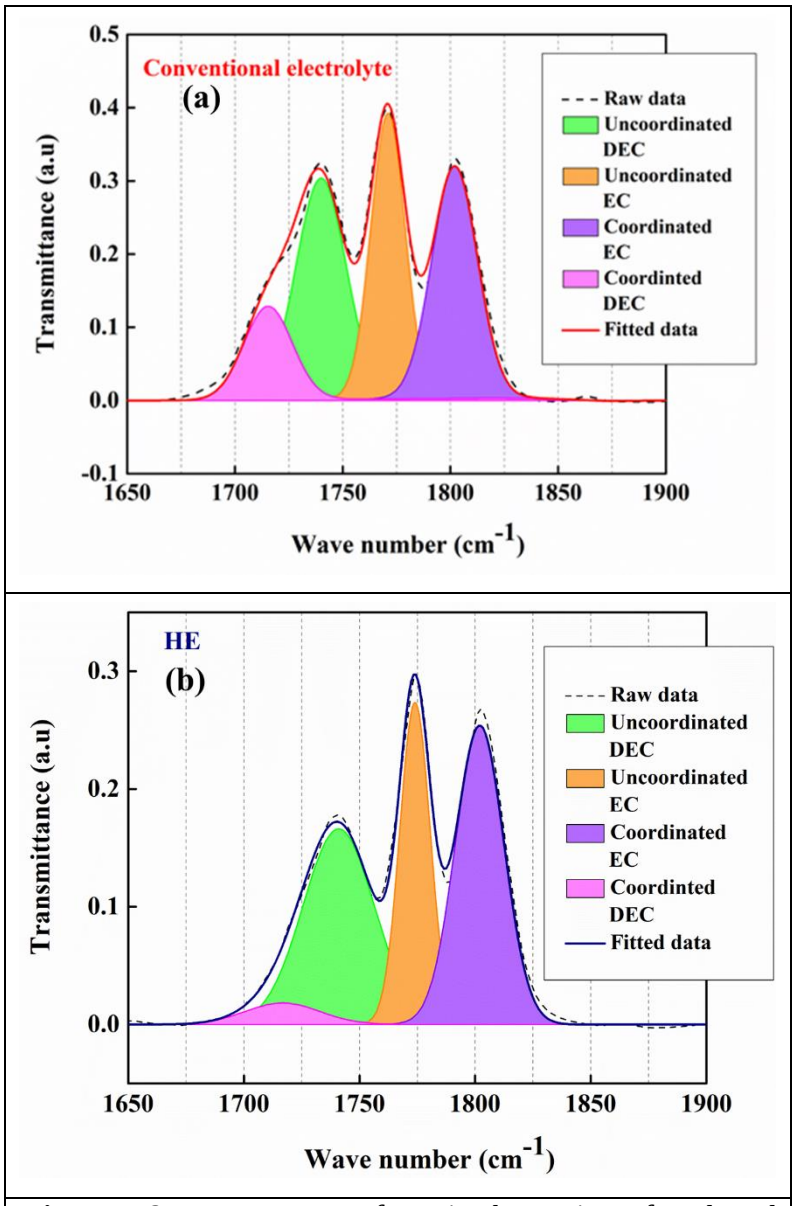

Figure 2.8 *FTIR spectra of HE in the region of carbonyl absorptions in comparison with the conventional electrolyte showing coordinated and uncoordinated bands.*

In the present case, we could observe the coordinated peaks of EC and DEC at 1802 and 1715 cm^{-1}, whereas the uncoordinated peaks of EC and DEC are seen at 1765 and 1735 cm^{-1}. We believe the minor changes in the peak positions may arise due to the difference in the operating conditions. The coordination of carbonates with the lithium ions is also observed in the HE as shown in Figure 2.8 (b). It can be seen that the coordination by DEC (peak at 1715 cm^{-1}) is lower in the HE, as compared to the conventional electrolyte. This may suggests some tendency towards participation of the ionic liquid anion in the co-ordination of lithium ion. The EC peaks show strong evidence of co-ordination by EC in

both HE and LP40 however, as discussed in detail by Seo et al.[43] due to overlapping issues the observations of the EC coordination cannot quantified further in the FTIR analysis. Aguilera et al. reported that organic carbonates can preferably solvate the lithium-ions when their concentration is above 25 percent in the solution[30] and this appears to be the case here. To further investigate the lithium solvation in the presence of the ionic liquid in the system mass spectroscopic studies were undertaken as described in the next section.

2.3.1.5.2 Mass Spectroscopy Studies

Mass spectrometric studies were carried out as shown in Figure 2.9. Electrospray ionization (ESI^+) mass spectroscopy is performed to add further evidence to the previously obtained spectroscopic data, because band-overlapping issues in Raman spectroscopy and FTIR spectroscopy can be circumvented by this technique[44].

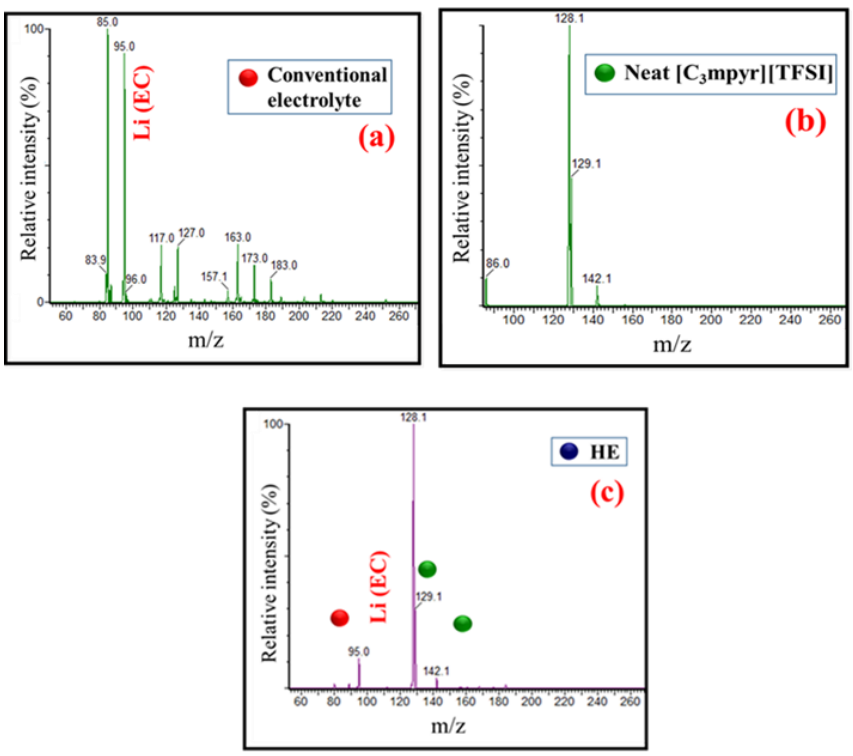

Figure 2.9 *Mass spectra of the electrolytes represented for an understanding of the ion coordination in the system (a) conventional electrolyte, (b) neat [C3mpyr][TFSI], and (c) HE.*

In addition, it was reported that the solvated ions in the first solvation sheath will not be disturbed during the first MS ionization process[8,44]. The current study confirms the

previous observation of the continued coordination of Li+ by the carbonate molecules even in the presence of the ionic liquid in the HE, though there is a suggestion of slightly lower participation of DEC in the FTIR. The preferential solvation of carbonate species, and EC in particular, in HE can be justified on the basis of their high dielectric constants[32].

2.3.2 Electrochemical Characterization

In addition to the physicochemical studies, an initial electrochemical characterization was carried out in order to have a preliminary understanding of the HE system. In this section, as mentioned earlier, the electrochemical potential window and electrode-electrolyte interfacial characteristics were studied. Since the linear carbonates will not contribute to any significant electrochemical performance[32], the performances of HE in this section can be compared with the conventional electrolyte (LP30).

2.3.2.1 LSV Studies

The electrochemical potential stability of the electrolytes needs to be understood in order to have an appropriate understanding of the electrochemical processes that occur in the system.

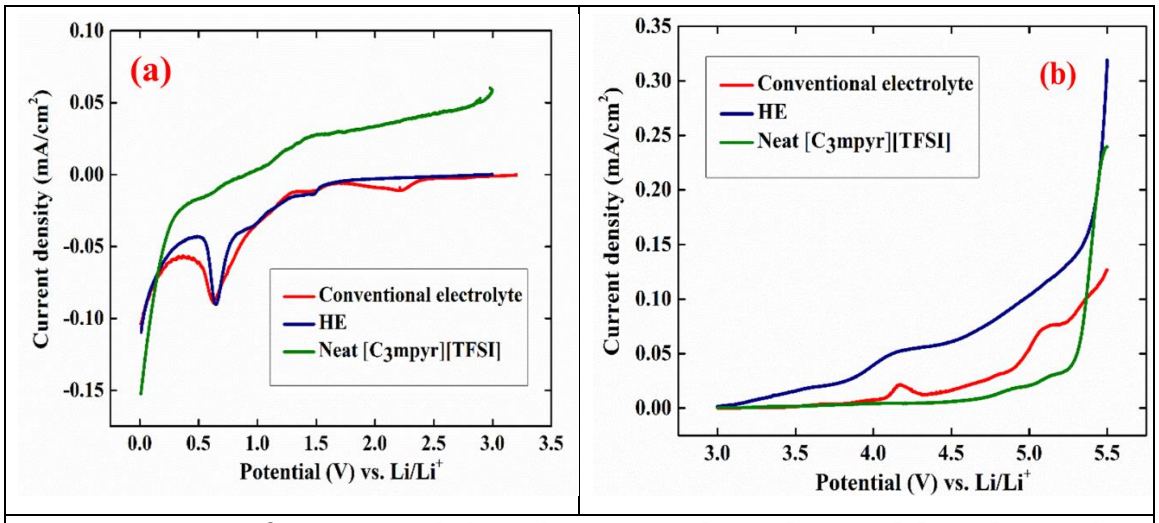

Figure 2.10 *LSV of conventional electrolyte, HE, and neat [C_3mpyr] [TFSI] on carbon binder-coated Copper current collector (swept from 2.5 V to 0.01 V* vs. *Li/Li$^+$) and Aluminum current collector (swept from 3 V to 5.5 V* vs. *Li/Li$^+$).*

This will further help in the understanding of the working mechanism of the batteries. There are several approaches to the study of the electrochemical potential window of the electrolytes by using voltammetry. It is customary to study, at a preliminary level, the

electrolyte potential window on inert electrodes such as platinum or on a glassy carbon electrode[45,46]. However, the behaviour of the electrolyte differs when it is subjected to practical conditions in which the current collector metal, carbon, and binder in the electrolyte system plays a role[47].

Though the literature reports the potential stability of the conventional electrolyte and the neat ionic liquid in inert electrodes, the intention here was to extend the studies to the real environment. As mentioned earlier, aluminum is used as a cathodic current collector and copper as the anodic current collector due to their stability in the anodic and cathodic regions. Since carbon and the binder serve as the common ingredient in the electrode, the working electrode used in the present work was a mixture of 90 percent carbon and 10 percent binder coated onto the respective current collectors.

Figure 2.10 presents the potential window of the conventional electrolyte, HE, and neat [C_3mpyr][TFSI] on the respective current collectors. In the cathodic regime, the potential was swept from 2.5–0.01 V vs. Li/Li^+ on the copper current collector. The reduction peak found at 0.65 V vs. Li/Li^+ may be due to the SEI formation that occurs on the electrode. It should be noted here that SEI formation of the lithium battery electrolyte on the graphite electrode occurs at potentials close to 0.9 V vs. Li/Li^+ [11]. In the present case, the shift to the lower potential may be due to the difference in the super P carbon and graphite surfaces[11,47]. In the case of neat [C_3mpyr][TFSI], the voltage current profile did not show any reduction peaks in the potential of our interest. Hence, it can be inferred that the main observation in the present case is that no significant decomposition (interference) of the ionic liquid cation occurs in the HE, which helps us to understand that the nature of SEI will not be disturbed by the presence of the ionic liquid in the system.

In the anodic regime, it was reported that the electrochemical potential stability of the ionic liquids that had pyrrolidinium cations was greater than 5V in comparison Li/Li^+ on inert electrodes such as platinum or glassy carbon. Similar behaviour was observed in neat [C_3mpyr][TFSI] that was cycled on carbon and binder electrodes in which the current density started to increase at potentials > 5.2 V when compared to Li/Li^+. However, in the conventional electrolyte, small humps at 4.2 V (in comparison to Li/Li^+) may be due to the passivation reaction on the aluminum substrate[48], and the hump at 4.8 V (in comparison to Li/Li^+) may be due to the decomposition of alkyl carbonates in the electrolyte[49]. However, in the case of HE, similar humps were not found at those potentials[49]. The main breakdown

of HE occurs at potentials > 5.45 V (in comparison to Li/Li^+), which can be due to the breakdown of [C_3mpyr] [TFSI], as seen earlier. These behaviors are investigated in more detail in the following chapters.

2.3.2.2 Transference Number Measurements

Transference number or transport number of an ionic species is defined as the fraction of the total current carried by it in an electrolyte. In lithium-ion batteries, the transference number of the lithium ion plays a significant role in the performance kinetics. A number of techniques such as potentiostatic polarization (PP), galvanostatic polarization (GP), very low frequency impedance spectroscopy (VLFIS), emf (electromotive force) method, and pulse-field NMR were used to determine the transference number of non-aqueous electrolytes especially those containing lithium salts[50–52,29,53,19,54–56]. However, accurate data on the transport number measurements are very rare due to experimental challenges[50,57]. Table 2.1 presents the transference numbers reported in literatures for common lithium battery electrolytes at room temperature using various measurement techniques.

In this work, transference number of HE was measured at room temperature using the potentiostatic polarisation method as proposed by Bruce et al[58,59]. The measurement was carried out by polarising lithium symmetric cell to a potential difference of 10 mV. The measurement was carried out until the system reached a steady state. EIS measurements were carried out to measure the resistance before and after the polarization measurements. The initial and steady state current values were noted. The plot of current versus time and the Nyquist plot are shown in Figure 2.11.

The lithium transference number, (t_{Li^+}) is calculated further using the following Bruce–Vincent equation[58],

$$t_{Li^+} = \frac{I_s(\Delta V - I_0 R_0)}{I_0(\Delta V - I_s R_s)} \qquad \text{(Equation. 2.3)}$$

where,

ΔV is the applied potential difference in Volt,

I_0 is the initial current in Ampere,

I_s is the steady-state current in Ampere,

R_0 is the initial resistance in Ohm,

R_s is the steady-state resistance in Ohm.

Table 2.1 *Transference numbers reported in literatures for common lithium battery electrolytes at room temperature using various measurement techniques.*

S.No	Electrolyte solution	Method	Salt concentration (mol/Kg)	Lithium transport number (t_{Li^+}) at room temperature	References
1.	$LiPF_6$ in EC/PC/DMC	GP	0.68	0.38±0.025	50
2.	$LiPF_6$ in EC/PC/DMC	PP	0.68	0.39±0.024	50
3.	$LiPF_6$ in EC/DEC	PP	0.68	0.34±0.0053	50
4.	$LiPF_6$ in EC/DEC	GP	0.76	0.24±0.0087	50
5.	$LiPF_6$ in EC/DEC	EMF	0.76	0.28±0.0003	50
6.	$LiPF_6$ in PC	PP	1.5 0.25	0.37 0.557	50
7.	$LiPF_6$ in PC	NMR	0.25 1.5	0.505 0.337	50
8.	$LiBF_4$ in PC	PP	0.68	0.35	50
9.	$LiPF_6$ in EC/DMC	NMR	0.077-1.152	0.37-0.43	19
10.	$LiPF_6$ in EC/DMC	NMR	0.78	0.38±0.01	52
11.	$LiPF_6$ in EC/DMC	VLFIS	1	0.071±0.01	56
12.	LiTFSI in [C_4mpyr][TFSI]	PP	0.2	0.22	51
13.	0.3 M LiTFSI in 0.5 wt. % [C_4mpyr][TFSI]+ 0.5 wt. % PC	NMR	--	~0.06	60
14.	*x*LiTFSI in (1-x) [C_4mpyr][TFSI] mixture with x =0.377	NMR	--	0.132	61

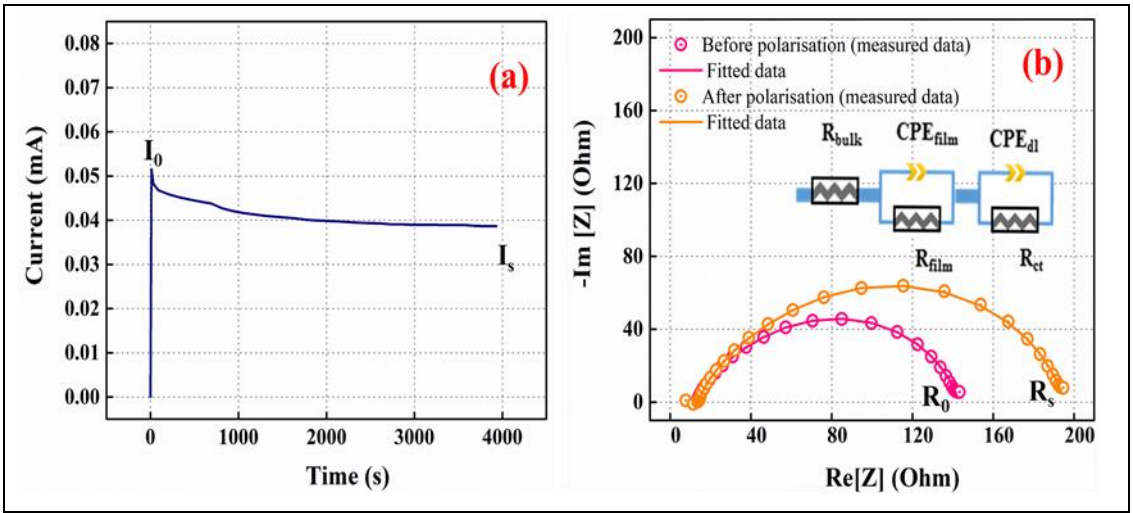

Figure 2.11 *(a) Plot of current versus time of HE for an applied potential of 10 mV in a lithium symmetric cell and (b) Nyquist plot of HE in a lithium symmetric cell before and after polarisation. The corresponding equivalent circuit is presented in the inset figure.*

The transference number of HE calculated using the Equation 2.3 was found to be 0.32± 0.0483. The calculated number lies in range with the values reported for the common electrolyte mixtures as shown in Table 2.1.

2.3.2.3 Lithium Interfacial Studies

In order to study the compatibility of lithium metal with HE, lithium symmetrical cells were made by using lithium electrodes at both sides. The aim of this study was to understand the changes that occur at the interfaces in the presence and the absence of current flow (ie at open circuit voltage (OCV)). Figure 2.12 shows the comparison of the overpotential profile of the conventional electrolyte, HE, and [C_3mpyr] [TFSI] at the 1st, 10th, 30th, 50th, 70th, and 100th cycles. The neat IL shows the highest overpotential due to its high viscosity, whereas the relatively lower overpotential of HE in comparison to the conventional electrolyte may be due to the synergistic effect of the ionic liquid, Li^+, and the PF_6^- ions in the mixture. Also, as supported by an earlier report[62], the TFSI anion, with its weaker basicity, may facilitate more rapid nucleation and growth kinetics during the deposition cycle.

Electrochemical impedance measurements (EIS) were carried out before cycling as well as after the 1st, 10th, 30th, 50th, 70th, and 100th platting/stripping cycles, in the frequency

range of 1 MHz–10 mHz, as shown in Figure 2.13.

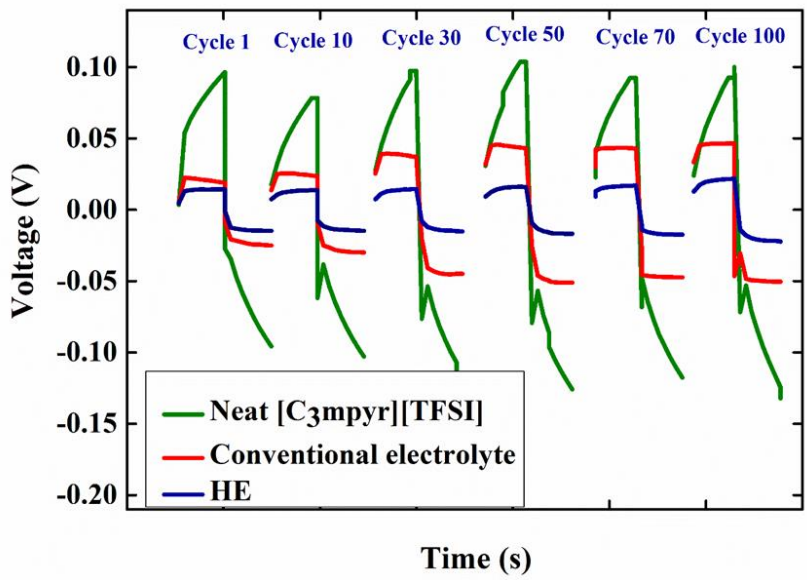

Figure 2.12 *Overpotential profile of the conventional electrolyte, HE, and [C_3mpyr] [TFSI] electrolytes on lithium electrodes at a polarization current density of 1mA/cm^2 with 16 minutes of each plating and stripping cycle at 20 ^{o}C.*

The obtained Nyquist plots were fitted by using an equivalent circuit that is presented as an inset in Figure 2.13. The use of a Constant Phase Element (CPE) instead of a capacitor in the equivalent circuit was due to the depressed semicircles in the system[63]. The Warburg diffusion impedance is not shown in the impedance plot in order to have a clearer view of the interfacial resistance after successive cycles. The interfacial resistance in this context takes into account both the passivation film resistance as well as the charge transfer resistance[64]. Significantly, it was found that the interfacial resistance of HE is lower than that of conventional electrolyte and [C_3mpyr] [TFSI], which is consistent with the lower overpotentials that are observed in Figure 2.12. Thus, it appears that in HE, the combination of the ionic liquid with the alkyl carbonate solvents provides favorable properties when compared to the combination of the two other electrolytes.

In the Nyquist plots (Figure 2.13), it was found that in the initial few cycles there is a slight decrease in the interfacial resistance of the cell when compared to the resistance before cycling. This can be explained by the initial occurrence of a porous lithium film on the surface, which increases the surface area of the electrode, thereby decreasing the resistance. Later, dissolution of this porous layer takes place by the formation of the SEI, which

increases the interfacial impedance[65]. The increase in the interfacial resistance with cycling is quite common; however, the difference between the initial interfacial resistance and the final interfacial resistance is small in HE in comparison to the other two cases. The increase in resistance after 100 cycles was in the order of 100 Ω in HE in comparison to 150 Ω in the conventional electrolyte, which can be attributed to the better stability of the interface upon cycling. The observations made from these EIS studies are consistent with the overpotential profiles shown in Figure 2.12.

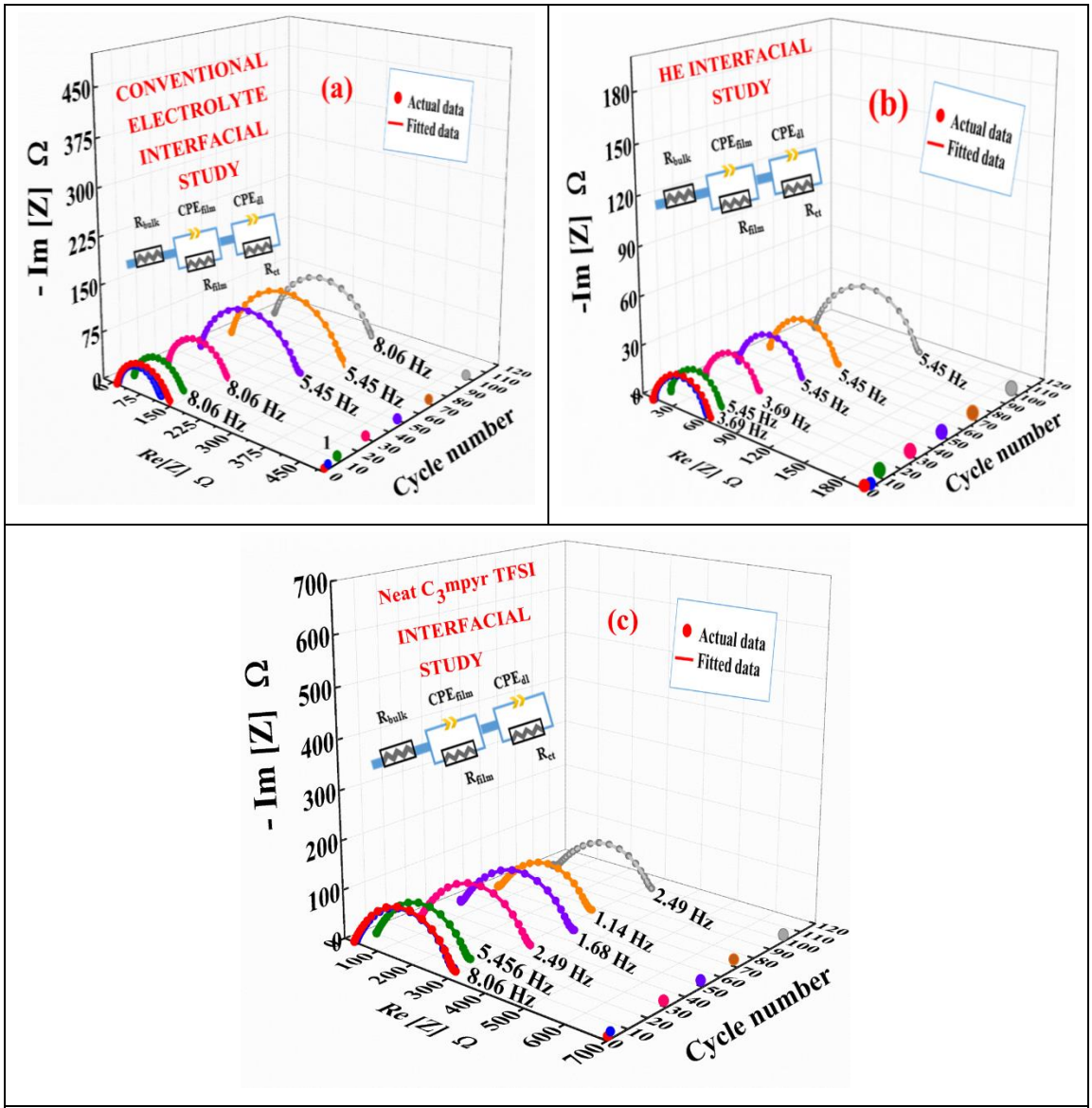

Figure 2.13 *Nyquist plot of the lithium symmetric cells with (a) conventional electrolyte, (b) HE and (c) Neat [C3mpyr][TFSI] electrolytes along with the corresponding equivalent circuits.*

We also studied the evolution of the interfacial resistance of Li/electrolyte/Li symmetric cells along with the conventional electrolyte and HE upon aging at 20 ^{o}C. The impedance of these cells was constantly monitored. Figure 2.14 shows the variation of the interfacial resistance in the symmetric cells when the conventional electrolyte and HE are used. It was observed that the interfacial resistance increases upon storage. It was also found that, in the case of the HE system, the increase in the interfacial resistance with time was quite high in the initial few days, but after 15 days it became quite constant.

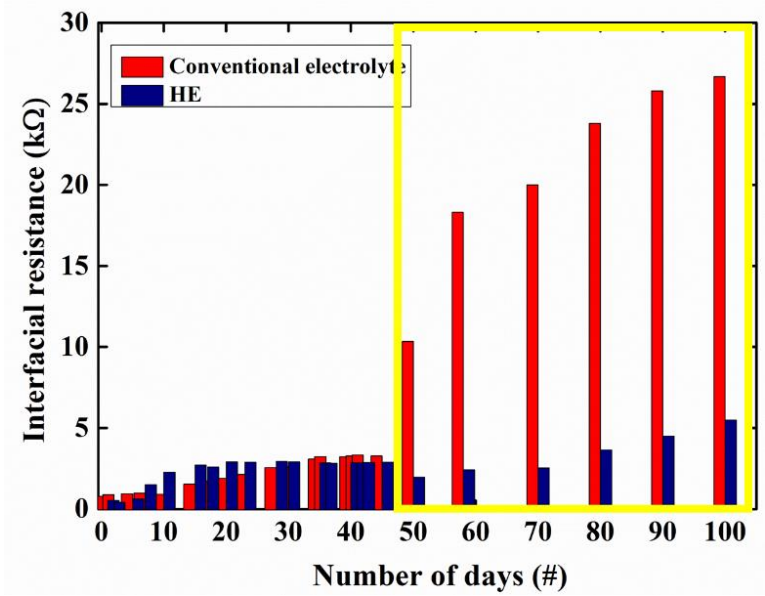

Figure 2.14 *Variation of interfacial resistance upon aging in symmetric cells in a conventional electrolyte and HE mixtures. The resistance values after the yellow highlighted region was measured to check the effect of short polarization at 1 mA/cm^2 for 60 minutes.*

The trend was such that from 1 to 15 days, the increases in the interfacial resistance for the conventional electrolyte and HE were 747 Ω and 2174 Ω, whereas, after 45 days, the interfacial resistances were 2486 Ω and 2353 Ω, respectively. It was also noted that after 10 to 15 days of storage, an extra semi-circle was clearly seen in the case of the HE system; however, this was not observed in the case of the conventional electrolyte. This shows that the ionic liquid component plays a role in the development of interfacial layers in this system, in addition to the conventional electrolyte components. After 45 days of storage, in order to check the nature of the surface layer that was formed; we disturbed the system

for 60 minutes with a current density of 1 mA/cm^2 and left it aging at 20 ^{o}C. The impedance of these cells was then monitored every 10 days. The increase in the interfacial resistance in the case of the conventional electrolyte was quite high, whereas in HE the increase was quite low. The increase in resistance in the case of the conventional electrolyte may be attributed to the presence of the PF_6 anion in the system. On the other hand, it can be expected that the combination of PF_6 and the bis(trifluoromethanesulfonyl)imide anion lowers the interfacial resistance in the HE system[62]. At the end of 100 days, it appears that the HE is capable of forming a stable interface with a low interfacial resistance, when compared to the conventional electrolyte system.

2.4 Concluding Remarks

In this chapter, we have studied the physicochemical properties and electrochemical properties of the HE that contains alkyl carbonate electrolytes. The physicochemical properties of HE were validated along with the conventional electrolyte for comparison studies. Further, the solution structure was also examined with the help of spectroscopic analysis. It was found that the lithium ion in the HE also showed preferential solvation by ethylene carbonate. This study supports the claim at a proportion of 40 percent ionic liquid in the system, the ionic liquid will not interfere with the lithium coordination in the system. Further electrochemical evaluation of the interfaces reveals the synergistic effect of the HE, which elicits better interfacial stability. In short, the initial characterization studies that were carried out in this chapter encouraged further understanding of the HE system.

2.5 References

(1) Armand, M.; Tarascon, J.-M. Building Better Batteries. Nature 2008, 451, 652–657.

(2) Etacheri, V.; Marom, R.; Elazari, R.; Salitra, G.; Aurbach, D. Challenges in the Development of Advanced Li-Ion Batteries: A Review. *Energy Environ. Sci.* **2011**, *4*, 3243–3262.

(3) Dunn, B.; Kamath, H.; Tarascon, J.-M. Electrical Energy Storage for the Grid: A Battery of Choices. *Science (80-.).* **2011**, *334*, 928–935.

(4) E. Peter Roth and Christopher J. Orendorff. How Electrolytes Influence Battery Safety. *Electrochem. Soc. Interface* 45–49.

(5) Scrosati, B.; Garche, J. Lithium Batteries: Status, Prospects and Future. *J. Power*

Sources **2010**, *195*, 2419–2430.

(6) Xu, K. Electrolytes and Interphases in Li-Ion Batteries and Beyond. *Chem. Rev.* **2014**, *114*, 11503–11618.

(7) Edström, K.; Gustafsson, T.; Thomas, J. The Cathode-Electrolyte Interface in a Li-Ion Battery. In *Lithium-Ion Batteries Solid-Electrolyte Interphase*; Balbuena, P. B.; Wang, Y., Eds.; Imperial College Press, 2004; pp. 337–364.

(8) von Cresce, A.; Xu, K. Preferential Solvation of Li^+ Directs Formation of Interphase on Graphitic Anode. *Electrochem. Solid-State Lett.* **2011**, *14*, A154.

(9) Verma, P.; Maire, P.; Novák, P. A Review of the Features and Analyses of the Solid Electrolyte Interphase in Li-Ion Batteries. *Electrochim. Acta* **2010**, *55*, 6332–6341.

(10) Cheng, X.-B.; Zhang, R.; Zhao, C.-Z.; Wei, F.; Zhang, J.-G.; Zhang, Q. A Review of Solid Electrolyte Interphases on Lithium Metal Anode. *Adv. Sci.* **2016**, *3*, 1500213.

(11) An, S. J.; Li, J.; Daniel, C.; Mohanty, D.; Nagpure, S.; Wood, D. L. The State of Understanding of the Lithium-Ion-Battery Graphite Solid Electrolyte Interphase (SEI) and Its Relationship to Formation Cycling. *Carbon N. Y.* **2016**, *105*, 52–76.

(12) Borodin, O.; Olguin, M.; Ganesh, P.; Kent, P. R. C.; Allen, J. L.; Henderson, W. A. Competitive Lithium Solvation of Linear and Cyclic Carbonates from Quantum Chemistry. *Phys. Chem. Chem. Phys.* **2016**, *18*, 164–175.

(13) Nie, M.; Abraham, D. P.; Seo, D. M.; Chen, Y.; Bose, A.; Lucht, B. L. Role of Solution Structure in Solid Electrolyte Interphase Formation on Graphite with $LiPF_6$ in Propylene Carbonate. *J. Phys. Chem. C* **2013**, *117*, 25381–25389.

(14) Appetecchi, G. B.; Montanino, M.; Passerini, S. Ionic Liquid-Based Electrolytes for High Energy, Safer Lithium Batteries. *ACS Symp. Ser.* **2012**, *1117*, 67–128.

(15) MacFarlane, D. R.; Forsyth, M.; Howlett, P. C.; Pringle, J. M.; Sun, J.; Annat, G.; Neil, W.; Izgorodina, E. I. Ionic Liquids in Electrochemical Devices and Processes: Managing Interfacial Electrochemistry. *Acc. Chem. Res.* **2007**, *40*, 1165–1173.

(16) Matsumoto, H.; Sakaebe, H.; Tatsumi, K.; Kikuta, M.; Ishiko, E.; Kono, M. Fast Cycling of Li/LiCoO2 Cell with Low-Viscosity Ionic Liquids Based on

Bis(fluorosulfonyl)imide [FSI]−. *J. Power Sources* **2006**, *160*, 1308–1313.

(17) Ueno, K.; Murai, J.; Ikeda, K.; Tsuzuki, S.; Tsuchiya, M.; Tatara, R.; Mandai, T.; Umebayashi, Y.; Dokko, K.; Watanabe, M. Li^+ Solvation and Ionic Transport in Lithium Solvate Ionic Liquids Diluted by Molecular Solvents. *J. Phys. Chem. C* **2015**.

(18) Le, M. L. P.; Cointeaux, L.; Strobel, P.; Leprêtre, J.-C.; Judeinstein, P.; Alloin, F. Influence of Solvent Addition on the Properties of Ionic Liquids. *J. Phys. Chem. C* **2012**, *116*, 7712–7718.

(19) Valøen, L. O.; Reimers, J. N. Transport Properties of LiPF[sub 6]-Based Li-Ion Battery Electrolytes. *J. Electrochem. Soc.* **2005**, *152*, A882.

(20) Kanamura, K. Anodic Oxidation of Nonaqueous Electrolytes on Cathode Materials and Current Collectors for Rechargeable Lithium Batteries. *J. Power Sources* **1999**, *81–82*, 123–129.

(21) Theivaprakasam, S.; MacFarlane, D. R.; Mitra, S. Electrochemical Studies of N-Methyl N-Propyl Pyrrolidinium Bis(trifluoromethanesulfonyl) Imide Ionic Liquid Mixtures with Conventional Electrolytes in LiFePO4/Li Cells. *Electrochim. Acta* **2015**, *180*, 737–745.

(22) Li, H.; Pang, J.; Yin, Y.; Zhuang, W.; Wang, H.; Zhai, C.; Lu, S. Application of a Nonflammable Electrolyte Containing Pp13TFSI Ionic Liquid for Lithium-Ion Batteries Using the High Capacity Cathode Material Li[Li0.2Mn0.54Ni0.13Co0.13]O2. *RSC Adv.* **2013**, *3*, 13907–13914.

(23) Fukushima, T.; Matsuda, Y.; Hashimoto, H.; Arakawa, R. Solvation of Lithium Ions in Organic Electrolytes of Primary Lithium Batteries by Electrospray Ionization-Mass Spectroscopy. *J. Power Sources* **2002**, *110*, 34–37.

(24) Matsuda, Y.; Fukushima, T.; Hashimoto, H.; Arakawa, R. Solvation of Lithium Ions in Mixed Organic Electrolyte Solutions by Electrospray Ionization Mass Spectroscopy. *J. Electrochem. Soc.* **2002**, *149*, A1045–A1048.

(25) Han, S.-D.; Borodin, O.; Seo, D. M.; Zhou, Z.-B.; Henderson, W. a. Electrolyte Solvation and Ionic Association: V. Acetonitrile-Lithium Bis(fluorosulfonyl)imide (LiFSI) Mixtures. *J. Electrochem. Soc.* **2014**, *161*.

(26) Cazzanelli, E.; Croce, F.; Appetecchi, G. B.; Benevelli, F.; Mustarelli, P. Li[sup +] Solvation in Ethylene Carbonate–propylene Carbonate Concentrated Solutions: A Comprehensive Model. *J. Chem. Phys.* **1997**, *107*, 5740.

(27) Xu, K.; von Wald Cresce, A. Li+-Solvation/desolvation Dictates Interphasial Processes on Graphitic Anode in Li Ion Cells. *J. Mater. Res.* **2012**, *27*, 2327–2341.

(28) von Wald Cresce, A.; Borodin, O.; Xu, K. Correlating Li $^{+}$ Solvation Sheath Structure with Interphasial Chemistry on Graphite. *J. Phys. Chem. C* **2012**, *116*, 26111–26117.

(29) Wohde, F.; Bhandary, R.; Moldrickx, J. M.; Sundermeyer, J.; Schönhoff, M.; Roling, B. Li+ Ion Transport in Ionic Liquid-Based Electrolytes and the Influence of Sulfonate-Based Zwitterion Additives. *Solid State Ionics* **2016**, *284*, 37–44.

(30) Aguilera, L.; Scheers, J.; Matic, A. Enhanced Low-Temperature Ionic Conductivity via Different Li + Solvated Clusters in Organic Solvent/ionic Liquid Mixed Electrolytes. *Phys. Chem. Chem. Phys.* **2016**, *18*, 25458–25464.

(31) Monti, D.; Jónsson, E.; Palacín, M. R.; Johansson, P. *Ionic Liquid Based Electrolytes for Sodium-Ion Batteries: Na+ Solvation and Ionic Conductivity*; 2014; Vol. 245.

(32) Xu, K. Nonaqueous Liquid Electrolytes for Lithium-Based Rechargeable Batteries. *Chem. Rev.* **2004**, *104*, 4303–4418.

(33) Sloop, S. E.; Pugh, J. K.; Wang, S.; Kerr, J. B.; Kinoshita, K. Chemical Reactivity of PF[sub 5] and LiPF[sub 6] in Ethylene Carbonate/Dimethyl Carbonate Solutions. *Electrochem. Solid-State Lett.* **2001**, *4*, A42.

(34) Kunze, M.; Jeong, S.; Paillard, E.; Winter, M.; Passerini, S. Melting Behavior of Pyrrolidinium-Based Ionic Liquids and Their Binary Mixtures. *J. Phys. Chem. C* **2010**, *114*, 12364–12369.

(35) Huang, J.; Hollenkamp, A. F. Thermal Behavior of Ionic Liquids Containing the FSI Anion and the Li+ Cation. *J. Phys. Chem. C* **2010**, *114*, 21840–21847.

(36) Zhou, Q.; Henderson, W. A.; Appetecchi, G. B.; Montanino, M.; Passerini, S. Physical and Electrochemical Properties of *N* -Alkyl- *N* -Methylpyrrolidinium

Bis(fluorosulfonyl)imide Ionic Liquids: $PY_{13}FSI$ and $PY_{14}FSI$. *J. Phys. Chem. B* **2008**, *112*, 13577–13580.

(37) Foley, M. P.; Seo, D. M.; Worosz, C. J.; Boyle, P. D.; Henderson, W. A.; De Long, H. C.; Trulove, P. C. Phase Behavior and Solvation of Lithium Triflate in Ethylene Carbonate. In *ECS Transactions*; The Electrochemical Society, 2012; Vol. 41, pp. 99–105.

(38) Masahiro Yoshizawa, †; Wu Xu, and; Angell*, C. A. Ionic Liquids by Proton Transfer: Vapor Pressure, Conductivity, and the Relevance of ΔpKa from Aqueous Solutions. **2003**.

(39) MacFarlane, D. R.; Forsyth, M.; Izgorodina, E. I.; Abbott, A. P.; Annat, G.; Fraser, K.; Endres, F.; Abedin, S. Z. El; Smiglak, M.; Metlen, A.; et al. On the Concept of Ionicity in Ionic Liquids. *Phys. Chem. Chem. Phys.* **2009**, *11*, 4962.

(40) Eshetu, G. G.; Jeong, S.; Pandard, P.; Lecocq, A.; Marlair, G.; Passerini, S. Comprehensive Insights into the Thermal Stability, Biodegradability and Combustion Chemistry of Pyrrolidinium-Based Ionic Liquids. *ChemSusChem* **2017**.

(41) Fu, Y.; Zhu, H.; Shen, J. Thermal Decomposition of Dimethoxymethane and Dimethyl Carbonate Catalyzed by Solid Acids and Bases. *Thermochim. Acta* **2005**, *434*, 88–92.

(42) Yang, H.; Zhuang, G. V; Jr., P. N. R. Thermal Stability of LiPF6 Salt and Li-Ion Battery Electrolytes Containing LiPF6. *J. Power Sources* **2006**, *161*, 573–579.

(43) Seo, D. M.; Reininger, S.; Kutcher, M.; Redmond, K.; Euler, W. B.; Lucht, B. L. Role of Mixed Solvation and Ion Pairing in the Solution Structure of Lithium Ion Battery Electrolytes. *J. Phys. Chem. C* **2015**, *119*, 14038–14046.

(44) Zheng, D.; Qu, D.; Yang, X.; Lee, H.; Qu, D. Preferential Solvation of Lithium Cations and Impacts on Oxygen Reduction in Lithium − Air Batteries. *Appl. Mater. Interfaces* **2015**, *7*, 19923–19929.

(45) Huggins, R. Electrolyte Stability Windows and Their Extension. In *Advanced Batteries SE - 16*; Springer US, 2009; pp. 375–392.

(46) Quinn, B. M.; Ding, Z.; Moulton, R.; Bard, A. J. Novel Electrochemical Studies of

Ionic Liquids. *Langmuir* **2002**, *18*, 1734–1742.

(47) Fransson, L.; Eriksson, T.; Edström, K.; Gustafsson, T.; Thomas, J. O. Influence of Carbon Black and Binder on Li-Ion Batteries. *J. Power Sources* **2001**, *101*, 1–9.

(48) Markovsky, B.; Amalraj, F.; Gottlieb, H. E.; Gofer, Y.; Martha, S. K.; Aurbach, D. On the Electrochemical Behavior of Aluminum Electrodes in Nonaqueous Electrolyte Solutions of Lithium Salts. *J. Electrochem. Soc.* **2010**, *157*, A423–A429.

(49) Lombardo, L.; Brutti, S.; Navarra, M. A.; Panero, S.; Reale, P. Mixtures of Ionic Liquid – Alkylcarbonates as Electrolytes for Safe Lithium-Ion Batteries. *J. Power Sources* **2013**, *227*, 8–14.

(50) Zugmann, S.; Fleischmann, M.; Amereller, M.; Gschwind, R. M.; Wiemhöfer, H. D.; Gores, H. J. Measurement of Transference Numbers for Lithium Ion Electrolytes via Four Different Methods, a Comparative Study. *Electrochim. Acta* **2011**, *56*, 3926–3933.

(51) Agostini, M.; Ulissi, U.; Di Lecce, D.; Ahiara, Y.; Ito, S.; Hassoun, J. A Lithium-Ion Battery Based on an Ionic Liquid Electrolyte, Tin-Carbon Nanostructured Anode, and Li2O-ZrO2-Coated Li[Ni0.8Co0.15Al0.05]O2Cathode. *Energy Technol.* **2015**, *3*, 632–637.

(52) Porion, P.; Dougassa, Y. R.; Tessier, C. C.; El Ouatani, L.; Jacquemin, J.; Anouti, M. M. Comparative Study on Transport Properties for LiFAP and LiPF6 in Alkyl-Carbonates as Electrolytes through Conductivity, Viscosity and NMR Self-Diffusion Measurements. *Electrochim. Acta* **2013**, *114*, 95–104.

(53) Ueno, K.; Yoshida, K.; Tsuchiya, M.; Tachikawa, N.; Dokko, K.; Watanabe, M. Glyme-Lithium Salt Equimolar Molten Mixtures: Concentrated Solutions or Solvate Ionic Liquids? *J. Phys. Chem. B* **2012**, *116*, 11323–11331.

(54) Shah, F. U.; Gnezdilov, O. I.; Gusain, R.; Filippov, A. Transport and Association of Ions in Lithium Battery Electrolytes Based on Glycol Ether Mixed with Halogen-Free Orthoborate Ionic Liquid. *Sci. Rep.* **2017**, *7*, 16340.

(55) Gélinas, B.; Natali, M.; Bibienne, T.; Li, Q. P.; Dollé, M.; Rochefort, D. Electrochemical and Transport Properties of Ions in Mixtures of Electroactive Ionic

Liquid and Propylene Carbonate with a Lithium Salt for Lithium-Ion Batteries. *J. Phys. Chem. C* **2016**, *120*, 5315–5325.

(56) Wohde, F.; Balabajew, M.; Roling, B. Li^{+} Transference Numbers in Liquid Electrolytes Obtained by Very-Low-Frequency Impedance Spectroscopy at Variable Electrode Distances. *J. Electrochem. Soc.* **2016**, *163*, A714–A721.

(57) Vardner, J. T.; Ling, T.; Russell, S. T.; Perakis, A. M.; He, Y.; Brady, N. W.; Kumar, S. K.; West, A. C. Method of Measuring Salt Transference Numbers in Ion-Selective Membranes. *J. Electrochem. Soc.* **2017**, *164*, A2940–A2947.

(58) Evans, J.; Vincent, C. A.; Bruce, P. G. Electrochemical Measurement of Transference Numbers in Polymer Electrolytes. *Polymer (Guildf).* **1987**, *28*, 2324–2328.

(59) Bruce, P. G.; Vincent, C. A. Steady State Current Flow in Solid Binary Electrolyte Cells. *J. Electroanal. Chem.* **1987**, *225*, 1–17.

(60) Kühnel, R.-S.; Balducci, A. Lithium Ion Transport and Solvation in N-Butyl-N-methylpyrrolidinium Bis(trifluoromethanesulfonyl)imide− Propylene Carbonate Mixtures. *J. Phys. Chem. C* **2014**, *118*, 5742–5748.

(61) Frömling, T.; Kunze, M.; Schönhoff, M.; Sundermeyer, J.; Roling, B. Enhanced Lithium Transference Numbers in Ionic Liquid Electrolytes.

(62) Fisher, A. S.; Khalid, M. B.; Widstrom, M.; Kofinas, P. Anion Effects on Solid Polymer Electrolytes Containing Sulfur Based Ionic Liquid for Lithium Batteries. *J. Electrochem. Soc.* **2012**, *159*, A592–A597.

(63) *Impedance Spectroscopy: Theory, Experiment, and Applications*; Evgenij, B.; Macdonald, J. R., Eds.; Second.; Wiley, 2005.

(64) Li, M.; Yang, L.; Fang, S.; Dong, S.; Hirano, S.; Tachibana, K. Polymer Electrolytes Containing Guanidinium-Based Polymeric Ionic Liquids for Rechargeable Lithium Batteries. *J. Power Sources* **2011**, *196*, 8662–8668.

(65) Illig, J. *Physically Based Impedance Modelling of Lithium-Ion Cells*; First Edit.; KIT Scientific Publishing, 2014.

Chapter 3

Studies of Hybrid Electrolyte with Lithium Cobalt Oxide Cathode

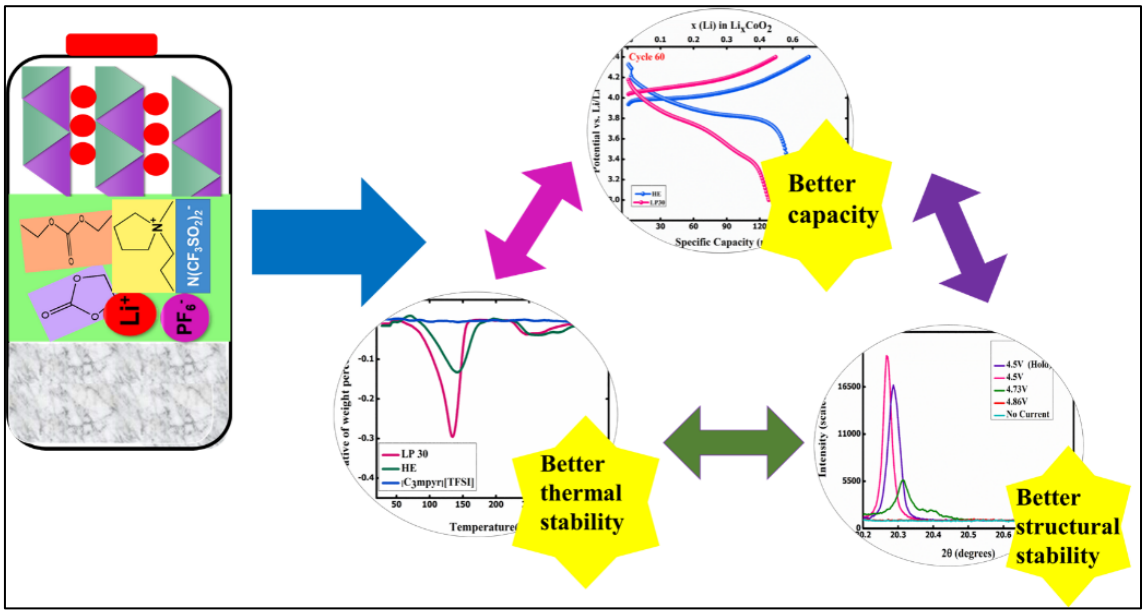

Part of this chapter is published as a journal publication:

Theivaprakasam, S.; Wu, J.; Pramudita, J. C.; Sharma, N.; MacFarlane, D. R.; Mitra, S. Understanding the Behavior of $LiCoO_2$ Cathodes at Extended Potentials in Ionic Liquid–Alkyl Carbonate Hybrid Electrolytes. *J. Phys. Chem. C* **2017**, *121*, 15630–15638.

3.1 Introduction

One of the current energy challenges is to make batteries more dense in energy so as to power electric vehicles and other large-scale energy-storage requirements[1,2]. To meet this high energy density goal, current research is focused on high-potential cathodes, high-capacity anodes, and electrolytes with wide electrochemical potential window[3–5]. Apart from the recently reported high-potential cathodes, lithium cobalt oxide ($LiCoO_2$) is still the most commercially successful cathode in lithium ion batteries[1,2,6].

Although the theoretical capacity of $LiCoO_2$ is 274 mAh/g, the safer limit for reversible lithium extraction is limited to one half of the theoretical capacity. In such cases, the control over lithium extraction is achieved by limiting the charging potential to 4.2 V vs. Li/Li^+. Elevating the potential beyond 4.2 V vs. Li/Li^+, will give rise to serious structural instabilities with the release of oxygen[7-12]. The evolved oxygen gas from the cathode reacts with the electrolyte ingredients which creates serious safety issues such as thermal runaway. The solution to the above issues can be obtained by concentrating on the region of interest i.e the cathode-electrolyte interface. Measures such as the coating of the cathode surface with ceramics, oxides or with electrolyte additives[13–16] have been found successful in extending the potential limit. However, the safety and thermal runaway issues still remains.

Ionic liquids have been proposed as safe electrolytes to avoid issues that arise due to the flammability of carbonate electrolytes[7,17–23]. Several studies have been carried out with ionic liquids; however the specific capacities of the systems as well as capacity retention were not convincing when compared to conventional electrolytes[18,24–27]. Studies about ionic liquids that were based on the fluorosulfonyl imide (FSI) anion presented better rate capability than the conventional electrolytes with $LiCoO_2$ cathodes[11,28]. However, the thermal stability of FSI anions is lower than that of trifluoromethanesulfonyl imide (TFSI) anions[29] and, typically, TFSI anions show better electrochemical stability[30]. Hence, an ionic liquid that was composed of TFSI anions was used in our study. In this work, we have investigated the hypothesis that some of the desirable features of ionic liquid electrolytes could be introduced via a hybrid electrolyte that consists of a mixture of an ionic liquid and traditional electrolytes with $LiCoO_2$ cathodes[19,31–34]. The hybrid electrolyte with 40 percent of ionic liquid in the mixture was considered as being an optimum

composition for the best compromise between thermal stability and viscosity[19,31–35]. Therefore, studies were carried out to explore the electrochemistry of this optimum composition in commercial cathodes. The current study is motivated by the need to explore the electrochemical performance of $LiCoO_2$ cathodes with this hybrid electrolyte. Thus, in this chapter, we focus on the voltage/capacity challenges and the thermal instability of $LiCoO_2$ cathodes by using hybrid electrolytes (HE).

3.2 Experimental

3.2.1 Electrode Preparation

An electrode slurry was prepared by mixing the $LiCoO_2$ cathode (BATSOL, India) with carbon black (Super C-65, Timcal, Switzerland) and polyvinylidene fluoride-hexafluoropropylene (Sigma–Aldrich) binder in the ratio of 90:5:5 with N-methyl-pyrrolidinone (Thermo Fisher Scientific) as a solvent. The well-mixed slurry is then coated on an aluminum current collector (MTI corp) using the doctor blade technique. The coated electrode foils were dried in an air oven for 24 hours. The dried electrode foil was then punched into small circular disks for cell fabrication.

3.2.2 Electrochemical Characterization

Electrochemical studies were carried out with $LiCoO_2$ as the working electrode and lithium metal (Alfa Aesar) as the counter and reference electrode in Swagelok two-electrode cells. The cells were tested with conventional carbonate electrolyte 1 M $LiPF_6$: ethylene carbonate: dimethyl carbonate (conventional electrolyte, LP30 Merck), and also with the Hybrid electrolyte (HE). The HE contained 40 percent of ionic liquid (N-methyl-N-propylpyrrolidinium bis(trifluoromethanesulfonyl) imide was added to the conventional electrolyte mixture of 1M $LiPF_6$ in ethylene carbonate and diethyl carbonate (1:1) (Solvionic).

The cells were tested with a glass fiber separator (GF/D Whatman). Neat N-methyl-N-propyl-pyrrolidinium bis (trifluromethanesulfonyl) imide ([C_3mpyr][TFSI], Solvoionic, France) was also used in certain reference studies. The cells were made in an argon glove box (Lab star, MBraun) with a water and oxygen content of 0.5 ppm and 1 ppm, respectively.

The charge-discharge studies were carried out galvanostatically at the C/5 rate at 20 ^{o}C by using an Arbin battery tester (BT-2000 model, Arbin Instruments). The schematic representation of the processes involved in the fabrication lithium cells for electrochemical measurement is shown in Figure 3.1.

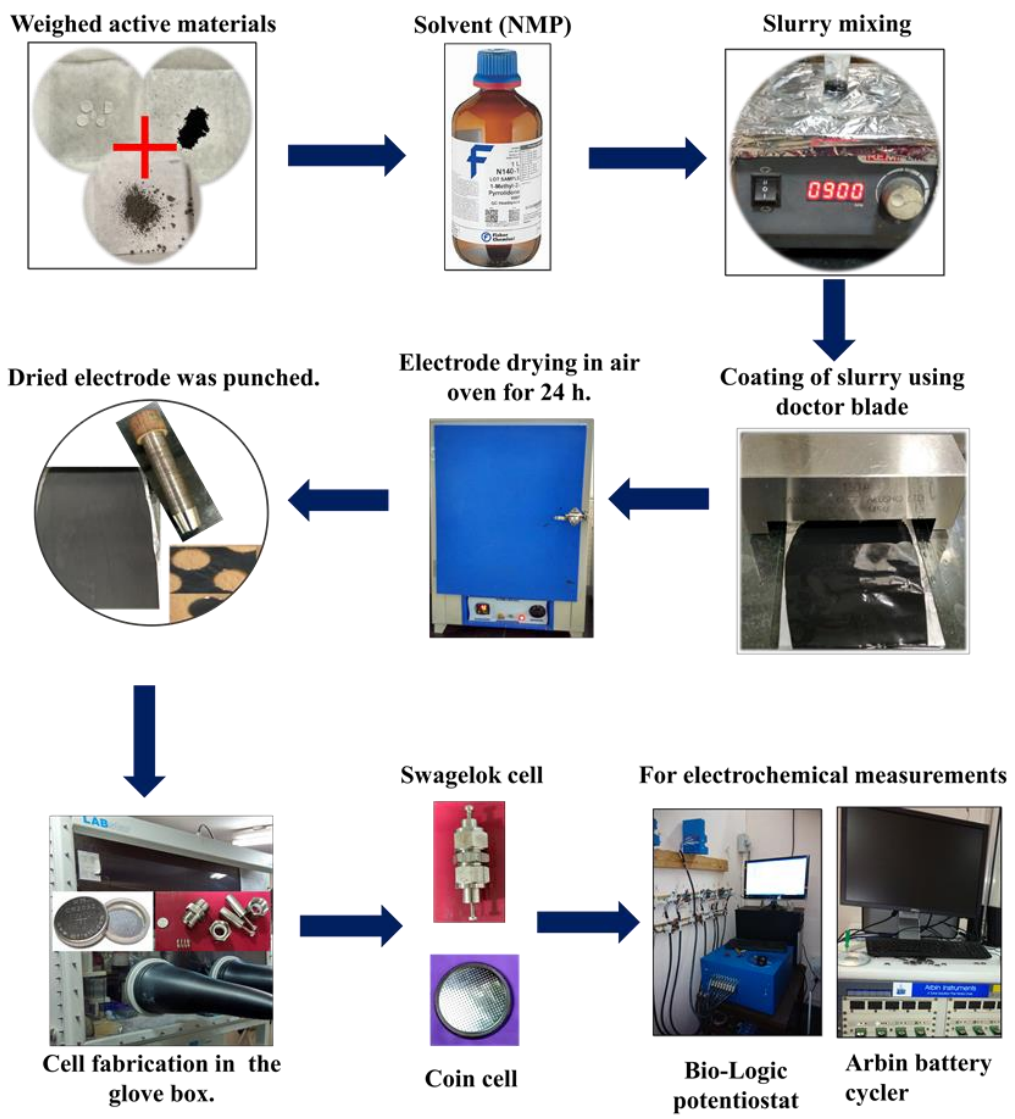

Figure 3.1 *Schematic representation of the steps involved in the fabrication of lithium cells for electrochemical measurements.*

3.2.3 Surface Characterization

The surface characterization of the $LiCoO_2$ electrodes was carried out by opening the cellsinside the glovebox after cycling and washing with diethyl carbonate. High-resolution transmission electron microscopy (HR-TEM, JEOL-2100F) and X-ray photoelectron

spectroscopy (XPS, AXIS Ultra) were carried out to provide a better understanding of the surface of the electrode. The XPS curves were fitted using the processing software package Casa XPS. Thermogravimetric analysis (TGA, NETZSCH STA 449F3) was carried out on delithiated $LiCoO_2$ electrodes in a nitrogen gas environment at a heating rate of 5 ^oC per minute.

3.2.4 Structural Characterization

Half-coin cells with 3 mm diameter holes in the casing and 5 mm diameter holes in the stainless spacer were used to construct coin cells for the in situ synchrotron X-ray diffraction (XRD) measurements. The coin cells contained the electrode, Li metal, and the glass fiber separator containing HE. Cells were made three days before the in situ synchrotron XRD experiments. Further details regarding the construction of the coin cell and the setup of the beamline can be found in the referenced literatures[36,37]. In situ synchrotron XRD data were collected on the Powder Diffraction beamline[38] at the Australian Synchrotron at X-ray wavelength, λ = 0. 0.708735(2) Å, which was determined using the NIST 660b LaB_6 standard reference material. Each data set was collected in three minute acquisitions (with detector position movement) on the coin cell in a transmission geometry throughout the charge-discharge cycles; the period between datasets was 28 minutes. This is an in situ experiment rather than an in operando experiment in which data are continuously collected. The structural analysis was carried out using the software package GSAS and EXPGUI[39,40].

3.3 Results and Discussion

3.3.1 Role of Potential Window in $LiCoO_2$ Cathodes

As mentioned earlier, the potential window plays a major role in controlling lithium extractionfrom $LiCoO_2$ cathodes.Though the maximum capacity of lithium extraction from the system is 274 mAh/g, due to irreversible structural changes, the safe and standard practice is to limit the maximum charging potential to 4.2 V versus Li/Li^+. As a result, 50 percent of lithium utilization is made possible in this system. Though lithium extraction above 50 percent increases the discharge capacity per gram of the cathode material, such extraction will contribute to the structural instabilities and safety issues in the system[16]. The following discussion reveals ways by which the potential limit can be extended without compromising the thermal and structural stability of the system.

3.3.2 Studies in the Standard Potential Window (3.0 - 4.2 V vs. Li/Li^+)

Initially, we carried out studies in the standard potential window to validate the performance of these HEs. The following section presents details of the charge-discharge studies, thermal studies, and postmortem surface analysis of the delithiated $LiCoO_2$.

3.3.2.1 Galvanostatic Charge-Discharge Studies

The galvanostatic charge-discharge studies were carried out at 20 °C. in the potential window of 3–4.2 V versus Li/Li^+. The first cycle discharge capacities in conventional electrolyte and HE electrolyte-based cells were 135 and 138 mAh/g, respectively. At the end of 60 cycles, the discharge capacities of the conventional electrolyte and HE electrolyte were 131 and 133 mAh/g, respectively, as shown in Figure 3.2.

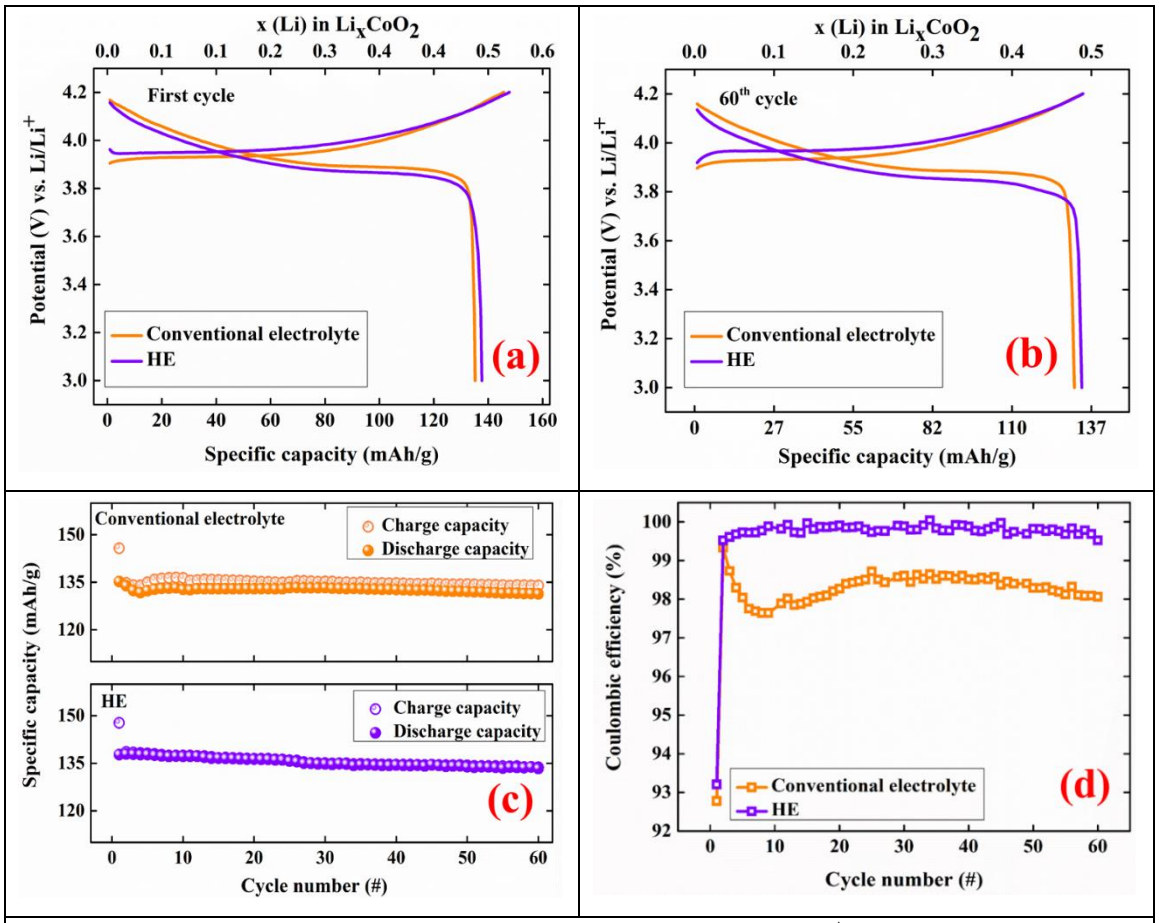

Figure 3.2 *Specific capacity at potential cutoff 4.2 V* vs. *Li/Li^+ of (a) Li/conventional electrolyte/$LiCoO_2$, (b) Li/HE/$LiCoO_2$, (c) Comparison of specific capacity over 60 cycles, and (d) comparison of coulombic efficiency in conventional electrolyte and HE. All the measurements were carried out at 20 °C.*

The plots of capacity and coulombic efficiency versus cycle number are shown in Figure 3.2 (c). It was observed that the HE showed better cyclic efficiency, as shown in Figure 3.2 (d). This suggests that there is a degradation in the case of the conventional electrolyte, which is negligible in HE, as has also been observed by other researchers[41].

3.3.2.2 Preliminary Studies

3.3.2.2.1 TEM Analysis

TEM analysis of the charged electrodes is shown in Figure 3.3. The analysis indicates the formation of a thin surface film on the electrode that is cycled with HE, that is not present in the conventional electrolyte and which could help in preventing the undesirable side reactions that can occur on direct contact with the electrolyte in a highly oxidative environment. Other researchers[18,19,42,43] have also reported that ionic liquid-assisted film formation on the cathodes improves cyclic stability.

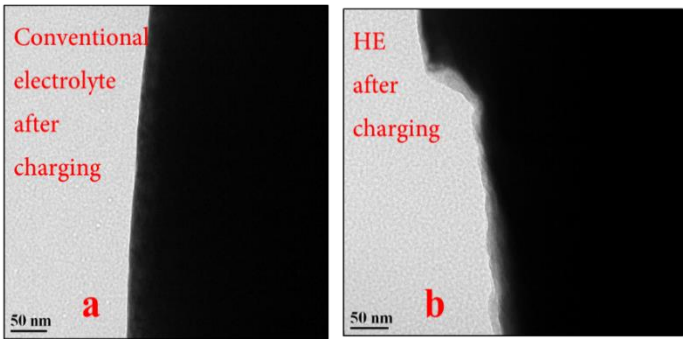

Figure 3.3 *TEM images of (a) Li/Conventional electrolyte/$LiCoO_2$ and (b) Li/HE/$LiCoO_2$ after cycling to 4.2 V* vs. *Li/Li^+.*

3.3.2.2.2 Thermal Analysis

Further, the intention was to investigate whether the surface film might also enhance the thermal stability of delithiated $LiCoO_2$. In order to evaluate the thermal behavior, differential thermal analysis and thermogravimetric analysis were carried out on delithiated $LiCoO_2$ cathodes, as shown in Figure 3.4 (a) (samples were removed directly from the cell, placed into the TGA instrument, and intentionally allowed to retain traces of electrolyte.) $LiCoO_2$ in the neat ionic liquid was also included as a control experiment.

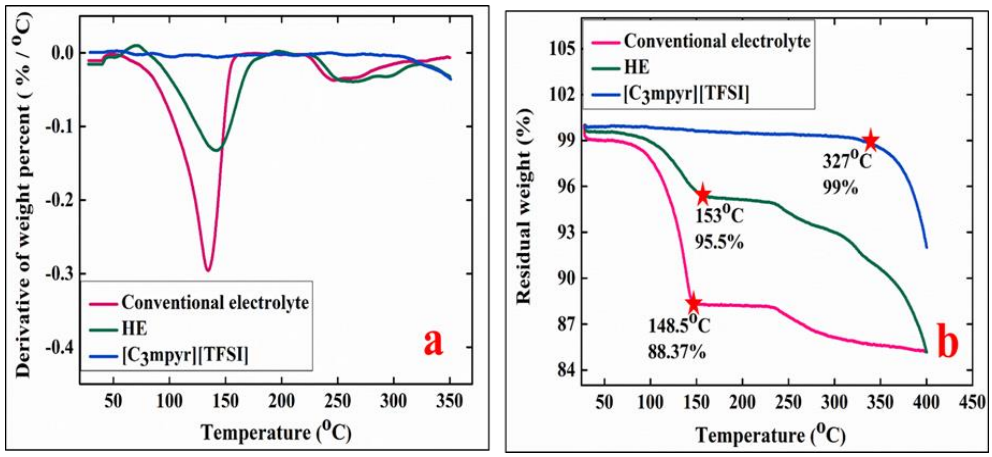

Figure 3.4 *Thermal Analysis of delithiated $LiCoO_2$ cycled in conventional electrolyte, HE, and neat [C_3mpyr] [TFSI] electrolytes with potential cutoff at 4.2 V* vs. *Li/Li$^+$. (a) DTA trace and (b) TGA trace.*

In Figure 3.4 (a), the peak at 133 °C in the conventional electrolyte is in accordance with the literature[16] and is understood to occur due to the volatile organic solvents in the electrolyte, whereas the corresponding peak occurs at 140 °C in the HE system, which indicates the lower volatility of the carbonate components in the mixture, as is expected from Henry's law. The second feature that starts near 230 °C can be attributed to the initiation of thermal decomposition of $LiPF_6$ in the system. This is also supported by the absence of such a feature in the pure [C_3mpyr] [TFSI]/$Li_{0.5}CoO_2$ sample and by the shift to higher temperatures in the HE. These results suggest that the cathode material is slightly more thermal stable in the HE.

The thermogravimetric trace in Figure 3.4 (b), shows that the delithiated cathodes that were cycled using neat ionic liquids showed stable behavior until around 300 °C, which confirms the thermal stability with neat ionic liquid electrolytes, whereas the HEs showed lesser mass loss with increasing temperatures, in comparison to the conventional electrolyte, as shown in Figure 3.4 (b).

3.3.3 Studies in the Extended (3.0 - 4.4 V) Potential Window

Further studies were carried out in the extended potential range of 4.4 V versus. Li/Li$^+$, in order to extract a greater amount of lithium from the system[35]. Further studies were carried out in the extended potential range of 4.4 V versus. Li/Li$^+$, in order to extract a greater amount of lithium from the system[35].

The potential cutoff was restricted to 4.4 V versus Li/Li^+, as a safe limit in order to avoid serious structural distortion in $LiCoO_2$ cathodes, as is shown in previous litreatures[14,44,45] and as investigated here via in situ synchrotron XRD and other surface studies. The relationship between the applied electrochemical potential and lithium extraction in $LiCoO_2$ will be discussed in the following sub section 3.3.3.2.4.

3.3.3.1 Galvanostatic Charge-Discharge Studies

The charge-discharge studies were carried out galvanostatically at C/5 rate in the potential window of 3–4.4 V versus Li/Li^+, as shown in Figure 3.5.

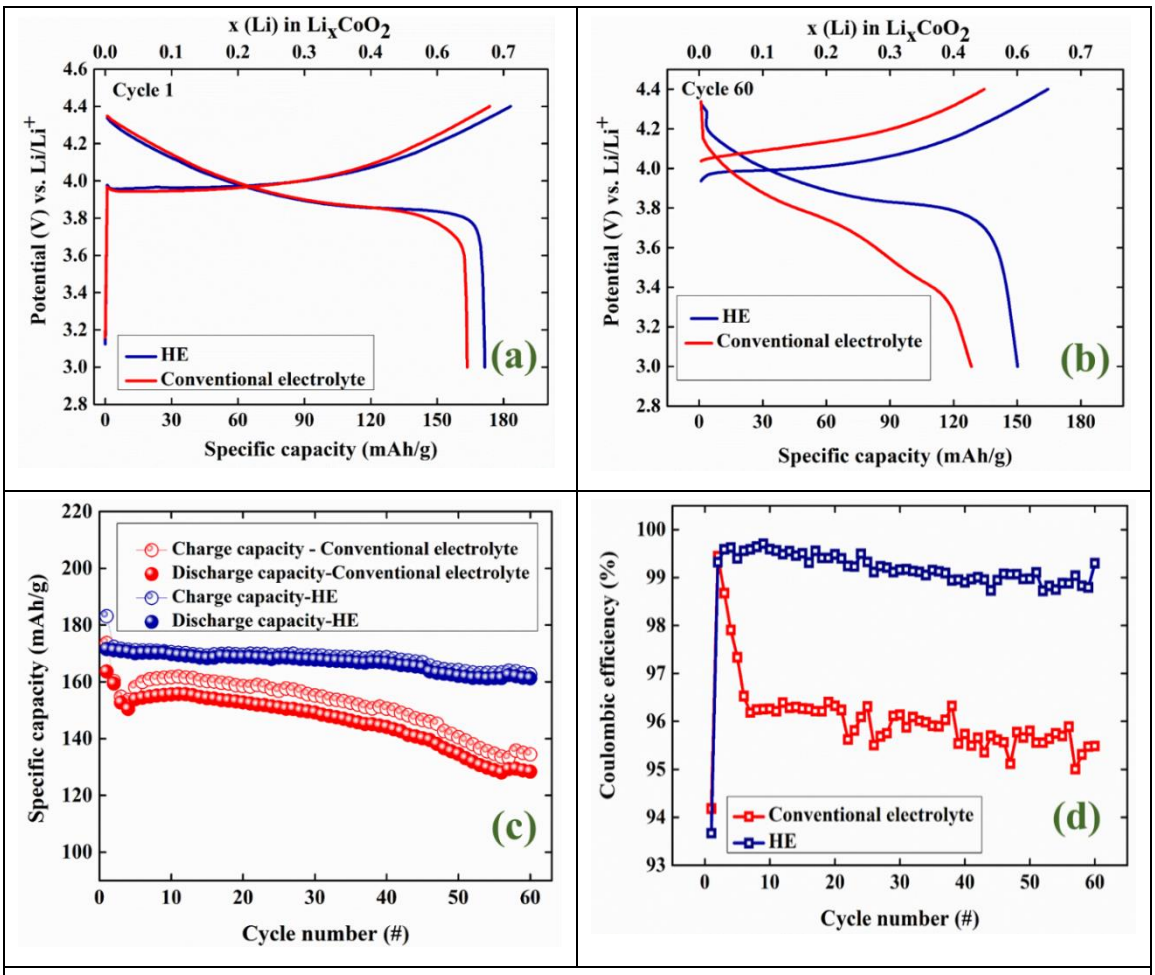

Figure 3.5 *Comparison of conventional electrolyte and HE cells in the potential window (3–4.4 V* vs. *Li/Li^+) after a) 1st cycle, b) 60th cycle, (c) cycle number* vs. *specific capacity and (d)comparison of coulombic efficiency of the conventional electrolyte and HE cells for 60 cycles. All the measurements were carried out at 20 °C.*

In the first cycle, the discharge capacity of the conventional electrolyte cell was 164

mAh/g, whereas the discharge capacity of the HE cell was 172 mAh/g. At the end of 60 cycles, the discharge capacity of the conventional electrolyte and the HE cycled cells were 128 and 161 mAh/g, respectively. The higher capacity in the HE suggests that a larger proportion of lithium is being reversibly cycled from the electrodes. The capacity fade at the end of 10th and 60th cycles in conventional electrolyte was 5 percent and 22 percent, whereas in HE it was only 1 percent and 6 percent, respectively. Further, the rate performance of these HEs was tested at various C rates of up to 1C. It was found that a better capacity of around 124 mAh/g was attained in the HE at the 1C rate, as shown in Figure 3.6.

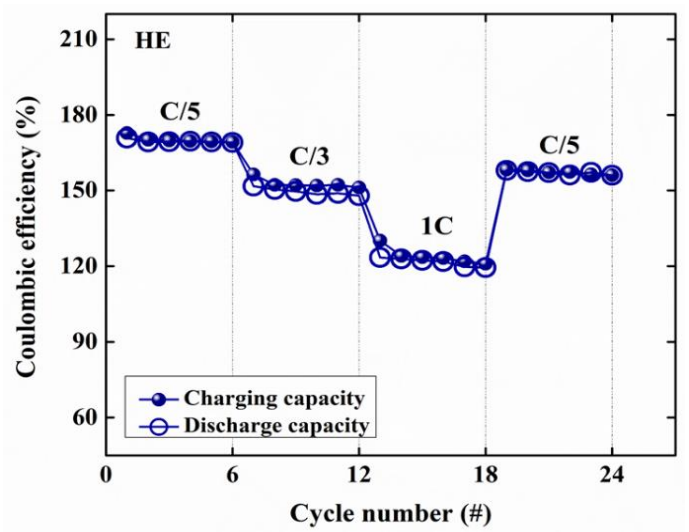

Figure 3.6 *Rate performance of HEs at various C rates carried out at 20 °C.*

3.3.3.2 Post Analysis of Delithiated $LiCoO_2$ Cathodes

Further insight into the improved performance in HEs was achieved with the help of post-cycling surface, thermal and structural analyses. Surface studies such as XPS and TEM studies were carried out to validate the presence of the surface film. Thermal analysis was carried out to evaluate the thermal stability of delithiated $LiCoO_2$ cathodes in the presence of the surface film. In addition, structural insights into the delithiated $LiCoO_2$ was studied using data from ex situ XRD studies and in situ synchrotron studies. The following subsections present a detailed account of these analyses.

3.3.3.2.1 TEM Analysis

The TEM micrographs of the delithiated $LiCoO_2$ are shown in Figure 3.7, which shows film formation in the HE cycled cathode, which is similar to that seen earlier in Figure 3.3. The similarity of the film formation in the cathodes was reported by various researchers [13,18,19,46,47], who claimed that this film formation would play a serious role in preventing further undesired reactions between the bare surface of the electrode and the electrolytes.

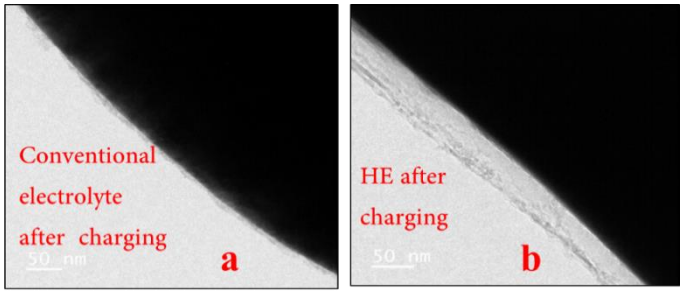

Figure 3.7 *TEM images of the electrodes after the first cycle in (a) Li/ conventional electrolyte/$LiCoO_2$ and (b) Li/HE/$LiCoO_2$ cells in the potential cutoff 4.4V* vs. *Li/Li^+*.

3.3.3.2.2 XPS Analysis

The XPS survey spectrum of the electrodes is illustrated in Figure 3.8. Table 3.1 shows the atomic percentage of the elements that are present on the surface of the electrodes. It is clear that both cycled electrodes feature electrolyte decomposition products on the surface; however, closer observation reveals that there is more carbon, oxygen and phosphorous on the electrode that is cycled in the conventional electrolyte, whereas in HE, trace quantities of sulfur are seen, but with smaller quantities of other electrolyte components. This supports our hypothesis that the ionic liquid assists in film formation, because sulfur can originate only from the anion in the ionic liquid.

The XPS spectra of carbon and oxygen for the conventional electrolyte and HE cycled cells are shown in Figure 3.9. The C1s peaks of fresh $LiCoO_2$ cathodes were found at 284.3 eV, 285.7 eV, and 290.1 eV, which correspond to C-C bonds from the added carbon additive in the electrode, C-H bonds, and C-F bonds from the PVDF-HFP binder[48–50].

In the cycled electrodes, the peaks mentioned above were found to have variable intensities; in addition, a peak at 286.2 eV represents the C-O peak. In the C1s core peak

of cycled electrodes, the intensity of the C-H peak in the HE cycled electrode is comparatively higher than that of the conventional electrolyte cycled electrode, which may be due to the presence of the ionic liquid component on the electrode surface. This in turn suggests an active role of the ionic liquid in the formation of the film on the surface of the electrode.

Table 3. 1 *Atomic percentage of the elements on the delithiated $LiCoO_2$ electrodes.*

S. No	$Li_{1-x}CoO_2$	C 1s	O 1s	F 1s	Co 2p	Li 1s	P 2p	S 2p
1.	Conventional electrolyte	40.3	12.9	16.4	0.3	28.5	1.6	--
2.	HE	34.2	6.6	7.2	0.6	51	---	0.4

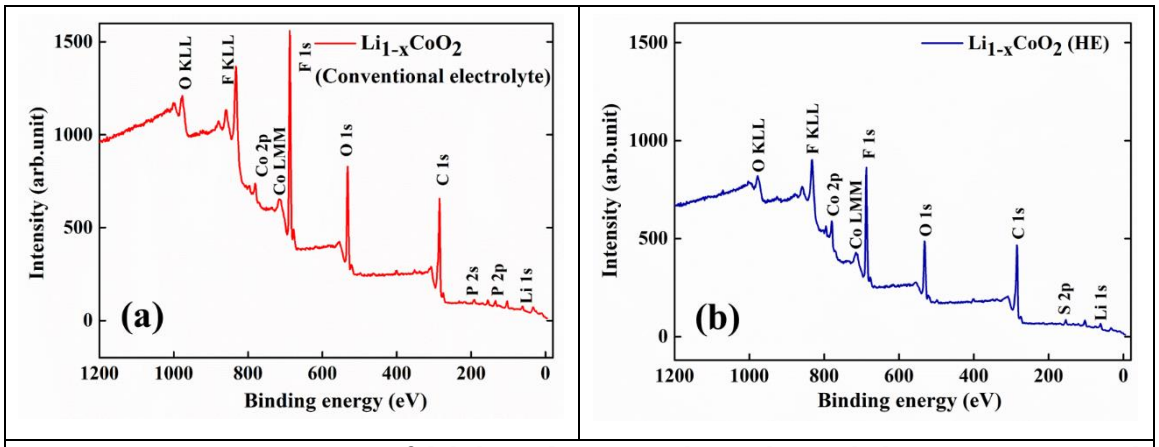

Figure 3.8 *Survey spectrum of delithiated $LiCoO_2$ electrodes cycled in (a) conventional electrolyte and (b) HE.*

The O1s spectrum of the fresh electrode includes two peaks. The one that is at 529.45 eV represents the cobalt-oxygen bond and the other that is at 530.9 eV represents the trace carbonate Li_2CO_3 species in the fresh cathode[48,51]. The O1s spectra of the cycled electrodes exhibit additional peaks at 532 eV and 533 eV due to the LiOH species and other oxidation products of the electrolytes on the electrode surface[48,52].

The XPS spectra of phosphorous and fluorine are shown in Figure 3.10. The P 2p spectrum of the cycled electrodes consists of two peaks. The one that is at 133.7 eV represents the phosphate species that arise from oxidation products of the electrolytes at the surface and the other that is at 136.4 eV represents the residual $LiPF_6$ salt that is present on the surface of the electrode[50]. These P 2p peaks suggest that the presence of $LiPF_6$ and its

decomposition products is lower on the HE cycled electrode. Earlier works[50,53,54] also suggest that a smaller degree of electrolyte decomposition, in turn, results in better performance of the electrode, which supports the improvement that is observed in the performance of the HE.

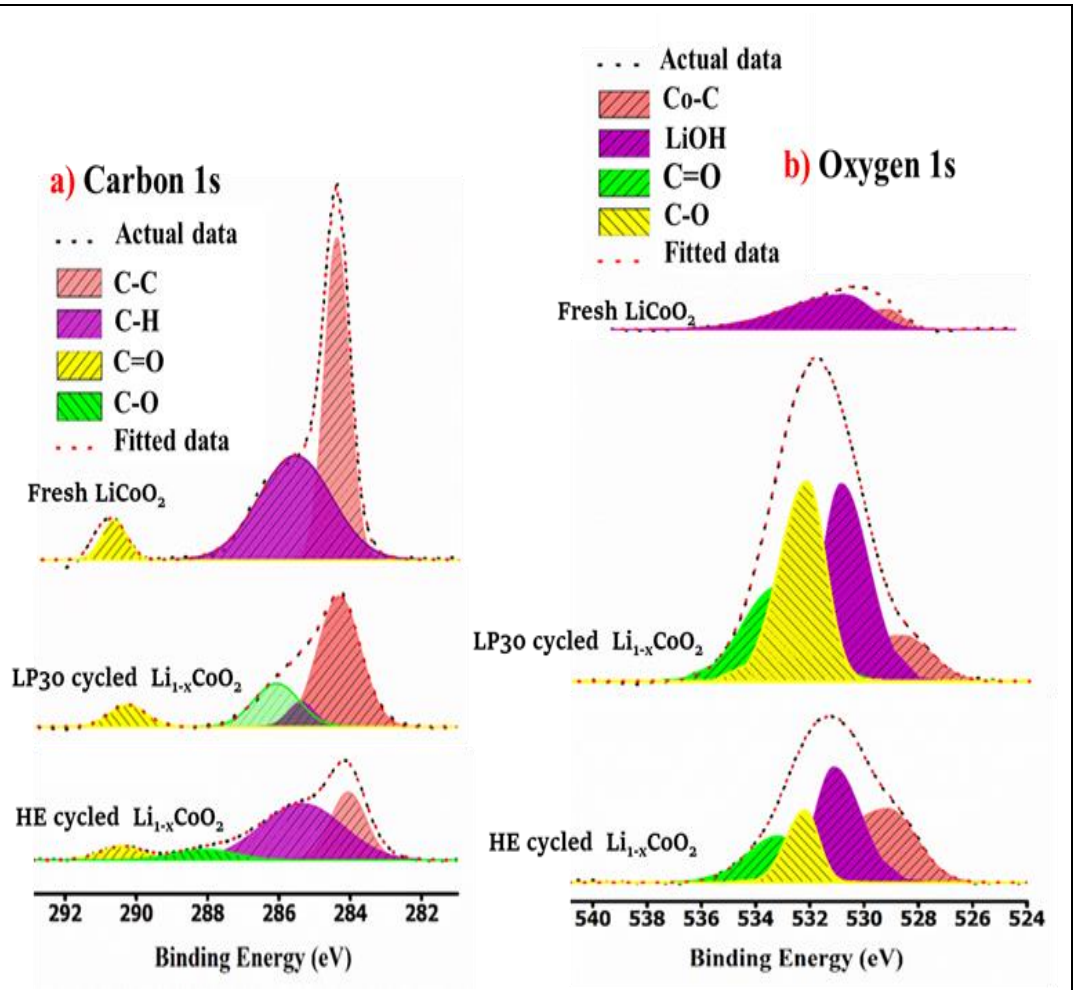

Figure 3.9 *C 1s and O 1s XPS spectra of the fresh and cycled $Li_{1-x}CoO_2$ electrodes in conventional electrolyte and HE.*

The F 1s spectrum of the fresh electrode consists of a peak at 687 eV, which represents the fluorine component in the binder; whereas the cycled electrodes have two peaks: one at 684.4 eV, which corresponds to the LiF component from the electrolyte, and the other at 687.3 eV, which stems from the binder as well as from trace amounts of $LiPF_6$ salt in the electrolyte[42,45].

The S 2p spectra on the HE cycled electrode is shown in Figure 3.11. It consists of a peak at 169.4 eV, which represents the SO_2F species on the electrode[14,42]. The oxidized sulfur

species on the surface of the electrode also further indicates the role of the ionic liquid in the surface film.

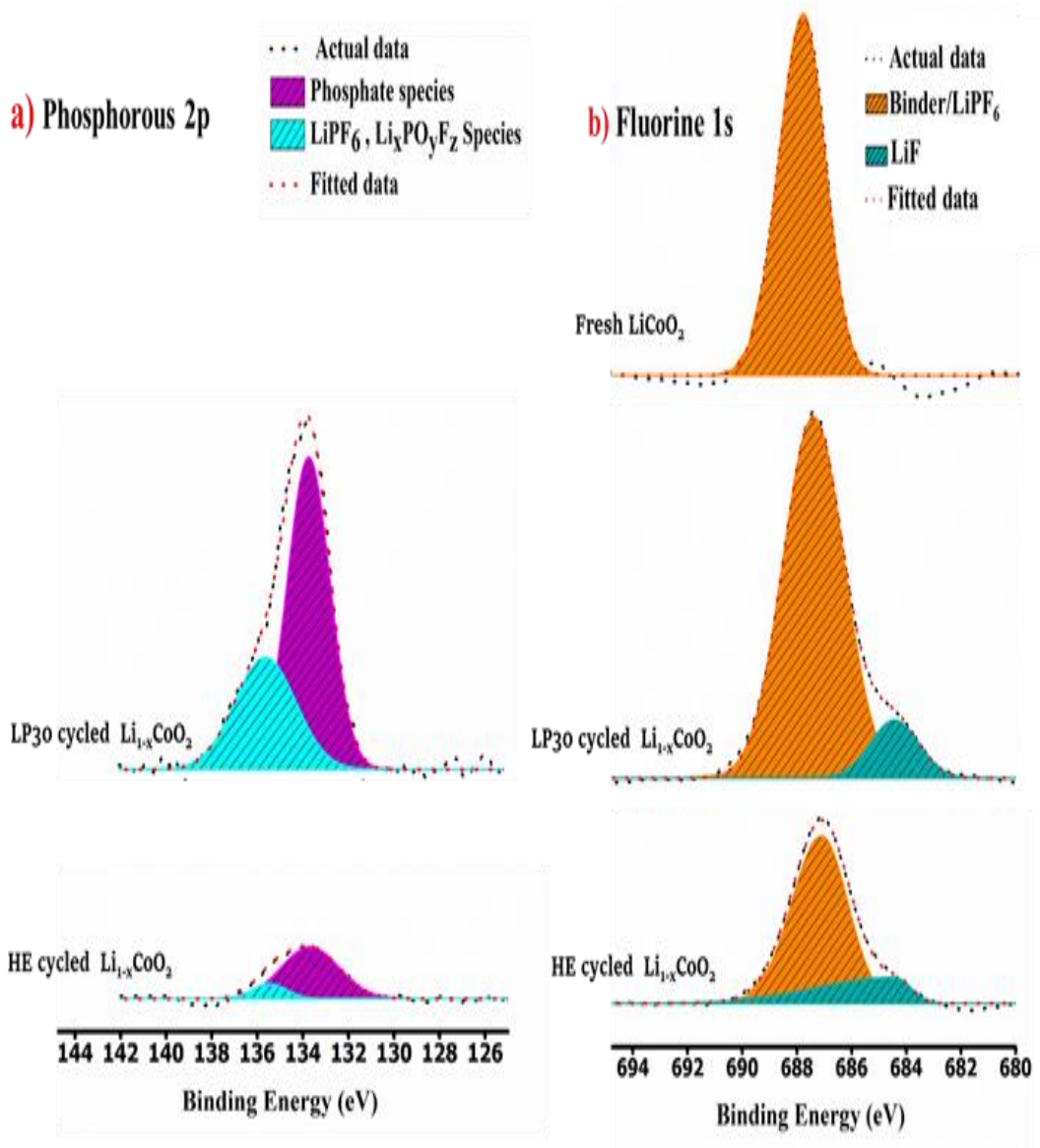

Figure 3.10 *P 2p and F 1s XPS spectrum of the fresh and delithiated $LiCoO_2$ electrodes cycled in conventional electrolyte and HE.*

In short, the film observed in this work is a composite film that contains carbon, fluorine, phosphorous, and sulfur species. Such film formation on the surface of cathodes ($LiCoO_2$) has been reported in addition to this work by several researchers[13,18,46,47] who suggest that the film that is formed in the first cycle will play a clear role in preventing further surface reactions of the electrolyte with the cathode. The effectiveness of such films can also be visualized through the better capacity retention of the cathodes in the subsequent cycles.

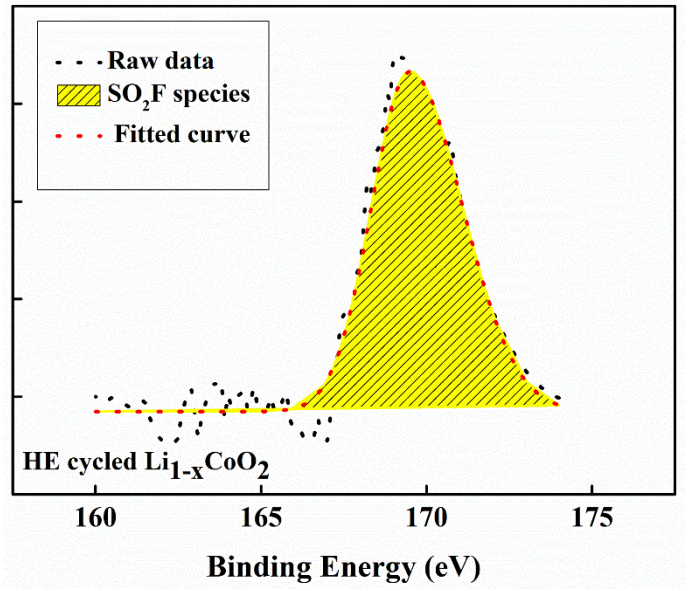

Figure 3.11 *S 2p XPS spectrum of $LiCoO_2$ electrodes cycled in HE*

3.3.3.2.3 Thermal Analysis

Differential thermal analysis carried out on delithiated $LiCoO_2$ cathodes exhibited trends similar, as reported in the section on the standard potential window (Figure 3.12).

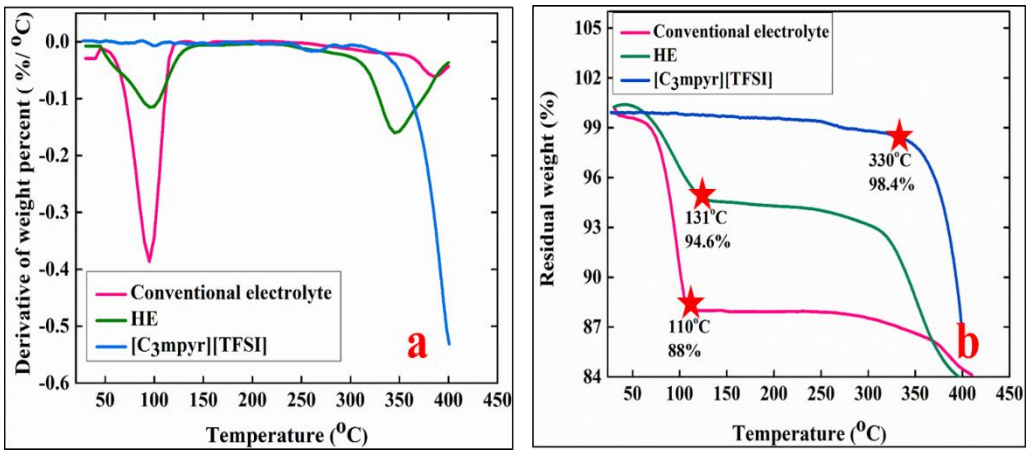

Figure 3.12 *Thermal Analysis of delithiated $LiCoO_2$ cycled in the conventional electrolyte, HE, and neat [C_3mpyr] [TFSI] electrolytes with the potential cutoff at 4.4 V* vs. *Li/Li^+. (a) DTA trace and (b) TGA trace.*

It was obvious that the weight losses slightly increased in the electrodes that were cycled in the extended potential window because extracting lithium beyond 0.5 makes it more thermally vulnerable[16].

3.3.3.2.4 Structural Insights into Delithiated $LiCoO_2$ Cathodes

The most common forms of $LiCoO_2$ used for battery applications exists in cubic (spinel) and hexagonal structures[55]. In such cases, the structure of $LiCoO_2$ is decided by the temperature of synthesis. In most cases, $LiCoO_2$ synthesized at low temperatures (<= 400 ^oC) exists in spinel form whereas those synthesized at high temperatures (~850-900 ^oC) exists in hexagonal structures[56]. The differential properties that occur in low temperature $LiCoO_2$ (LT-$LiCoO_2$) and high temperature $LiCoO_2$ (HT-$LiCoO_2$) are outlined in Table 3.2.

Table 3.2 *Outline of the difference in properties of LT-$LiCoO_2$ and HT-$LiCoO_2$.*

S.No.	Properties	LT-$LiCoO_2$		HT-$LiCoO_2$	
1.	Synthesis temperature[55,56]	<=400 ^oC		850-900 ^oC	
2.	Crystal structure[56]	Cubic (Spinel)		Hexagonal	
3.	Space group[56]	Fd3m		R3m	
4.	Cell parameters[55,60]	a value	2.8297 Å	a value	2.815-2.816Å
		c value	13.868 Å	c value	14.05-14.08 Å
		c/a ratio	4.914	c/a ratio	4.98-5.00
5.	Cation arrangement[55,56]	Co and Li compositions lie perpendicular to each of the four cubic [111] direction in AB and BA pattern.		Co and Li planes alternate in ABC-ABC oxygen stacking.	
6.	Safe potential window of operation[55]	3.3-3.9 V vs. Li/Li^+		3.8-4.3 V vs. Li/Li^+	

Nevertheless, the HT-$LiCoO_2$ is most commonly used $LiCoO_2$ among battery researchers due to its better electrochemical performance than the LT-$LiCoO_2$[56,57]. In this chapter, $LiCoO_2$ is referred to as HT-$LiCoO_2$. Figure 3.13 shows the structure and arrangements of atoms in the hexagonal structure of $LiCoO_2$. As mentioned earlier, before charging $LiCoO_2$ occurs in hexagonal structure. However, after 50 percent lithium extraction ($Li_{0.5}CoO_2$), there occurs a transition to a monoclinic structure which, upon further lithium extraction, will convert to hexagonal structure[58]. The end member (Li_0CoO_2) is found with the hexagonal single layered structure[58,59]. The amount of lithium extracted and the structure

of $LiCoO_2$ can be tuned by the applied electrochemical potential. The extent of lithium extracted as a function of the applied electrochemical potential is detailed in Table 3.3.

Table 3.3 *Relation between the extent of lithium extraction and the applied electrochemical potential*[59,61]

S.No.	Percent of lithium extraction in $LiCoO_2$ (%)	Electrochemical potential (vs. Li/Li^+)
1.	100	5.2
2.	80	4.65
3.	75-78	4.55
4.	55	4.35
5.	50	4.2

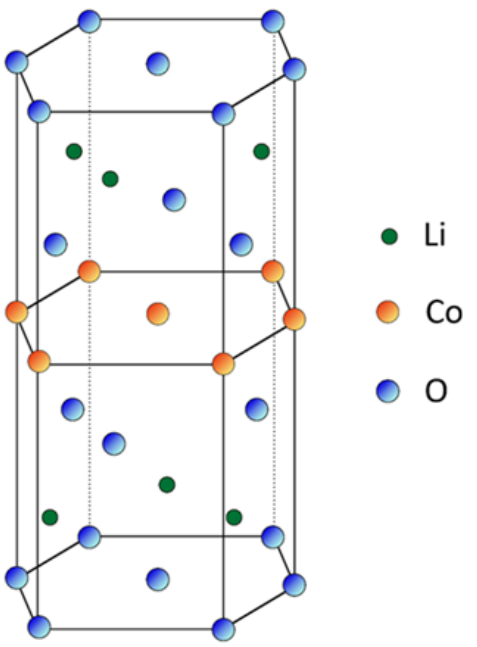

Figure 3.13 *Arrangement of atoms in $LiCoO_2$ hexagonal structure.*

In the above context, the present study was carried out to understand the structural stability of $LiCoO_2$ during the lithium extraction at extended potentials with the help of ex situ and in situ XRD studies.

3.3.3.2.4.1 Ex situ XRD studies

XRD studies were carried out on the delithiated electrodes at the end of the first charge and after 60 cycles, as shown in Figure 3.14. As reported by Chung et al.[11], the capacity fading is predominantly due to surface reactions on the cathode, but structural changes in the bulk do have some impact[61].

Literature reports that structural changes in $LiCoO_2$ are notably seen in the (003) peak [13,57,59,62]. It was found that after the first charging cycle, the (003) peak moved to lower angles when compared to the fresh electrodes. This is due to the delithiation process[32] with the HE showing a lower 2θ value than the conventional electrolyte which in turn suggests a greater amount of lithium extraction with the HE.

Similarly, after the 61st charging, the (003) peak of the conventional electrolyte cycled cell shows a drop in intensity and is found at higher 2θ values than those of the HE cycled electrode. This indicates better structural stability in the HE cycled electrodes and, possibly, a greater amount of lithium extraction[11,59].

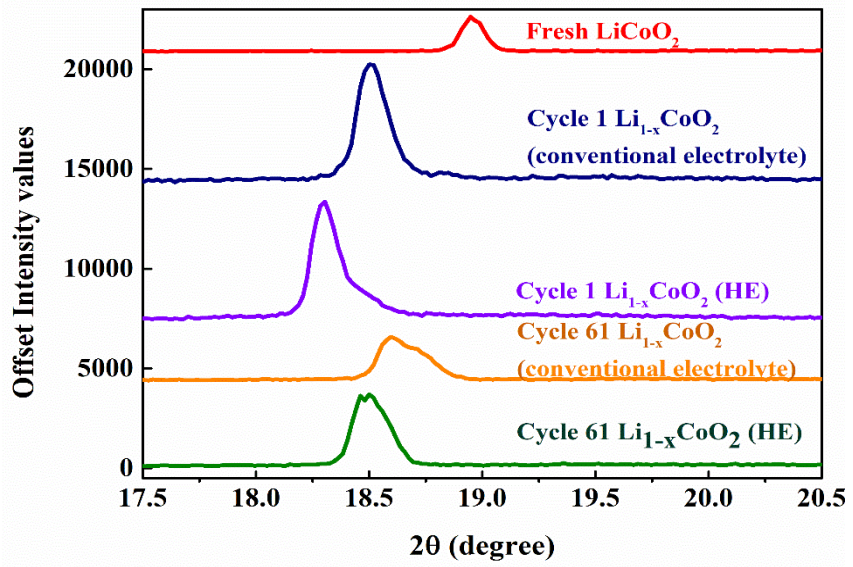

Figure 3.14 *XRD data of fresh $LiCoO_2$, after 1st charging and 61st charging in the conventional electrolyte and HE.*

3.3.3.2.4.2 In situ XRD studies

To shed further light on the structural evolution, in situ synchrotron XRD data were collected. The Rietveld refined fit for the electrode in the coin cell for the first XRD pattern

is shown in Figure 3.15 and the lattice evolution using a single *R*-3*m* phase structural model with the electrochemical charge curve shown is in Figure 3.16. Stacked individual patterns at selected potentials are shown in Figure 3.17 (a) and 3.17 (b). On charge, the cell was held at 4.2 V for 30 minutes followed by charging to 4.5 V and holding at 4.5 V for 60 minutes, which was again followed by further charging.

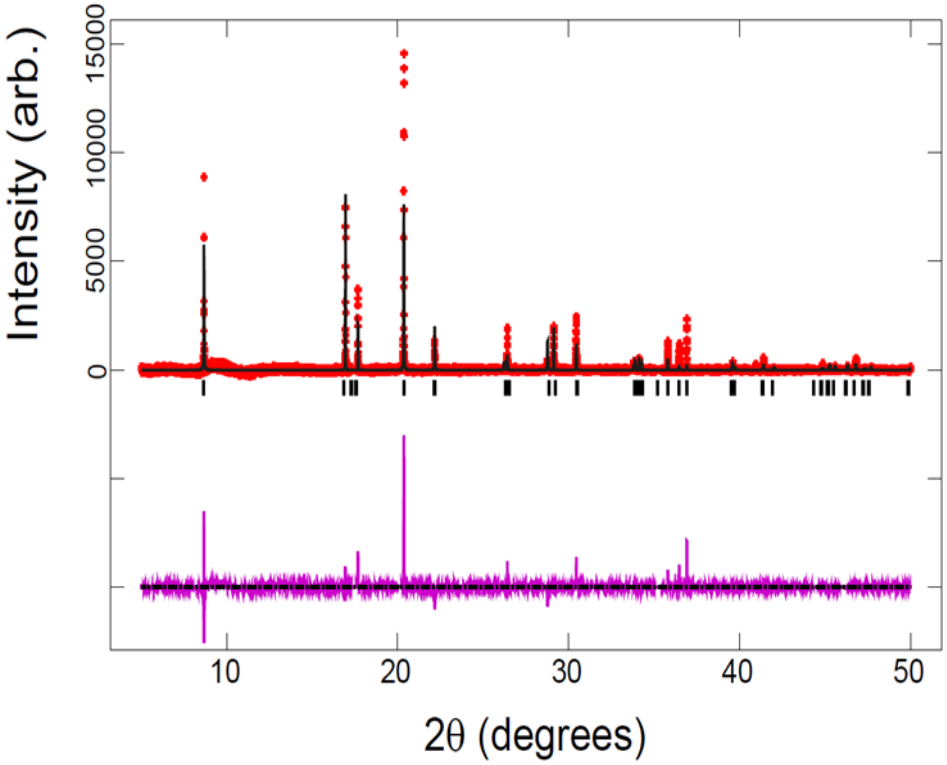

Figure 3.15 *Rietveld refined fit of the $LiCoO_2$ structural model to the first in situ synchrotron XRD dataset. Data are shown as crosses, the calculated Rietveld model as a line through the data, and the difference between the data and the model as the line below the data. The vertical reflection markers are for $LiCoO_2$. Some preferred orientation is found in this sample. See reflection $2\theta \sim 20°$.*

The lattice evolution shows that the *c* lattice parameter and the volume increase, while the *a* lattice parameter decreases until 4.3 V; the parameters then stabilize, which shows a minimal amount of change in the ramp from 4.3 V to 4.45 V. During the 4.5 V hold, the opposite trend is observed, with a decrease in the *c* lattice parameter and the volume and an increase in the *a* lattice parameter. This behavior to 4.3 V is consistent with the literature, which shows that the removal of Li ions leads to a repulsion of the CoO_2^- layers that expand the *c* lattice parameter or the stacking axis, and a partial decrease in the *a* lattice

parameter, partly due to the oxidation of Co^{3+} to Co^{4+}. Early work in which $LiCoO_2$ was close to equilibrium suggested that the expansion of the *c* or the stacking axis stabilizes around 4.12 V, which corresponds to 0.5 Li that was extracted from $LiCoO_2$ [61]. Additionally a monoclinic splitting was observed for the 104 reflection between 4.05–4.2 V, which was also observed around 4.2 V in related studies under different electrochemical conditions[57]. Although slightly different electrochemical conditions are used in our study, the monoclinic splitting of the (104) reflection is only observed at 4.73 V with some evidence of the presence of multiple phases at 4.57 V with the (003) reflection; see Figure 3.18 (a). Interestingly, the *R*-3*m* layered structure is preserved to at least 4.3 V; see Figure 3.18 (b) for a Rietveld refined fit, with no evidence of peak splitting or secondary phases. Minor additional reflections appear at 4.45 V, as seen in Figure 3.17 (a).

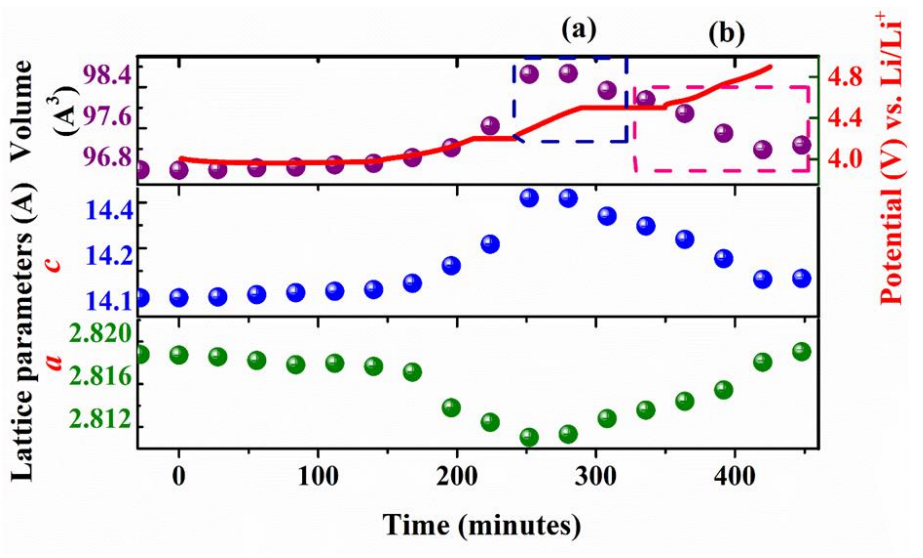

Figure 3.16 *(a) Lattice and volume evolution of the $LiCoO_2$ during charging, as determined from Rietveld analysis of in situ synchrotron XRD data; the boxed regions indicate patterns shown in Figure 3.17 (a) and (b).*

The lattice evolution shows that the *c* lattice parameter and the volume increase, while the *a* lattice parameter decreases until 4.3 V; the parameters then stabilize, which shows a minimal amount of change in the ramp from 4.3–4.45 V. During the 4.5 V hold, the opposite trend is observed, with a decrease in the *c* lattice parameter and the volume and an increase in the *a* lattice parameter. This behavior to 4.3 V is consistent with the literature, which shows that the removal of Li ions leads to a repulsion of the CoO_2^- layers

that expand the *c* lattice parameter or the stacking axis, and a partial decrease in the *a* lattice parameter, partly due to the oxidation of Co^{3+} to Co^{4+}. Early work in which $LiCoO_2$ was close to equilibrium suggested that the expansion of the *c* or the stacking axis stabilizes around 4.12 V, which corresponds to 0.5 Li that was extracted from $LiCoO_2$[61]. Additionally a monoclinic splitting was observed for the 104 reflection between 4.05–4.2 V, which was also observed around 4.2 V in related studies under different electrochemical conditions[57]. Although slightly different electrochemical conditions are used in our study, the monoclinic splitting of the (104) reflection is only observed at 4.73 V with some evidence of the presence of multiple phases at 4.57 V with the (003) reflection; see Figure 3.18 (a). Interestingly, the *R*-3*m* layered structure is preserved to at least 4.3 V; see Figure 3.18 (b) for a Rietveld refined fit, with no evidence of peak splitting or secondary phases. Minor additional reflections appear at 4.45 V, as seen in Figure 3.17 (a).

In any case, the *R*-3*m* structure is preserved through the use of the HE at least to 4.3 V, which suggests that the combination of the surface layer and HE may play a role in stabilizing this structure to lower lithium contents (allowing a larger amount of reversible Li insertion/extraction while maintaining the *R*-3*m* structure). This in turn allows the electrode to function at higher potentials with reasonable capacity retention.

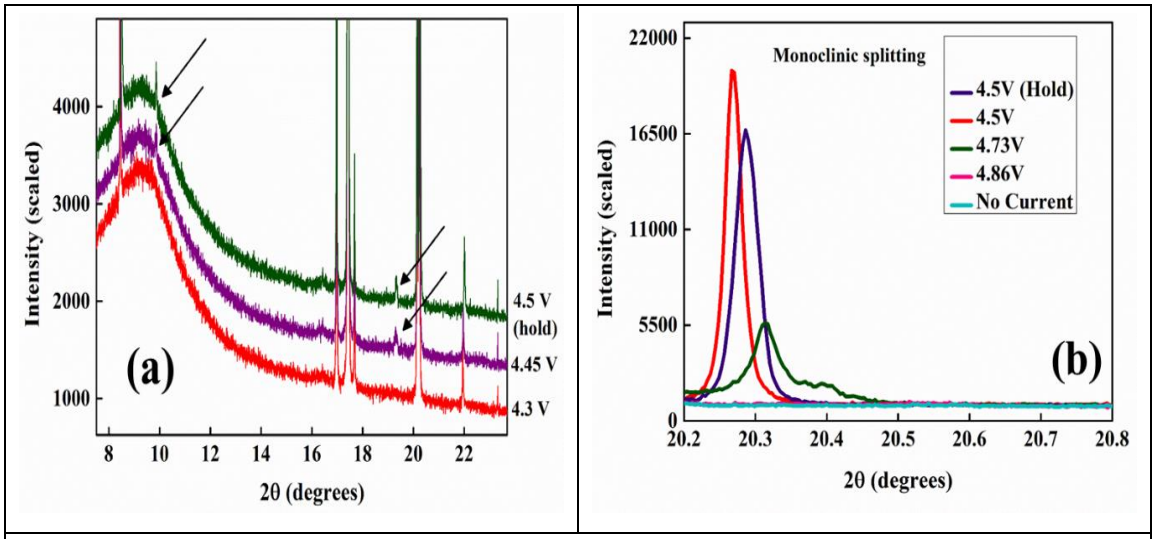

Figure 3.17 *Stacked XRD data of selected 2θ regions that correspond to higher potential regions are shown in Figure 3.16 (a) and (b). In particular, (a) refers to new reflections that are observed at around 4.45 V and (b) monoclinic splitting of the 104 reflection, which is illustrated at around 4.73 V.*

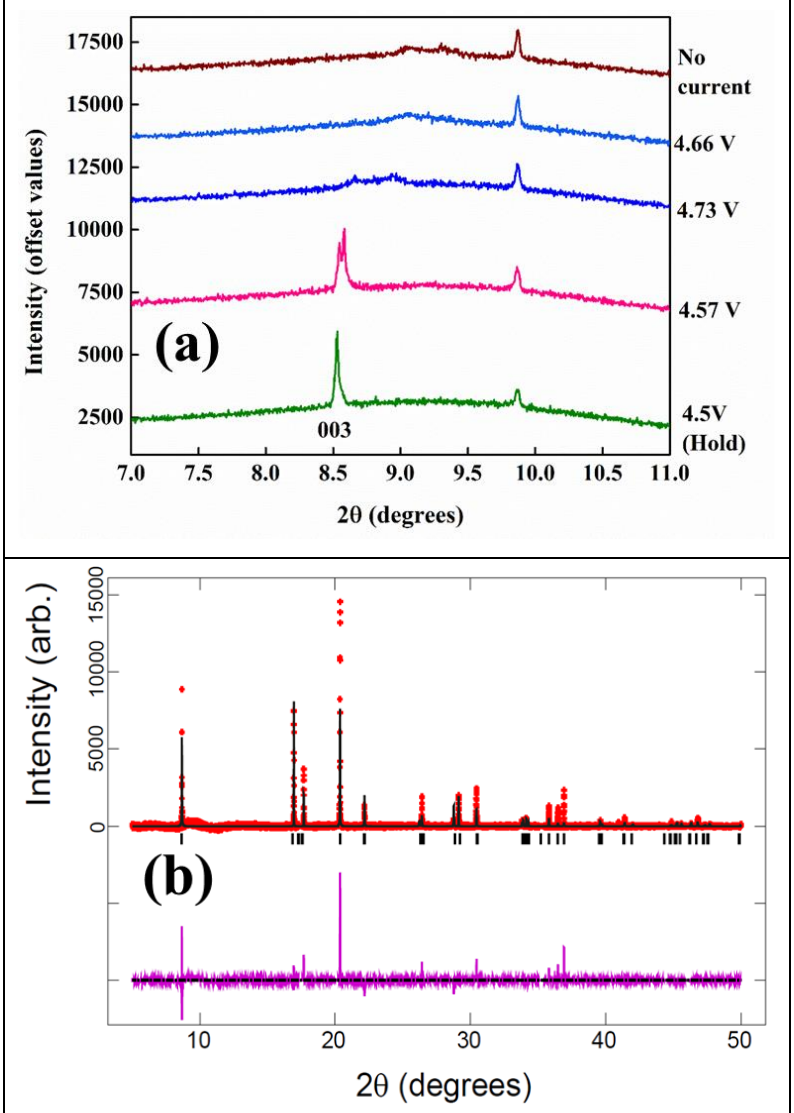

Figure 3.18 *(a) Stacked plot of* in situ *synchrotron XRD data, which correlates to the potential and corresponds to the lower angle region that is shown in Figure 3.17 (b), Splitting of the (003) reflection is seen at around 4.57 V and (b) Rietveld refined fit of the* Li_xCoO_2 *structural model to the* in situ *synchrotron XRD dataset at 4.3 V. Data are shown as crosses, the calculated Rietveld model as a line through the data, and the difference between the data and the model as the line below the data. The vertical reflection markers are for* $LiCoO_2$*. Some preferred orientation remains in this sample; see reflection* $2\theta \sim 20°$*.*

In addition, the surface film may be amorphous, because there is no significant peak contribution of the surface film in the ex situ XRD that is taken after cycling (1st and 60th cycles) as well as in the in situ synchrotron studies of the cathodes that are cycled with this HE.

The exact mechanism of the role of the HE in potentially stabilizing the *R*-3*m* structure is intriguing and unknown at this time. Speculatively solvent or a component of intercalation could be occurring or the interface layer is stabilizing the outer layers of the Li_xCoO_2 particle which in turn stabilizes the core. All of these hypotheses require further work for the the underlying mechanism to be understood.

3.4 Concluding Remarks

In this chapter, the use of HEs with $LiCoO_2$ cathodes in the standard potential window, as well as the elevated cutoff potential of 4.4 V versus Li/Li^+ was demonstrated. The presence of ionic liquid in the electrolyte plays a key role in the improving of the capacity retention and thermal stability with delithiated cathodes especially close to x ~ 0.7 where it appears that the phase transitions (monoclinic and other phases) do not appear until higher potentials. With the help of surface studies, it was shown that the film formation on the cathode surface involves the ionic liquid species, forming a thinner, more stable film that reduces further electrolyte decomposition at elevated potentials (4.4 V). It was shown that the electrode maintains the *R*-3*m* structure to at least 4.3 V, and no new phases are formed. In short, without the use of any ceramic surface coatings or metal dopants in the cathodes, it was shown that HE provides better performance and safety in $LiCoO_2$ cathodes.

3.5 References

(1) *Advances in Lithium-Ion Batteries*; Schalkwijk, W. A. van; Scrosati, B., Eds.; Kluwer Academic Publishers, 2002.

(2) Scrosati, B.; Garche, J. Lithium Batteries: Status, Prospects and Future. *J. Power Sources* **2010**, *195*, 2419–2430.

(3) Nithya, C.; Sowmiya, T.; Vijaya Baskar, K.; Selvaganeshan, N.; Kalaiyarasi, T.; Gopukumar, S. High Capacity $Sn_xSb_yCu_z$ Composite Anodes for Lithium Ion Batteries. *Solid State Sci.* **2013**, *19*, 144–149.

(4) Sarkar, S.; Banda, H.; Mitra, S. High Capacity Lithium-Ion Battery Cathode Using LiV 3O8 Nanorods. Electrochim. Acta 2013, 99, 242–252.

(5) Sen, U. K.; Mitra, S. High-Rate and High-Energy-Density Lithium-Ion Battery Anode Containing 2D MoS_2 Nanowall and Cellulose Binder. *ACS Appl. Mater. Interfaces* **2013**, *5*, 1240–1247.

(6) M. Julien, Christian and Mauger, Alain and Zaghib, Karim and Groult, H. Comparative Issues of Cathode Materials for Li-Ion Batteries. *Inorganics* **2014**, *2*, 132–154.

(7) Cho, J.; Kim, Y. J.; Park, B. Novel $LiCoO_2$ Cathode Material with Al_2O_3 Coating for a Li Ion Cell. *Chem. Mater.* **2000**, *12*, 3788–3791.

(8) Takahashi, M.; Tobishima, S.; Takei, K.; Sakurai, Y. Reaction Behavior of $LiFePO_4$ as a Cathode Material for Rechargeable Lithium Batteries. *Solid State Ionics* **2002**, *148*, 283–289.

(9) Wang, H.; Jang, Y.; Huang, B.; Sadoway, D. R.; Chiang, Y. TEM Study of Electrochemical Cycling-Induced Damage and Disorder in $LiCoO_2$ Cathodes for Rechargeable Lithium Batteries. *J. Electrochem. Soc.* **1999**, *146*, 473–480.

(10) Xia, H.; Lu, L.; Meng, Y. S.; Ceder, G. Phase Transitions and High-Voltage Electrochemical Behavior of $LiCoO_2$ Thin Films Grown by Pulsed Laser Deposition. *J. Electrochem. Soc.* **2007**, *154*, A337–A342.

(11) Chung, K. Y.; Yoon, W.-S.; McBreen, J.; Yang, X.-Q.; Oh, S. H.; Shin, H. C.; Cho, W. Il; Cho, B. W. Structural Studies on the Effects of ZrO_2 Coating on $LiCoO_2$ during Cycling Using In Situ X-Ray Diffraction Technique. *J. Electrochem. Soc.* **2006**, *153*, A2152–A2157.

(12) Erol, S.; Orazem, M. E.; Muller, R. P. Influence of Overcharge and over-Discharge on the Impedance Response of $LiCoO_2$|C Batteries. *J. Power Sources* **2014**, *270*, 92–100.

(13) Dai, X.; Zhou, A.; Xu, J.; Lu, Y.; Wang, L.; Fan, C.; Li, J. Extending the High-Voltage Capacity of $LiCoO_2$ Cathode by Direct Coating of the Composite Electrode with Li_2CO_3 via Magnetron Sputtering. *J. Phys. Chem. C* **2016**, *120*, 422–430.

(14) Cho, J.; Kim, C.; Yoo, S. Improvement of Structural Stability of $LiCoO_2$ Cathode during Electrochemical Cycling by Sol-Gel Coating of SnO_2 . *Electrochem. Solid-State Lett.* **2000**, *3*, 362–365.

(15) Kannan, A. M.; Rabenberg, L.; Manthiram, A. High Capacity Surface-Modified $LiCoO_2$ Cathodes for Lithium-Ion Batteries . *Electrochem. Solid-State Lett.* **2003**, *6*, A16–A18.

(16) Lee, K. T.; Jeong, S.; Cho, J. Roles of Surface Chemistry on Safety and Electrochemistry in Lithium Ion Batteries. *Acc. Chem. Res.* **2013**, *46*, 1161–1170.

(17) Navarra, M. A. Ionic Liquids as Safe Electrolyte Components for Li-Metal and Li-Ion Batteries. *MRS Bull.* **2013**, *38*, 548–553.

(18) Mun, J.; Yim, T.; Park, J. H.; Ryu, J. H.; Lee, S. Y.; Kim, Y. G.; Oh, S. M. Allylic Ionic Liquid Electrolyte-Assisted Electrochemical Surface Passivation of $LiCoO_2$ for Advanced, Safe Lithium-Ion Batteries. *Sci. Rep.* **2014**, *4*, 5802.

(19) Theivaprakasam, S.; MacFarlane, D. R.; Mitra, S. Electrochemical Studies of N-Methyl N-Propyl Pyrrolidinium Bis(trifluoromethanesulfonyl) Imide Ionic Liquid Mixtures with Conventional Electrolytes in $LiFePO_4$/Li Cells. *Electrochim. Acta* **2015**, *180*, 737–745.

(20) Marczewski, M. J.; Stanje, B.; Hanzu, I.; Wilkening, M.; Johansson, P. "Ionic Liquids-in-Salt" - a Promising Electrolyte Concept for High-Temperature Lithium Batteries? *Phys. Chem. Chem. Phys.* **2014**, *16*, 12341–12349.

(21) Forsyth, S. A.; Pringle, J. M.; MacFarlane, D. R. Ionic Liquids—an Overview. *Aust. J. Chem.* **2004**, *57*, 113–119.

(22) MacFarlane, D. R.; Pringle, J. M.; Howlett, P. C.; Forsyth, M. Ionic Liquids and Reactions at the Electrochemical Interface. *Phys. Chem. Chem. Phys.* **2010**, *12*, 1659–1669.

(23) MacFarlane, D. R.; Forsyth, M.; Howlett, P. C.; Pringle, J. M.; Sun, J.; Annat, G.; Neil, W.; Izgorodina, E. I. Ionic Liquids in Electrochemical Devices and Processes: Managing Interfacial Electrochemistry. *Acc. Chem. Res.* **2007**, *40*, 1165–1173.

(24) Matsumoto, H.; Sakaebe, H.; Tatsumi, K.; Kikuta, M.; Ishiko, E.; Kono, M. Fast Cycling of Li/$LiCoO_2$ Cell with Low-Viscosity Ionic Liquids Based on Bis(fluorosulfonyl)imide $[FSI]^-$. *J. Power Sources* **2006**, *160*, 1308–1313.

(25) Egashira, M.; Tanaka-Nakagawa, M.; Watanabe, I.; Okada, S.; Yamaki, J. Charge–discharge and High Temperature Reaction of $LiCoO_2$ in Ionic Liquid Electrolytes Based on Cyano-Substituted Quaternary Ammonium Cation. *J. Power Sources* **2006**, *160*, 1387–1390.

(26) Chou, S.-L.; Wang, J.-Z.; Sun, J.-Z.; Wexler, D.; Forsyth, M.; Liu, H.-K.; MacFarlane, D. R.; Dou, S.-X. High Capacity, Safety, and Enhanced Cyclability of Lithium Metal Battery Using a V_2O_5 Nanomaterial Cathode and Room Temperature Ionic Liquid Electrolyte. *Chem. Mater.* **2008**, *20*, 7044–7051.

(27) Howlett, P. C.; MacFarlane, D. R.; Hollenkamp, A. F. High Lithium Metal Cycling Efficiency in a Room-Temperature Ionic Liquid. *Electrochem. Solid-State Lett.* **2004**, *7*, A97--A101.

(28) Yoon, H.; Howlett, P. C.; Best, A. S.; Forsyth, M.; MacFarlane, D. R. Fast Charge/discharge of Li Metal Batteries Using an Ionic Liquid Electrolyte. *J. Electrochem. Soc.* **2013**, *160*, A1629–A1637.

(29) Huang, J.; Hollenkamp, A. F. Thermal Behavior of Ionic Liquids Containing the FSI Anion and the Li^+ Cation. *J. Phys. Chem. C* **2010**, *114*, 21840–21847.

(30) Howlett, P. C.; Izgorodina, E. I.; Forsyth, M.; Macfarlane, D. R. Electrochemistry at Negative Potentials in Bis(trifluoromethanesulfonyl)amide Ionic Liquids. *Z. Phys. Chem* **2006**, *220*, 1483–1498.

(31) Guerfi, A.; Dontigny, M.; Charest, P.; Petitclerc, M.; Lagacé, M.; Vijh, A.; Zaghib, K. Improved Electrolytes for Li-Ion Batteries: Mixtures of Ionic Liquid and Organic Electrolyte with Enhanced Safety and Electrochemical Performance. *J. Power Sources* **2010**, *195*, 845–852.

(32) Quinzeni, I.; Ferrari, S.; Quartarone, E.; Tomasi, C.; Fagnoni, M.; Mustarelli, P. Li-Doped Mixtures of Alkoxy-N-Methylpyrrolidinium Bis(trifluoromethanesulfonyl)-Imide and Organic Carbonates as Safe Liquid Electrolytes for Lithium Batteries. *J. Power Sources* **2013**, *237*, 204–209.

(33) Lombardo, L.; Brutti, S.; Navarra, M. A.; Panero, S.; Reale, P. Mixtures of Ionic Liquid – Alkylcarbonates as Electrolytes for Safe Lithium-Ion Batteries. *J. Power Sources* **2013**, *227*, 8–14.

(34) Kühnel, R.-S.; Böckenfeld, N.; Passerini, S.; Winter, M.; Balducci, A. Mixtures of Ionic Liquid and Organic Carbonate as Electrolyte with Improved Safety and Performance for Rechargeable Lithium Batteries. *Electrochim. Acta* **2011**, *56*, 4092–4099.

(35) Aguilera, L.; Scheers, J.; Matic, A. Enhanced Low-Temperature Ionic Conductivity via Different Li^+ Solvated Clusters in Organic Solvent/ionic Liquid Mixed Electrolytes. *Phys. Chem. Chem. Phys.* **2016**, *18*, 25458–25464.

(36) Sharma, N.; Han, M. H.; Pramudita, J. C.; Gonzalo, E.; Brand, H. E. A.; Rojo, T.; Peterson, V. K.; Rojo, T.; Huang, X.; Ogumi, Z.; et al. A Comprehensive Picture of the Current Rate Dependence of the Structural Evolution of P2-$Na_{2/3}Fe_{2/3}Mn_{1/3}O_2$. *J. Mater. Chem. A* **2015**, *3*, 21023–21038.

(37) Sharma, N.; Tapia-Ruiz, N.; Singh, G.; Armstrong, A. R.; Pramudita, J. C.; Brand, H. E. A.; Billaud, J.; Bruce, P. G.; Rojo, T. Rate Dependent Performance Related to Crystal Structure Evolution of $Na_{0.67}Mn_{0.8}Mg_{0.2}O_2$ in a Sodium-Ion Battery. *Chem. Mater.* **2015**, *27*, 6976–6986.

(38) Wallwork, K. S.; Kennedy, B. J.; Wang, D. The High Resolution Powder Diffraction Beamline for the Australian Synchrotron. In *AIP Conference Proceedings*; AIP, 2007; Vol. 879, pp. 879–882.

(39) Toby, B. H. EXPGUI, a Graphical User Interface for GSAS. *J. Appl. Cryst* **2001**, *34*, 210–213.

(40) Larson, A. C.; Von Dreele, R. B. General Structure Analysis System (GSAS). *Rep. laur 86-748, Los Alamos Natl. Lab.* **2004**, *748*.

(41) Wu, F.; Zhu, Q.; Li, L.; Chen, R.; Chen, S. A Diisocyanate/sulfone Binary Electrolyte Based on Lithium Difluoro(oxalate)borate for Lithium Batteries. *J. Mater. Chem. A* **2013**, *1*, 3659–3666.

(42) Mun, J.; Kim, S.; Yim, T.; Ryu, J. H.; Kim, Y. G.; Oh, S. M. Comparative Study on Surface Films from Ionic Liquids Containing Saturated and Unsaturated Substituent for $LiCoO_2$. J. Electrochem. Soc. 2010, 157, A136–A141.

(43) Zheng, J.; Gu, M.; Chen, H.; Meduri, P.; Engelhard, M. H.; Zhang, J.-G.; Liu, J.; Xiao, J. Ionic Liquid-Enhanced Solid State Electrolyte Interface (SEI) for Lithium-Sulfur Batteries. *J. Mater. Chem. A* **2013**, *1*, 8464–8470.

(44) Jung, Y. S.; Cavanagh, A. S.; Dillon, A. C.; Groner, M. D.; George, S. M.; Lee, S.-H. Enhanced Stability of $LiCoO_2$ Cathodes in Lithium-Ion Batteries Using Surface Modification by Atomic Layer Deposition. *J. Electrochem. Soc.* **2010**, *157*, A75–A81.

(45) Takahashi, Y.; Tode, S.; Kinoshita, A.; Fujimoto, H.; Nakane, I.; Fujitani, S. Development of Lithium-Ion Batteries with a $LiCoO_2$ Cathode Toward High Capacity by Elevating Charging Potential. *J. Electrochem. Soc.* **2008**, *155*, A537–A541.

(46) El Ouatani, L.; Dedryvère, R.; Siret, C.; Biensan, P.; Reynaud, S.; Iratçabal, P.; Gonbeau, D. The Effect of Vinylene Carbonate Additive on Surface Film Formation on Both Electrodes in Li-Ion Batteries. *J. Electrochem. Soc.* **2009**, *156*, A103.

(47) Xia, J.; Petibon, R.; Sinha, N. N.; Dahn, J. R. One Sulfonate and Three Sulfate Electrolyte Additives Studied in Graphite/$LiCoO_2$ Pouch Cells. *J. Electrochem. Soc.* **2015**, *162*, A2227–A2235.

(48) Xu, M.; Zhou, L.; Dong, Y.; Chen, Y.; Demeaux, J.; MacIntosh, A. D.; Garsuch, A.; Lucht, B. L. Development of Novel Lithium Borate Additives for Designed Surface Modification of High Voltage $LiNi_{0.5}Mn_{1.5}O_4$ Cathodes. *Energy Environ. Sci.* **2016**, *9*, 1308–1319.

(49) Wongittharom, N.; Wang, C.-H.; Wang, Y.-C.; Fey, G. T.-K.; Li, H.-Y.; Wu, T.-Y.; Lee, T.-C.; Chang, J.-K. Charge-Storage Performance of Li/$LiFePO_4$ Cells with Additive-Incorporated Ionic Liquid Electrolytes at Various Temperatures. *J. Power Sources* **2014**, *260*, 268–275.

(50) Verdier, S.; El Ouatani, L.; Dedryvère, R.; Bonhomme, F.; Biensan, P.; Gonbeau, D. XPS Study on Al_2O_3- and $AlPO_4$-Coated $LiCoO_2$ Cathode Material for High-Capacity Li Ion Batteries. *J. Electrochem. Soc.* **2007**, *154*, A1088–A1099.

(51) Niehoff, P.; Passerini, S.; Winter, M. Interface Investigations of a Commercial Lithium Ion Battery Graphite Anode Material by Sputter Depth Profile X-Ray Photoelectron Spectroscopy. *Langmuir* **2013**, *29*, 5806–5816.

(52) Budi, A.; Basile, A.; Opletal, G.; Hollenkamp, A. F.; Best, A. S.; Rees, R. J.; Bhatt, A. I.; O'Mullane, A. P.; Russo, S. P. Study of the Initial Stage of Solid Electrolyte Interphase Formation upon Chemical Reaction of Lithium Metal and N-Methyl-N-Propyl-Pyrrolidinium-Bis(Fluorosulfonyl)Imide. *J. Phys. Chem. C* **2012**, *116*, 19789–19797.

(53) Herstedt, M.; Abraham, D. P.; Kerr, J. B.; Edström, K. X-Ray Photoelectron Spectroscopy of Negative Electrodes from High-Power Lithium-Ion Cells Showing Various Levels of Power Fade. *Electrochim. Acta* **2004**, *49*, 5097–5110.

(54) Dedryvère, R.; Laruelle, S.; Grugeon, S.; Poizot, P.; Gonbeau, D.; Tarascon, J.-M. Contribution of X-Ray Photoelectron Spectroscopy to the Study of the Electrochemical Reactivity of CoO toward Lithium. *Chem. Mater.* **2004**, *16*, 1056–1061.

(55) Rossen, E.; Reimers, J.; Dahn, J. Synthesis and Electrochemistry of Spinel LT-$LiCoO_2$. *Solid State Ionics* **1993**, *62*, 53–60.

(56) Antolini, E. $LiCoO_2$: Formation, Structure, Lithium and Oxygen Nonstoichiometry, Electrochemical Behaviour and Transport Properties. *Solid State Ionics* **2004**, *170*, 159–171.

(57) Sharma, N.; Peterson, V. K.; Elcombe, M. M.; Avdeev, M.; Studer, A. J.; Blagojevic, N.; Yusoff, R.; Kamarulzaman, N. Structural Changes in a Commercial Lithium-Ion Battery during Electrochemical Cycling: An in Situ Neutron Diffraction Study. *J. Power Sources* **2010**, *195*, 8258–8266.

(58) Dahn, J.; Fuller, E.; Obrovac, M.; Vonsacken, U. Thermal Stability of Li_xCoO_2, Li_xNiO_2 and λ-MnO_2 and Consequences for the Safety of Li-Ion Cells. *Solid State Ionics* **1994**, *69*, 265–270.

(59) Amatucci, G. G.; Tarascon, J. M.; Klein, L. C. CoO_2, The End Member of the $Li_X CoO_2$ Solid Solution. *J. Electrochem. Soc.* **1996**, *143*, 1114–1123.

(60) Reimers, J. N.; Dahn, J. R. Electrochemical and In Situ X-Ray Diffraction Studies of Lithium Intercalation in Li_XCoO_2 . *J. Electrochem. Soc.* **1992**, *139*, 2091–2097.

(61) Gummow, R.; Thackeray, M.; David, W.; Hull, S. Structure and Electrochemistry of Lithium Cobalt Oxide Synthesised at 400°C. *Mater. Res. Bull.* **1992**, *27*, 327–337.

(62) Taminato, S.; Hirayama, M.; Suzuki, K.; Tamura, K.; Minato, T.; Arai, H.; Uchimoto, Y.; Ogumi, Z.; Kanno, R. Lithium Intercalation and Structural Changes at the $LiCoO_2$ Surface under High Voltage Battery Operation. *J. Power Sources* **2016**, *307*, 599–603.

Chapter 4

$LiFePO_4$ Based Batteries with Hybrid Electrolytes and Applications at Subzero Temperatures

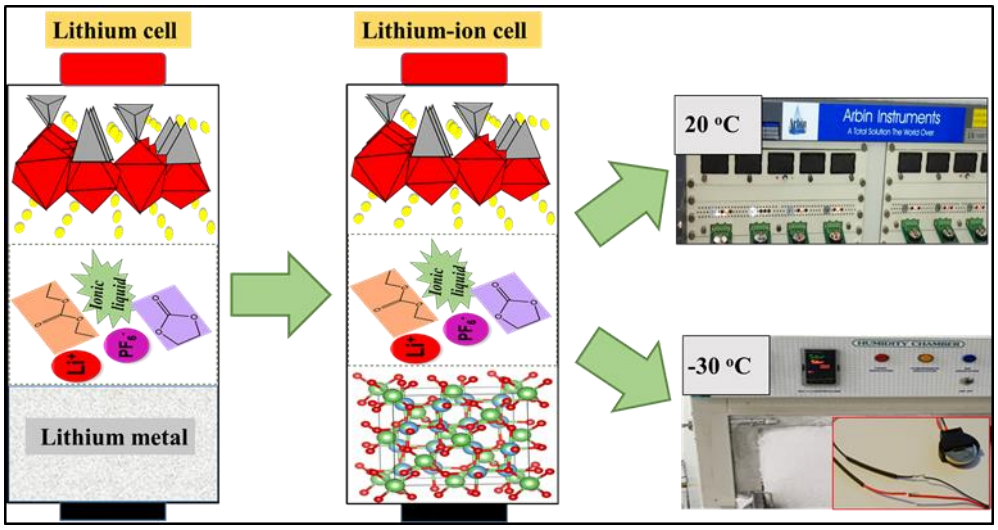

- Part of this chapter is published as a journal publication:

Theivaprakasam, S.; MacFarlane, D. R.; Mitra, S. Electrochemical Studies of N-Methyl N-Propyl Pyrrolidinium Bis(trifluoromethanesulfonyl) Imide Ionic Liquid Mixtures with Conventional Electrolytes in $LiFePO_4$/Li Cells. *Electrochim. Acta* **2015**, *180*, 737–745.

- Part of this chapter is filed as a patent:

Patent number 201721017681, dated 19 May 2017.

4.1 Introduction

The electrode–electrolyte chemistry is the most researched area in the development of LiB technology[1]. The compatibility of the electrolyte with the anode and the cathode, plays an important role in the performance of the battery[2]. The replacement of lithium metal anodes to graphite anodes had significantly reduced the safety issues of lithium batteries; however, the thermal instability of the alkyl carbonates and $LiPF_6$ salt poses safety risks[3–6]. Further at high temperatures, the gaseous products formed as a result of electrolyte decomposition serves as the potential source of battery explosion which is a major safety concern[3]. Therefore, the search to enhance the thermal stability of the electrolyte constituents is an important goal in the area of LiB technology. Apart from the electrolyte, the safety of LiB also dependent on the choice of cathode and anode. The following section details the safety aspects of the common anode and cathode materials in LiBs.

In the case of cathode materials, the most commonly used are the lithium-intercalated metal oxides. These metal oxide cathodes possess the risk of thermal instability, due to the evolution of oxygen from the crystal lattice at high temperatures which may led to collapse of the battery[7,8]. In such cases, the lithium iron phosphate ($LiFePO_4$) cathode introduced in 1997 by Padhi et al.[9] is considered as the safe cathode material. The strong metal phosphate bonds help in the stability of $LiFePO_4$ cathodes and, as a result, they are safe in comparison to the metal oxide cathodes[10]. Due to their inherent safety, $LiFePO_4$ is the most commonly preferred cathode material in electric vehicle applications[11–13]. However, the most common problem that is associated with $LiFePO_4$ cathodes is their low electronic conductivity in comparison to other oxide cathode materials. However, the conductivity issues are being addressed by particle size reduction or by using suitable dopants[14–16].

In the case of anodes, the most commonly used material is graphite. In spite of the wide range of cathodes that were proposed and commercialized from the time of the inception of LiBs, graphite is the most successful commercial anode material used in almost all LiB. This is due to the following reasons.

1. Low redox potential of graphite anodes, close to that of lithium metal
2. The effective SEI formed on the graphite surface, which in turn leads to better capacity retention and cycle life of LiBs[17].

3. In low temperature applications, the issues of lithium plating on the graphite electrodes creates a severe safety threat to the batteries[18,19].

In such circumstances, an alternative safe anode can be the lithium titanium oxide ($Li_4Ti_5O_{12}$) anodes with a theoretical capacity of 175 mAh/g[19]. $Li_4Ti_5O_{12}$ has spinel structure which operates at a higher potential of ~ 1.5 V vs. Li/Li^+. Since this anode material operates at higher potential, SEI/passivation is not pronounced[1]. However, at elevated temperatures, $Li_4Ti_5O_{12}$ anodes have severe gassing issues in the electrolyte which may lead to the swelling of batteries. Further, this anode cannot be compared with graphite in terms of its theoretical capacity and redox potential; however, it is desirable in terms of its safety and higher reversibility. Further, steps were taken to increase the lithium storage capacity and rate capability of $Li_4Ti_5O_{12}$ anodes through nanostructuring and doping with reduced graphene oxides[20–22]. Nevertheless, $Li_4Ti_5O_{12}$ anodes and $LiFePO_4$ are the preferred candidates in LiB for electric vehicle applications[1,23].

Besides safety, another important concern in LiBs, is their narrow operating temperature of –10 ^oC to 60 ^oC. In such circumstances, the electrolyte in LiB was seen as one of the reason for their limited temperature window[24,25]. However, the LiBs are expected to operate beyond these temperature limits in various applications. The performance at higher temperatures (above 60 ^oC) is restricted to the low thermal stability of the solvents that are used in the electrolytes. The limited performances at low temperatures is predominantly due to the freezing of the solvents that are used in the electrolyte and the slow lithium ion diffusion kinetics[5,6,26–28]. Other concerns are the serious capacity fade and the plating of lithium on graphite anodes at low temperatures[18]. However, the actual mechanism that is responsible for the poor performance at low temperatures is not clear[25,27,29,30]. This problem can be addressed by the careful selection of the electrode materials and electrolyte ingredients.

Commonly preferred electrode materials and electrolyte ingredients for low temperature operations are as follows,

- In the case of anodes, graphite is not preferred due to its lithium platting issues whereas $Li_4Ti_5O_{12}$ is preferred for its better performances at low temperatures[1].

- In the case of the cathodes, $LiFePO_4$, lithium manganese oxide ($LiMn_2O_4$), and lithium nickel cobalt aluminum oxide doped ($LiNiCoAlO_2$) cathodes were studied for their appreciable low temperature performances[25,31].
- In the case of the electrolytes, efforts were taken to increase the ionic conductivity through the addition of organic solvents in the electrolyte composition.

There are several reported patents[32–41] and publications[24,27,31,42] that explain the impact of various organic solvents in the electrolyte composition. Nevertheless, most of those compositions have limited room temperature applications due to flammability and undesired electrochemical side reactions of the solvents that are used in the electrolyte.

In this chapter, the choice of lithium-ion configuration is the $Li_4Ti_5O_{12}$/HE/$LiFePO_4$ system for low temperature applications. Initial studies involved the understanding of $LiFePO_4$ cathodes with HE. Later, $LiFePO_4$ cathodes were coupled with $Li_4Ti_5O_{12}$ anodes to study their performance in the lithium-ion configuration.

Further, efforts were taken to study the subzero temperature performance of the $Li_4Ti_5O_{12}$/$LiFePO_4$ system using a special composition (HE*). HE* was initially characterized for low temperature applications. Subsequently, the electrolyte was tested in $Li_4Ti_5O_{12}$/$LiFePO_4$ to study battery performance.

4.2 Experimental

The outline on the materials used for the study, the details of the electrochemical, surface, and structural characterizations are elaborated in this section. The modus operandi of the subzero performance analysis is discussed separately in the section 4.2.4. The methods discussed in this chapter refers to the experiments carried out at room temperatures unless specified otherwise.

4.2.1 Materials

Similarly, $Li_4Ti_5O_{12}$ (Batsol, India), carbon black and polyvinylidene fluoride–hexa fluoro propylene (PVDF-HFP) were mixed with N-Methyl Pyrrolidone in the ratio of 70:20:10 for the slurry. The slurry was then coated onto copper current collector (MTI corp., USA, 10µm thickness) using the doctor blade technique. The coated electrode was then dried for

24 h in an air oven. After drying, the ($LiFePO_4$/$Li_4Ti_5O_{12}$) electrodes were punched into circular disks of required diameter 12 mm. These circular electrode disks were used further for the cell fabrication. The HE composition is the mixture of 40 percent N-methyl-N-propylpyrrolidinium bis(trifluoromethanesulfonyl)imide ([C_3mpyr] [TFSI]) in 1M $LiPF_6$ in ethylene carbonate (EC): diethyl carbonate (DEC) (1:1). Neat [C_3mpyr] [TFSI] (Solvionic, France) is also used as the electrolyte for reference studies. The initial studies on HE were compared with the conventional electrolyte (1M $LiPF_6$ in ethylene carbonate: dimethyl carbonate (DMC) (1:1) (LP30)).

Borosilicate glass microfiber separators (GF/D, Whatman) were used as separators for the Li/electrolyte/$LiFePO_4$ cells and polypropylene separators were used for the $Li_4Ti_5O_{12}$/electrolyte/$LiFePO_4$ cells.

For better clarity, Li/electrolyte/$LiFePO_4$ cells will be referred to as lithium cells and $Li_4Ti_5O_{12}$/electrolyte/$LiFePO_4$ cells as lithium-ion cells in the rest of this chapter.

4.2.2 Cell Fabrication

The lithium cell fabrication was carried out similar as explained in the Chapter 3 whereas the modus operandi for the lithium-ion cell will be discussed in this chapter. The lithium-ion cells were made in 2016 coin cell configuration by using $Li_4Ti_5O_{12}$ and $LiFePO_4$ electrodes. The steps involved in the fabrication of coin cell for electrochemical measurements are illustrated in Figure 4.1. Initially, the cell components were arranged as per the sequence inside the glove box by using an automatic coin cell crimper (Hohsen Corp.). The sealed cell can be used further for the electrochemical measurements. It is to be noted that the moisture and oxygen levels of the glove box were maintained as 0.5 ppm and 1.2 ppm, respectively.

4.2.3 Electrochemical Characterization

Cyclic Voltammetry (CV) studies were carried out in Biologic VMP-3 instrument by using a two-electrode cell with $LiFePO_4$ as the working electrode, lithium metal as the reference and counter electrode.

Galvanostatic charge-discharge studies were carried out in Arbin Instruments, USA (BT2000 model) at the C rate of C/5. It is to be noted that the potential window of operation varies with the electrode and cell configuration and are mentioned as follows,

i. The $Li/LiFePO_4$ cells were cycled in the potential window of 2.5– 4.1 V vs. Li/Li^+.
ii. The $Li/Li_4Ti_5O_{12}$ cells were cycled in the potential window of 2–0.95 V vs. Li/Li^+.
iii. The lithium-ion ($Li_4Ti_5O_{12}$/electrolyte/$LiFePO_4$) cells were cycled in the potential window of 1.5–2.3 V.

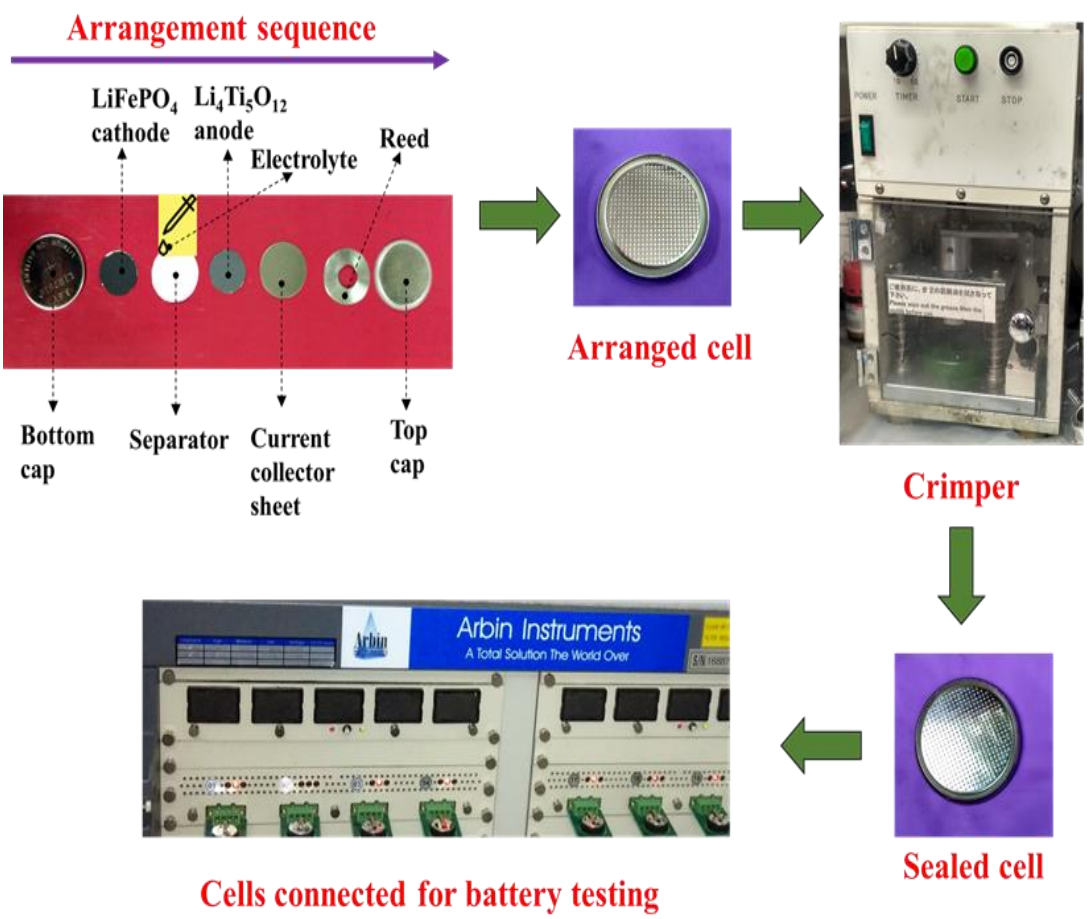

Figure 4.1 *Steps involved in the fabrication of lithium-ion cell for battery testing.*

4.2.4 Post Analysis of $LiFePO_4$ Electrodes

4.2.4.1 Electrode Washing

Electrodes, after the cycling events (first charging, first discharging, and after 100 cycles as mentioned) were opened inside the glove box. The electrodes that were cycled in HE were washed by using DEC and the electrodes that were cycled with the conventional electrolyte were washed with DMC. The electrodes were then dried in a vacuum oven at 60 ^oC overnight and then stored in the glove box.

4.2.4.2 Post Analysis Techniques

X-ray diffraction (XRD) studies of $LiFePO_4$ samples were carried out in an X-ray Diffractometer (Rigaku Smart lab X-ray Diffractometer, Japan) with a Cu K alpha radiation of 1.514 Å over a scan range of 10 to 40 ^{o}C with a step size of 5 degree/minute.

Field emission gun scanning electron microscopy (FEG-SEM, ZEISS Ultra-55) and High-resolution transmission electron microscopy (HR-TEM, JEOL-2100F]) were used to study the surface morphology of the electrodes.

The surface composition of the cycled electrodes was studied by Energy Dispersive X-ray Analysis (Oxford EDS system) as well as with ex situ Fourier-transform infrared spectroscopy (FTIR) in the Attenuated Total Reflection (ATR) mode. Care was taken to minimize the exposure of the samples to the atmosphere while analyzing them in the ex situ mode.

4.2.5 Subzero Temperature Battery Tests

For subzero battery cycling, lithium-ion cells were cycled inside a Eurotherm temperature-controlled chamber that was connected to the Biologic SP 150 potentiostat, as shown in Figure 4.2.

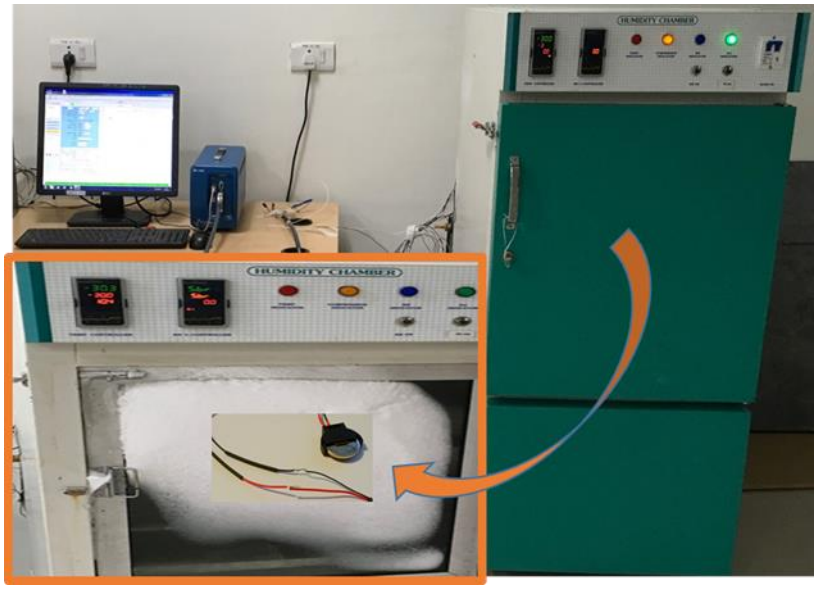

Figure 4.2 *Photograph illustrating the cycling of the lithium-ion cell at –30 ^{o}C, a closer view of which is presented in the inset figure.*

The subzero temperature analyses were focused mainly at –30 ºC whereas some experiments were carried out at –20 ºC for comparison purpose. HE* is a mixture of 40 percent N-Methyl-N-propylpyrrolidinium bis(fluorosulfonyl)imide in 1 M $LiPF_6$ salt in 1:1 EC : DEC mixture (Indian patent 201721017681 dated 19/05/17). The ionic conductivity and DSC of the HE* were measured by using the same protocol as that which was discussed in Chapter 2.

Galvanostatic charge discharge studies for subzero temperature analysis was carried out in the potential window of 1.5 to 2.3 V. Electrochemical Impedance Spectroscopy (EIS) measurements were carried out in the frequency range of 1 MHz to 0.1 Hz.

4.3 Results and Discussion

In this section, the electrochemical performances of $LiFePO_4$ were studied by using CV and Galvanostatic charge-discharge studies. Further, characterization of the delithiated $LiFePO_4$ electrodes were carried out by using EIS, XRD, FEG-SEM, FE TEM, and FTIR analysis. Further, $LiFePO_4$ cathodes were combined with $Li_4Ti_5O_{12}$ anodes for lithium-ion cell studies. The lithium-ion cells were cycled initially at room temperatures.

The second part of this section deals with the subzero temperature cycling of the lithium-ion cells by using HE*. In this section, the change in the interfacial resistance with the cycle numbers and the battery performances were focused at –30 ºC. The performances at –30 ºC were further compared to the performances at –20 ºC and 20 ºC for comparison purposes.

4.3.1 Studies on Li/$LiFePO_4$ cells

4.3.1.1 CV Studies

The CV studies were carried out on $LiFePO_4$ electrodes with the conventional electrolyte, HE and [C_3mpyr][TFSI] electrolytes, as shown in Figure 4.3. At a scan rate of 0.5 mV/s, the peak current was normalized to the mass of the electrode which was then compared across the three systems. It was found that the neat [C_3mpyr][TFSI] with its higher viscosity and low conductivity, has the lowest peak current, whereas, the HE shows a peak current performance that was better than the conventional system. The increase in the peak

current may be an effect of the increased rate of diffusion of the lithium ions in the electrolytes or the $LiFePO_4$ cathodes.

To investigate the diffusion-controlled behavior, the effect of the scan rate on the peak current was studied as shown in Figure 4.4. Denis et al. demonstrated that the intercalation process in $LiFePO_4$ can be described in terms of a reversible model[43], hence the Randles–Sevcik equation (Equation 4.1) can be applied to calculate the apparent diffusion coefficient in the system[44]:

$$\frac{i_p}{\mathrm{m}} = 0.4463\mathrm{F}\left(\frac{F}{RT}\right)^{0.5} C_{Li} v^{0.5} A_e D^{0.5} \qquad \text{(Equation 4.1)}$$

where,

$\frac{i_p}{\mathrm{m}}$ is the peak current per unit mass of the $LiFePO_4$ cathode in A/g,

F is the Faraday constant in C/mol,

υ is the scan rate in V/s,

C_{Li} is the initial concentration of lithium-ions in $LiFePO_4$ (equivalent to 0.0228 mol /cm^3)

A_e is the effective surface area per unit mass in cm^2/g,

D is the apparent diffusion coefficient in cm^2/s.

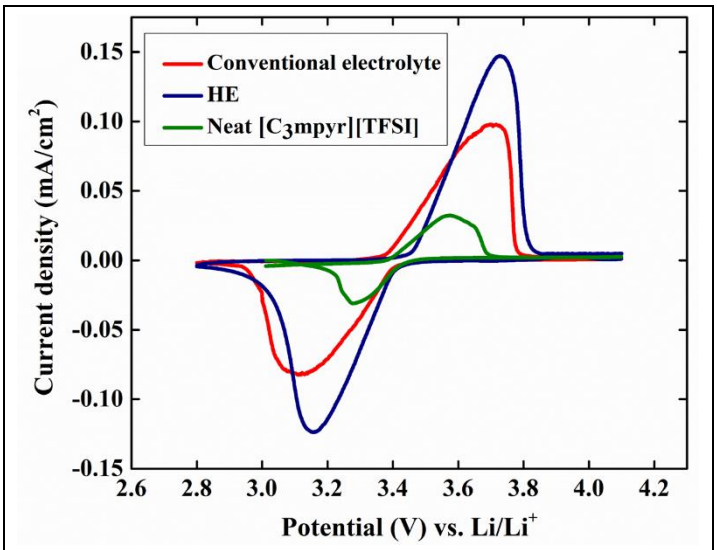

Figure 4.3 *CV of the $LiFePO_4$ electrode carried out at 20 °C with the conventional electrolyte, HE, and neat [C_3mpyr][TFSI] electrolyte at a scan rate of 0.5 mV/s .*

Diffusion controlled behavior can be further illustrated with the help of a plot of the square root of the scan rate as opposed to the peak current and is expected that the plot would yield a straight line[43] as shown in Figure 4.5. The apparent diffusion coefficient was

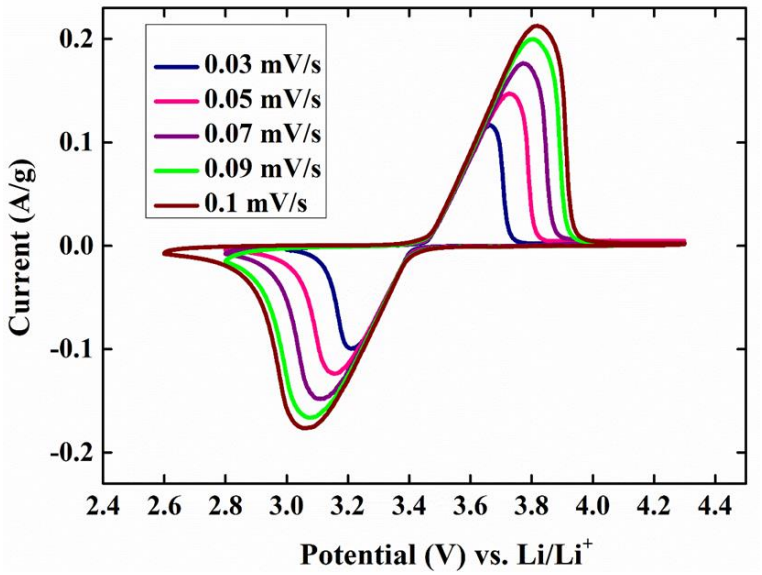

Figure 4.4 *Variation of scan rate with peak current in Li/HE/LiFePO4 system at 20 °C.*

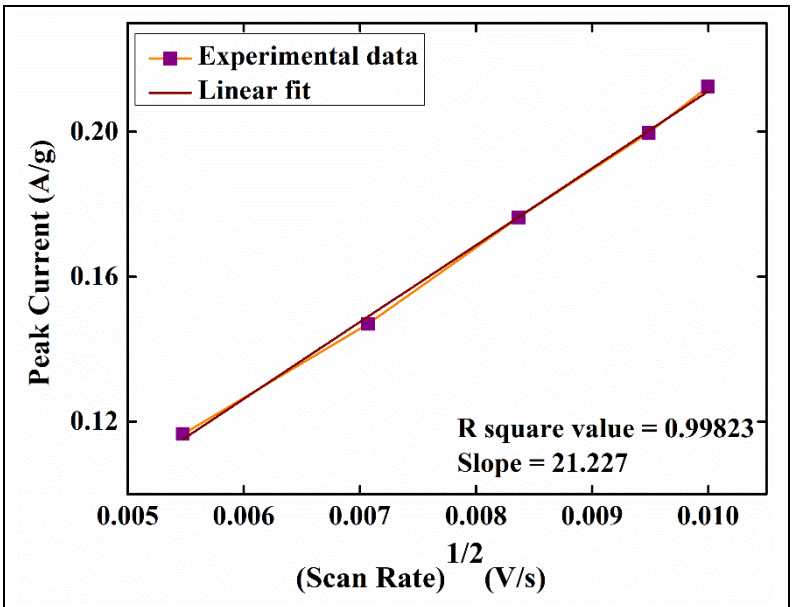

Figure 4.5 *Plot of square root of scan rate versus oxidation peak current per unit mass of the active material.*

calculated by using Equation 4.1 with the help of the slope of the plot of the square root of the scan rate versus the peak current. The values obtained for the conventional electrolyte and HE-cycled electrodes are 1.4 x 10^{-15} cm^2/s and 4.7 x 10^{-15} cm^2/s, respectively. (Due to the random distribution of the lattices, one third of the actual BET surface area (15 m^2/g as provided by the supplier) of the $LiFePO_4$ powders was used to calculate the apparent diffusion coefficient). From the calculated values, it can be observed that the HE mixture has higher apparent lithium diffusion kinetics compared to that of the conventional electrolyte system. The magnitude of these values is clearly that of a solid-state diffusion process as opposed to a solution-state process. Nonetheless, the electrolyte has an effect on the apparent diffusion coefficient (as observed in Figure 4.3) that is obtained here, as also observed by Denis et al.[43]; this may be the result of the uncertainty that surrounds the value of C_{Li} in this context, and the possible role of electrolyte factors in this quantity.

4.3.1.2 Galvanostatic Charge-Discharge Studies on $LiFePO_4$

The charge–discharge studies of $LiFePO_4$ were carried out galvanostatically at C/5 rate as shown in Figure 4.6. In the case of the conventional electrolyte, the discharge capacity was

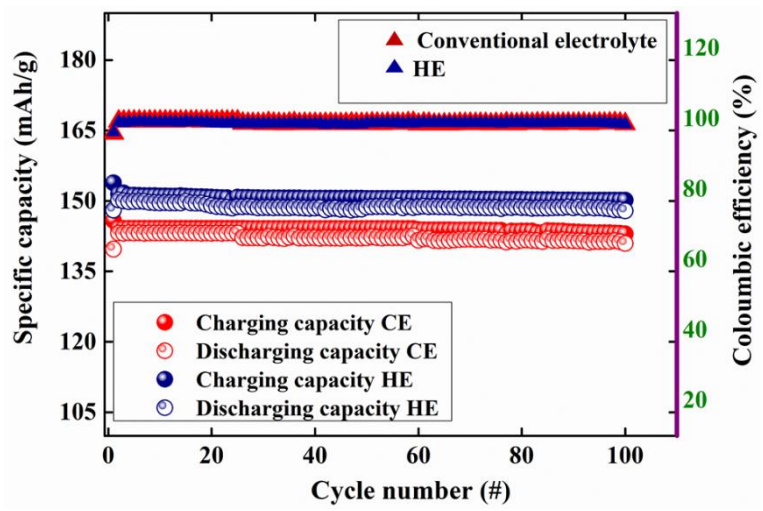

Figure 4.6 *Comparison of specific capacity and columbic efficiency versus cycle number of conventional electrolyte and HE electrolyte at C/5 rate.*

comparable to the capacities of commercial $LiFePO_4$ electrodes such as 140 mAh/g at the end of the first cycle, 143 mAh/g after the second cycle, and 141 mAh/g at the end of 100th

cycles. In the case of HE, the first discharge capacity was 148 mAh/g at the end of the first cycle, 150 mAh/g and 148 mAh/g at the end of the second and 100th cycles, respectively. The plot of the cycle number versus the specific capacity is shown in Figure 4.6. The greater ease of lithium-ion transfer on the HE interface, as explained in chapter 2, may be the origin of the slightly increased capacity in the HE mixture[45].

4.3.1.3 Interface study of $LiFePO_4$ cathodes upon aging

The most common problem that is associated with the capacity fade and stability of $LiFePO_4$ cathodes is the dissolution of the transition metal ion into the solution[12]. In this section, studies were carried out to understand the extent of iron dissolution in the presence of HE. Hence, Li/$LiFePO_4$ cells that were created by using the conventional electrolyte and HE after charging were aged at 20 ^{o}C for 30 days. At the end of 30 days, the cells were dismantled in a glove box and opened for observation. The separator in the cells, with the respective electrolytes, exhibited a clear difference which can be seen by the naked eye.

The separator from the cell which was aged by using the conventional electrolyte was brownish, whereas the separator in the cell which was cycled with HE was clear white, as shown in the inset of Figure 4.7 (a) and (b). We assumed that the color change was due to iron dissolution from $LiFePO_4$ in the system. In order to confirm this, we carried out EDS analysis of the separators, as shown in Figure 4.7. The bare glass fiber separator had traces of alkali metals and Si. As a result, the analysis of the separator in EDS showed those elements in addition to the electrolyte constituents. The conventional electrolyte aged cell showed the separator with traces of iron, while the separator that was aged with HE did not show such iron traces in the analysis.

EIS studies were also carried out on the two cells, that are shown in Figure 4.7 (c). It is observed that in the case of the conventional electrolyte/$LiFePO_4$ combination there is a slight decrease in the interfacial resistance in the initial days, which might be due to the iron dissolution[12,46]. After 30 days of storage, only a minor increase in resistance is noted, while in the case of HE, there is a notable increase in interfacial resistance which may be due to the existence of a new surface film in the HE-aged $LiFePO_4$ electrodes. Such a film has been labeled as a cathode electrolyte interface layer by Kristina et al.[47]. It is believed that the acidic reactions that occur on the cathode surface due to $LiPF_6$ can be alleviated by the ionic liquid-assisted film formed on the surface of the cathode[48].

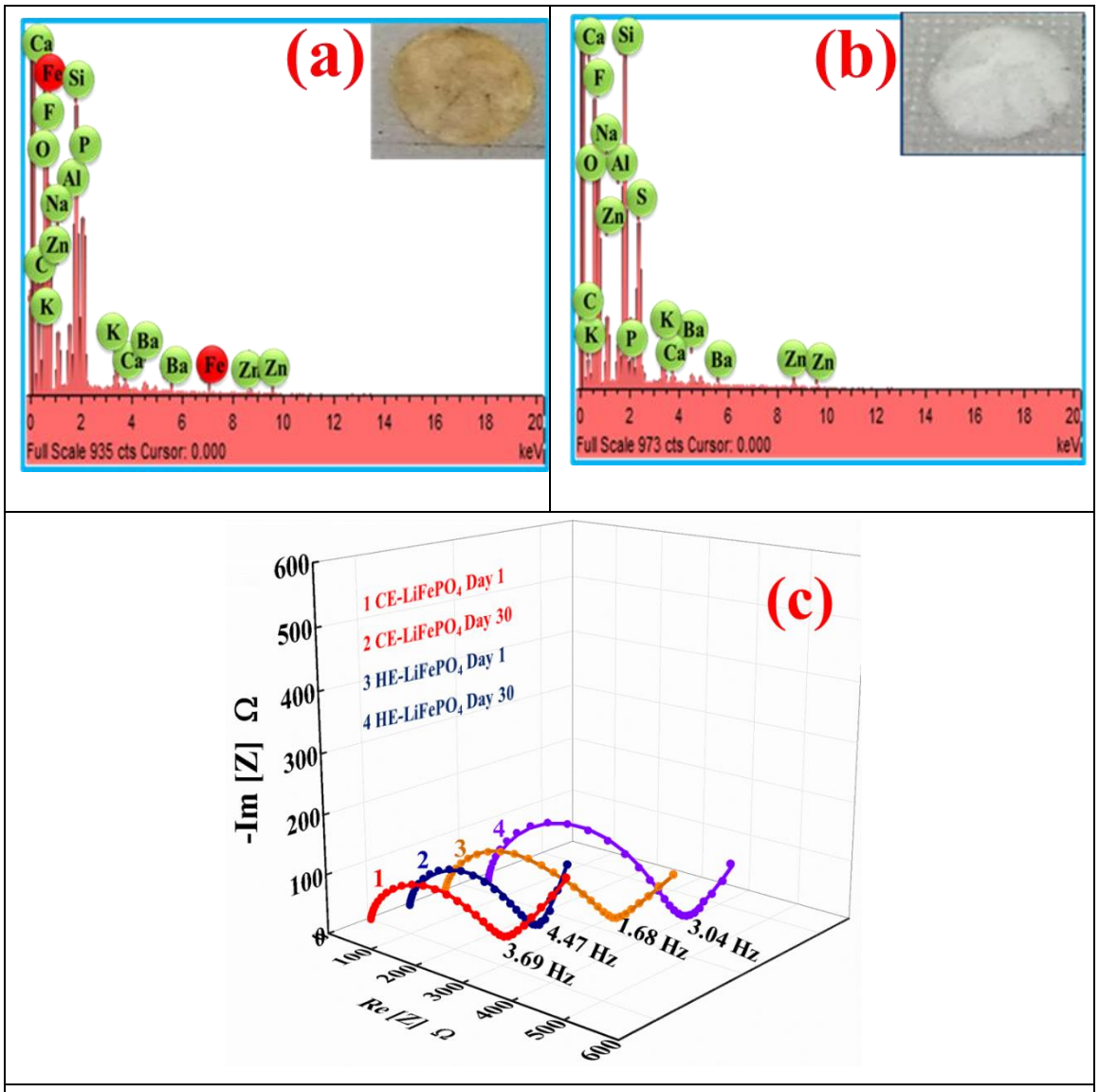

Figure 4.7 *FEG-SEM-EDS analysis of the separator in (a) Li/conventional electrolyte/$LiFePO_4$ aged cell (b) Li/HE/$LiFePO_4$ aged cell. (c) EIS study of aged $LiFePO_4$ electrodes at 20 ^oC in conventional electrolyte and HE electrolytes.*

4.3.1.4 Post Analyses of the Cycled Electrodes

Post-cycling analyses of the cycled electrodes were carried out XRD, FTIR, FEG-SEM, EDS, and HR TEM analyses, to obtain better understanding on the surface morphology, composition, and structural stability of the system.

4.3.1.4.1 XRD Analysis

Post-cycling XRD analysis was carried out on the washed electrode films after first charging, after first discharging, and after final discharge at the end of 100 cycles as shown in Figure 4.8. After the first discharge, the profile shows the typical pattern of delithiated $LiFePO_4$ electrodes in HE. A comparison of the XRD profiles of the first charging in both the electrolytes shows that the introduction of [C_3mpyr][TFSI] into the HE did not cause any structural changes in the cathode after the first charging as well as after 100 cycles.

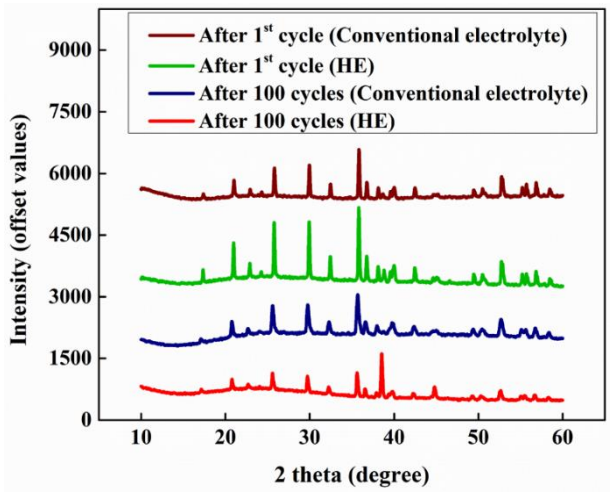

Figure 4.8 *Ex situ XRD analysis of $LiFePO_4$ electrodes on conventional electrolyte and HE.*

4.3.1.4.2 FTIR Analysis

FTIR studies were carried out on cycled $LiFePO_4$ electrode foils before cycling, after first charging cycle, the first discharging cycle in the conventional electrolyte and HE. The comparison of the FTIR spectrum of the electrode foils at various stages is shown in Figure 4.9. In the fresh electrode, which is a mixture of carbon and the binder with $LiFePO_4$, the typical carbon stretching and P-O stretching of $LiFePO_4$ was seen from the peaks[49] at 1139 –945 cm^{-1}. The singlet peak at 930 cm^{-1} and doublet peaks in the regions of 538–493 cm^{-1} can be attributed to the stretching of the phosphate anion[50], as exhibited in all four FTIR plots of Figure 4.9. From Figure 4.9 (b) and 4.9 (c), slight distinctions were noted for the $LiFePO_4$ electrode that was charged in the conventional electrolyte and HE. Since the HE electrolyte is a mixture of conventional electrolyte constituents, certain similar peaks

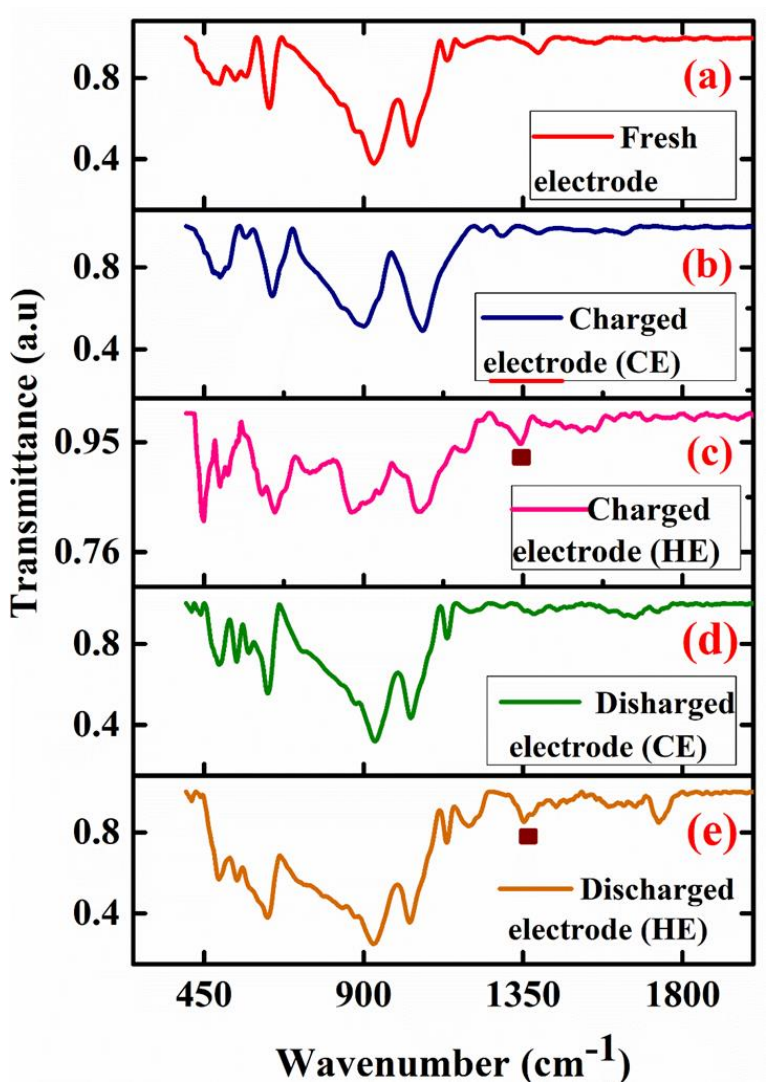

Figure 4.9 *FTIR-ATR analysis of $LiFePO_4$ cycled electrodes after first charging, discharging in conventional electrolyte and HE mixture.*

in the $LiFePO_4$ electrodes are cycled in both the electrolytes. On the other hand, certain peaks were introduced in the HE-cycled $LiFePO_4$ such as at 1352 cm^{-1} which can also be attributed to the effect of the S=O=S stretching[51] of the added [C_3mpyr][TFSI]. It is noticed that the peak was not observed on the fresh $LiFePO_4$ electrode and the conventional electrolyte cycled $LiFePO_4$ electrodes. The peak due to [C_3mpyr][TFSI] occurs in the $LiFePO_4$ electrode after the first discharge cycle in HE, as shown in Figure 4.9 (d). This indicates that the added ionic liquid has an influence on the composition of the surface that is quite constant after cycling as well. Hence, it was believed that the change in the surface film composition may alter the interfacial behavior in the HE system.

4.3.1.4.3 SEM Analysis

The FEG-SEM-EDS analysis of the $LiFePO_4$ electrode before cycling, after the first charge in the conventional electrolyte and HE reveals that there is a difference in the surface morphology of the electrodes that are cycled in conventional electrolyte, HE, and neat [C_3mpyr] [TFSI] (Figure 4.10). On a closer view, it can be seen that a thin film is present on the surface of the HE-cycled electrodes but not in the conventional electrolyte-cycled electrodes. We believe that the surface film might be due to [C_3mpyr] [TFSI] in the mixture. Such surface film formation was also observed in $LiCoO_2$ cathodes cycled using HE as described in Chapter 3. The corresponding EDS profile (Figure 4.10) shows that there exists a trace of sulfur that comes from the anion of the ionic liquid and may be a component of the surface film in HE-cycled electrodes.

Bare $LiFePO_4$ electrodes	**Conventional electrolyte - $LiFePO_4$ after 1st charge**	**HE-$LiFePO_4$ after 1st charge**

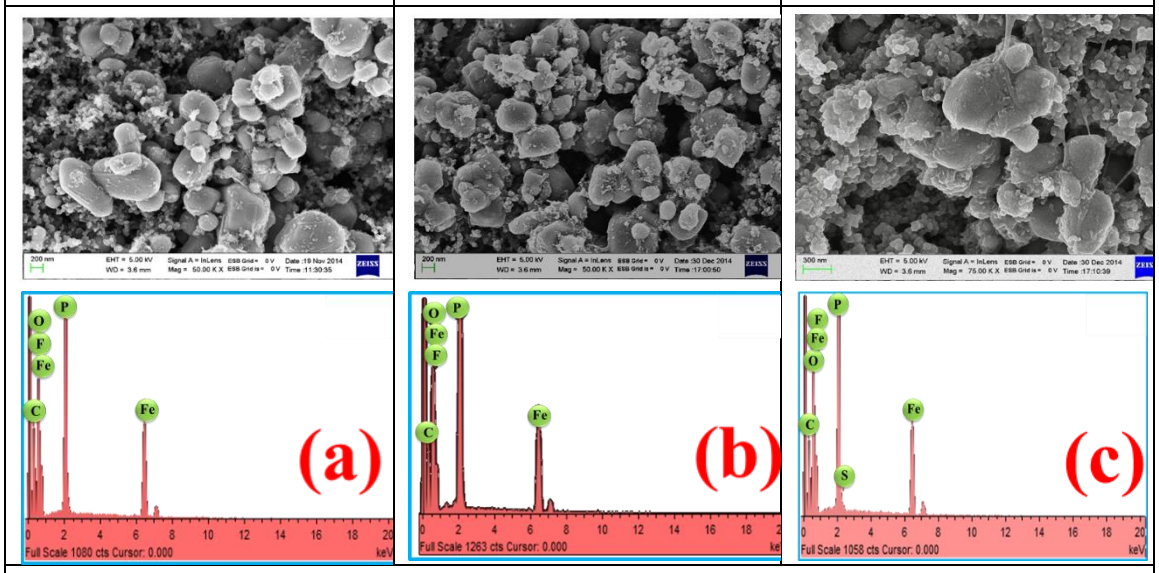

Figure 4.10 *FEG-SEM analysis of $LiFePO_4$ electrodes. (a) Before cycling along with EDS profile, (b) After first charging in conventional electrolyte along with EDS profile and (c) After first charging in HE along with the EDS profile.*

To understand the nature of the surface film as well as the sulfur constituent at the end of 100 cycles, we took FEG-SEM images at the end of 100 cycles as shown in Figure 4.11. In Figure 4.11 (a) and 4.11 (b), it was found that with conventional electrolyte-cycled electrodes show some distortion on the surface after 100 cycles and the similar was not

observed in HE. The surface film resembles that on the $LiFePO_4$ electrode after first charging. It is important to note that there is no significant surface degradation during the 100 cycles of charge-discharge, as evidenced by the EDS in Figure 4.11 (b) and (c). It was believed that unwanted surface reactions can be prevented on the electrode surface through these surface films[52].

Conventional electrolyte-$LiFePO_4$ 100th cycle	HE-$LiFePO_4$ 100th cycle	[C_3mpyr][TFSI]-$LiFePO_4$ 100th cycle
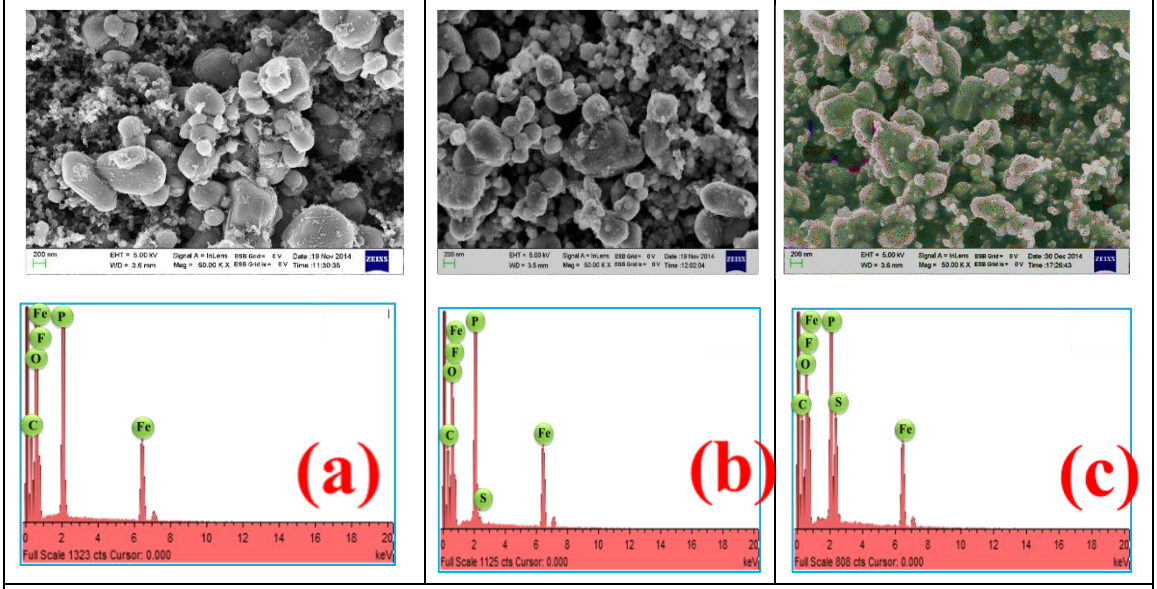		

Figure 4.11 *FEG-SEM analysis of $LiFePO_4$ electrodes. (a) After 100 cycles in conventional electrolyte along with EDS profile (b)After 100 cycles in HE along with EDS profile, and (c) After 100 cycles in neat [C_3mpyr][TFSI] along with the EDS profile.*

4.3.1.4.4 TEM Analysis

The cycled electrodes were analyzed by using HRTEM in order to acquire further insights on the surface film on $LiFePO_4$ cathodes. In Figure 4.12 (b), a thin homogenous surface film surrounds the $LiFePO_4$ electrodes whereas the same film was quite thick in [C_3mpyr][TFSI] cycled electrodes as shown in Figure 4.12 (c). Hence it can be suggested that the presence of [C_3mpyr][TFSI] helps in forming the surface film on the cathode surface. With 40 percent of [C_3mpyr][TFSI], the cathode-electrolyte interface in the case

of HE was quite thin which helps in preventing the cathode surface from adverse $LiPF_6$ induced reactions.

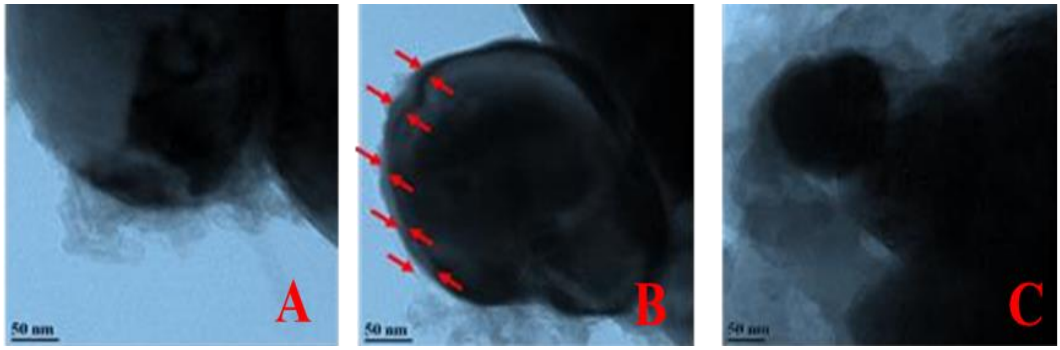

Figure 4.12 *TEM analysis of the $LiFePO_4$ electrode after first cycling in (a)conventional electrolyte, (b)HE, and (c) neat [C_3mpyr][TFSI].*

4.3.2 Lithium-ion Cell Studies

The lithium-ion cells were fabricated by using the $LiFePO_4$ cathodes and $Li_4Ti_5O_{12}$ anodes. As mentioned earlier, $Li_4Ti_5O_{12}$ anodes operate at a higher anodic potential of 1.5 V vs. Li/Li^+ on the basis of insertion mechanism[1,53,54]. The charge-discharge profile of $Li/Li_4Ti_5O_{12}$ for 10 cycles in the potential window of 0.01–2.5 V vs. Li/Li^+ at C/5 rate is shown in Figure 4.13. It was observed that the commercial $Li_4Ti_5O_{12}$ anodes used in this study can deliver an average capacity of 143 mAh/g when charged at C/5 rate.

Since $Li_4Ti_5O_{12}$ anodes operates around 1.5 V vs. Li/Li^+, the most common SEI/passivation mechanism is not strongly observed in this system[1,55]. As a result, little efforts have been dedicated to the understanding the of $Li_4Ti_5O_{12}$ which is beyond the scope of this work. It is believed that the efforts taken in this section will help to fabricate lithium-ion cells by using HE. The operating potential window of the lithium-ion cell depends on the electrode materials of choice. Figure 4.14 depicts the variation of operating potential window from the lithium cells to the lithium-ion cells with different electrodes of interest.

In the present case, 1.5–2.3 V vs. Li/Li^+ is considered as the operating potential window for the $Li_4Ti_5O_{12}$/HE/$LiFePO_4$ cell configuration. The cells were cycled for 200 cycles at the C/5 rate. The cycling performance of the lithium-ion cells is shown in Figure 4.15. In the present case, the capacity of the lithium-ion cell is calculated with reference to the

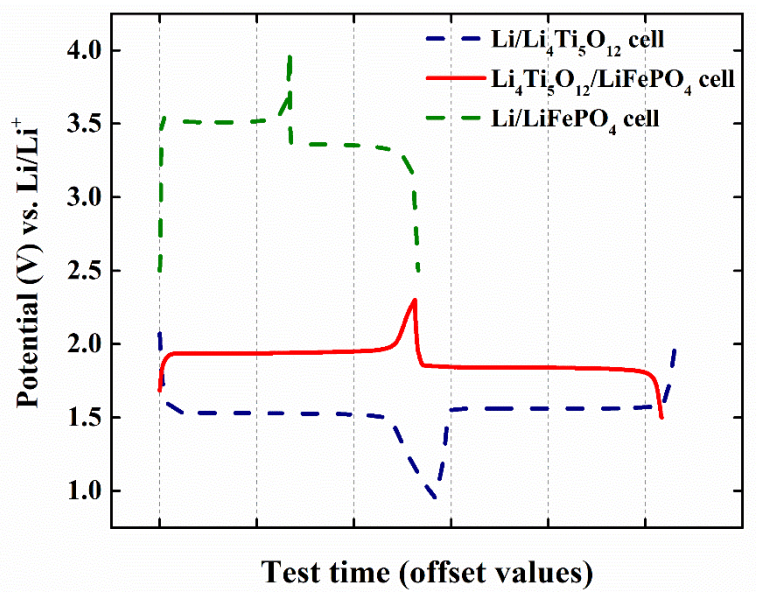

Figure 4.13 *Schematic representation of the plateau region in lithium and lithium-ion cells at* 20 °C.

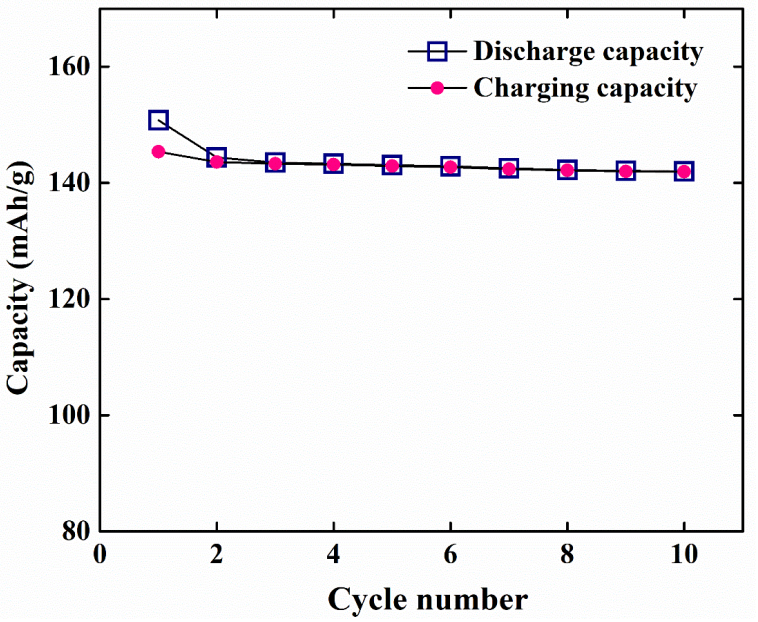

Figure 4.14 *Plot of cycle number versus specific capacity of* $Li/Li_4Ti_5O_{12}$ *cell cycled at C/5 rate cycled at 20 °C.*

anodic mass due to the relatively lower loading of $Li_4Ti_5O_{12}$ anodes. The plot of the capacity in (mAh) and the specific capacity versus the cycle number is shown in Figure 4.15. It was observed that the first discharge capacity of the lithium-ion is around 149 mAh/g. Since the anode loading is lower than the cathode loading, the specific capacity was calculated with reference to the anode loading mass.It was observed that the total capacity loss after 200 cycles is about 6.5 percent and further work is required to optimize the electrode loading and the performance of lithium- ion cells by using HE. The next section will focus on the performance of $Li_4Ti_5O_{12}$/HE/$LiFePO_4$ cells at subzero temperatures.

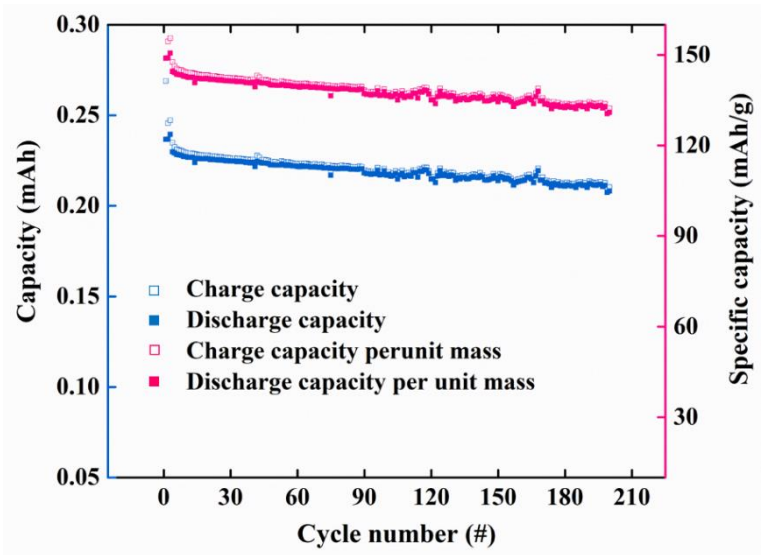

Figure 4.15 *Cyclic performance of* $Li_4Ti_5O_{12}$/HE/$LiFePO_4$ *cell at C/5 rate at 20 °C*

4.3.3 Subzero Temperature Analysis

In this section, the electrolyte for subzero applications, HE* is studied to find the phase behavior and ionic conductivity as a prerequisite to understanding their performance at subzero temperatures. Further CV, EIS, and galvanostatic charge discharge studies were performed to understand the performance and the interfacial resistance over the cycles at subzero temperatures.

4.3.3.1 Electrolyte Characterization

4.3.3.1.1 DSC Analysis

The experimental parameters for the DSC studies of HE* were similar to those described in Chapter 2. The phase behavior of HE* was studied in comparison with the conventional electrolyte, as shown in Figure 4.16. Figure 4.17 gives the naked eye view of the electrolytes at –40 °C, indicating little freezing of HE* at subzero temperatures. In the conventional electrolyte as shown in Figure 4.16, several phase changes exist from –58 °C to 20 °C, whereas in HE*only a small change was observed at –4 °C.

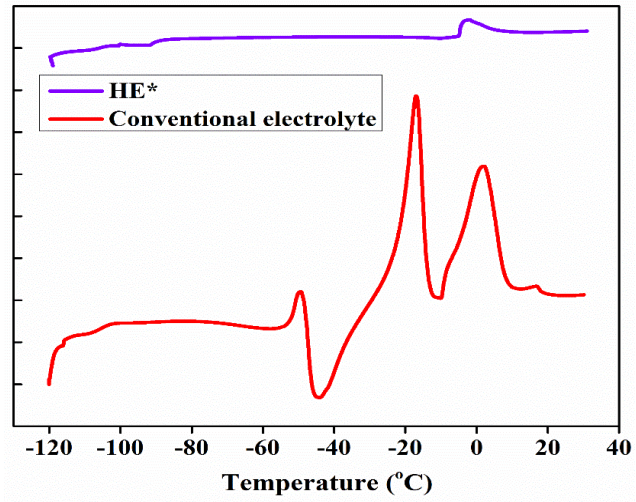

Figure 4.16 *DSC Analysis of the conventional electrolyte in comparison to HE* from –120 °C to 30 °C at a ramp rate of 5°/min.*

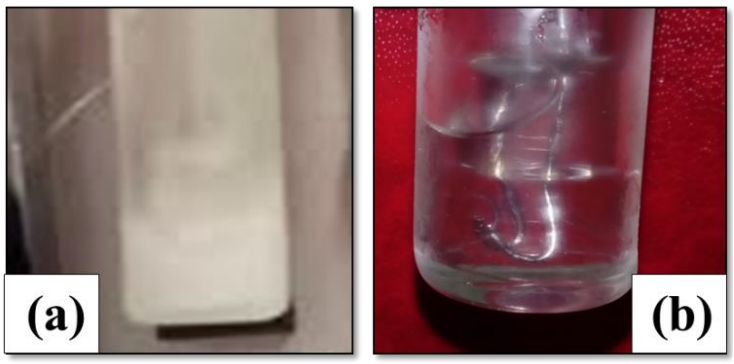

Figure 4.17 *Photograph of electrolytes in the conductivity cell (a) Conventional electrolyte and (b) HE*.*

The dominant phase change in the conventional electrolyte is due to the crystallization and melting of the organic solvents EC, DMC, and DEC. Only a small extent of this phase change is seen in HE* due to the suppression of crystallization in the mixture[56].

4.3.3.1.2 Ionic Conductivity Studies

Ionic conductivity was measured by using the similar protocol described in Chapter 2. HE* is filled in a dip cell inside the glove box. The ionic conductivity was tested in the temperature range of –40 °C to 100 °C. The plot of ionic conductivities of HE* in comparison to the conventional electrolyte is shown in Figure 4.18. The better ionic conductivities of HE* may be due to the lesser degree of crystallisation in HE* at low temperatures. However, the ionic conductivity values are not the only the factors to determine the low temperature performance of the batteries as the performance is further governed by the lithium-ion diffusion kinetics[25,30].

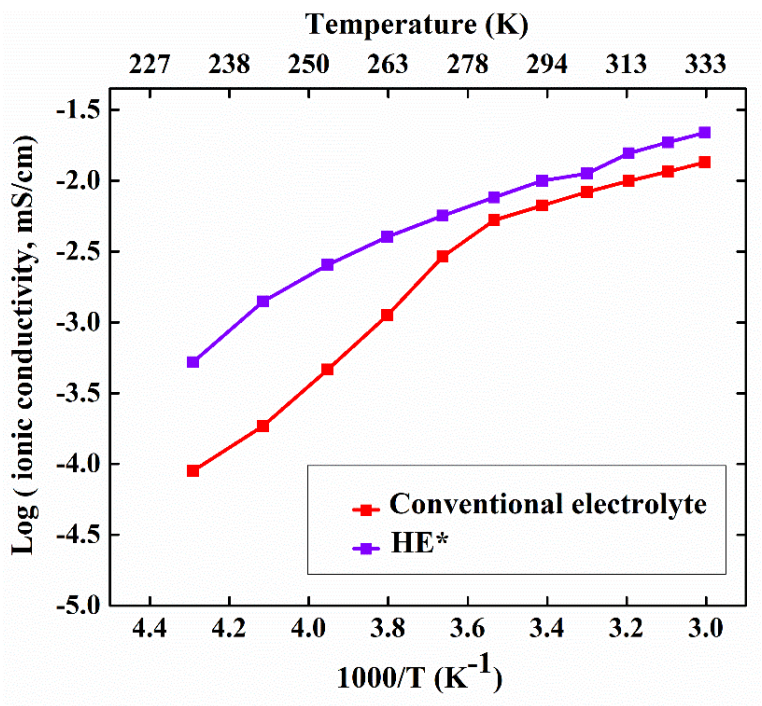

Figure 4.18 *Ionic conductivity values of HE* in comparison to conventional electrolyte from –40 °C to 10 0 °C.*

4.3.3.2 Performance Analysis

The modus operandi for electrochemical performance analysis is shown in Figure 4.19. The aim of this protocol was to understand the effect of temperature on interfacial resistance and the aging process. In addition to the electrochemical charge-discharge studies, the EIS was measured at intermittent stages to understand the change in interfacial resistance over time. The EIS data were fitted with the equivalent circuit[57] as shown in the left inset of Figure 4.20.

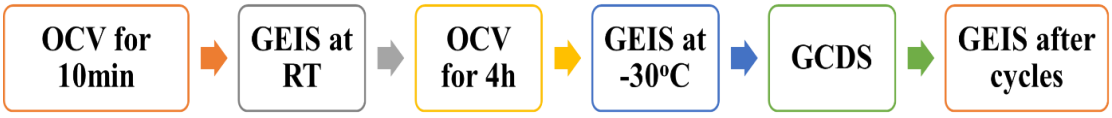

Figure 4.19 *Schematic representation of the sequence of experiments carried out to understand the performance at –30 °C. *GCDS- Galvanostatic charge discharge studies, GEIS - Galvanostatic Electrochemical Impedance Spectroscopy and RT - Room temperature.*

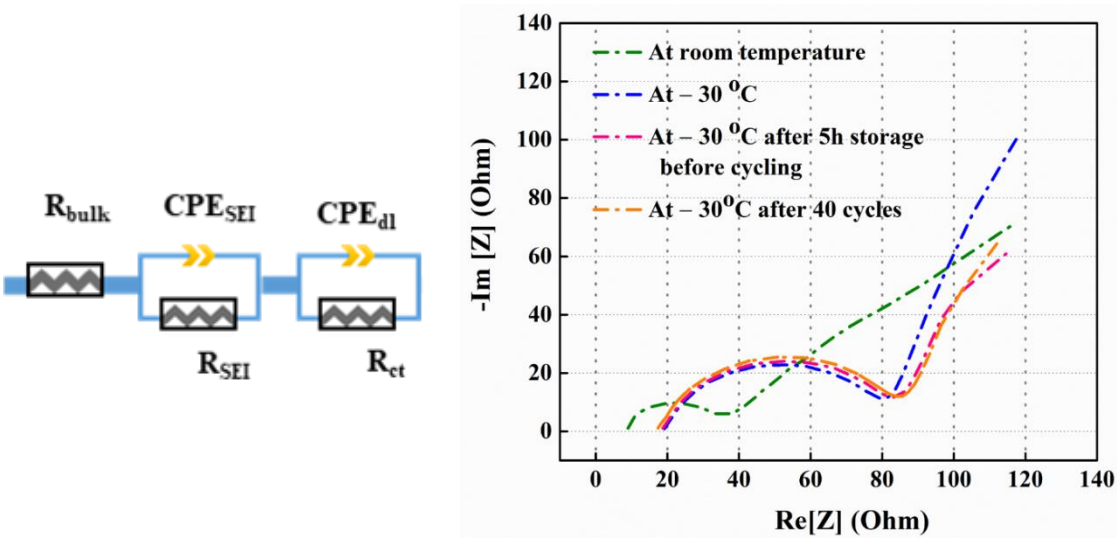

Figure 4.20 *EIS studies of $Li_4Ti_5O_{12}$/HE*/$LiFePO_4$ at –30 °C before, intermittent, and at the end of 40 cycles. The corresponding equivalent circuit is described as an inset in the left side of the figure.*

The initial resistance of the lithium-ion cell at room temperatures was found to be 35 Ω whereas the interfacial resistance at –30 °C was found to be 80 ± 2 Ω. After aging at –30 °C for 5 hours, the cell resistance was found to be 81 ± 3 Ω. The interfacial resistance after 40 cycles was found to be similar at around 82 ± 3 Ω. Thus no significant change in the interfacial resistance was observed during aging and cycling of lithium-ion cells at subzero temperatures. The galvanostatic charge-discharge studies that are shown in Figure 4.21 were performed at –30 °C with the charging and discharging time of ten hours. It was observed that the average capacity value was around 70 mAh/g along with good capacity retention. The better capacity retention can be attributed to the negligible change in the interfacial resistance of the lithium-ion cell over the cycles.

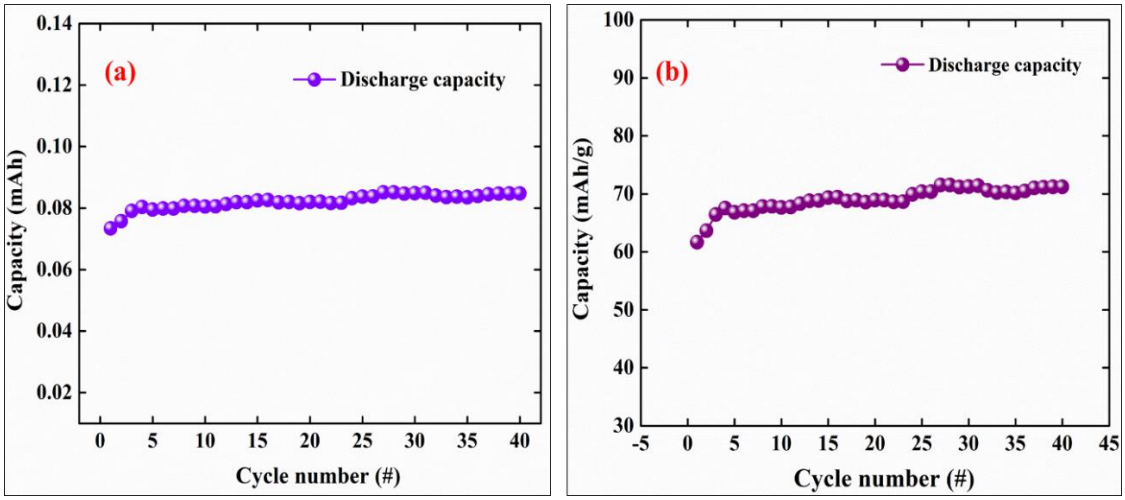

Figure 4.21 *Discharge capacity at –30 °C for the $Li_4Ti_5O_{12}$/HE*/$LiFePO_4$ cell cycled for ten hours. (a) Capacity vs. cycle number studies in mAh and (b) Specific discharge capacity at –30 °C in reference to the anodic mass loading in the electrodes.*

Further, efforts were taken to understand the effect of the charging time on capacity at subzero temperatures in HE*. The capacity values measured at different charging times are tabulated in Table 4.1 with reference to the capacity that was obtained after ten hours of charging at –30 °C. It can be seen that there is a notable rate performance of HE* at –30 °C. Further, it can be inferred from Table 4.1, that the decrease in capacity with respect to the reduction in charging time was non-linear. It can be seen that when the charging time was reduced to 2.5 h, the cell yielded 50 percent of the capacity obtained after 10 h of charging. Thus, lithium-ion cells made of HE* can also be used for better lithium-ion storage with lesser charging times.

Table 4.1 *Relative discharge capacity with respect to 10h charging time at –30 °C.*

S.No.	Charging time (h)	Discharging time (h)	$C / C_{(10)}$ (%)
1	10	10	100
2	6	6	72
3	2.5	2.5	50
4	1.2	1.2	36
5	0.5	0.5	21

*$C/C_{(10)}$ is the percent of the 10 h discharge capacity obtained at a particular discharge time.

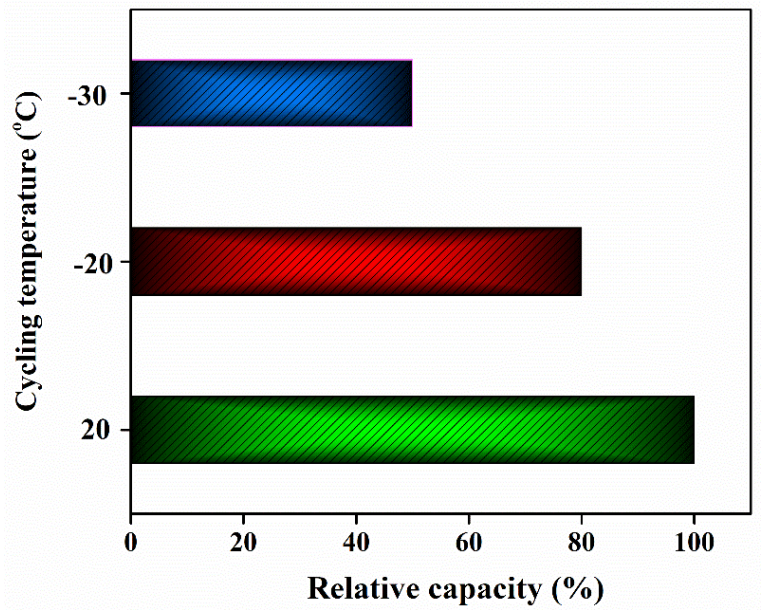

Figure 4.22 *Statistics of the capacity obtained at subzero temperatures (– 20 °C and – 30 °C) in relation to the room temperature performance.*

Relative capacity ($C_{relative}$) defines the ratio of the capacity that is obtained at subzero temperatures to the performance obtained at room temperatures. Figure 4.22 shows the relative capacity at subzero temperatures (–20 °C and –30 °C) to the room temperature performance. It can be seen that 80 percent of the room temperature capacity was obtained at –20 °C and 50 percent of the room temperature performance was obtained at –30 °C.

Thus it appears that HE* supports excellent performance at subzero temperatures. Notably this is achieved without sacrificing the high temperature stability and safety.

4.4 Concluding Remarks

In this chapter, commercial $LiFePO_4$ cathodes were studied initially by using the HE in comparison to the conventional electrolyte. The studies demonstrated negligible iron dissolution from $LiFePO_4$ cathodes cycled in HE as compared to those cycled in conventional electrolyte. Further, the possibility of HE in lithium-ion cells was demonstrated with $Li_4Ti_5O_{12}$/HE/$LiFePO_4$ cells for 200 cycles.

Further, the behavior of HE at subzero temperatures was studied by using the special composition HE*. Initial physicochemical analyses shows lesser degree of crystallization and better ionic conductivity at subzero temperatures. The charge/discharge studies showed better performance and capacity retention for HE* than the conventional electrolyte in lithium-ion cells. Further, the EIS analysis demonstrated the non-varying interfacial resistance with better ionic conductivity at subzero temperatures. Thus, the above studies demonstrate the application of hybrid electrolyte formulations for subzero battery operation.

4.5 References

(1) Etacheri, V.; Marom, R.; Elazari, R.; Salitra, G.; Aurbach, D. Challenges in the Development of Advanced Li-Ion Batteries: A Review. Energy Environ. Sci. 2011, 4, 3243–3262.

(2) Xu, K. Nonaqueous Liquid Electrolytes for Lithium-Based Rechargeable Batteries. Chem. Rev. 2004, 104, 4303–4418.

(3) E. Peter Roth and Christopher J. Orendorff. How Electrolytes Influence Battery Safety. *Electrochem. Soc. Interface* 45–49.

(4) MacFarlane, D. R.; Forsyth, M.; Howlett, P. C.; Pringle, J. M.; Sun, J.; Annat, G.; Neil, W.; Izgorodina, E. I. Ionic Liquids in Electrochemical Devices and Processes: Managing Interfacial Electrochemistry. *Acc. Chem. Res.* **2007**, *40*, 1165–1173.

(5) Arbizzani, C.; Gabrielli, G.; Mastragostino, M. Thermal Stability and Flammability of Electrolytes for Lithium-Ion Batteries. *J. Power Sources* **2011**, *196*, 4801–4805.

(6) Yang, H.; Zhuang, G. V; Jr., P. N. R. Thermal Stability of $LiPF_6$ Salt and Li-Ion Battery Electrolytes Containing $LiPF_6$. *J. Power Sources* **2006**, *161*, 573–579.

(7) Nitta, N.; Wu, F.; Lee, J. T.; Yushin, G. Li-Ion Battery Materials: Present and Future. *Mater. Today* **2015**, *18*, 252–264.

(8) Dahn, J.; Fuller, E.; Obrovac, M.; Vonsacken, U. Thermal Stability of Li_xCoO_2, Li_xNiO_2 and λ-MnO_2 and Consequences for the Safety of Li-Ion Cells. *Solid State Ionics* **1994**, *69*, 265–270.

(9) Padhi, A. K.; Nanjundaswamy, K. S.; Goodenough, J. B. Phospho-Olivines as Positive-Electrode Materials for Rechargeable Lithium Batteries. *J. Electrochem. Soc.* **1997**, *144*, 1188.

(10) Nolis, G. M.; Omenya, F.; Zhang, R.; Fang, B.; Upreti, S.; Chernova, N. A.; Wang, F.; Graetz, J.; Hu, Y.-Y.; Grey, C. P.; et al. Structure, Defects and Thermal Stability of Delithiated Olivine Phosphates. *J. Mater. Chem.* **2012**, *22*, 20482.

(11) $LiFePO_4$ Batteries: A Breakthrough For Electric Vehicles - Meta Efficient https://metaefficient.com/rechargeable-batteries/innovative-lifepo4-batteries-electric-vehicles.html (accessed May 29, 2017).

(12) Koltypin, M.; Aurbach, D.; Nazar, L.; Ellis, B. On the Stability of $LiFePO_4$ Olivine Cathodes under Various Conditions (Electrolyte Solutions, Temperatures). *Electrochem. Solid-State Lett.* **2007**, *10*, A40–A44.

(13) Wang, J.; Sun, X.; Wang, D.; Yue, D.; Li, C.; Amine, K.; Julien, C. M.; Komana, S.; Vaaland, O.; Wang, C.; et al. Olivine $LiFePO_4$: The Remaining Challenges for Future Energy Storage. *Energy Environ. Sci.* **2015**, *8*, 1110–1138.

(14) Hu, J.; Xie, J.; Zhao, X.; Yu, H.; Zhou, X.; Cao, G.; Tu, J. Doping Effects on Electronic Conductivity and Electrochemical Performance of $LiFePO_4$. *J. Mater. Sci. Tech.* **2009**, *25*, 405.

(15) Sun, Y.-K.; Chen, Z.; Noh, H.-J.; Lee, D.-J.; Jung, H.-G.; Ren, Y.; Wang, S.; Yoon, C. S.; Myung, S.-T.; Amine, K. Nanostructured High-Energy Cathode Materials for Advanced Lithium Batteries. *Nat Mater* **2012**, *11*, 942–947.

(16) Rajoba, S. J.; Jadhav, L. D.; Patil, P. S.; Tyagi, D. K.; Varma, S.; Wani, B. N.

Enhancement of Electrical Conductivity of $LiFePO_4$ by Controlled Solution Combustion Synthesis. *J. Electron. Mater.* **2017**, *46*, 1683–1691.

(17) Lu, W.; Xiong, S.; Xie, K.; Pan, Y.; Zheng, C. Identification of Solid Electrolyte Interphase Formed on Graphite Electrode Cycled in Trifluoroethyl Aliphatic Carboxylate-Based Electrolytes for Low-Temperature Lithium-Ion Batteries. *Ionics* . **2016**, *22*, 2095–2102.

(18) Birkenmaier, C.; Bitzer, B.; Harzheim, M.; Hintennach, A.; Schleid, T. Lithium Plating on Graphite Negative Electrodes: Innovative Qualitative and Quantitative Investigation Methods. *J. Electrochem. Soc.* **2015**, *162*, A2646–A2650.

(19) Evarts, E. C. Lithium Batteries: To the Limits of Lithium. *Nature* **2015**, *526*, S93–S95.

(20) Ge, H.; Hao, T.; Osgood, H.; Zhang, B.; Chen, L.; Cui, L.; Song, X.-M.; Ogoke, O.; Wu, G. Advanced Mesoporous Spinel $Li_4Ti_5O_{12}$/rGO Composites with Increased Surface Lithium Storage Capability for High-Power Lithium-Ion Batteries. *ACS Appl. Mater. Interfaces* **2016**, *8*, 9162–9169.

(21) Tian, Q.; Zhang, Z.; Yang, L.; Xiang, Y. Improving the Lithium Storage Properties of Li_4 Ti_5O_{12} Anodes by Facile Two-Phase Formation and Nanostructure Engineering Strategy. *J. Alloys Compd.* **2017**, *705*, 638–644.

(22) Zaghib, K.; Dontigny, M.; Guerfi, A.; Charest, P.; Rodrigues, I.; Mauger, A.; Julien, C. M. Safe and Fast-Charging Li-Ion Battery with Long Shelf Life for Power Applications. *J. Power Sources* **2011**, *196*, 3949–3954.

(23) Zaghib, K.; Mauger, A.; Julien, C. M. Olivine-Based Cathode Materials. In; 2015; pp. 25–65.

(24) Friesen, A.; Horsthemke, F.; Mönnighoff, X.; Brunklaus, G.; Krafft, R.; Börner, M.; Risthaus, T.; Winter, M.; Schappacher, F. M. Impact of Cycling at Low Temperatures on the Safety Behavior of 18650-Type Lithium Ion Cells: Combined Study of Mechanical and Thermal Abuse Testing Accompanied by Post-Mortem Analysis. *J. Power Sources* **2016**, *334*, 1–11.

(25) Singer, J. P.; Birke, K. P. Kinetic Study of Low Temperature Capacity Fading in

Li-Ion Cells. *J. Energy Storage* **2017**, *13*, 129–136.

(26) Gachot, G.; Grugeon, S.; Eshetu, G. G.; Mathiron, D.; Ribière, P.; Armand, M.; Laruelle, S. Thermal Behaviour of the Lithiated-Graphite/electrolyte Interface through GC/MS Analysis. *Electrochim. Acta* **2012**, *83*, 402–409.

(27) Smart, M. C.; Ratnakumar, B. V.; Surampudi, S. Electrolytes for Low-Temperature Lithium Batteries Based on Ternary Mixtures of Aliphatic Carbonates. *J. Electrochem. Soc.* **1999**, *146*, 486.

(28) Ratnakumar, B. V.; Smart, M. C.; Surampudi, S. Effects of SEI on the Kinetics of Lithium Intercalation. *J. Power Sources* **2001**, *97–98*, 137–139.

(29) Plichta, E. J.; Behl, W. K. A Low-Temperature Electrolyte for Lithium and Lithium-Ion Batteries. *J. Power Sources* **2000**, *88*, 192–196.

(30) Huang, C.-K.; Sakamoto, J. S.; Wolfenstine, J.; Surampudi, S. The Limits of Low-Temperature Performance of Li-Ion Cells. *J. Electrochem. Soc.* **2000**, *147*, 2893.

(31) Chang, W.; Kim, S.-J.; Park, I.-T.; Cho, B.-W.; Chung, K. Y.; Shin, H.-C. Low Temperature Performance of $LiFePO_4$ Cathode Material for Li-Ion Batteries. *J. Alloys Compd.* **2013**, *563*, 249–253.

(32) Kunlin, X.; Qun, H.; Xiangyun, Y.; Xiaorong, C.; Sheng, Y. A Method for Improving the Low Temperature Performance of Lithium Manganese Battery Organic Electrolyte. CN103378360A, 2015.

(33) Xuedong, Y.; Meizhi, P.; Changhe, C. Low-Temperature Lithium Iron Phosphate Ion Battery Electrolyte and Preparation Method Thereof. CN103779605, 2014.

(34) Liu Pengpeng; Jing, D.; Zhaoqiang, L.; Bo, H.; Xisheng, F. A Low Temperature Ratio Lithium Ion Battery Electrolyte. CN103078136 B, 2015.

(35) Yan Xuedong; Meizhi, P.; Changhe, C. Lithium Iron Phosphate Lithium Ion Battery Cryogenic Electrolyte and Its Preparation Method. CN103779605, 2014.

(36) Shijiang, L.; Hongjun, H.; Huachun, Y.; Xujin, X.; Shengjun, G.; Xi, L.; Jianjun, H.; Fengfeng, X.; Chengguo, L. A Cryogenic Lithium Ion Battery and a Lithium Ion Battery Electrolyte. CN103107364B, 2016.

(37) Suojiang, Z.; Tao, D.; Yingjun, C.; Liang, Z. Ester-Based Ionic Liquid Electrolyte Solution for Low Temperature Lithium Ion Battery. CN201310046352, 2013.

(38) Li, B.; Amiruddin, S. Low Temperature Electrolyte for High Capacity Lithium Based Batteries. US20130157147A1, US20130157147, WO2013090417A1, 2013.

(39) Sun, L. Non-Aqueous Electrolytes Having an Extended Temperature Range for Battery Applications. US20050123835, 2005.

(40) Hallac, B.; Smart, M. C.; Frederick C. Krause, Bernhard M. Metz, R. V. B. Lithium Ion Electrolytes with Lifsi for Improved Wide Operating Temperature Range. US 20160149263A1, 2016.

(41) Cheng, G.; Zhu, Y.; Strand, D.; Hallac, B.; Metz, B. M. Electrolyte Formulations for Lithium Ion Batteries. US9466857 B1; US20160380308; WO2016209839A1, 2016.

(42) Zhang, S. S.; Xu, K.; Jow, T. R. The Low Temperature Performance of Li-Ion Batteries. *J. Power Sources* **2003**, *115*, 137–140.

(43) Yu, D. Y. W.; Fietzek, C.; Weydanz, W.; Donoue, K.; Inoue, T.; Kurokawa, H.; Fujitani, S. Study of LiFePO4 by Cyclic Voltammetry. *J. Electrochem. Soc.* **2007**, *154*, A253–A257.

(44) Takahashi, M.; Tobishima, S.; Takei, K.; Sakurai, Y. Reaction Behavior of $LiFePO_4$ as a Cathode Material for Rechargeable Lithium Batteries. *Solid State Ionics* **2002**, *148*, 283–289.

(45) Theivaprakasam, S.; MacFarlane, D. R.; Mitra, S. Electrochemical Studies of N-Methyl N-Propyl Pyrrolidinium Bis(trifluoromethanesulfonyl) Imide Ionic Liquid Mixtures with Conventional Electrolytes in $LiFePO_4$/Li Cells. *Electrochim. Acta* **2015**, *180*, 737–745.

(46) Aurbach, D.; Markovsky, B.; Salitra, G.; Markevich, E.; Talyossef, Y.; Koltypin, M.; Nazar, L.; Ellis, B.; Kovacheva, D. Review on Electrode–electrolyte Solution Interactions, Related to Cathode Materials for Li-Ion Batteries. *J. Power Sources* **2007**, *165*, 491–499.

(47) Edström, K.; Gustafsson, T.; Thomas, J. The Cathode-Electrolyte Interface in a Li-

Ion Battery. In *Lithium-Ion Batteries Solid-Electrolyte Interphase*; Balbuena, P. B.; Wang, Y., Eds.; Imperial College Press, 2004; pp. 337–364.

(48) Yamaki, J. Liquid Electrolytes. In *Advances in Lithium-Ion Batteries*; Van Schalkwijk, W.; Scrosati, B., Eds.; Springer US: Boston, MA, 2002; pp. 155–187.

(49) Ait Salah, A.; Jozwiak, P.; Zaghib, K.; Garbarczyk, J.; Gendron, F.; Mauger, A.; Julien, C. M. FTIR Features of Lithium-Iron Phosphates as Electrode Materials for Rechargeable Lithium Batteries. *Spectrochim. Acta Part A Mol. Biomol. Spectrosc.* **2006**, *65*, 1007–1013.

(50) Rulmont, A.; Cahay, R.; Liegeois-Duyckaerts, M.; Tarte, P. Vibrational Spectroscopy of Phosphates: Some General Correlations between Structure and Spectra. *Eur. J. Solid State Inorg. Chem.* **1991**, *28*, 207–219.

(51) Chen, R.; Chen, Y.; Zhu, L.; Zhu, Q.; Wu, F.; Li, L. A Facile Approach of Adopting DMS into LiODFB–PYR14TFSI Electrolyte for Lithium-Ion Batteries. *J. Mater. Chem. A* **2015**.

(52) Mun, J.; Yim, T.; Park, J. H.; Ryu, J. H.; Lee, S. Y.; Kim, Y. G.; Oh, S. M. Allylic Ionic Liquid Electrolyte-Assisted Electrochemical Surface Passivation of $LiCoO_2$ for Advanced, Safe Lithium-Ion Batteries. *Sci. Rep.* **2014**, *4*, 5802.

(53) Huggins, R. A. *Advanced Batteries Materials Science Aspects*; Springer, 2009.

(54) Mekonnen, Y.; Sundararajan, A.; Sarwat, A. I. A Review of Cathode and Anode Materials for Lithium-Ion Batteries. In *SoutheastCon 2016*; IEEE, 2016; pp. 1–6.

(55) Kurc, B.; Swiderska-Mocek, A. Properties of $Li_4Ti_5O_{12}$ as an Anode Material in Non-Flammable Electrolytes. *J. Appl. Electrochem.* **2014**, *44*, 245–253.

(56) Aguilera, L.; Scheers, J.; Matic, A. Enhanced Low-Temperature Ionic Conductivity via Different Li^+ Solvated Clusters in Organic Solvent/ionic Liquid Mixed Electrolytes. *Phys. Chem. Chem. Phys.* **2016**, *18*, 25458–25464.

(57) Zhang, S. S.; Xu, K.; Jow, T. R. Electrochemical Impedance Study on the Low Temperature of Li-Ion Batteries. *Electrochim. Acta* **2004**, *49*, 1057–1061.

Chapter 5

Passivation Behaviour of Aluminum Current Collector in Hybrid Electrolytes with [FSI] and [TFSI] anions

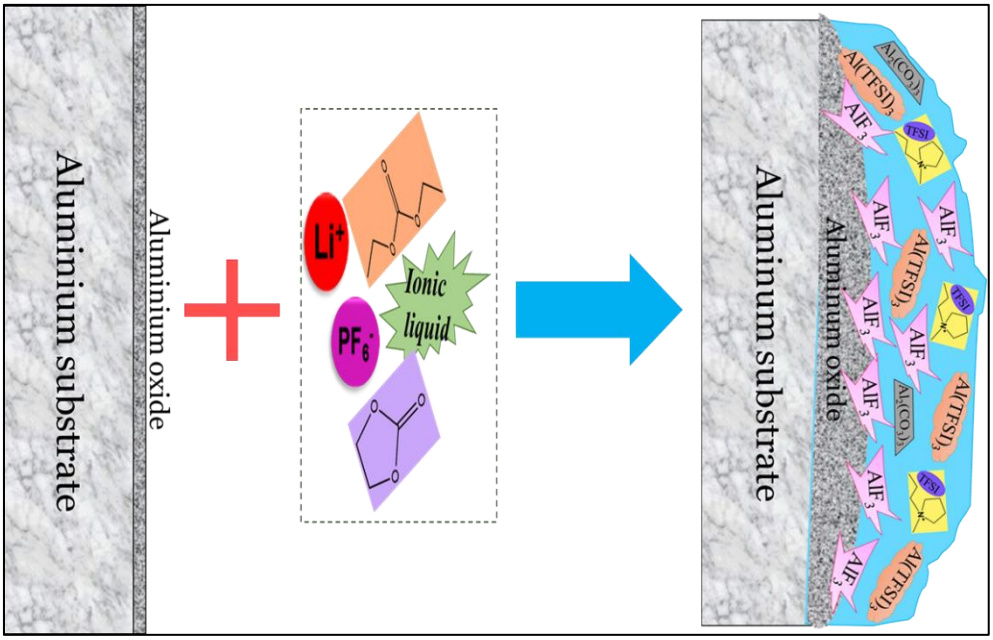

This chapter is published as a journal publication:

Theivaprakasam, S.; Girard, G.; Howlett, P.; Forsyth, M.; Mitra, S.; MacFarlane, D. Passivation Behaviour of Aluminium Current Collector in Ionic Liquid Alkyl Carbonate (Hybrid) Electrolytes. npj Mater. Degrad. **2018**, 2, 13.

5.1 Introduction

In a LiB, the flow of lithium ions between the electrodes occurs along with the electron transfer in the external circuit. The electron transfer is achieved with the help of thin metal foil current collectors, which are coated with the active electrode materials in the battery[1–3]. Since the primary role of the current collectors is electron conduction, high electronic conductivity as well as high stability in the electrochemical environment are of crucial importance[1–4]. Although thin foils of nickel, copper, platinum, zinc, titanium and other similar metals have been studied as current collectors, aluminum is the most preferred cathodic current collector in lithium-ion batteries due to its ability to form a passive film, making the electrolyte/Al interface stable, even at potentials > 4V *vs.* Li/Li^+. Al also offers benefits such as lightness of weight, low cost, good adhesion, and good electronic conductivity to the active materials[3,4]. The current use of lithium-ion batteries in electric vehicles requires safe, high energy density batteries[5,6]. An area that is widely studied in the realm of high-energy lithium batteries is the development of high-potential cathodes[7,8]. Improved stability of the aluminium current collector is also important for improvement in the performance offered by these high-potential cathodes[3,9–11]. In addition, several reports[12–14] in the literature also claim that the electrolyte composition, especially the nature of the salt, plays a major role in the corrosion of aluminum current collectors; certain other reports claim that the solvents play a significant role[15,16]. In most commercially-used electrolytes, lithium hexafluorophosphate ($LiPF_6$) is the preferred salt (despite its thermal instability), because of its mechanism of passivation on aluminum.[11,13,17] Salts with better thermal stability (such as lithium bis(trifluoromethanesulfonyl)imide (LiTFSI)) are not preferred, because they tend to corrode aluminum current collectors[13,18]. Although state-of-the-art electrolytes with $LiPF_6$ salts work well at current operating potentials, they still cause corrosion of current collectors at potentials in which high-potential cathodes are expected to operate[19].

Recent studies examined the use of ionic liquids as electrolyte components in lithium batteries, and certain ionic liquids were found to possess wide electrochemical stability, better safety[15,17,20–22] and corrosion-inhibition properties[23–26]. It is interesting to note that the well-known corrosive nature of the LiTFSI salt decreased when ionic liquids were added to the electrolyte composition[17,27,28]. In addition to corrosion inhibition, the so-called

passive films formed on the substrates in the presence of ionic liquid electrolytes show better thermal stability[27]. On the other hand, in spite of the corrosive nature of the bis(fluorosulfonyl) imide anion [FSI^-] at high oxidation potentials (> 4.0 V *vs.* Li/Li^+), Cho et al. demonstrated that the addition of $LiPF_6$ to *N*-methyl-*N*-propyl pyrrolidinium bis(fluorosulfonyl)imide [C_3mpyr][FSI] reduced the pitting corrosion[29].

Despite their remarkable thermal stability, the use of ionic liquid mixtures as electrolytes in lithium batteries is limited by their low ionic conductivity at room temperature, and by certain issues in the formation of a solid electrolyte interface[30–32]. To overcome these disadvantages, researchers have explored the concept of hybrid electrolytes, by which an organic solvent is added to the ionic liquid electrolytes so as to increase the ionic conductivity at room temperature and to achieve better interfacial behavior[15,20,33–36]. In this chapter, studies were carried out by using hybrid electrolytes that were composed of 40 percent of the ionic liquid by weight in a conventional electrolyte system in order to understand the role of the interaction between the ionic liquid and the organic carbonate system in the passivation mechanism that occurs on the aluminum foil. The proportion of 40 percent of ionic liquid by weight was chosen as a compromise between the safety and the viscosity of these electrolytes at room temperatures[20,34,37,38]. The most promising ionic liquids in lithium battery applications are N-methyl-*N*-propyl pyrrolidinium bis(fluorosulfonyl)imide, [C_3mpyr][FSI] and N-methyl-N-propylpyrrolidinium bis (trifluoromethanesulfonyl)imide [C_3mpyr][TFSI][20,33,39,40]. Hence, in this chapter, the synergistic role of these ionic liquids in conventional electrolytes will be studied with regard to the corrosion of the cathodic current collector (aluminum) in LiB.

5.2 Experimental

5.2.1 Materials

Battery grade aluminum foils (MTI Corp.) were pre-cleaned in a dimethyl carbonate solution and dried in a vacuum oven at 120 ^oC. The dried aluminum foils were immediately transferred to the glove box. The conventional electrolyte solution that was used comprised 1M $LiPF_6$ in ethylene carbonate and diethyl carbonate (LP40, Sigma–Aldrich , <15 ppm H_2O and <50 ppm HF). Two hybrid electrolyte compositions that had 40 percent of ionic liquid by weight *N*-methyl-*N*-propyl pyrrolidinium bis(trifluoromethanesulfonyl)imide, [C_3mpyr][TFSI] (Solvionic, France, 99.9 percent purity) in the conventional electrolyte

(HE 1), and *N*-methyl-*N*-propyl pyrrolidinium bis (fluorosulfonyl) imide, [C_3mpyr][FSI] (Solvionic, France, 99.9 percent purity) in the conventional electrolyte (HE 2)—were studied. In addition, the neat ionic liquids, [C_3mpyr][TFSI] and [C_3mpyr][FSI], were used in comparison studies.

5.2.2 Pre-treatment of aluminum

The clean, dried aluminum foils were washed once more (inside the glove box) with dimethyl carbonate before the electrochemical measurements.

5.2.3 Electrochemical measurements

Electrochemical measurements were carried out in a pipette cell by using a Biologic VMP3 multi-channel potentiostat, which was controlled by Biologic EC-Lab version 11.01 software. The pipette cell that was used in this study is shown in Figure 5.1, which has been also previously described elsewhere[26].

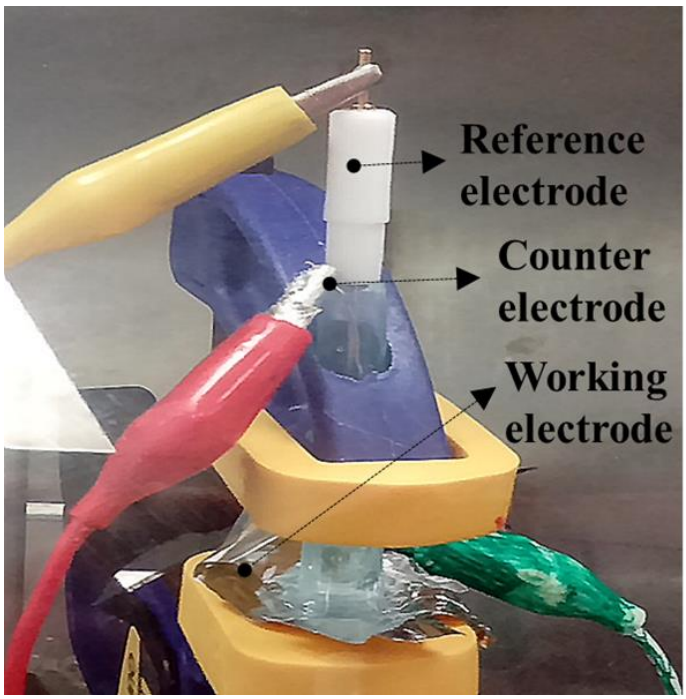

Figure 5.1 *Arrangement of pipette tip cell used for electrochemical measurements inside the glove box.*

The inner surface area of the pipette (equal to that of the working electrode,W.E.) was 0.38 ± 0.05 cm^2. The cell consisted of a polyethylene pipette tip with a Ag/AgOTf reference

and a Pt wire counter electrode that had a diameter of 0.5mm.

Cyclic Potentiodynamic Polarisation (CPP) was carried out over the potential range of 2.7 – 5 V *vs*. Li/Li^+ at a scan rate of 10 mV/min. It should be noted that all electrochemical measurements were carried out inside a nitrogen glove box.

The Tafel curves were fitted by using the EC lab software V10.44 (Bio-Logic Science & Instruments). Cyclic voltammetry (CV) was used over a range of 2.7 – 4.7 V vs. Li/Li^+ at a scan rate of 1 mV/s for three cycles, after which chronoamperometry (CA) was carried out for 3 hours at 4.7 V vs. Li/Li^+. After treatment, surfaces were rinsed with DMC to wash off any excess IL and were finally dried under a nitrogen stream. It is to be noted that all measurements were carried out at room temperature. All surface characterisations were carried out further in the electrochemically treated samples. For convenience, these samples will be referred to as aluminum coupons in future discussions.

5.2.4 Fourier-Transformed Infrared Spectroscopy (FTIR)

Infrared spectra were acquired on a Perkin Elmer IR 101820 series spectrometer by using the Spectrum (v.10.4) software. Ex situ attenuated total reflectance (ATR) spectra were obtained by using a diamond ATR crystal in the mid-IR range (4000-450 cm^{-1}). The aluminum coupons were hermetically transferred and loaded onto the sample stage after brief exposure to air. Firm pressure was applied in order to press the aluminum disk against the diamond window of the sample stage. All spectra were recorded at a resolution of 4 cm^{-1} and 256 scans.

5.2.5 Scanning Electron Microscopy (SEM) with Energy Dispersive X-ray Spectroscopy (EDXS)

Al coupons were further characterised by Scanning Electron Microscopy (SEM). SEM images of the Al electrodes were obtained by using a JEOL JSM-IT300 at an accelerating voltage of 10 kV. An Oxford Instruments X-Max 50 mm^2 Energy Dispersive X-ray Spectroscopy (EDS) detector was used to analyse the Al surfaces and the attachment at 10–11 mm W.D. with a collection time of five minutes. The Oxford Instruments Aztec (version 1.0) software was used.

5.2.6 Optical Profilometry

The aluminum coupons were examined by using a Contour GT-K1 optical profilometer, and the data were analysed by using Vision 64 software v. 5.30, Bruker Instruments. The measurements were carried out by using the following parameters: VSI - 20X or 50X lens, Magnifier 1.0X, Speed 1X with a 25 µm back scan, 50 µm Length, and 0.5 percent threshold.

5.2.7 X-ray Photoelectron Spectroscopy (XPS)

For all XPS experiments, the binding energy scale was calibrated from the aliphatic hydrocarbon C 1s peak at 284.8 eV. The samples were mounted on an XPS sample stud by using conductive carbon adhesive tape, after which they were placed in a hermetic vessel for transfer to the instrument. X-ray photoelectron spectroscopic measurements were carried out at the Victorian node of the Australian National Fabrication Facility (CMSS, La Trobe University, Australia).

X-ray photoelectron spectroscopy was performed by using an AXIS Ultra instrument (Kratos Analytical, Manchester, UK) by using a monochromatic Al Kα X-ray source that was operated at 150 W (15 kV, 10 mA). The hybrid analysis mode that was used provided a sampling area of 300 x 700 μm^2. Survey spectra were acquired at 80 eV pass energy, and high-resolution region spectra were acquired at 20 eV pass energy. Etching experiments were performed on the sample surface by using an argon ion beam gun, which operated at 5 keV and beam current of 2 µA, resulting in an estimated etching rate of 2 $Å.s^{-1}$. The pressure in the analysis chamber was maintained at 4.0×10^{-10} mbar. Instrument operation was performed by using XPS software (Vision 2.0).

XPS data were analysed by using CASAXPS software (v. 2.3.16). Relative sensitivity factors (RSF) were taken from the Kratos Library and were used to determine the relative atomic percentages from survey and high-resolution scans of the most intense photoelectron peak for each element. Peak areas were measured after performing a two-point Shirley background subtraction. A Gaussian:Lorentzian algorithm (70:30 percent) was used to fit the peaks to obtain quantitative results. The fit produces an estimated ± 10 percent error in the atomic concentration that was determined for each peak.

5.3 Results and Discussion

The extent of corrosion performance in various electrolytes can be better understood at the early stages by investigating their electrochemical behaviour. For electrochemical characterization, the pre-cleaned aluminum foils were subjected to electrochemical characterisations such as potentiodynamic measurements, CV, and CA experiments. After the CV and CA experiments, the aluminum coupons were studied by using various surface techniques such as scanning electron microscopy (SEM), Energy Dispersive X-ray spectroscopy (EDXS), and optical profilometry in order to understand the extent of aluminum passivation. Further, information about the passive film composition and mechanism were obtained by using Fourier Transform Infrared spectroscopy (ATR-FTIR) and X-ray photoelectron spectroscopy (XPS) studies.

5.3.1 Electrochemical Measurements

5.3.1.1 Tafel Studies

Tafel studies involve the evaluating of the corrosion potential and corrosion current density by using a Tafel plot. The Tafel plot is drawn by subjecting the system to several hundred mV potentials to and away from the corrosion potential. In cases in which the corrosion potential is unknown, the system is subjected to a range of potentials in which the reaction of interest is expected. This method will help us to understand the corrosion kinetics much faster than the conventional weight loss methods do. A typical example of a Tafel plot is shown in Figure 5.2. The curves obtained after the potential-current measurements are plotted in the form of potential versus logarithmic current density. The obtained curves are extrapolated to obtain a straight line region for each of the anodic and cathodic domains. The intersection of the cathodic and anodic potential regions determines the corrosion potential (E_{corr}) and corrosion current (I_{corr}). Further analysis involves the measurement of Tafel slopes and understanding of the exchange current density. In this section, the corrosion current densities in different lithium battery electrolytes were compared. Tafel curves of aluminum surfaces were obtained in hybrid, conventional electrolytes, and neat ionic liquids and are presented in Figure 5.3. The corrosion current densities were lower in those electrolytes that contained ionic liquids, when compared to the conventional electrolytes. In hybrid electrolytes, the corrosion potential and the corrosion current density initially follow the same trend as that which is seen in the neat ionic liquids; however, at

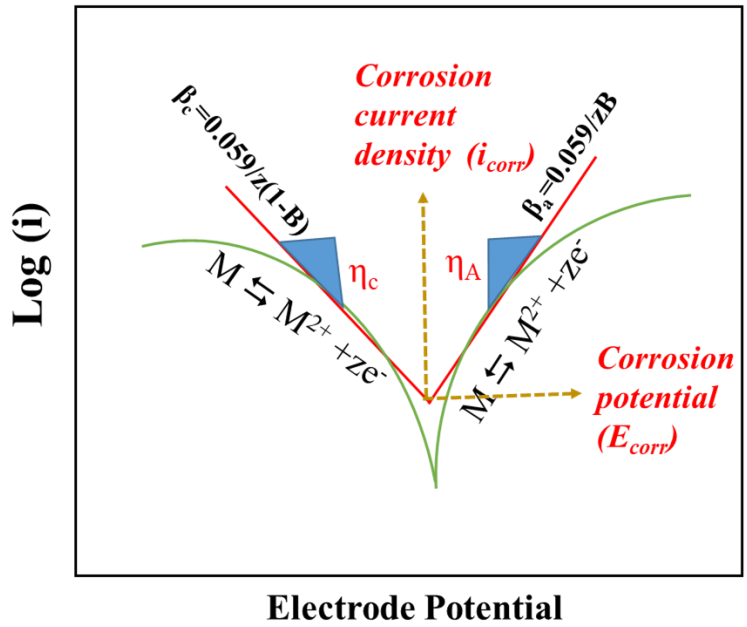

Figure 5.2 *Pictorial representation of a typical Tafel plot. In this figure, M represents any metal, z refers to the number of electrons, β_a and βc represent the anodic and cathodic slope and surface.*

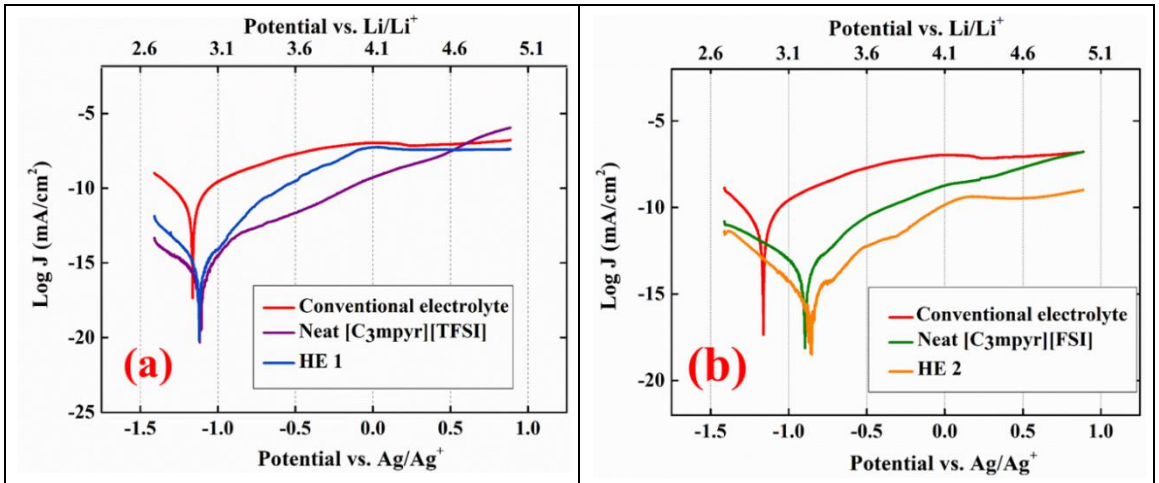

Figure 5.3 *Tafel plots of aluminum foils in (a) [C_3mpyr][TFSI] ionic liquid and HE 1 in comparison with the conventional electrolyte; (b) [C_3mpyr][FSI] ionic liquid and HE 2 in comparison with the conventional electrolyte.*

more positive potentials, the presence of $LiPF_6$ in the system creates passivation. The passivation can be seen in the flat regions in the curves for both conventional and hybrid

electrolytes. This clearly shows that the hybrid electrolytes can help decrease corrosion of aluminum current collectors.

5.3.1.2 CV and CA measurements

Further insight into corrosion was obtained by performing CV on the aluminum current collectors in the electrolyte under study. The electrochemical measurements carried out in this section aims:

i) To verify the formation of the passive film,
ii) To understand whether the formation is a one-time process or whether the film is self-healing, and
iii) To establish the mechanism of passive film formation as well as the composition of the film.

Initially, CV measurements were carried out on aluminum current collectors over a potential range of 2.7 to 4.7 V vs. Li/Li^+, as shown in Figure 5.4. The cycle was repeated twice at a rate of 0.1mV/s to understand the formation of the passive film. Quasi-flat profiles in CV in the second and third cycles at very low currents were found in ionic liquid-based electrolytes, as shown in Figure 5.3. In contrast, a significant constant increase in current density during the potential sweep was observed in the conventional electrolyte. Following the CV measurements, CA was carried out, in which the samples were subjected to a potential of 4.7 V vs. Li/Li^+ for 3 hours to further examine passive film formation. The flat lines (constant current in the system) indicate that a passive film further impedes corrosion reactions, as shown in Figure 5.4 (f).

The current *vs.* time profiles confirm the following observations:

1. The film formed in the conventional electrolyte is not sufficiently passive to prevent the corrosion on the surface, as can be seen from the steady increase of the current.

2. The film formed in neat ionic liquids and in the HE prevented further corrosion in the system, as can be seen from the steady current density values. However, the increase in current density values within 1.5 h in HE 2 may be due to damage in the passive film that is formed on the surface. Further surface characterisation was

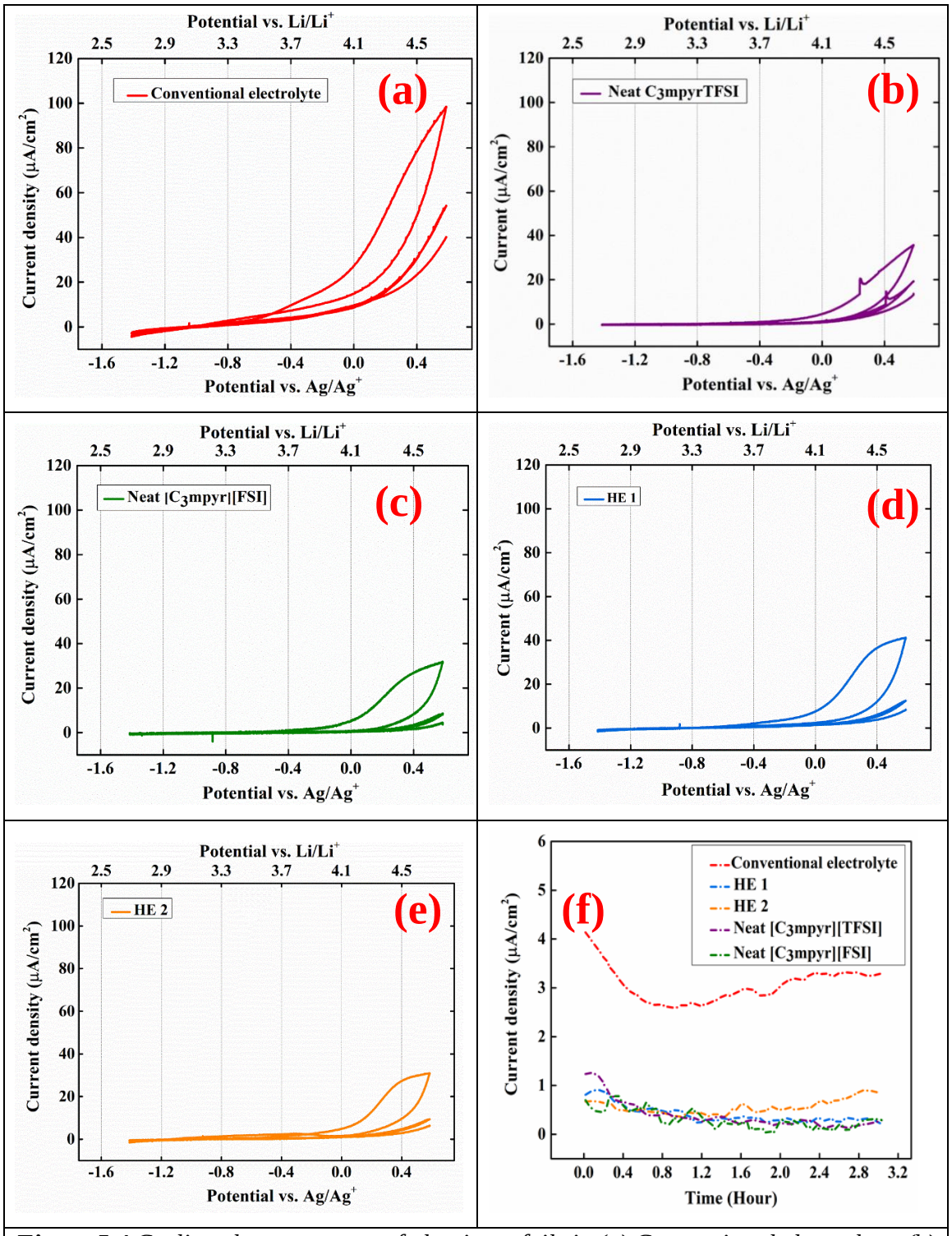

Figure 5.4 *Cyclic voltammograms of aluminum foils in (a) Conventional electrolyte, (b) [C3mpyr][TFSI], (c) [C3mpyr][FSI], (d) HE 1, (e) HE 2 at a scan rate of 0.1 mV/s over a potential window of 2.7-4.7V vs. Li / Li+, and (f) CA of aluminum foil at 4.7 V vs. Li/Li+ in conventional electrolyte, [C3mpyr] [TFSI], [C3mpyr] [FSI], HE 1, and HE 2.*

conducted on the samples to understand the formation mechanism and the composition of the passive film.

5.3.2 Surface Analysis

After CV and CA tests, the surface morphologies of the electrochemically-treated aluminum current collectors were examined by using SEM, EDXS, and optical profilometry, while the surface composition was further analysed by FTIR and XPS.

5.3.2.1 SEM & EDXS studies

Figure 5.5 shows SEM images of aluminum current collectors after electrochemical treatment in different solutions. Close observation of the SEM images indicates the formation of a layer on the surface in all cases, showing passivation by chemical attack.

The SEM micrograph of Figure 5.5 (a) shows the surface morphology of the pristine surface before any treatment.

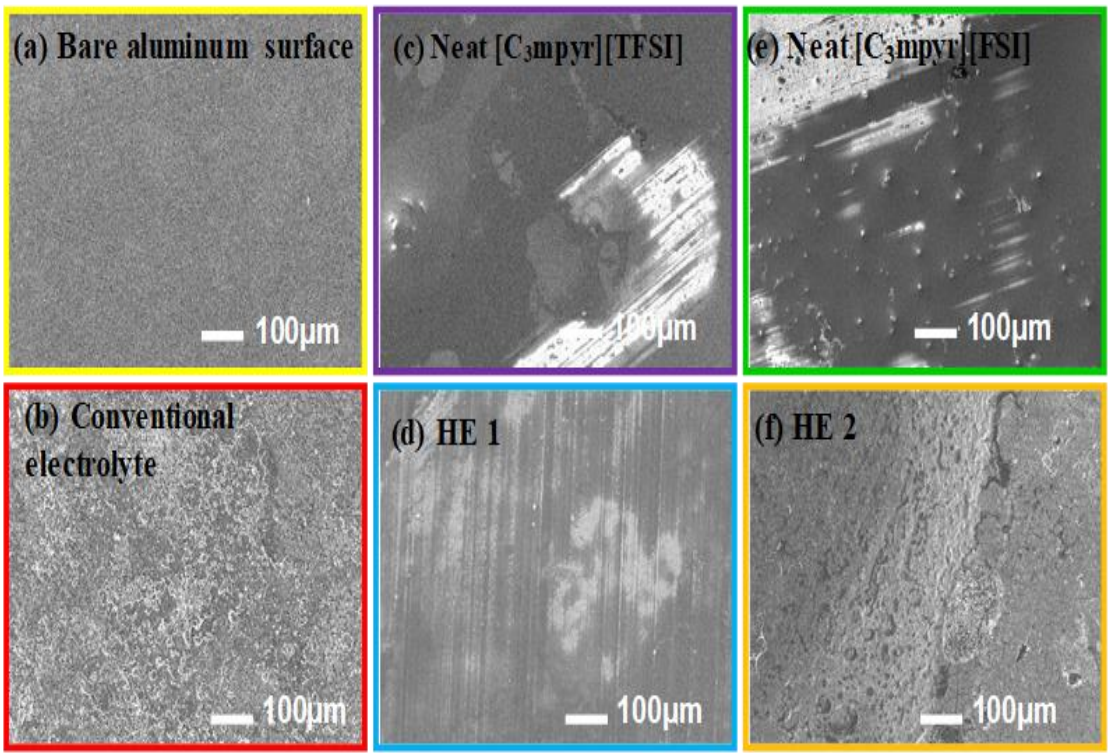

Figure 5.5 *SEM images (EHT = 10 kV) of (a) bare Aluminum surface; and aluminum foil treated in (b) conventional electrolye, (c) [C_3mpyr][TFSI], (d) [C_3mpyr][FSI], (e) HE 1, and (f) HE 2.*

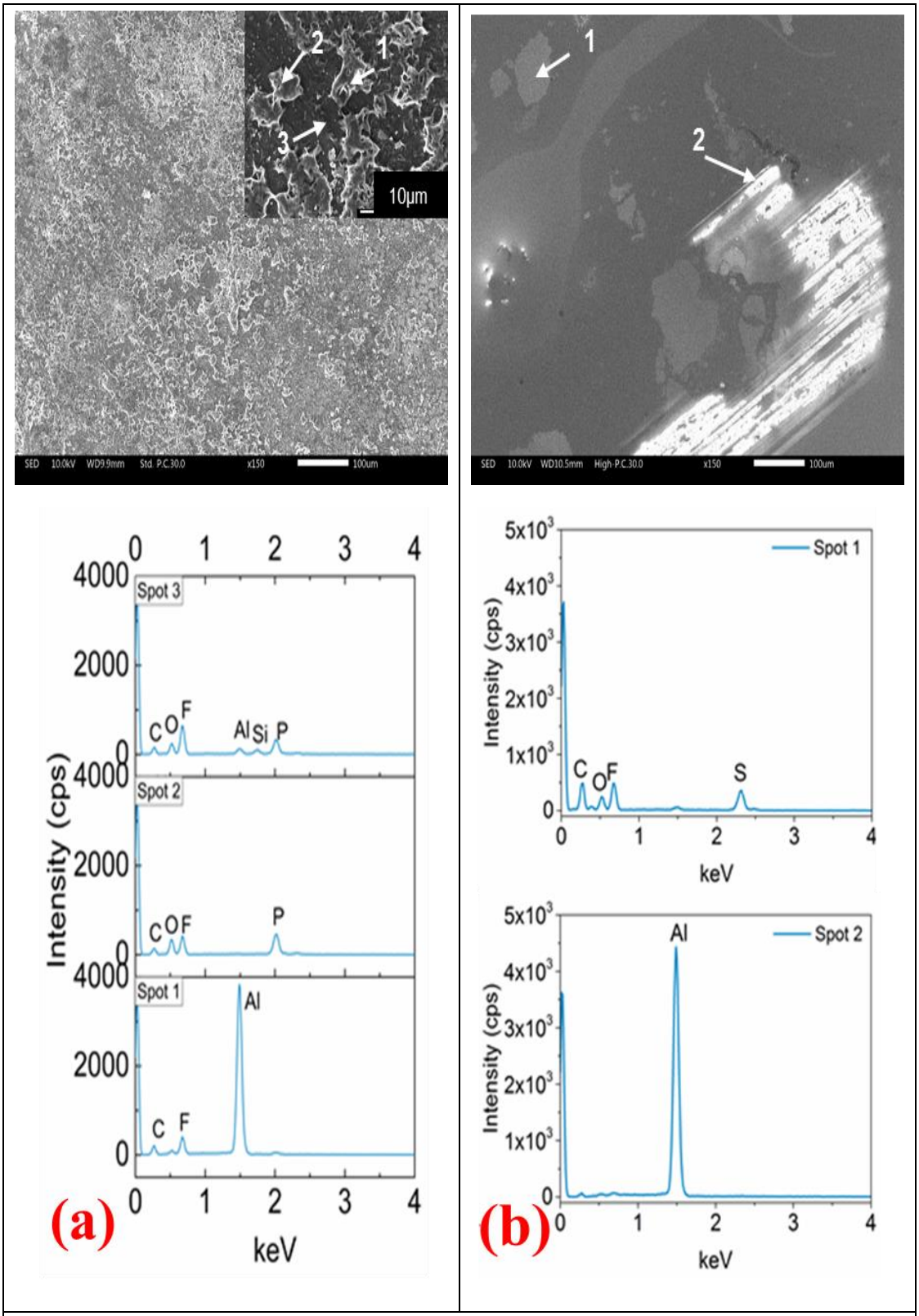

Figure 5.6 *SEM and EDXS spectra of Al surfaces electrochemically treated in a) conventional electrolyte and b) neat [C_3mpyr] [TFSI].*

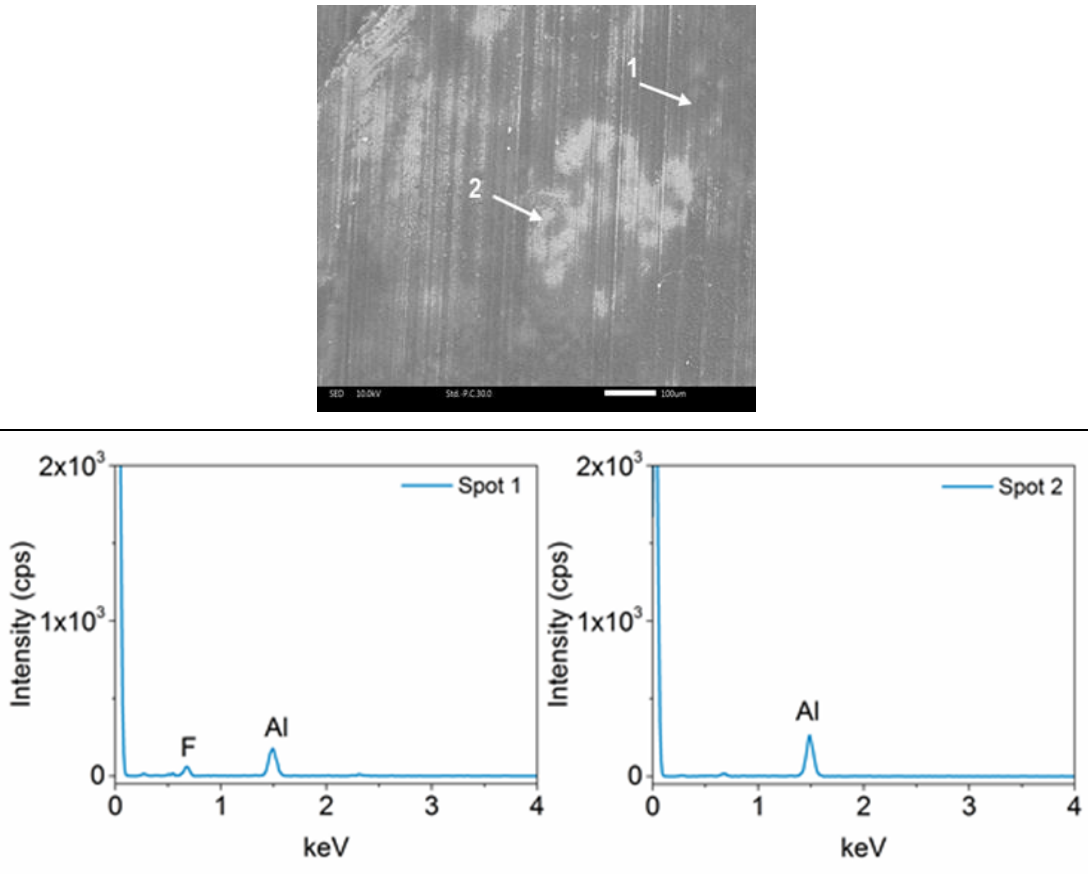

Figure 5.7 *SEM and EDXS spectra of Al surfaces electrochemically treated in HE 1.*

The treated surface in the organic carbonate solvent (conventional electrolyte) appears significantly roughened, as can be seen in Figure 5.5 (b). Closer observation reveals the formation of a very thick and non-uniform passive layer in the sample that was treated with the conventional electrolyte. EDXS analysis confirmed the presence of a relatively thick layer on the Al surface, in which the chemical composition is dominated by P, C, F, and O, as shown in Figure 5.6. The surface morphologies in Figures 5.6 (b) and 5.7 present evidence of the [$TFSI^-$] anion helping in the protecting of the aluminum surface through the formation of a protective layer that is stable against the anodizing treatment, which results in a smoothened surface. Small amounts of elements that are associated with the [$TFSI^-$] anion were detected by EDXS (Figures 5.6 (b) and 5.7)), although these need to be further confirmed by XPS analysis. The samples that were treated in neat [C_3mpyr] [TFSI] and neat [C_3mpyr] [FSI] show very different surface morphologies (Figures 5.8 (a) and (b)). The FSI-treated sample has a very uneven surface, suggesting a heterogeneous passivation layer on the Al surface (Figure 5.8). This suggests that (in contrast to the

behaviour seen in the TFSI-treated sample) the passivating layer that is formed on the neat FSI-treated sample did not withstand the anodising treatment.

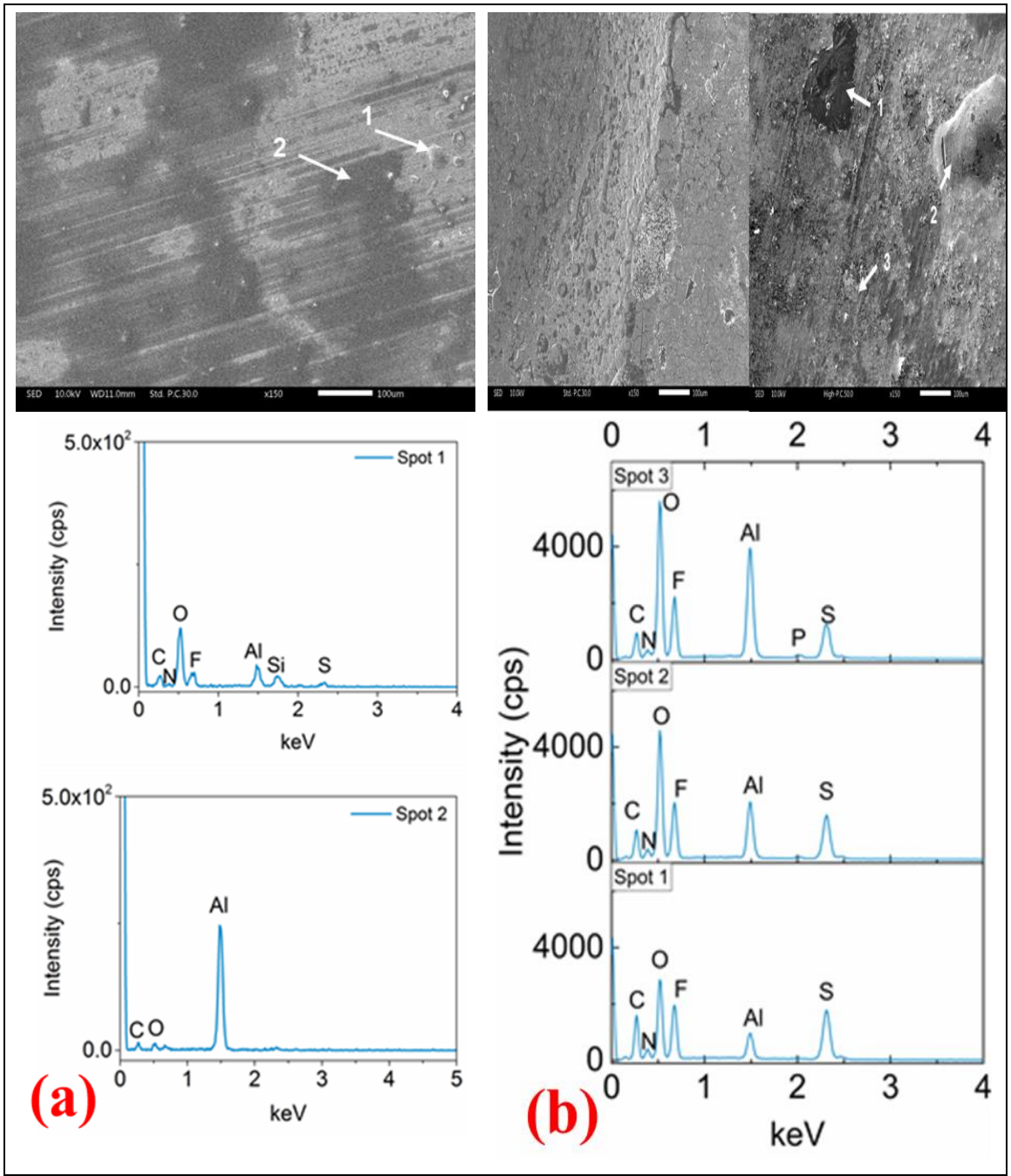

Figure 5.8 *SEM and EDXS spectra of Al surfaces after electrochemical treatment in a) neat [C3mpyr] [FSI], and b) HE 2.*

The main difference between in the SEM analyses of the surfaces treated in the hybrid electrolytes is in the presence of a thicker layer when the FSI^- anion is mixed with the conventional electrolyte solution, as can be seen in Figure 5.5 (f) (HE 2 sample). The

cracks that were visible on the surface were interpreted as being a result of the vacuum in the SEM chamber. Larger quantities of elements such as O, F and S, which are associated with the anion in the case of the HE 2 surface, were confirmed by EDXS analysis (Figure 5.8 (b)) as being characteristic of the strong interaction between the IL anion and the surface that may form a passivating layer on the Al.

5.3.2.2 Optical profilometric study

To obtain quantitative information about the roughness of the surface, the samples that were treated in the neat ionic liquids, HE 1 and HE 2, were tested by optical profilometry. 3D images are presented in Figure 5.9.

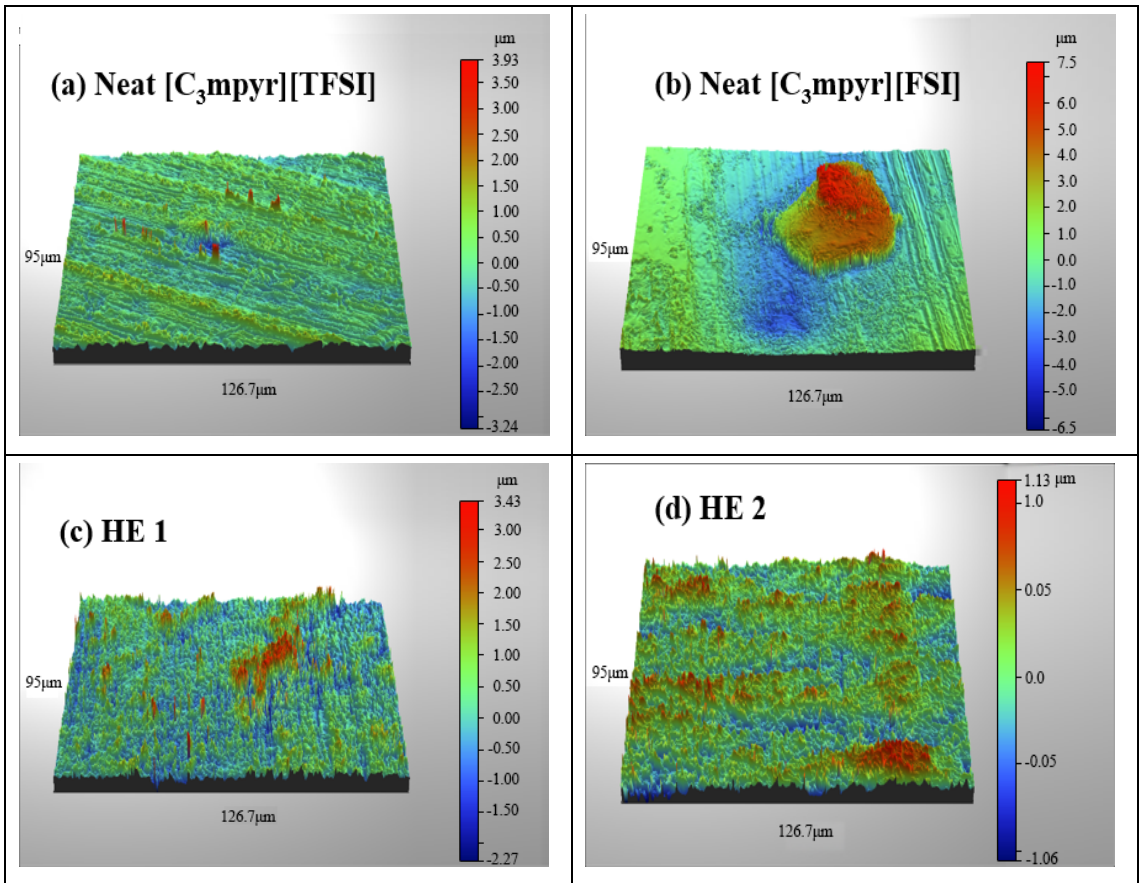

Figure 5.9 *Optical profilometric 3D images collected for aluminum surfaces after anodizing treatment in (a) [C3mpyr][TFSI], (b) [C3mpyr][FSI], (c) HE 1, and (d) HE 2.*

After treatment in neat ILs (Figures 5.9 (a) and 5.9 (b), respectively, for the neat TFSI and neat FSI samples), there were rough, distributed deposits on the surface, and the roughness

was significantly more pronounced in the case of the neat FSI sample. Whereas, after treatment in the hybrid solutions (Figures 5.9 (c) and 5.9 (d), respectively, for HE 1 and HE 2) a more evenly distributed, thin layer appears to have been deposited onto the surface of the aluminum. These images are consistent with those from SEM (Figure 5.5). Here it must be noted that the color legend at the right side of the images in Figure 5.9 is different for each sample.

Table 5.1 *Average roughness of aluminum surfaces after anodizing treatment in [C_3mpyr][TFSI], [C_3mpyr][FSI], HE 1, and HE 2, obtained by optical profilometry.*

Sample	S_a / µm (average roughness)
Neat [C_3mpyr][TFSI]	0.52 ± 0.2
HE 1	0.48 ± 0.1
Neat [C_3mpyr][FSI]	0.79 ± 0.7
HE 2	0.53 ± 0.01

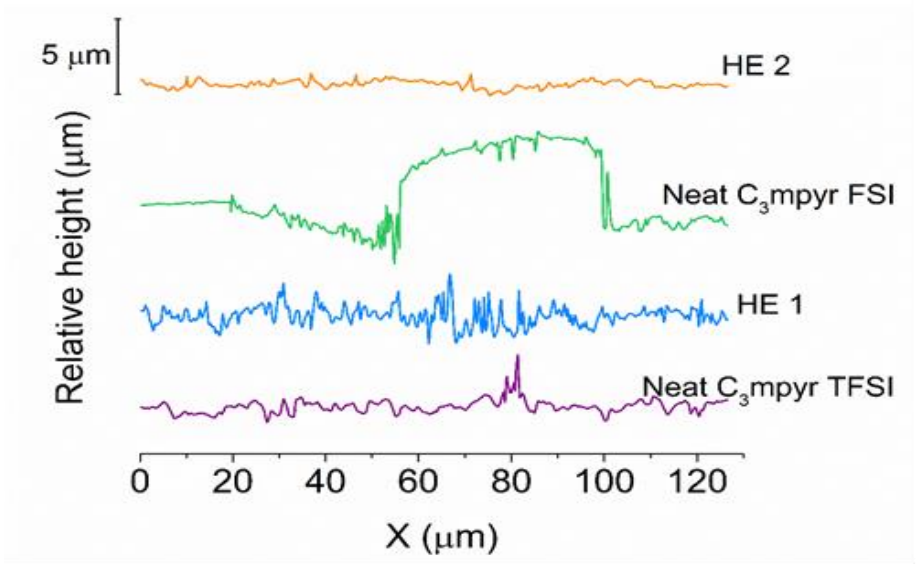

Figure 5.10 *Average Roughness and relative height (2 D contour profile) across the aluminum surface after anodizing treatment in [C_3mpyr][TFSI], [C_3mpyr][FSI], HE 1, and HE 2 obtained by optical profilometry.*

The observations from the profilometric study concur with previous SEM analyses. The results provide evidence of a more uniform protective layer that is formed with the hybrid systems. The average roughness was measured on multiple spots, and small deviations that were obtained in the case of hybrid samples reflect the uniformity of the surface, as shown in Table 5.1. This could explain the electrochemical results (CV), which were previously described.

In the case of the samples that were treated with neat TFSI and neat FSI, the surface was not flat. (This observation is confirmed by a relative height variation of ± 10 µm, seen in Figure 5.10.) However, a smoother surface was confirmed in the case of the HE 2 sample.

5.3.2.3 FTIR Analysis

FTIR analyses of the electrochemically treated aluminum foils are presented in Figure 5.11. In the case of hybrid electrolytes, the strong peaks that correspond to SO_2 asymmetrical and symmetrical stretching were found at 1177 and 1348 cm^{-1} for the sample that was treated in HE 1 and 1174 and at 1381 cm^{-1} for that which was treated in HE 2, respectively. This indicates that the SO_2 portion of the anion has remained intact and is present on or very near the surface[41–43] (when the penetration depth of the IR beam is taken into account).

The SO_2 group may belong to multiple species on the surface of the aluminum, but the FTIR spectra do not enable any conclusion about the exact structure. There does not seem to be a peak that could be assigned to the S-F stretch[42]. The strong peaks that correspond to the SN stretch are clearly present at ~ 740 and 843 cm^{-1} for the sample that was treated in HE 1, and at ~ 740 and 832 cm^{-1} for the sample that was treated in HE 2, respectively[42,44–46]. All C-H-based vibrations that do not arise from DMC reaction residues must be due to the C_3mpyr^+ cation. Clear peaks are associated with the CH_3 stretch at 2888, 2947, and 2980 cm^{-1} in the spectrum of the sample treated with HE 2, which precisely match the peak positions[42,43,46,47] found in the spectra of neat [C_3mpyr][TFSI] and [C_3mpyr][FSI], as shown in Figure 5.11 This indicates that, at least in most cases, the alkyl chains are preserved, which suggests the presence of the intact pyrrolidinium cation on the surface. During the anodizing process, the surface of the Al becomes positively charged, so it is expected that migration of the anion towards Al will be promoted, while the cation will

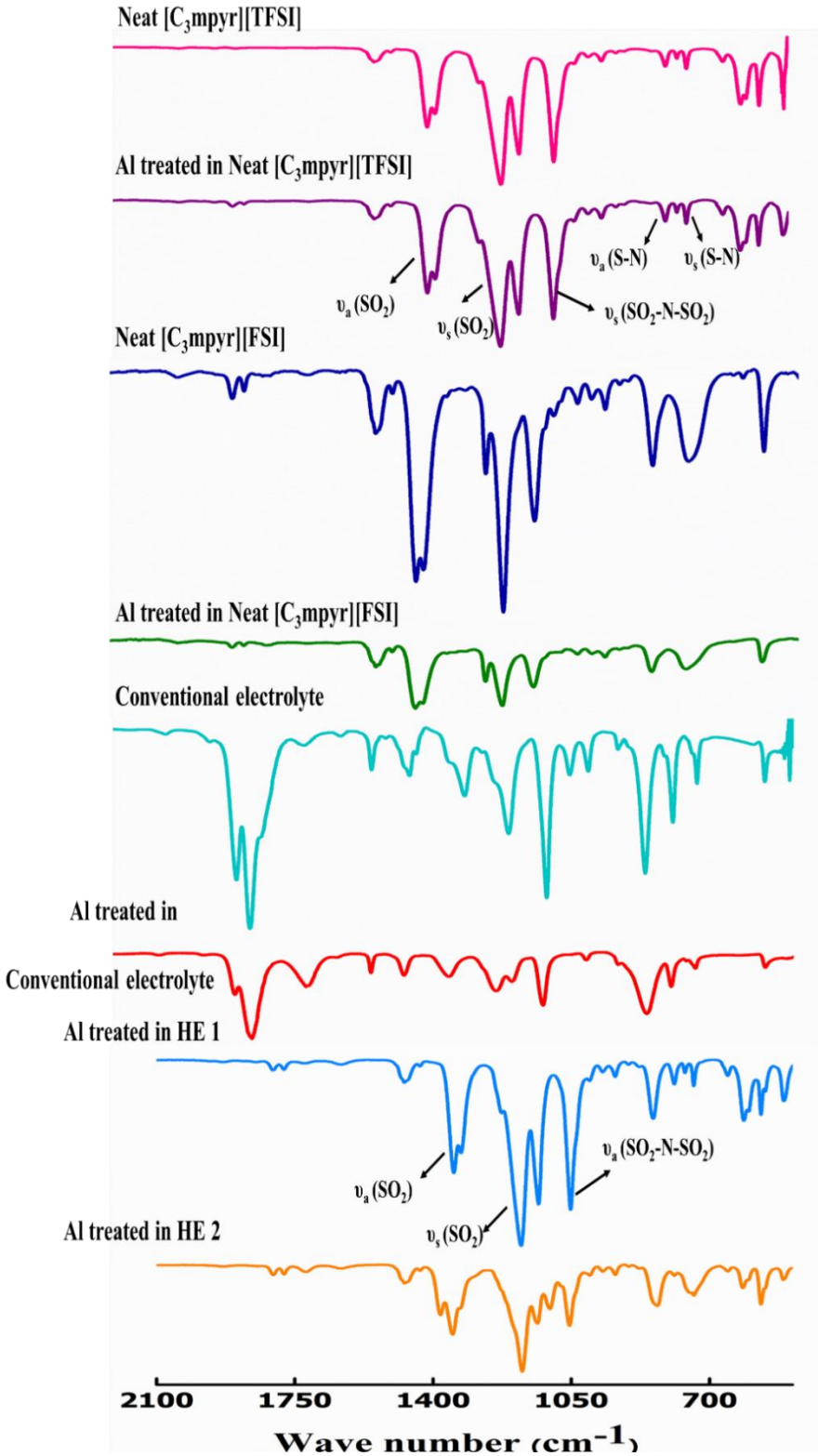

Figure 5.11 *FTIR spectra of neat [C3mpyr][TFSI], [C3mpyr][FSI], and aluminum foils treated in the conventional electrolyte, [C3mpyr][TFSI],[C3mpyr][FSI], HE 1, and HE 2.*

Table 5.2 *FTIR spectra of neat [C_3mpyr][TFSI],[C_3mpyr][FSI], and the aluminum foils treated in [C_3mpyr][TFSI],[C_3mpyr][FSI], HE 1, and HE 2. The yellow highlighted rows represent the peak positions from the conventional electrolyte.*

S.No	Assignment	Samples								
		Neat [C_3mpyr][TFSI]	Neat [C_3mpyr][TFSI]-Al	Neat [C_3mpyr][FSI]	Neat [C_3mpyr][FSI]-Al	Conventional electrolyte	Conventional electrolyte on Al	HE 1	HE 2	References
1.	$\delta_a(SO_2)$	569 (s)	570 (w)	567 (s)	570			570	570	[42]
2.	ν_s (SNS)	740	740	729 (b)	745			740 (w)	740	[42,44–46]
3.	ν_a (SNS) & ν(SF)	789	789		828			843	832	[41,44,46]
4.	ν_s (R-C-R)					835 (s)	835 (s)			[48]
5.	ν (CO)					1079 (s)	1079 (s)			[48]
6.	$\nu_a(SO_2$-N-$SO_2)$	1051 (s)	1051 (s)	1101	1103			1052 (s)	1054	[41–43]
7.	ν_a (R-C-R)					1152 (s) 1189	1153 (s) 1189			[48]
8.	ν_s (SO_2-N-SO_2	1133 (s) 1175 (s)	1133 (w) 1176 (s)	1172 1216	1175 1216			1133 1177 (s)	1104 1136 1174 (s)	[41–43]
9.	ν_a (SO_2)	1330 (s)	1329 (s)	1360 (s)	1360			1329	1332 (w) 1350	[41,42,46]
10.	ν_a (SO_2)	1348 (s)	1347 (s)	1377 (s)	1378			1348	1381	[41,42]
11.	ν (CH_2) ν(CH_3)	1473	1472 (m)	1471	1472			1473	1472	[42,47,49]

(Continued)

S.No	Assignment	Samples								
		Neat [C_3mpyr][TFSI]	Neat [C_3mpyr] [TFSI]-Al	Neat [C_3mpyr] [FSI]	Neat [C_3mpyr][FSI]-Al	Conventional electrolyte	Conventional electrolyte on Al	HE 1	HE 2	References
12.	ν (C=O) from R-O-COOR					1763 (s)	1764 (s)			[48]
13.	ν (CH_2)	2889	2889 (w)	2887	2887			2889	2888	[42,43,46,47]
14.	ν (CH_2)	2950	2948 (w)	2945	2946	2940	2940	2949	2947	[42,43,46,47]
15.	ν (CH_2)	2982	2981	2980	2979			2981	2980	[42,43,46,47]
16.	ν (CH_2)					3004	3008			[42,46,47]
17.	ν (CH_2)		3042 (w)		3042 (w)					[47]
18.	ν (OH)					3630 (s,b)	3630 (s,b)			[48]

move away from the surface. The peak positions and their corresponding significance are collated in Table 5.2. Literature reports that are based on the elemental composition of ionic liquid films on various reactive metals show that the ionic liquid anion greatly dominates the surface chemistry[50]. Another study on the basis of ToF-SIMS revealed that both the cation and anion are present in the film; however, only the cation could be identified as a whole molecule[26]. This confirms that the anion chemistry plays a dominant role in the passivation of aluminum current collectors.

5.3.2.4 XPS Analysis

5.3.2.4.1 XPS Initial Measurements

XPS high-resolution region spectra peak identities were determined from published values[51,52] and from reports of XPS studies of aluminum surfaces[53,54]. The data obtained initially (before etching) are indicative of the outer surface.

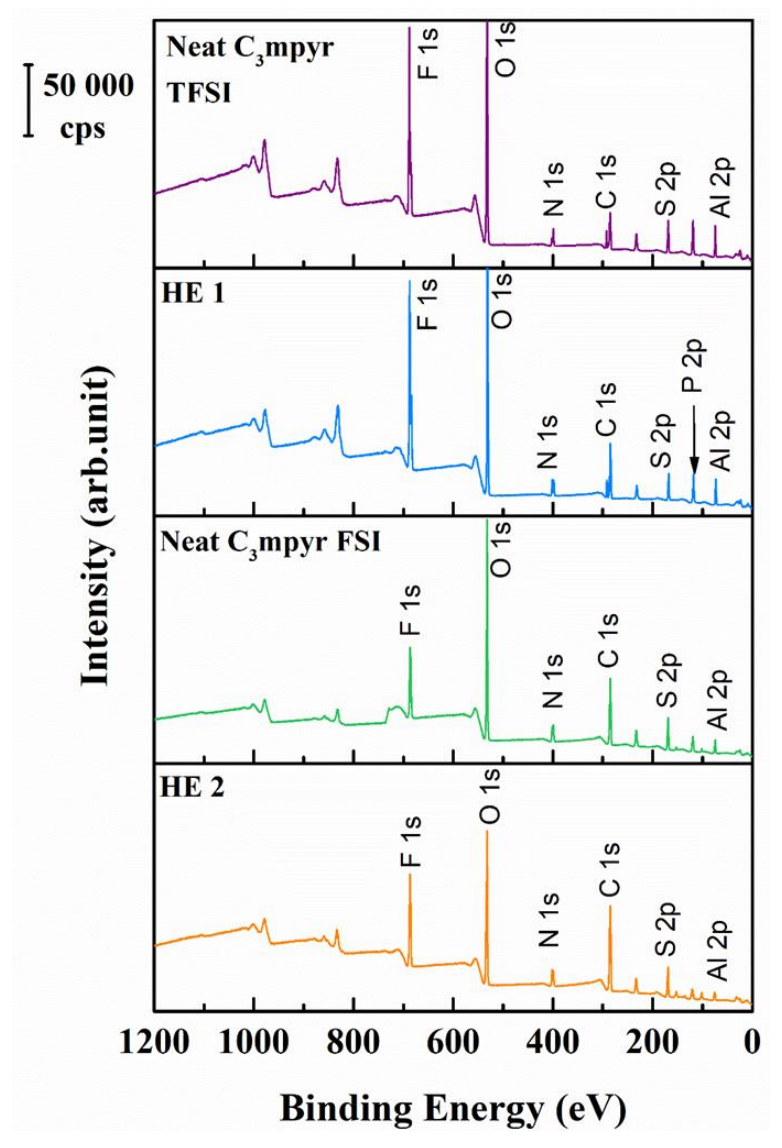

Figure 5.12 *XPS survey scan for the Al surfaces treated in neat [C3mpyr][TFSI], HE 1, neat [C3mpyr][FSI], and HE 2 solutions before and after etching.*

Figure 5.12 presents the survey spectra that were obtained from the neat IL samples and the corresponding hybrid samples. Chemical compositions (atomic percentage) are included in Table 5.3.

Measurements clearly indicate that the elements that were associated with the IL anions were present on the surface of the samples in significant quantities. Differences in the chemical composition before and after etching are more pronounced in the case of neat ILs, suggesting that the surfaces that are treated in the HE are more homogeneous. As

expected, larger amounts of F and, interestingly, larger amounts of Al, were detected in the sample surfaces that were treated in [TFSI]-containing electrolytes (neat [C_3mpyr] [TFSI] and HE 1), whereas more C was detected in the [FSI]-treated samples (neat [C_3mpyr] [FSI] and HE 2).

Table 5.3 *Atomic percent (± 0.1 - 1 %) summary determined from the survey spectra for the aluminium surfaces before (initial) and after etching (etched) for five minutes*

Element	Atomic concentration (%)							
	Neat [C_3mpyr][TFSI]		HE 1		Neat [C_3mpyr][FSI]		HE 2	
	Initial	Etched	Initial	Etched	Initial	Etched	Initial	Etched
F (1s)	16.4	30.9	18.6	20.7	9.2	18.8	10.0	14.2
O (1s)	41.7	28.3	31.2	22.4	31.7	31.0	24.3	20.0
N (1s)	3.6	1.8	4.3	3.3	6.0	3.9	5.4	6.3
C (1s)	17.9	8.0	19.9	19.6	34.3	17.8	45.1	36.3
S ($2p_{3/2}$)	6.2	2.7	5.1	3.9	8.8	5.2	7.6	8.8
P ($2p_{3/2}$)	-	-	8.3	12.0	-	-	-	2.2
Al (2p)	14.2	28.3	12.7	18.2	9.9	23.3	7.6	12.2

5.3.2.4.2 XPS Etching Measurements

Although the etching procedure is destructive and sample compositions must be analyzed with care, it may be useful to identify existing species that are likely to be present in the passivating layer, which will provide significant insight into the chemical nature of the film. As the etching rate was estimated to be 2 Å.s^{-1}, the experiment is estimated to have removed approximately 60 nm of material.

High-resolution region spectra were acquired initially and after 5 min of etching. The results that were obtained from the Al 2p and F 1s for the four samples are summarized in Figures 5.13 and 5.14. Region spectra from C 1s, N 1s, O 1s, and S 2p are provided in Figures 5.15, 5.16, 5.17, and 5.18 along with peak assignments (Tables 5.4 and 5.5).

Table 5.4 *Summary of XPS data and assignments for the aluminum surfaces of neat [C_3mpyr][TFSI] and HE 1 samples (before and after etching).*

Element	Assignment	Peak position (eV)			
		Neat [C_3mpyr][TFSI]		HE 1	
		Initial	Etched	Initial	Etched
F (1s)	$-CF_3$	689.4 (37.7)	688.7 (45.5) 688.2 (7.3)	690.6 (0.4) 688.7 (35.2)	689.9 (5.6)
	$-SO_2F$	688.9 (31.4)	687.6 (4) 687.0 (8.4)	688.2 (30.4)	688.2 (41.9)
	AlF_3 (686.3) metal fluoride (684-685.5)	686.8 (8) 685.7 (23)	686.6 (34.7)	685.6 (14.1) 685.1 (19) 684.2 (0.8)	686.2 (50) 684.4 (2.5)
O (1s)	O-F (ca. 535)	534.3 (6)	534.1 (42.5)	-	534.6 (1.8)
	Organic C=O (ca. 533)	533.3 (41.1) 533.0 (3.2)	533.6 (9.6) 533.1 (1.2)	533.8 (2.3)	533.4 (5.7) 532.7 (46.8)
	CO_3^{2-} (531.5-532) organic C-O or SO_2^-	532.6 (47.5)	532.6 (5.4) 531.9,532 (41.4)	532.2 (59.2) 531.7 (5.5) 531.5 (32)	532.0 (26.3) 530.8 (19.5)
	Al oxide (529-530)	531.1 (2.3)	-	529.9 (1)	-
N (1s)	N^+	403.6 (2.9) 402.7 (22.4) 402.1 (0.5) 401.5 (5.0)	404.5 (8.5) 402.2 (47.8)	403.9 (1) 402.6 (10.4) 402.1 (34.7) 401.1 (0.2)	403.3 (10.7) 401.9 (36.2)
	N^-	400.7 (13.4) 399.7 (43.1) 399.6 (12.7)	400.6 (21.2) 399.9 (2.1) 399.1 (20.5)	399.5-20.8 399.1-28.1 398.1-4.9	400.4 (7.4) 398.8 (45.7)

(Continued)

Element	Assignment	Peak position (eV)			
		Neat [C_3mpyr][TFSI]		HE 1	
		Initial	Etched	Initial	Etched
C (1s)	$-CF_3$	293.5 (9.2) 292.9 (10.3)	292.9 (6)	292.6 (14.1)	292.6 (3.5) 292.3 (5.6)
	C_{hetero} CO_3^{2-} O-C=O	289.4 (6.5)	290.8 (6.1) 288.9 (6.2)	288.3 (3.1)	289.7 (4.4)
	C-O-C (ca. 286 eV) C-N	287.1 (17.4) 286.4 (19.4)	286.9 (47.3)	286.3 (41.8)	287.1 (12.5) 286.1 (21.7)
S (2p)	$-SO_2CF_3$	169.7 (31.4) 170.9 (15.7) 169.0 (31.9) 170.2 (16)	173.7 (1.4) 172.5 (2.8) 170.2 (30.6) 171.4 (15.3)	168.6 (45.8) 169.7 (22.9)	169.9,170 (2.9) 171.1 (1.4) 168.3 (24.8) 169.5 (12.4)
	Oxidized S (sulfone, sulfite)	167.3 (3.4) 168.4 (1.7)	168.5 (16.4) 169.6 (8.2)	167.9 (19.2) 169.0 (9.6)	168.1 (19.8) 169.2 (9.9)
	Sulfide species (160-165) and S_0 (164.1, 164)	-	165.4 (11.3) 166.5 (5.7) 163.8 (5.6) 164.9 (2.8)	163.8 (1.7) 164.9 (0.9)	163.5 (13.8) 164.7 (6.9) 164.2 (2.7) 163.0 (5.4)
Al ($2p_{3/2}$)	AlF_3 (76.6)	-	77.2 (23.1) 78.4 (11.5)	74.8 (23) 76.6 (2.3)	76.8 (18.8) 75.7 (37.7)
	Al oxide on Al foil (75.6)	76.0 (31) 75.4 (8) 74.9 (61.3)	75.4 (42.5) 76.6 (21.3)	-	-
	Al oxide (74.4-74.6)	-	-	74.4 (47.5) 74.1 (26.4)	75.5 (14.5) 74.4 (28.9)
	Al_0 (72.6-72.9)	-	70.8 (1.6)	-	-

Table 5.5 *Summary of XPS data and assignments for the aluminum surfaces of neat [C_3mpyr][FSI] and HE 2 samples (before and after etching).*

Element	Assignment	Peak position (eV)			
		Neat [C_3mpyr][FSI]		HE 2	
		Initial	Etched	Initial	Etched
F (1s)	$-CF_3$	-	-	-	-
	$-SO_2F$	688.2 (18.5) 687.6 (20.3)	688.0 (58.4)	688.5 (16.1) 687.9 (30.8) 687.1 (41.3)	688.7 (0.2) 688.3 (37.3) 687.4 (34.6)
	AlF_3 (686.3) Metal fluoride (684-685.5)	686.7 (61.2)	686.6 (29.4) 685.2 (12.1)	686.2 (3.3) 685.8 (8.6)	686.4 (22.9) 685.1 (5.1)
O (1s)	O-F (ca. 535)	535.0 (3.9) 534.2 (6.9)	534.2 (30.3)	534.5 (8.9)	-
	Organic C=O (ca. 533)	533.5 (47.4)		533.4 (43.7)	533.6 (25.1) 533.3 (31.8)
	CO_3^{2-} (531.5-532) organic C-O or SO_2^-	532.5 (41.8)	532.7 (67.1) 531.1 (2.4)	532.7 (36.5) 532.0 (10.8)	532.7 (26.1) 531.5 (17)
	Al oxide (529-530)	-	529.6 (0.3)	-	-
N (1s)	N^+	403.2 (28.9) 401.9,402 (3.8)	404.3 (9.8) 403.0 (14.2) 401.7 (36.9)	403.9,404 (5.3) 402.4 (41.5)	402.7 (34.2) 402.4 (7.9)
	N^-	400.5 (59.9) 399.1 (7.5)	400.4 (6.9) 399.3 (32.2)	400.6 (10) 399.5 (38.2) 398.3 (5)	400.3 (28.3) 399.5 (18) 398.7 (11.7)
C (1s)	$-CF_3$	-	-	-	-
	C_{hetero} CO_3^{2-} O-C=O	289.8 (2.5) 287.1(37.1)	287.2 (59.3)	287.6 (7.4) 287.1 (6)	-

(Continued)

Element	Assignment	Peak position (eV)			
		Neat [C_3mpyr][FSI]		HE 2	
		Initial	Etched	Initial	Etched
C (1s)	C-O-C (ca. 286 eV) C-N	285.9,286 (38.3)	286.2 (9) 285.9 (9.5)	286.4 (35.1) 285.3 (19.4)	286.5 (50.8) 286.4 (16.1) 285.4 (13.4)
	$C_{aliphatic}$ C-C / C-H	284.8 (22.2)	284.8 (22.1)	284.8 (32.1)	284.8 (19.8)
S ($2p_{3/2}$)	$-SO_2F$	170.5 (8.4) 171.7-4.2 169.7 (55.5) 170.9 (27.8) 169.3 (2.8) 170.4 (1.4)	170.9,171 (23.7) 172.1 (11.9) 170.3 (0.9) 171.4 (0.5) 169.5 (11) 170.6 (5.5)	171.4 (5.3) 172.6 (2.6) 170.8 (3) 171.98 (1.5)	170.8 (10) 171.9,172.0 (5) 169.7 (19.3) 170.9 (9.6)
	Oxidized S (sulfone, sulfite)	-	168.9 (11.2) 170.0 (5.6) 167.5 (6) 168.6 (3)	169.6 (51.9) 170.8 (25.9) 168.3 (6.5) 169.4 (3.3)	168.7 (14.7) 169.9 (7.3)
	Sulfide species (160-165) and S^0 (164.1, 164)	-	164.9,165 (10.2) 166.1 (5.1) 163.1 (3.7) 164.3 (1.9)	-	164.2 (18.2) 165.3 (9.1) 163.5 (4.5) 164.7 (2.3)
Al ($2p_{3/2}$)	AlF_3 (76.6)	76.1 (24.9) 77.2 (12.5)	76.8 (37.3) 77.2 (18.7)	77.6 (7.1) 78.8 (3.6) 75.8 (59.6) 76.9,77.0 (29.8)	76.1 (43.8) 77.3 (21.9) 76.0 (3.6) 77.2 (1.8)
	Al oxide on Al foil (75.6)	75.2 (40.9) 76.3 (20.5)	75.1 (28.9) 76.3 (14.4)	-	75.2 (19.2) 76.4 (9.6)
	Al oxide (74.4-74.6)	-	-	-	-
	Al^0 (72.6-72.9)	71.2 (1.2)	70.2 (0.8)	-	-

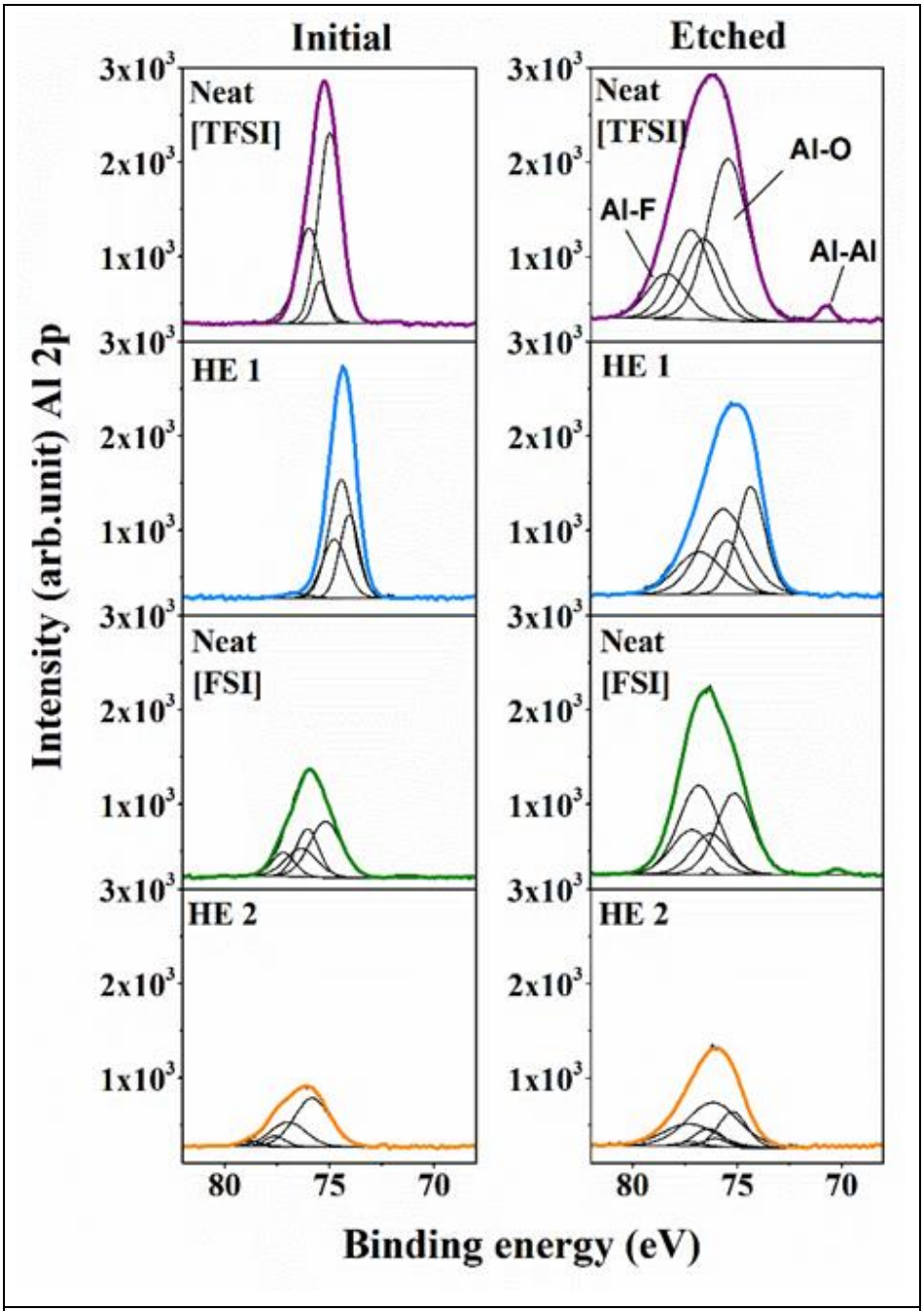

Figure 5.13 *C 1s High-resolution spectra for the Al surfaces treated in neat [C3mpyr][TFSI], HE 1, neat [C3mpyr][FSI], and HE 2 solutions before and after etching.*

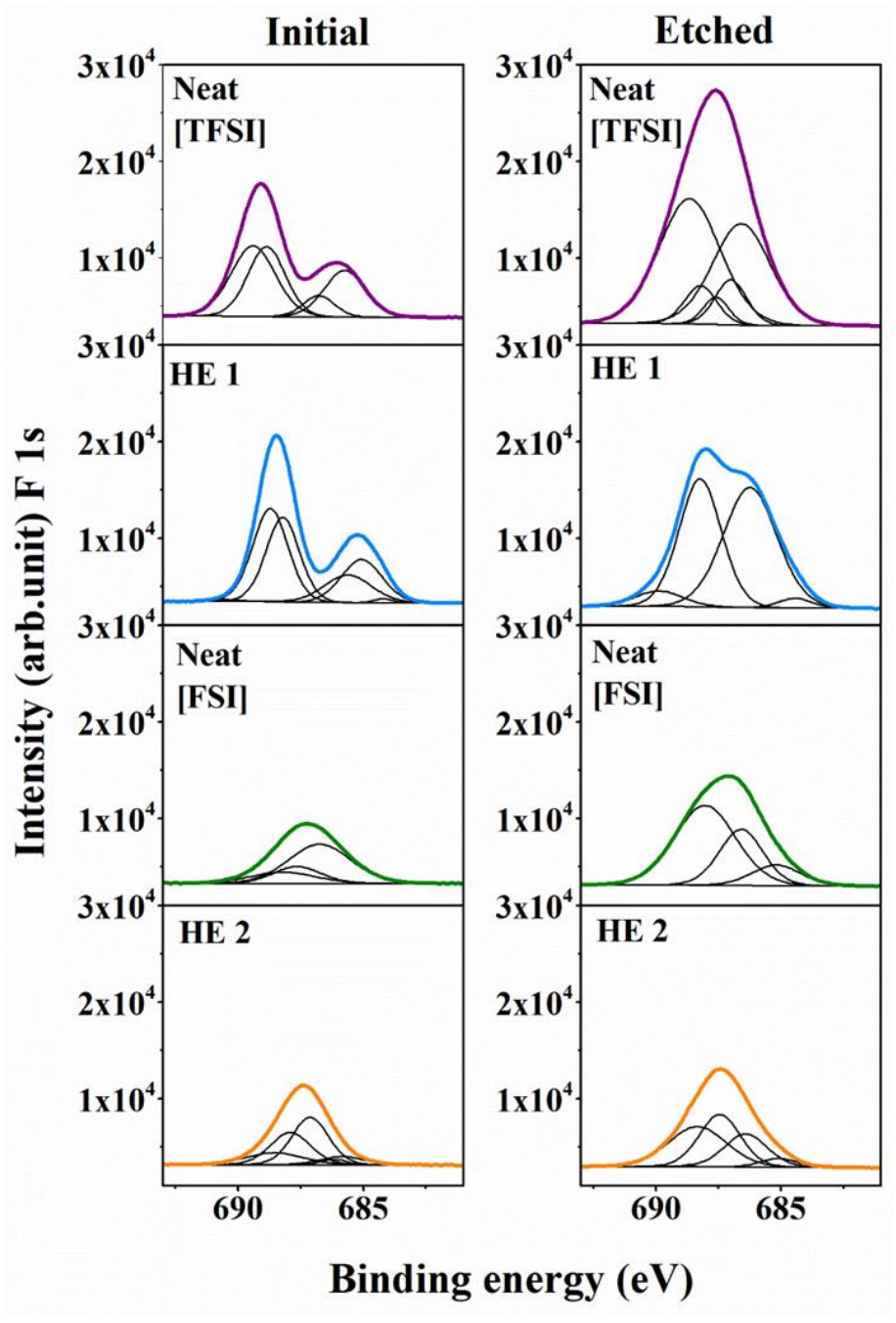

Figure 5.14 *High-resolution F 1s region spectra for the Al surfaces treated in neat [C_3mpyr][TFSI], HE 1, neat [C_3mpyr][FSI],and HE 2 solutions before and after etching.*

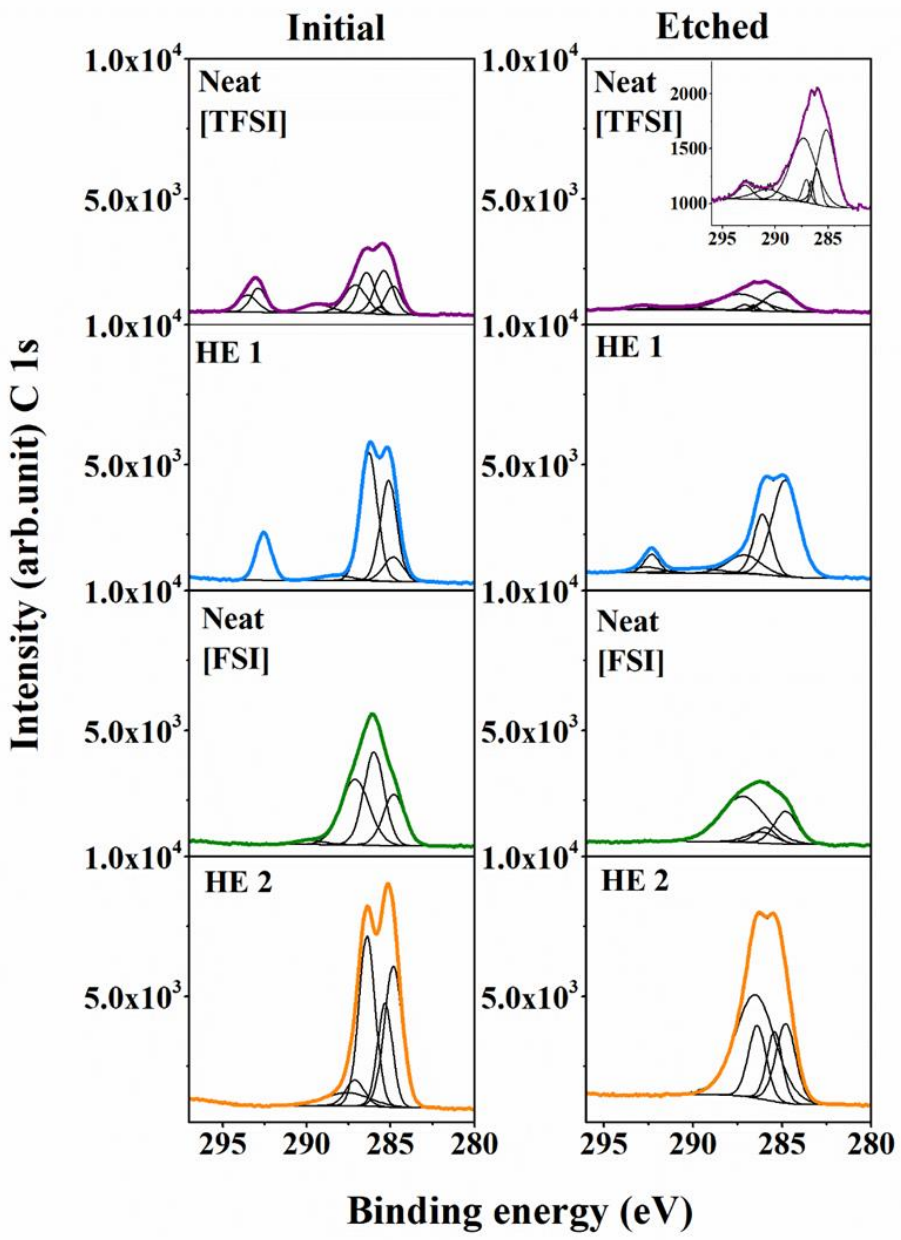

Figure 5.15 *C 1s High-resolution spectra for the Al surfaces treated in neat [C3mpyr][TFSI], HE 1, neat [C3mpyr][FSI], and HE 2 solutions before and after etching.*

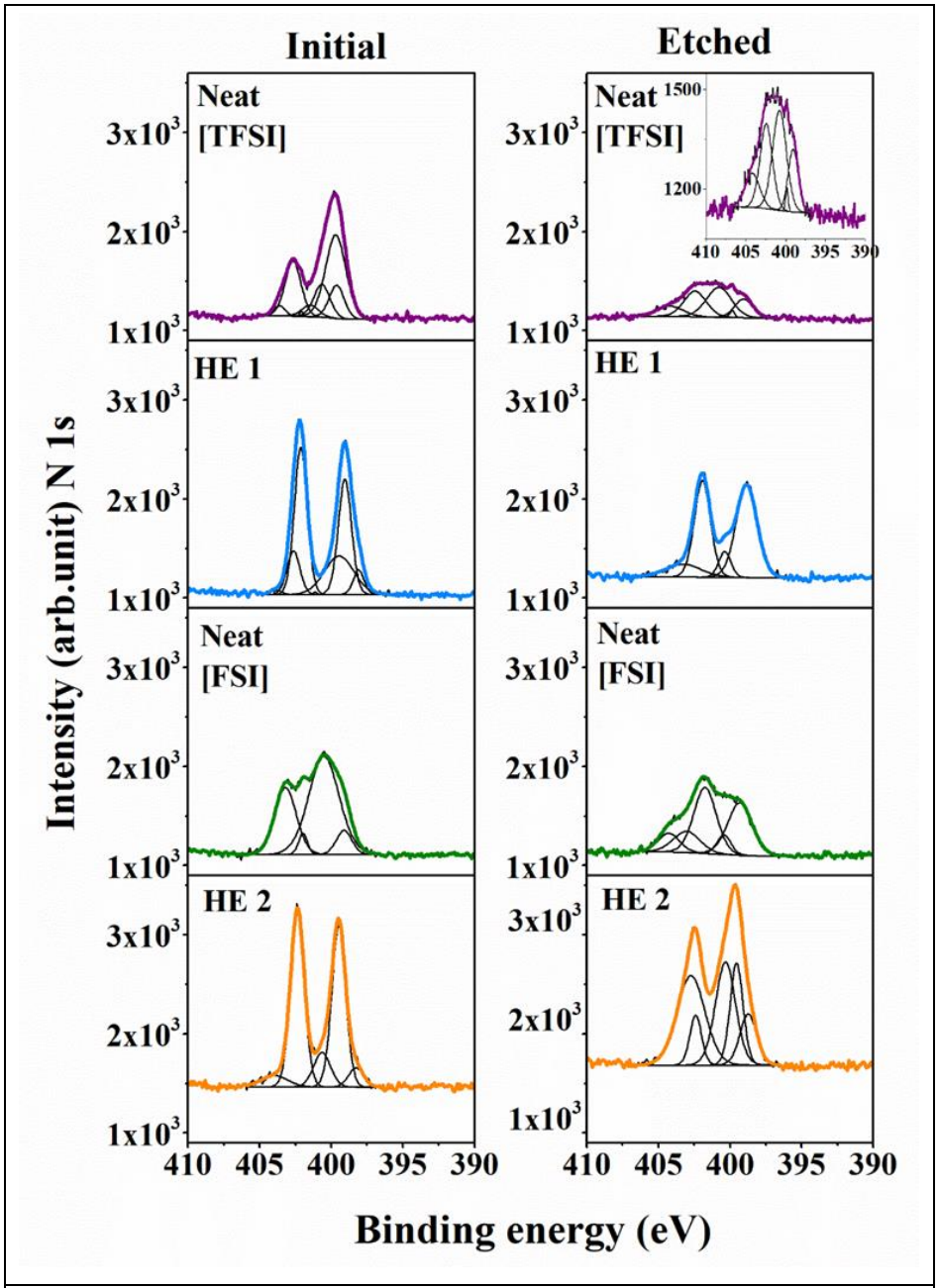

Figure 5.16 *N 1s High-resolution spectra for the Al surfaces treated in neat [C3mpyr][TFSI], HE 1, neat [C3mpyr][FSI], and HE 2 solutions before and after etching.*

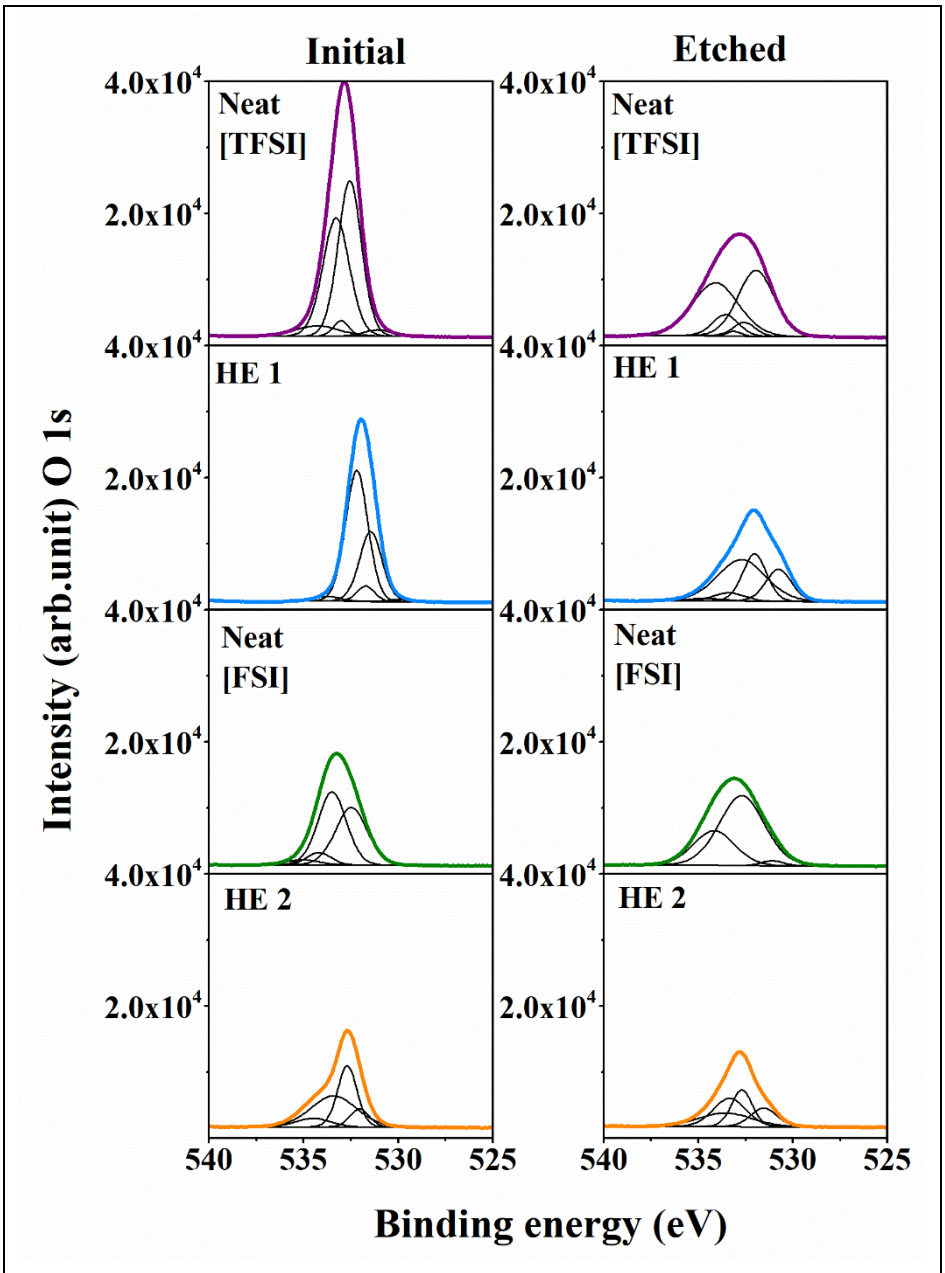

Figure 5.17 *O 1s High-resolution spectra for the Al surfaces treated in neat [C_3mpyr][TFSI], HE 1, neat [C_3mpyr][FSI], and HE 2 solutions before and after etching.*

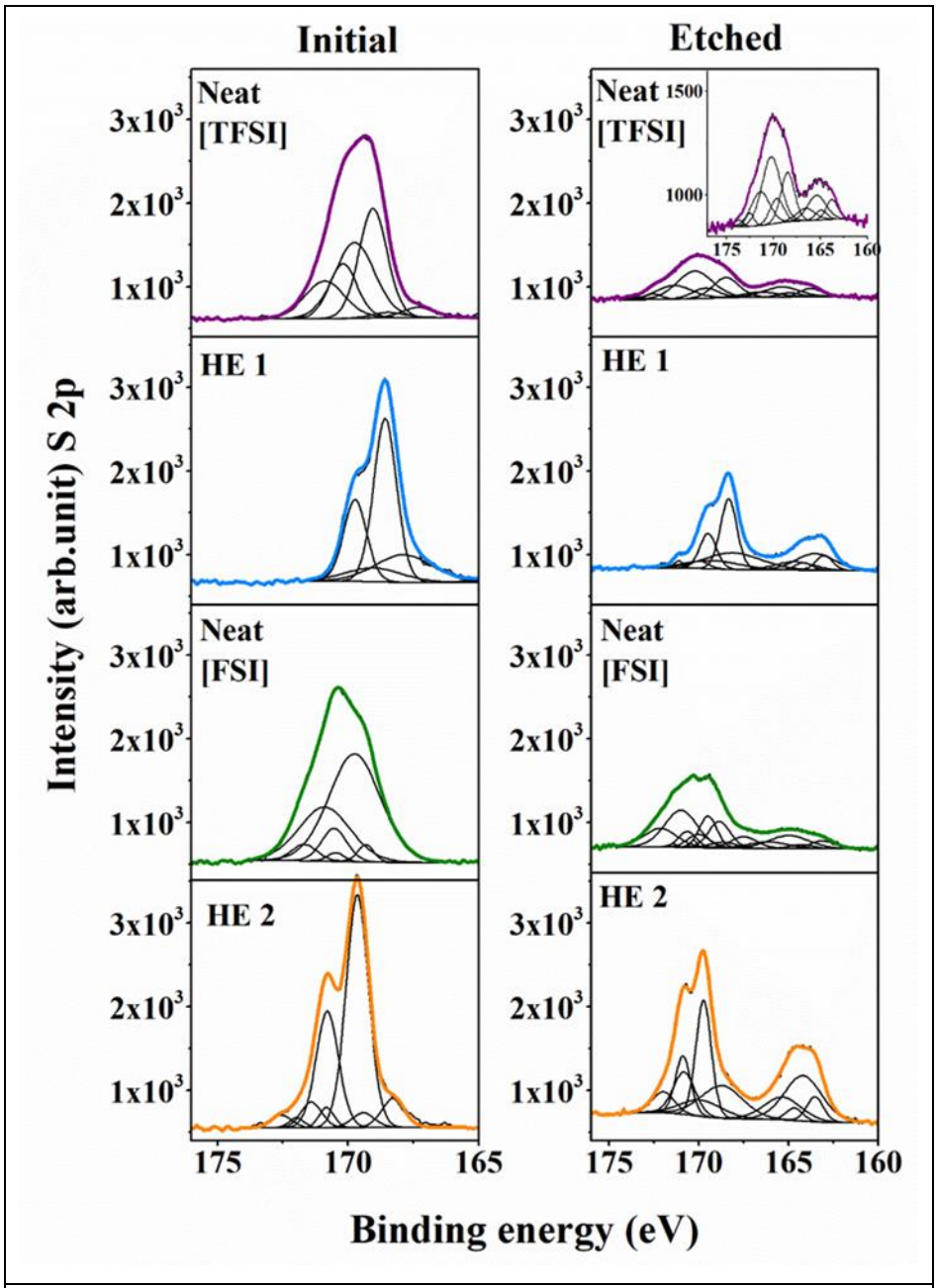

Figure 5.18 *S 2p High-resolution spectra for the Al surfaces treated in neat [C_3mpyr][TFSI], HE 1, neat [C_3mpyr][FSI], and HE 2 solutions before and after etching.*

By taking into account the F 1s spectra, peaks were identified for aluminum fluoride (AlF_3) at ca. 686.3 eV and $–SO_2F$ at ca. 688 eV for all samples. There was an increase in the quantity of AlF_3 in all samples except for the neat [FSI]-treated sample. The results suggest that a layer of AlF_3 is present close to the surface of the aluminum. Peaks that were associated with $–CF_3$, a "fingerprint" of the [TFSI] anion, were identified in the [TFSI]-treated samples at ca. 688.7-689 eV; similar amounts were detected in the neat [TFSI] treated sample before and after etching, whereas the amount of $-CF_3$ present in the hybrid HE 1-treated sample decreased drastically with etching.

There are significant differences between the samples: the surface films on the samples that were treated with neat ILs or HE 1 contained mainly $–SO_2F$ and AlF_3, after a small amount of etching. In contrast, a more steady variation in composition with etching was exhibited by the HE 2-treated sample, which suggests that the passive film formed on the surface may be thicker, or that significant amounts of other species may be present on the surface of the Al in this case.

The Al 2p high-resolution region spectra displayed peaks that corresponded to Al^0 at 71-72 eV, Al oxide at ca. 74.6 eV, aluminum oxide (Al_2O_3) on Al foil at ca. 75.6 eV, and AlF_3 at ca. 76.6 eV. The initial spectra of the surface of the Al indicated the presence of a considerable quantity of Al oxide that did not persist after etching and was present most likely as a contaminant from sample handling. A substantial amount of AlF_3 was indicated in the FSI-treated samples (neat [FSI] and HE 2), and the quantity of AlF_3 continued to increase with etching. Al^0 that was associated with the Al substrate was only detected in the surfaces that were treated in neat ILs, which suggests the formation of thinner films in the case of neat ILs; this observation is in agreement with the survey scan that was described previously and results that were obtained from other techniques. If the etching experiment is estimated to have removed 60 nm of material, then it may be concluded that the X-ray beam has not penetrated through the passivating film in the case of hybrid samples. After etching, a relatively complex mixture of aluminum species was identified in most samples, and the response to the fitting parameters was satisfying. Spin orbit splitting generates a doublet that corresponds to one Al 2p species; the doublet separation should be of 1.15 eV with a ratio of 2:1[52].

From the C 1s high-resolution region spectra, peaks that were associated with C-C/C-H at 284.8 eV, C-N at ca. 286.5 eV and carbonate (CO_3^{2-}) at ca. 290 eV were identified.

Peaks that were detected in the O 1s high-resolution region spectra were assigned to CO_3^{2-}, organic C-O or SO_2^- at ca. 531.5 eV, C=O at 533 eV. The C 1s and S 2p spectra indicate that SO_2 was predominately detected. The spectra show that the amount of CO_3^{2-} and SO_2^- decreased upon etching, except in the case of the neat [FSI]-treated sample.

Peaks that were present in the N 1s high-resolution region spectra were associated with N^+ at 402-403 eV and N^- at 399-400 eV. For the [FSI]-treated samples, the results were consistent with the removal of ionic liquid during the etching process. Small quantities of nitrides at ca. 398 eV were also identified on the etched surfaces.

The S 2p high-resolution spectra displayed peaks that corresponded to $-SO_2CF_3$ species for the [TFSI]-treated samples at ca. 169 eV and 170.2 eV (doublet). The $-SO_2F$ species for the [FSI]-treated samples at ca. 169.7 eV and 170.9 eV, oxidized sulfur species from 167.5 to 169.0 eV. This range of peaks were detected only in the etched samples and associated with the sulfide species ranging from 163 to 165 eV. The overall quantity of sulfur-based species remained the same before and after etching.

A clear difference is visible between the Al surfaces that were treated in the neat ILs and in the hybrid solutions. The results suggest that the film that was formed on the Al foil was thicker in the hybrid solutions, with a significant amount of reduced species associated with the IL anion. The film that was formed on the Al foil was composed of an outer layer of Al oxide. The etching process indicated that AlF_3 dominates the film further in. The cation structure does not seem to be affected by the treatment, according to the N 1s region spectra, and this is in agreement with FTIR analysis that was described previously.

5.3.3 Mechanism of Action of HE on Aluminum Surfaces

It has been reported in the literatures that the aluminum substrate dissolves as Al^{3+} ions when subjected to higher oxidation potentials[13]. The dissolved aluminum ions react with the electrolyte mixture to form aluminum salts, the nature of which depends on the salt and solvents in the electrolyte system. It has been shown previously that the $[FSI]^-$ anion is corrosive on the aluminum substrate upon anodic polarization (> 4.0 V vs. Li/Li+)[29]. It was also reported that the extent of corrosion was suppressed in LiTFSI electrolytes by the addition of $LiPF_6$ salt, which resulted in passivation of the Al substrate[14,55]. The layer that was formed on the Al substrate was found to be composed mainly of AlF_3, as a result of the chemical attack of $LiPF_6$ on the native oxide layer (Al_2O_3).

In this work, the electrochemical studies indicate the corrosion-inhibiting properties of the hybrid electrolytes in comparison to the conventional electrolyte. Poor passivating properties were exhibited in the aluminum substrate that was cycled by using the conventional (LP40) electrolyte. The anodized Al foil displayed signs of corrosion which was identified from the electrochemical tests (Tafel plots and CV) was in agreement with SEM images. In the case of the hybrid electrolytes, the flat CV profiles from the second cycle of CV measurements indicate the effectiveness of the passivation on surface. The pictorial representation of the mechanism of passive film formation in HE and neat ionic liquids are presented in Figure 5.19.

By correlating depth-profiling Al 2p XPS spectra of the aluminum samples with SEM images further clarifies the corrosion-inhibiting properties of the hybrid electrolytes. Al_2O_3 is the major Al species on the Al foil that was anodized in the neat ILs (without LP40).

In contrast, AlF_3 dominates Al_2O_3 when the Al foil is anodized in the hybrid electrolytes that contain LP40. It is believed that the composite passive film that is formed with the help of the ionic liquid and the PF_6 anion from the lithium salt in the electrolyte help in the formation of the passive film, which remains stable over the cycles (confirmed by CV and chronoamperometry measurements). In particular, the [TFSI]-based hybrid electrolyte (HE 1) allowed the formation of a film that was mainly composed of AlF_3. This suggests the formation of a passivating layer more resistant to electrochemical treatment. Significant amounts of the layer remained, as can be observed in the optical, microscopic and spectroscopic analyses, which indicates the involvement of the anions, most likely as precipitates of $Al(FSI)_3$ or $Al(TFSI)_3$.

EDXS analysis of SEM images and XPS results confirm a different coordination environment between [FSI] and [TFSI] anions and aluminum. More uniform coverage on the Al foil was observed in HE 1, whereas a larger amount of species with a relatively rough surface was observed in the [FSI]-based hybrid solution. The results support the reported literatures that state that the solubility of the Al-FSI species that are formed in this manner are much more pronounced in the [FSI]-based ionic liquids[56,57], as opposed to the insoluble Al-TFSI species in TFSI-based ionic liquid. A comparison of the [TFSI] and [FSI] hybrid electrolytes reveals that the nature of the anion had significant effects on the thickness of the passivating film and its composition.

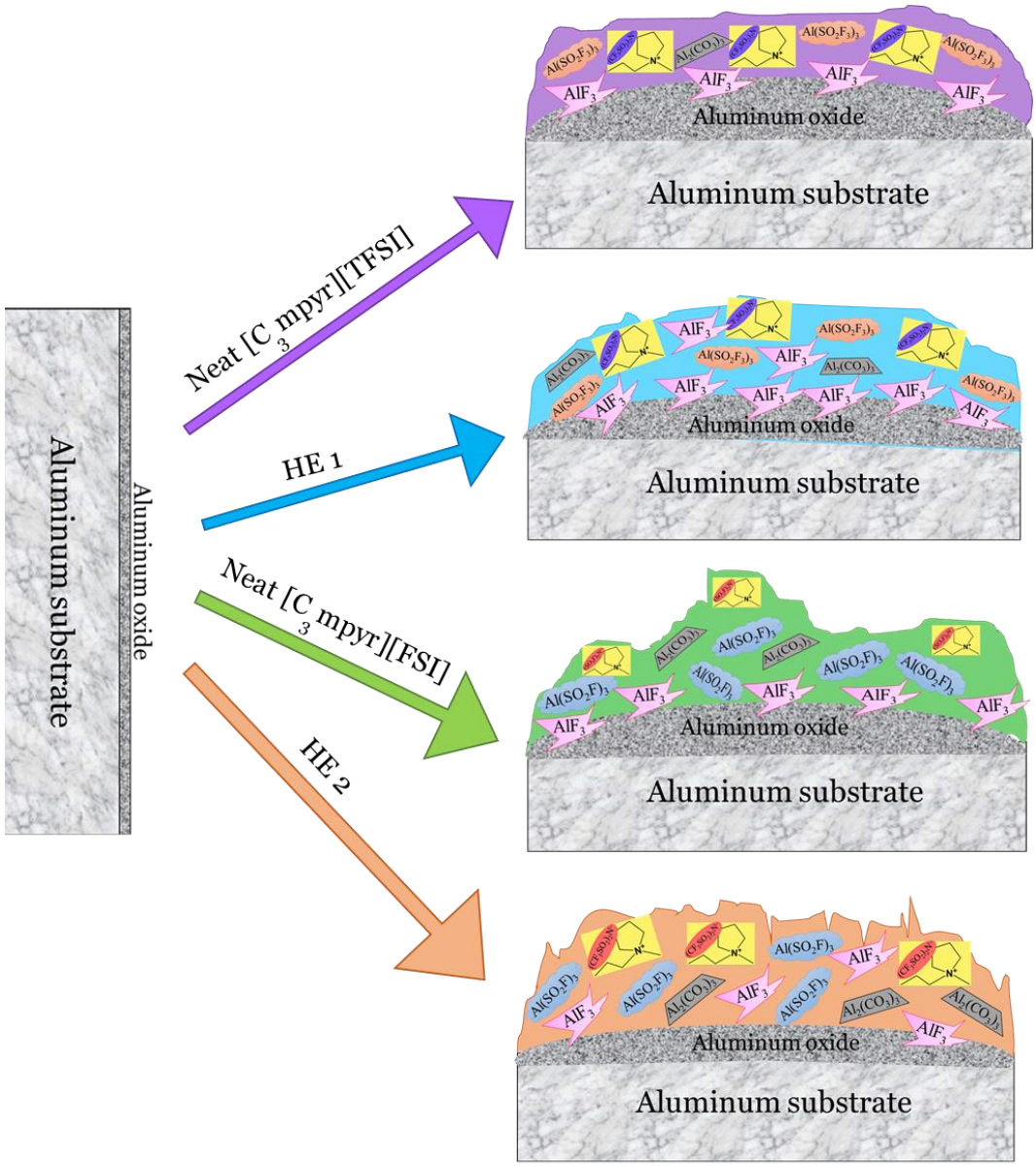

Figure 5.19 *Schematic representation of the moieties present in the passivation layer of aluminum current collector treated with different electrolytes. (The position or the number of moieties in the picture were chosen based on our interpretation of microscopic and spectroscopic analysis).*

Although TFSI-based lithium salts are known for their corrosive behavior on aluminium substrates [13,55,58], such behavior was not observed when [TFSI] anion was associated with the ionic liquid.[17,56,59] The present work also confirms the corrosion inhibition and better passivation of the TFSI-based hybrid electrolyte (HE 1) in comparison to the [FSI] ionic liquid-based hybrid electrolyte (HE 2) and the conventional electrolyte. It is reported that

the poor solubility of the passive film in the ionic liquid electrolytes helps to prevent the corrosion[56,59]. Nevertheless, the better corrosion properties of HE 1 may be due to the synergistic effect from the ionic liquid and the $LiPF_6$ salt present in the electrolyte. In other words, the insoluble Al-TFSI species that was formed from the ionic liquid and the AlF_3 that was formed from the $LiPF_6$ salt will form the principal inhibitors that would prevent the corrosion of aluminum substrate in HE 1. Thus, the addition of an [TFSI] ionic liquid to LP40 was found to have a significant positive impact on the protection of the aluminum surface from corrosion.

5.4 Concluding Remarks

This work has confirmed the significant corrosion inhibition properties of hybrid electrolytes-based on a pyrrolidinium ionic liquid and commercial liquid electrolyte for lithium batteries. The hybrid electrolyte-based on the bis(trifluoromethanesulfonyl)imide $[TFSI]^-$ anion performs better than both the neat $[TFSI]^-$ ionic liquid electrolyte and bis(fluorosulfonyl)imide $[FSI]^-$ hybrid electrolyte in contact with aluminum at high anodic potentials (4.7 V *vs.* Li/Li^+). The neat $[FSI]^-$ ionic liquid electrolyte and organic carbonate electrolyte (conventional electrolyte) did not exhibit appreciable passivating performance at such high anodic potential.

The observations that improved passivating properties were more evident with the presence of $[TFSI]^-$ anion in the hybrid electrolyte and that this correlated with an excess of AlF_3 and anionic moieties, strongly suggests that the speciation of the ionic liquid anion is critical to the anodic stability and high efficiency of aluminum corrosion inhibition. Further work is required to investigate the influence of the chemistry of both the ionic liquid and organic solvent on speciation in a lithium cell configuration and to correlate it with inhibitor performance. This could lead to improved combinations to yield even better passivating properties of these hybrid electrolytes.

5.5 References

(1) Zhang, Z.; Zhang, S. S. Challenges of Key Materials for Rechargeable Batteries. In *Rechargeable Batteries*; Zhang, Z.; Zhang, S. S., Eds.; Springer, Cham, 2015; pp. 1–24.

(2) Huggins, R. A. *Advanced Batteries Materials Science Aspects*; Springer, 2009.

(3) Whitehead, A. H.; Schreiber, M. Current Collectors for Positive Electrodes of Lithium-Based Batteries. *J. Electrochem. Soc.* **2005**, *152*, A2105-A2113.

(4) Braithwaite, J. W.; Gonzales, A.; Nagasubramanian, G.; Lucero, S. J.; Peebles, D. E.; Ohlhausen, J. A.; Cieslak, W. R. Corrosion of Lithium-Ion Battery Current Collectors. *J. Electrochem. Soc.* **1999**, *146*, 448–456.

(5) Evarts, E. C. Lithium Batteries: To the Limits of Lithium. *Nature* **2015**, *526*, S93–S95.

(6) Etacheri, V.; Marom, R.; Elazari, R.; Salitra, G.; Aurbach, D. Challenges in the Development of Advanced Li-Ion Batteries: A Review. *Energy Environ. Sci.* **2011**, *4*, 3243–3262.

(7) Yuge, R.; Tamura, N.; Kuroshima, S.; Maeda, K.; Narita, K.; Tabuchi, M.; Doumae, K.; Shibuya, H.; Heishi, M.; Toyokawa, T.; et al. High Energy Density Lithium Ion Batteries with Iron- and Nickel-Substituted Lithium-Rich Layered Oxide Cathode. *J. Electrochem. Soc.* **2016**, *163*, A1881–A1885.

(8) Choi, J. W.; Aurbach, D. Promise and Reality of Post-Lithium-Ion Batteries with High Energy Densities. *Nat. Rev. Mater.* **2016**, *1*, 16013.

(9) Li, F.; Gong, Y.; Jia, G.; Wang, Q.; Peng, Z. A Novel Dual-Salts of LiTFSI and LiODFB in $LiFePO_4$ -Based Batteries for Suppressing Aluminum Corrosion and Improving Cycling Stability. *J. Power Sources* **2015**, *295*, 47–54.

(10) Hyams, T. C.; Go, J.; Devine, T. M. Corrosion of Aluminum Current Collectors in High-Power Lithium-Ion Batteries for Use in Hybrid Electric Vehicles. *J. Electrochem. Soc.* **2007**, *154*, C390.

(11) Zhang, X.; Winget, B.; Doeff, M.; Evans, J. W.; Devine, T. M. Corrosion of Aluminum Current Collectors in Lithium-Ion Batteries with Electrolytes Containing $LiPF_6$. *J. Electrochem. Soc.* **2005**, *152*, B448–B454.

(12) Kramer, E.; Schedlbauer, T.; Hoffmann, B.; Terborg, L.; Nowak, S.; Gores, H. J.; Passerini, S.; Winter, M. Mechanism of Anodic Dissolution of the Aluminum Current Collector in 1 M LiTFSI EC:DEC 3:7 in Rechargeable Lithium Batteries. *J. Electrochem. Soc.* **2012**, *160*, A356–A360.

(13) Xu, K. Nonaqueous Liquid Electrolytes for Lithium-Based Rechargeable Batteries. *Chem. Rev.* **2004**, *104*, 4303–4418.

(14) Morita, M.; Shibata, T.; Yoshimoto, N.; Ishikawa, M. Anodic Behavior of Aluminum in Organic Solutions with Different Electrolytic Salts for Lithium Ion Batteries. *Electrochim. Acta* **2002**, *47*, 2787–2793.

(15) Evans, T.; Olson, J.; Bhat, V.; Lee, S. H. Effect of Organic Solvent Addition to PYR13FSI + LiFSI Electrolytes on Aluminum Oxidation and Rate Performance of $Li(Ni_{1/3}Mn_{1/3}Co_{1/3})O_2$ Cathodes. *J. Power Sources* **2014**, *265*, 132–139.

(16) Kramer, E.; Passerini, S.; Winter, M. Dependency of Aluminum Collector Corrosion in Lithium Ion Batteries on the Electrolyte Solvent. *ECS Electrochem. Lett.* **2012**, *1*, C9–C11.

(17) Moosbauer, D.; Zugmann, S.; Amereller, M.; Gores, H. J. Effect of Ionic Liquids as Additives on Lithium Electrolytes: Conductivity, Electrochemical Stability, and Aluminum Corrosion. *J. Chem. Eng. Data* **2010**, *55*, 1794–1798.

(18) Xu, K. Electrolytes and Interphases in Li-Ion Batteries and Beyond. *Chem. Rev.* **2014**, *114*, 11503–11618.

(19) Kühnel, R.-S.; Lübke, M.; Winter, M.; Passerini, S.; Balducci, A. Suppression of Aluminum Current Collector Corrosion in Ionic Liquid Containing Electrolytes. *J. Power Sources* **2012**, *214*, 178–184.

(20) Theivaprakasam, S.; MacFarlane, D. R.; Mitra, S. Electrochemical Studies of N-Methyl N-Propyl Pyrrolidinium Bis(trifluoromethanesulfonyl) Imide Ionic Liquid Mixtures with Conventional Electrolytes in $LiFePO_4$/Li Cells. *Electrochim. Acta* **2015**, *180*, 737–745.

(21) Chen, R.; Chen, Y.; Zhu, L.; Zhu, Q.; Wu, F.; Li, L. A Facile Approach of Adopting DMS into LiODFB/PYR_{14}TFSI Electrolyte for Lithium-Ion Batteries. *J. Mater. Chem. A* **2015**.

(22) Peng, C.; Yang, L.; Wang, B.; Zhang, Z.; Li, N. Electrochemical Behavior of Aluminum Foil in 1-Alkyl-3-Methylimidazolium Tetrafluoroborate Ionic Liquids Electrolytes. *Chinese Sci. Bull.* **2006**, *51*, 2824–2830.

(23) Huang, P.; Somers, A.; Howlett, P. C.; Forsyth, M. Film Formation in Trihexyl (Tetradecyl) Phosphonium Diphenylphosphate ([P 6, 6, 6, 14][dpp]) Ionic Liquid on AA5083 Aluminium Alloy. *Surf. Coatings Technol.* **2016**, *303*, 385–395.

(24) Chong, A. L.; Mardel, J. I.; MacFarlane, D. R.; Forsyth, M.; Somers, A. E. Synergistic Corrosion Inhibition of Mild Steel in Aqueous Chloride Solutions by an Imidazolinium Carboxylate Salt. *ACS Sustain. Chem. Eng.* **2016**, *4*, 1746–1755.

(25) Somers, A. E.; Chong, A. L.; MacFarlane, D. R.; Forsyth, M. Imidazolinium Inhibitor for Mild Steel in Aggressive Conditions. In *C&P2015: Corrosion and Prevention 2015*; The Australasian Corrosion Association, 2015; pp. 1–8.

(26) Latham, J.-A.; Howlett, P. C.; MacFarlane, D. R.; Somers, A.; Forsyth, M. Anodising AZ31 in a Phosphonium Ionic Liquid: Corrosion Protection through Composite Film Deposition. *J. Electrochem. Soc.* **2012**, *159*, C539–C545.

(27) Cha, E.-H.; Mun, J.-Y.; Cho, E.-R.; Yim, T.-E.; Kim, Y.-G.; Oh, S.-M.; Lim, S.-A.; Lim, J.-W. The Corrosion Study of Al Current Collector in Phosphonium Ionic Liquid as Solvent for Lithium Ion Battery. *J. Korean Electrochem. Soc.* **2011**, *14*, 152–156.

(28) Allen, J. L.; McOwen, D. W.; Delp, S. A.; Fox, E. T.; Dickmann, J. S.; Han, S. D.; Zhou, Z. Bin; Jow, T. R.; Henderson, W. A. N-Alkyl-N-Methylpyrrolidinium Difluoro(oxalato)borate Ionic Liquids: Physical/electrochemical Properties and Al Corrosion. *J. Power Sources* **2013**, *237*, 104–111.

(29) Cho, E.; Mun, J.; Chae, O. B.; Kwon, O. M.; Kim, H.-T.; Ryu, J. H.; Kim, Y. G.; Oh, S. M. Corrosion/passivation of Aluminum Current Collector in Bis(fluorosulfonyl)imide-Based Ionic Liquid for Lithium-Ion Batteries. *Electrochem. commun.* **2012**, *22*, 1–3.

(30) Yang, B.; Li, C.; Zhou, J.; Liu, J.; Zhang, Q. Pyrrolidinium-Based Ionic Liquid Electrolyte with Organic Additive and LiTFSI for High-Safety Lithium-Ion Batteries. *Electrochim. Acta* **2014**, *148*, 39–45.

(31) Liu, C.; Ma, X.; Xu, F.; Zheng, L.; Zhang, H.; Feng, W.; Huang, X.; Armand, M.; Nie, J.; Chen, H.; et al. Ionic Liquid Electrolyte of Lithium bis(fluorosulfonyl)imide /N-Methyl-N-Propylpiperidinium Bis(fluorosulfonyl)imide for Li/natural Graphite

Cells: Effect of Concentration of Lithium Salt on the Physicochemical and Electrochemical Properties. *Electrochim. Acta* **2014**, *149*, 370–385.

(32) Navarra, M. A. Ionic Liquids as Safe Electrolyte Components for Li-Metal and Li-Ion Batteries. *MRS Bull.* **2013**, *38*, 548–553.

(33) Li, H.; Pang, J.; Yin, Y.; Zhuang, W.; Wang, H.; Zhai, C.; Lu, S. Application of a Nonflammable Electrolyte Containing Pp13TFSI Ionic Liquid for Lithium-Ion Batteries Using the High Capacity Cathode Material $Li[Li_{0.2}Mn_{0.54}Ni_{0.13}Co_{0.13}]O_2$. *RSC Adv.* **2013**, *3*, 13907–13914.

(34) Guerfi, A.; Dontigny, M.; Charest, P.; Petitclerc, M.; Lagacé, M.; Vijh, A.; Zaghib, K. Improved Electrolytes for Li-Ion Batteries: Mixtures of Ionic Liquid and Organic Electrolyte with Enhanced Safety and Electrochemical Performance. *J. Power Sources* **2010**, *195*, 845–852.

(35) Choi, J. A.; Shim, E. G.; Scrosati, B.; Kim, D. W. Mixed Electrolytes of Organic Solvents and Ionic Liquid for Rechargeable Lithium-Ion Batteries. *Bull. Korean Chem. Soc.* **2010**, *31*, 3190–3194.

(36) Matsuda, Y.; Fukushima, T.; Hashimoto, H.; Arakawa, R. Solvation of Lithium Ions in Mixed Organic Electrolyte Solutions by Electrospray Ionization Mass Spectroscopy. *J. Electrochem. Soc.* **2002**, *149*, A1045–A1048.

(37) Kühnel, R.-S.; Böckenfeld, N.; Passerini, S.; Winter, M.; Balducci, A. Mixtures of Ionic Liquid and Organic Carbonate as Electrolyte with Improved Safety and Performance for Rechargeable Lithium Batteries. *Electrochim. Acta* **2011**, *56*, 4092–4099.

(38) Theivaprakasam, S.; Wu, J.; Pramudita, J. C.; Sharma, N.; Macfarlane, D. R.; Mitra, S. Understanding the Behavior of $LiCoO_2$ Cathodes at Extended Potentials in Ionic Liquid - Alkyl Carbonate Hybrid Electrolytes. *J. Phys. Chem. C* **2017**, *121*, 15630-15638.

(39) Yoon, H.; Howlett, P. C.; Best, A. S.; Forsyth, M.; MacFarlane, D. R. Fast Charge/discharge of Li Metal Batteries Using an Ionic Liquid Electrolyte. *J. Electrochem. Soc.* **2013**, *160*, A1629--A1637.

(40) Zhou, Q.; Henderson, W. A.; Appetecchi, G. B.; Montanino, M.; Passerini, S.

Physical and Electrochemical Properties of *N* -Alkyl- *N* -Methylpyrrolidinium Bis(fluorosulfonyl)imide Ionic Liquids: $PY_{13}FSI$ and $PY_{14}FSI$. *J. Phys. Chem. B* **2008**, *112*, 13577–13580.

(41) Li, L.; Zhou, S.; Han, H.; Li, H.; Nie, J.; Armand, M.; Zhou, Z.; Huang, X. Transport and Electrochemical Properties and Spectral Features of Non-Aqueous Electrolytes Containing LiFSI in Linear Carbonate Solvents. *J. Electrochem. Soc.* **2011**, *158*, A74-A82.

(42) Howlett, P. C.; Brack, N.; Hollenkamp, A. F.; Forsyth, M.; MacFarlane, D. R. Characterization of the Lithium Surface in N-Methyl-N-Alkylpyrrolidinium Bis (Trifluoromethanesulfonyl) Amide Room-Temperature Ionic Liquid Electrolytes. *J. Electrochem. Soc.* **2006**, *153*, A595--A606.

(43) Bednarska-Bolek, B.; Jakubas, R.; Bator, G.; Baran, J. Vibrational Study of the Structural Phase Transition in Bis(pyrrolidinium)-Chloride-hexachloroantimonate(V) by Infrared Spectroscopy. *J. Mol. Struct.* **2002**, *614*, 151–157.

(44) Yoon, H.; Best, A. S.; Forsyth, M.; MacFarlane, D. R.; Howlett, P. C. Physical Properties of High Li-Ion Content N-Propyl-N-Methylpyrrolidinium Bis(fluorosulfonyl)imide Based Ionic Liquid Electrolytes. *Phys. Chem. Chem. Phys.* **2015**, *17*, 4656–4663.

(45) Rey, I.; Lassègues, J. C.; Grondin, J.; Servant, L. Infrared and Raman Study of the PEO-LiTFSI Polymer Electrolyte. *Electrochim. Acta* **1998**, *43*, 1505–1510.

(46) Colthup, N. B.; Dalyse, H. L.; Wiberley, S. E. *Introduction to Infrared and Raman Spectroscopy*; Colthup, N. B.; Dalyse, H. L.; Wiberley, S. E., Eds.; Third Edit.; Academic Press: San Diego, 1990.

(47) Nyquist, C. L. P. R. A.; Leugers, M. A. *Handbook of Infrared and Raman Spectra of Inorganic Compounds and Organic Salts*; Academic Press, 1997.

(48) Nyquist, R. A.; Potts, W. J. Infrared Absorptions Characteristic of Organic Carbonate Derivatives and Related Compounds. *Spectrochim. Acta* **1961**, *17*, 679–697.

(49) Adebahr, J.; Johansson, P.; Jacobsson, P.; MacFarlane, D. R.; Forsyth, M. Ab Initio

Calculations, Raman and NMR Investigation of the Plastic Crystal Di-Methyl Pyrrolidinium Iodide. *Electrochim. Acta* **2003**, *48*, 2283–2289.

(50) Forsyth, M.; Neil, W. C.; Howlett, P. C.; Macfarlane, D. R.; Hinton, B. R. W.; Rocher, N.; Kemp, T. F.; Smith, M. E. New Insights into the Fundamental Chemical Nature of Ionic Liquid Film Formation on Magnesium Alloy Surfaces. *ACS Appl. Mater. Interfaces* **2009**, *1*, 1045–1052.

(51) Wagner, C. D.; Muilenberg, G. E. *Handbook of X-Ray Photoelectron Spectroscopy: A Reference Book of Standard Data for Use in X-Ray Photoelectron Spectroscopy*; Physical Electronics Division, Perkin-Elmer Corp., 1979.

(52) Crist, B. A Review of XPS Data-Banks. *XPS Int.* **2007**, *1*, 1–52.

(53) Minami, I. Ionic Liquids in Tribology. *Molecules* **2009**, *14*, 2286–2305.

(54) Marcus, P.; Hinnen, C.; Imbert, D.; Siffre, J. M. An In Situ XPS Study of the Formation of Aluminium-Polymer Interfaces. *Surf. Interface Anal.* **1992**, *19*, 127–132.

(55) Krause, L. J.; Lamanna, W.; Summerfield, J.; Engle, M.; Korba, G.; Loch, R.; Atanasoski, R. Corrosion of Aluminum at High Voltages in Non-Aqueous Electrolytes Containing Perfluoroalkylsulfonyl Imides; New Lithium Salts for Lithium-Ion Cells. *J. Power Sources* **1997**, *68*, 320–325.

(56) Kühnel, R.-S.; Balducci, A. Comparison of the Anodic Behavior of Aluminum Current Collectors in Imide-Based Ionic Liquids and Consequences on the Stability of High Voltage Supercapacitors. *J. Power Sources* **2014**, *249*, 163–171.

(57) Mcowen, D. W.; Seo, D. M.; Borodin, O.; Vatamanu, J.; Boyle, P. D.; Henderson, W. A. Concentrated Electrolytes: Decrypting Electrolyte Properties and Reassessing Al Corrosion Mechanisms. *Energy Environ. Sci.* **2014**, *7*, 416–426.

(58) Yang, H.; Kwon, K.; Devine, T. M.; Evans, J. W. Aluminum Corrosion in Lithium Batteries An Investigation Using the Electrochemical Quartz Crystal Microbalance Aluminum Corrosion in Lithium Batteries. *J. Electrochem. Soc.* **2000**, *147*, 4399–4407.

(59) Kühnel, R.-S.; Reiter, J.; Jeong, S.; Passerini, S.; Balducci, A. Anodic Stability of

Aluminum Current Collectors in an Ionic Liquid Based on the (Fluorosulfonyl)(trifluoromethanesulfonyl)imide Anion and Its Implication on High Voltage Supercapacitors. *Electrochem. commun.* **2014**, *38*, 117–119.

Chapter 6

Inferences and Scope for Future Research

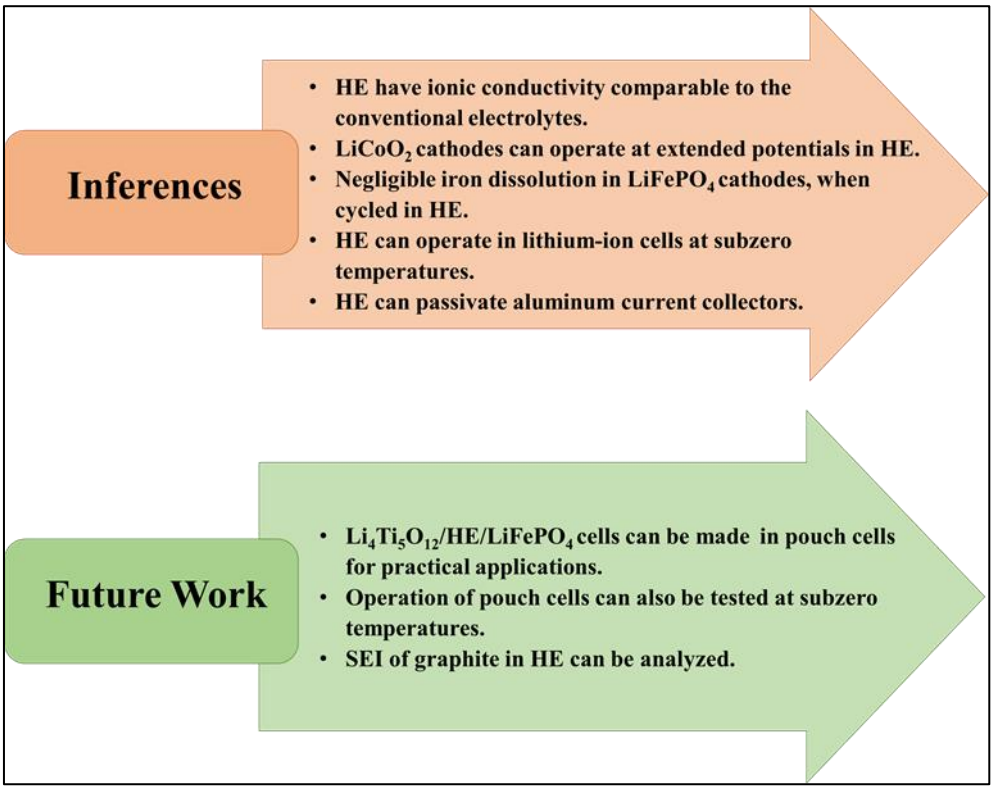

6.1 Introduction

The present chapter provides a brief outline of the significant contributions, and inferences from the works that were carried out as a part of this thesis. In addition, the scope for future work is also discussed in this chapter.

6.2 Inferences

The concept of a Hybrid Electrolyte (HE), which involves the addition of ionic liquids to the conventional electrolytes was studied in this work for the lithium/lithium-ion battery applications. An optimized proportion of 40 percent of ionic liquid was added to the conventional electrolyte mixture as described in the literature. The entire thesis was focused on the ionic liquid N-methyl-N-propyl pyrrolidinium bis (trifluoro methane sulfonyl) imide . However, in Chapter 5, additional insights to the effect of anion in the passivation of aluminum current collector was studied by comparing the present system with the ionic liquid, N-Methyl-N-propylpyrrolidinium bis(fluorosulfonyl)imide.

The idea behind HE was to attain the beneficial properties from both the ionic liquids and the conventional battery electrolytes. A pictorial representation of the inferences made out of this work is represented in Figure 6.1. The initial studies in this work were focused on understanding the physicochemical effects of ionic liquid addition in the HE. It was observed that the addition of 40 percent of ionic liquid in the system will not contribute to a significant increase in the density and viscosity of the electrolyte. Further, the room temperature ionic conductivity in HE was comparable to the conventional battery electrolytes, irrespective of the ionic liquid involved. The most interesting aspect was that the operating temperature of the batteries was extended by the addition to subzero temperatures. As reported in this work, HE can be used to operate lithium-ion batteries (LiBs) at –30 °C. Furthermore, as explained in Chapter 2, the presence of ionic liquid helps to reduce the evaporation losses in HE during operating above room temperature.

The Solid Electrolyte Interface (SEI) is considered as a significant phenomenon in the performance of LiBs. The decomposition of the electrolyte on the anode surface results in the formation of an anode SEI. As a result, the electrolyte constituents and their lithium solvation play an important role in the SEI formation. In this context, efforts were taken to study the lithium solvation in HE experimentaslly. From the spectroscopic studies, it can

be seen that the lithium solvation in HE resembles the conventional electrolytes in such a way that the lithium solvation is not hindered by the ions from the ionic liquid in the electrolyte. The presence of 60 percent of organic solvents in the conventional electrolytes helps the preferential solvation of lithium ion by ethylene carbonate. Further, the electrolyte was tested for its compatibility with the lithium interface in lithium symmetric cells. It was apparent from the overpotential measurements that the interfacial resistance of anything was a little lower while using HE.

The next stage of analysis was about understanding the performance of HE with the commercial cathodes to establish their application in the LiBs. The initial studies on Li/HE/$LiCoO_2$ cells operating in the standard potential window provided comparable performance to the conventional electrolytes. It is believed that the ionic liquid addition may contribute positively to the (otherwise poor) thermal and oxidative stability of $LiCoO_2$ cathodes. As a result, the $LiCoO_2$ cathodes were able to be operated to an extended potential cutoff of 4.4 V vs. Li/Li^+ to extract more lithium ions from the system. It is commonly reported in the literature that structural distortions reduces the cycle life of $LiCoO_2$ cathodes operating at extended potentials. On the contrary, it was inferred from this work that the surface film formed in the HE, prevents the structural instability until 4.7 V vs. Li/Li^+ as shown by the in situ synchrotron studies. Thus, the safe application of $LiCoO_2$ cathodes in the extended potential window was demonstrated in this work.

Presently, the application of LiBs in electric vehicles is one of the most researched areas. The most commonly preferred safe electrodes for LiBs in electric vehicles are the $LiFePO_4$ cathodes and $Li_4Ti_5O_{12}$ anodes. It is believed that the safety of LiBs is assured by the safety of its electrodes and electrolytes. As a result, the current study is focused on the $Li_4Ti_5O_{12}$/HE/ $LiFePO_4$ system to ensure safety of the operating devices.

Initially, $LiFePO_4$ cathodes in the Li/He/$LiFePO_4$ cell configuration demonstrated better performance and cyclic retention. The most common problem associated with the transition metal cathodes was the dissolution of transition metal ions into the electrolyte solution, which further influence the battery cycle life. Nevertheless, it was inferred from this work, that the iron dissolution in the $LiFePO_4$ cathodes was negligible when cycled in HE whereas it is common in conventional electrolytes with increasing cycle numbers. Further, the $LiFePO_4$ cathodes were studied with $Li_4Ti_5O_{12}$ anodes to test HE in lithium ion cells. The cells demonstrated better performance over 200 cycles at C/5 rate.

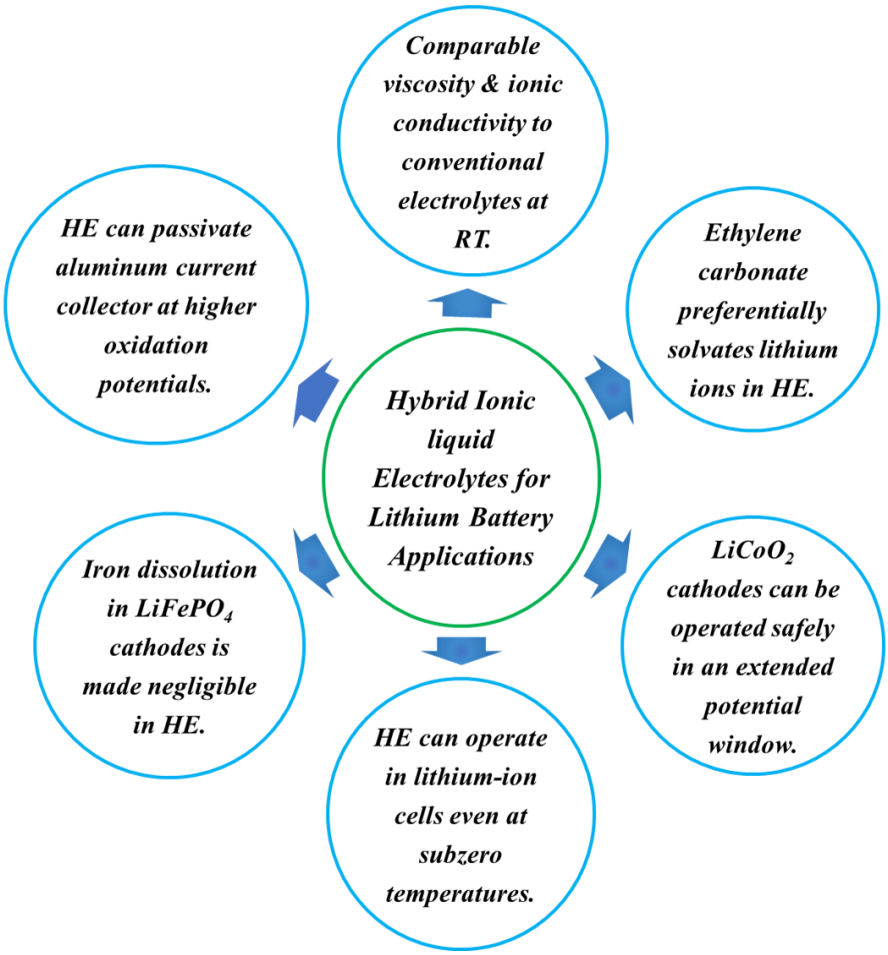

Figure 6.1 *Schematic representation of the findings of the current work.*

The most remarkable application of this work is a special HE formulation (HE*) for subzero LiB applications. Initially, the electrolyte was characterized to ascertain suitability for LiB applications. It was observed that the addition of ionic liquids prevents the freezing of electrolyte solvent components at subzero temperatures. Further, the electrolyte was tested in $Li_4Ti_5O_{12}$/HE/$LiFePO_4$ cells for 40 cycles at –30 °C. It was observed that 50 percent of the room temperature capacity was retained at –30 °C and 80 percent was retained when cycled at –20 °C. Electrochemical Impedance Spectroscopy (EIS) studies carried out before and after 40 cycles at –30 °C show that the interfacial resistance after 40 cycles was similar to that obtained before charging. Thus, the better cyclic stability at subzero temperatures may be attributed to the stable interfacial resistance in HE* electrolyte. In addition, the effect of charging time on lithium storage shows that half of the capacity obtained from ten hours of charging at –30 °C is retained when the charging

time was reduced to 2.5 h. Thus, HE* can be considered as the potential electrolyte for wide temperature range of operations, though rate performance is limited at low temperatures.

The electrolyte should also be compatible with the current collector at high oxidation potentials. In this work, efforts were taken to understand the passivation behavior of aluminum current collectors in HE in comparison to the conventional electrolyte and neat ionic liquids. It was observed that HE could passivate the aluminum surface with the help of the IL anion. The morphology and roughness of the passivation layer were also investigated in this work. It was observed that the passivation layer formed was a composite film made up of aluminum fluoride and aluminum carbonates along with Al salts of the ionic liquid anion, which appear to form a film capable of passivating the substrate at higher oxidation potentials.

Thus, the fundamental understanding on the application of HE for lithium as well as lithium-ion batteries was developed in this work contributing towards safe and high performance batteries.

6.3 Scope for Future Research

Future research directions could involve the further engineering and optimization of $Li_4Ti_5O_{12}$/HE/$LiFePO_4$ configuration in pouch cells for practical applications. Further, the pouch cells can also be tested using HE* at subzero temperatures.

The electrochemistry and SEI of graphite electrodes has a direct dependence on the electrolyte under study. Hence, the nature of the SEI on graphite electrodes should be studied using HE. Once an understanding is developed in this aspect, lithium-ion cells employing graphite anodes, high potential cathodes and HE can be used to fabricate high energy density safe batteries.

Further, the most important aspect of HE is their safety in comparison to the conventional electrolytes. Hence, it will be interesting to perform the safety tests in abusive conditions for lithium-ion cells using HE to assess their safety at various temperatures and operating conditions.

In future, it is expected that the HE could play a potential role in the safety of lithium-ion batteries for electric vehicle applications.

Research Outcomes

International Peer-Reviewed Journals

(1) Theivaprakasam, S.; Girard, G.; Howlett, P.; Forsyth, M.; Mitra, S.; MacFarlane, D. Passivation Behaviour of Aluminium Current Collector in Ionic Liquid Alkyl Carbonate (Hybrid) Electrolytes. npj Mater. Degrad. 2018, 2, 13.

(2) Theivaprakasam, S.; Wu, J.; Pramudita, J. C.; Sharma, N.; MacFarlane, D. R.; Mitra, S. Understanding the Behavior of $LiCoO_2$ Cathodes at Extended Potentials in Ionic Liquid-Alkyl Carbonate Hybrid Electrolytes. J. Phys. Chem. C 2017, 121.

(3) Theivaprakasam, S.; MacFarlane, D. R.; Mitra, S. Electrochemical Studies of N-Methyl N-Propyl Pyrrolidinium Bis(trifluoromethanesulfonyl) Imide Ionic Liquid Mixtures with Conventional Electrolytes in $LiFePO_4$/Li Cells. Electrochim. Acta 2015, 180, 737–745.

Patent

(1) Theivaprakasam, S.; Mitra, S.; MacFarlane, D. R. Electrolytes For Lithium Ion Batteries. 201721017681, 2017.

Conference Presentations

(1) Theivaprakasam, S.; Mitra, S.; MacFarlane, D. R., Hybrid ionic liquid electrolytes for safer room temperature lithium batteries, 12th Indian Society of Electroanalytical Chemistry discussion meeting, Mumbai, 7-8 December 2016, ***(Oral presentation)***.

(2) Theivaprakasam, S.; MacFarlane, D. R.; Mitra, S. Ionic Liquid - Alkyl Carbonate hybrid electrolytes: Understanding their interfacial electrochemistry in lithium batteries, International Meeting on Lithium Batteries (IMLB 2016), Jun 19-23, Chicago, ***(Poster presentation)***.

(3) Theivaprakasam, S.; MacFarlane, D. R.; Mitra, S. Ionic liquids as electrolytes for lithium batteries, The 7th Australian Symposium on Ionic Liquids, Newcastle, Australia,23-26 May 2016, ***(Oral presentation)***.

(4) Theivaprakasam, S.; Howlett P. C.; Forsyth M.; MacFarlane, D. R.; Mitra, S. Alkyl carbonate-ionic liquid mixture electrolytes for lithium batteries, 11th Annual International Electromaterials Science Symposium, Deakin University, Melbourne, Australia,10 – 12 February 2016, ***(Poster presentation)***.

Manuscript to be Submitted

(1) Theivaprakasam, S.; Mitra, S.; MacFarlane, D. R., Solution structure and physicochemical properties of ionic liquid-alkyl carbonate (hybrid) electrolytes for lithium batteries, *Manuscript*.

Acknowledgements

Firstly, I would like to thank the Almighty for giving me the opportunity, especially to work on the topic which was always my field of interest. I also thank him for the perseverance, knowledge and strength bestowed on me to carry out this work.

I had the wonderful opportunity to work with two supervisors Prof. Douglas MacFarlane and Prof. Sagar Mitra. I am very thankful to them for the faith they had in me and the space they had given me to learn each and every aspect of this project.

It was a wonderful one year time I had spent with Prof. Douglas MacFarlane in Monash University. I should say the interactions I had during the one year stay at Monash University had really shaped me and motivated me to carry out this work better. He is a great source of my inspiration and had taught me the ways to approach and deal with research problems.

I would also extend my deepest gratitude to my other supervisor, Prof. Sagar Mitra for his constant support and encouragement to carry out this work. I feel extremely grateful for the freedom he had given to me to carry out this project. It was always an answer of 'Yes' from him whenever I asked for permissions to avail various experimental facilities outside IITB to solve my research problems. Such encouragements exposed me to various techniques during this research journey.

It was a splendid opportunity to work in Deakin University under Prof. Maria Forsyth and A/Prof. Patrick Howlett during my stay in Australia. I specially thank them for giving full access and freedom to work in the Deakin IFM labs. I am highly grateful for the extremely helpful suggestions and guidance from A/Prof. Patrick Howlett to initiate the aluminum corrosion experiments.

I would also like to acknowledge the industrial sponsor of this project, Reliance Industries and the constant support from the industrial mentors Dr. Parasuveera Uppara and Dr. Pavan Kumar. I am also grateful to the funding of NCPRE and SAIF-IITB for various analytical facilities. The funding strength from all these agencies played a crucial role in the execution of this project.

I thank my research progress committee members Dr. Xinyi Zhang and Dr. Venkatasaila -nathan Ramadesigan for their constructive comments at various stages of this work. I really appreciate the time they had devoted to analyze my research progress every year through the annual progress seminar.

Im very much grateful to Prof. Murali Sastry, the CEO of IITB Monash research academy for his constant support and encouragement to carry out this work. I would also like to thank Dr. Kyatanahalli Nagabhushana, the COO of the Academy for his great help to patent a part of this work. I am also thankful to each staff in the Academy for their friendly and amazing support in easing the official formalities. I extend my special thanks to the Academy for providing me an office space in the Academy building, which created an excellent atmosphere for writing my thesis. I can never think of any better environment for writing.

It is also time to thank Dr. Neeraj Sharma, James Christian Pramudita, and Jimmy Wu for their help and contribution in the synchrotron measurements. Special thanks to Dr. Neeraj Sharma for his support and patience to teach me the interpretations of synchrotron data.

I owe a big thanks to Dr. Gaetan Girard for his great contribution to the aluminum passivation studies. Gaetan, your help had really marked a significant part in this thesis.

It is about not only the research but also the comfort zone, which helps to work better and ease to solve problems in the labs. I am extremely thankful to my lab mates in Monash Dr. Mega Kar, Dr. Alison Chong, Diogo Cabral, Zheng Ma, Dr. Fengling Zhou and Dr. Tiago Correia Mendes for creating such platform. My special thanks to Dr. Vijayaraghavan Ranganathan, Dr. Gary Annat, and Dr. Peter Newman for their great assistance and huge support during my stay at Monash.

It is always the initial basement, which matters a lot. I am very thankful to my seniors at IITB Dr. Alok Mani Tripathi, Dr. Uttam Kumar Sen, Dr. Sudeep Sarkar, Mr. Apoorv Shaligram and Dr. Pavan Kumar Veluri for their great patience in answering and helping with all my questions during the initial days of my Ph.D. It was not only those days, even now,I am fortunate to get their assistance with the research questions anytime in a day.

I am also thankful to Dr. Matthias Hilder, Dr. Rob Kerr, Dr. RuhamaYunis, Dr. Xiaoen Wang, Dr. Antony Somers, Mr. Shannon Biddulph and Mrs. Faezah Makhlooghiazad for their assistance and great support to carry out the work in Deakin IFM labs.

I also extend my big thanks to my lab mates at ECEL in IITB specially Mrs. Shivani Singh, Mr. C.V Manohar, Mr. Ananta Sarkar, Mr. Anish Raj, Ms. Ishita Vadagama and others for the help they had contributed towards this research project. I specially thank Ms. Divyamahalakshmi for helping me all times especially at times of hand inflammation. I still thankfully remember the times when Divya's left hand and my right hand worked together in the glove box for an experiment. It was due to the infinite assistance of Dr. Pavan Kumar Veluri and Ms. Divyamahalakshmi, I could able to continue my work even at times of tendon inflammation in my hand. I owe a big thanks to them.

Further, the assistance of Mr. Vilas Raut is highly appreciated while designing the three electrode cells and canister for my experiments. I also thank Mr. Ajay, lab assistant at ECEL for his help during the experiments. A lab mate outside my lab, I would like to thank Mr. Bapi Bera for all his help throughout the stay at IITB. I also thank each and every member of the short circuit lab who had actively contributed to this work. In addition, the assistance of Dr. Binayak Roy and Mr. Ajay Krishnan for the TGA measurements is highly appreciated. My special thanks to Mrs. Sheba Sanjay for the tremendous effort she had taken to correct the language aspects of this thesis. Her corrections had made me to understand the significant role of the language in scientific writing.

Apart, from the scientific assistance, the supportive environment created by the friends plays a significant role to tackle the difficulties during this Ph.D. These acknowledgements will not be enough for the support given by my friends Mr. T. Praveen Raj, Mrs. Sweta Shrinivasan, Ms. Lavanya Sethuraman, Mr. Naresh Chandrasekaran, Ms. Anjali Sairaman and Mrs. Gloria Josephine.

Above all, it will never be possible to complete this work without the support and dedication from my father, mother and brothers. I am highly grateful for the freedom they had given me to execute my dreams the way I like. I am also thankful to my parents-in-law for their support and prayers for the successful completion of this work. Finally, I could not find any word to express the thanks to my husband Mr. Srinivasan Mahendran for the infinite support, especially at times during this thesis writing. He had generously proofread this thesis infinite number of times and actively contributed to its betterment.

All, Thanks infinite!

Sowmiya Theivaprakasam.